UNIVERSITÀ DEGLI STUDI DI NAPOLI "FEDERICO II"

FACOLTÀ DI INGEGNERIA

Dottorato di ricerca in "Ingegneria Industriale" – XXX Ciclo

Settore scientifico disciplinare ING-IND/05:

Impianti e Sistemi Aerospaziali

DISSERTATION

New on-board multipurpose architecture integrating modern estimation techniques for generalized GNSS based autonomous orbit navigation

Francesco Menzione

Tutor:

Ch.mo Prof. Michele Grassi

Cotutor:

Ch.mo Prof. Alfredo Renga

Coordinatore:

Ch.mo Prof. Michele Grassi

to my Mom

"Aye, fight and you may die. Run, and you'll live... at least a while. And dying in your beds, many years from now, would you be willin' to trade all the days, from this day to that, for one chance, just one chance, to come back here and tell our enemies that they may take our lives, but they'll never take...our Freedom! "

William Wallace, Bravehearth

" Ever tried. Ever failed. No matter. Try again. Fail again. Fail better"

Samuel Beckett

ACKNOWLEDGMENTS

Before proceeding to thanking, I want to underline what this goal represents for me, beyond its academic value. My sacrifices have been worth proving a fundamental fact: anyone and I mean anyone, whether limited in any way or hindered by misfortune, can achieve what he wants to by striving and the help of those people who believe in him. This involves immense sacrifices that may seem discouraging and disappointing on the wisdom of one's choice. However, the fact that you have only thought of raising the goals of your life must make you proud. Even as the least among the PhD students, scientists and workers, a person can be the greatest of dreamers if he tried to be, , at any price, better than at the outset. The passion for what one does and the beautiful idea of following a dream in spite of everything will not meet with indifference. Just as in my case, it is possible to see that those people, whom I am also going to thank, will not have simply helped me, but they will have shared the same dream.

I begin by thanking my advisor, Professor Michele Grassi. He has been an amazing mentor by allowing me to chase after my own ideas and insights. A special mention goes to my supervisor, Professor Alfredo Renga, served as a constant source of inspiration early on in my graduate career: he continuously pushed me to expand the breadth of my research interests. Beyond tremendous academic support, they gave me the opportunity to demonstrate what I was worth, all the while guiding me towards becoming a better engineer and man.

This results project could not have been achieved without the support of my Thales Alenia Space responsible, Giovanni Campolo. He has always supported me on this route, promoting the possibility of making my ideas materialize in the world of space applications. I want also to thank Giuseppe Catastini and Luigi Galvagni, who were fundamental mentors for all my activities. They instilled in me the desire to improve by giving me novel and interesting point of view on the topics of my studies and encouraging me every day. Special mention goes to all my Thales colleagues, especially Marco M., Marco A., Dario, Simone, Francesco, Chiara, Domenico, Emiliano, Claudio, Vincenzo, Andrea, Massimiliano, who have taught me what I know today on space system, software, avionics and testing. Working with them is the greatest experience of my life: they are the right people to teach how you can fly your projects on a spacecraft platform.

My research could not have achieved any result without people who have collaborated with me on my research projects Raffaele Ferraro, David Sarrocco and Francesco Santoni: guys the road ahead is still too long but if the MEONS will fly it will mainly be thanks to you.

I want to thank all my childhood friends, Mario, Vincenzo, Sarah, Raffaele, Stefano, Peppe, G.Schiano

Daniele, Nando, who not only kept me in line, but also would constantly remind me to smile.

I wish to give thanks all my relatives: there has not been a day that they have not supported me allowing to go on in the personal ordeal of the last few years.

I want to thank my father, Giovanni. Now, I understand what you mean and I will manage to make you even more proud of me.

Last, but certainly not least, I want to thank the unsung heroin of my life, my mother Rossella, and my greatest love, Liliana.

Mother, I will never be able to repay you for what you gave me. However, this achievement shows that I will always continue to be the man you wanted me to be and for whom you have sacrificed your life.

Liliana, no matter what happened to the subject of a painting before or after, the beauty of the canvas will make it forever an eternal masterpiece.

This thesis is dedicated to these two women who probably will not be with me for much of what remains of my life. But for better or for worse they were my joy, my love and my strength to get here today, even if I was not always able show to them that they were my everything. Now I shall have to do simply everything that is in the life of a man to fill their spaces. The future awaits me, but you will always be the idea of strength and love that will support my shoulders and that will guide my choices.

My life what you want it to be, it all ends, what is left is today, the eternal heavenly nostalgia.

RINGRAZIAMENTI

Prima di procedere con ringraziamenti, voglio ricordare cosa questo traguardo rappresenta per me, al di là del suo valore accademico. I miei sacrifici sono serviti a dimostrare un fondamentale principio: chiunque e intendo chiunque, limitato o ostacolato, può raggiungere quello che desidera per mezzo della propria volontà e dell'aiuto delle persone che credono in lui. Ciò comporta immensi sacrifici che possono scoraggiare e disilludere, mettendo in dubbio la giustezza della vostra scelta. Tuttavia, il fatto stesso di aver pensato di elevare gli obiettivi della vita deve rendere orgogliosi. Anche se ultimi tra gli studenti di dottorato, tra gli scienziati e i lavoratori, si può essere il più grande dei sognatori se si è cercato di essere, ad ogni costo, migliori. La passione per ciò che si fa e la bellissima idea di seguire un sogno nonostante tutto non lascerà indifferente le persone intorno a voi. Proprio come è successo a me, vi renderete conto che quelle persone, che anche io mi appresto a ringraziare, non vi avranno semplicemente aiutato, ma avranno condiviso con voi quello stesso sogno

Comincio ringraziando il mio relatore, il Professor Michele Grassi. È stato un mentore straordinario, permettendomi di rincorrere le mie idee e intuizioni. Una menzione speciale va al mio supervisore, Alfredo Renga, da sempre fonte di ispirazione costante nella mia carriera universitaria: mi ha continuamente spinto ad ampliare i miei interessi di ricerca. Al di là dell'enorme sostegno accademico, devo assolutamente ringraziarli per avermi dato l'opportunità di dimostrare ciò che valevo, guidandomi nel frattempo nel mio percorso per essere un ingegnere e un uomo migliori.

Tutti i risultati non sarebbero stati ottenuti senza il supporto del mio responsabile di Thales Alenia Space, Giovanni Campolo. Mi ha sempre supportato in questo percorso, promuovendo la possibilità di rendere concrete le mie idee nella realtà delle applicazioni spaziali. Devo assolutamente ringraziare Giuseppe Catastini, Luigi Galvagni e Arturo Intelisano che sono stati i riferimenti fondamentali per tutte le mie attività. Mi hanno instillato il desiderio di migliorare e mi hanno sempre dato un punto di vista nuovo e

interessante sulle tematiche che affrontavo nel corso dei miei studi senza smettere di incoraggiarmi ogni giorno a dare il massimo. Una menzione speciale va a tutti i miei colleghi di Thales ed in particolare a Marco Maffei, Marco Anania, Massimiliano, Dario, Simone, Francesco, Chiara, Domenico, Emiliano, Claudio, Vincenzo, Andrea che mi hanno insegnato quello che so oggi sui sistemi spaziali, sulla progettazione software, sull'avionica e sul testing. Lavorare con loro è stata la più grande esperienza della mia vita: sono le persone giuste per insegnare come poter far volare i propri progetti su una vera piattaforma spaziale.

La mia ricerca non avrebbe potuto produrre questi risultati senza Raffaele Ferraro, David Sarrocco e Francesco Santoni, le persone che hanno direttamente collaborato con me ai miei progetti di ricerca: ragazzi la strada da percorrere è ancora lunga ma se il MEONS volerà sarà soprattutto grazie a voi.

Voglio ringraziare tutti i miei amici d'infanzia, Mario, Vincenzo, Sarah, Raffaele, Stefano, Peppe, Giuseppe Schiano, Daniele, Nando, che non solo mi ha tenuto in riga, ma mi hanno sempre ricordava e dato un motivo per sorridere.

Desidero rendere grazie a tutti i miei parenti: non c'è stato un giorno in cui non mi abbiano supportato permettendo di continuare la dura prova personale degli ultimi anni.

Voglio ringraziare mio padre, Giovanni. Ora capisco cosa intendi e riuscirò a renderti ancora più orgoglioso di me.

Ultimo, ma certamente non meno importante, voglio ringraziare l'eroina non celebrata della mia vita, mia madre Rossella, e il mio più grande amore, Liliana.

Madre, non potrò mai ripagarti per quello che mi hai dato. Tuttavia, questo risultato dimostra che continuerò sempre a essere l'uomo che volevi che io fossi e per il quale hai sacrificato la tua vita.

Liliana, non importa cosa sia successo al soggetto di un dipinto prima o dopo, la bellezza della tela lo renderà per sempre un eterno capolavoro.

Questa tesi è dedicata a queste due donne che probabilmente non saranno con me per gran parte di ciò che rimane della mia vita. Ma nel bene e nel male sono state la mia gioia, il mio amore e la mia forza per arrivare qui oggi e anche se non sono stato sempre in grado di dimostrarlo, loro sono state il mio tutto. Ora dovrò fare semplicemente tutto, tutto ciò che è nella vita di un uomo per colmare la loro mancanza. Il futuro mi attende, ma voi sarete sempre l'idea di forza e amore che sosterrà le mie spalle e che guiderà le mie scelte.

La mia vita cosa volete che sia, tutto finisce, quello che resta è oggi, l'eterna celeste nostalgia.

TABLE OF CONTENTS

LIST OF FIGURES

LIST OF TABLES

LIST OF ACRONYMS

AOC	**Attitude and Orbit Control**
C/N0	**Carrier To Noise Ratio**
CDGNSS	**Carrier phase Differential GNSS**
CPU	**Central Processing Unit**
CRB	**Cramer Rao lower Bound**
DoD	**Department of Defence**
DSP	**Digital Signal Processor**
ECEF	**Earth Centred Earth Fixed**
ECI	**Earth Centred Inertial**
EO	**Earth Observation**
EOR	**Earth Orbit Rising**
ESA	**European Space Agency**
FF	**Formation Flying**
FPGA	**Field Programmable Gate Array**
GEO	**Geostationary Earth orbit**
GGKF	**Generalized Gaussian Kalman Filtering**
GNC	**Guidance Navigation and Control**
GNSS	**Global Navigation Satellite System**
GOES-R	**Geostationary Operational Environmental Satellite-R**
GPS	**Global Positioning System**
GRAPHIC	**Group and Phase Ionospheric Calibration**
GTO	**Geostationary Transfer Orbit**
HEO	**High Earth Orbit**
LEO	**Low Earth Orbit**
LO	**Local Oscillator**
MAP	**Maximum A Posteriori**
MEO	**Medium Earth Orbit**
MMS	**Magnetospheric Multiscale mission**
MMSE	**minimum mean square error**
NASA	**National Aeronautic and Space Administration**
OCXO	**Oven-Controlled Crystal Oscillator**
PPS	**Pulse Per Second**
RAAN	**Right Ascension of the Ascending Node**
RF/IF	**Radio Frequency / Intermediatete Frequency**
RFFE	**Radio Frequency Front End**
RHS	**Right Hand Side**
S/S	**Subsystem**
SABRINA	**System for Advanced Bistatic and Radar INterferometric Application**
SAR	**Synthetic Aperture Radar**
SAR	**Synthetic Aperture Radar**
SBIRS	**Space Based InfraRed Sensor**
SISRE	**Signal in Space Range Error**
SOFTT	**Space Optimal Finite Thrust Transfer**
SVs	**Space vehicles**
SVs	**Space vehicles**
TAS-I	**Thales Alenia Space Italy**
TLC	**Telecommunication**
TT&C	**Telemetry, tracking, and command**

CHAPTER I

INTRODUCTION

I.1 BACKGROUND

Orbit Determination (OD) addresses the application of specifically devised estimation techniques aiming to determine the state of a satellite in order to support mission operations (Figure I-1). Post-flight processing generally integrates high fidelity propagation of spacecraft dynamic model with a set of observations and measurements collected by ground-based tracking stations. Different levels of accuracy can be reached varying from preliminary Initial Orbit Determination (or IOD) to high precision one referred as Precise Orbit Determination (POD).

The Orbit Navigation (ON) problem deals with the same issue, but it relies on real time spacecraft positioning by the direct on-board processing of avionic sensor and auxiliary observables. The primary aim is to support platform autonomous operations as trajectory and attitude control tasks, even though payload and data handling can benefit of a precise position tag.

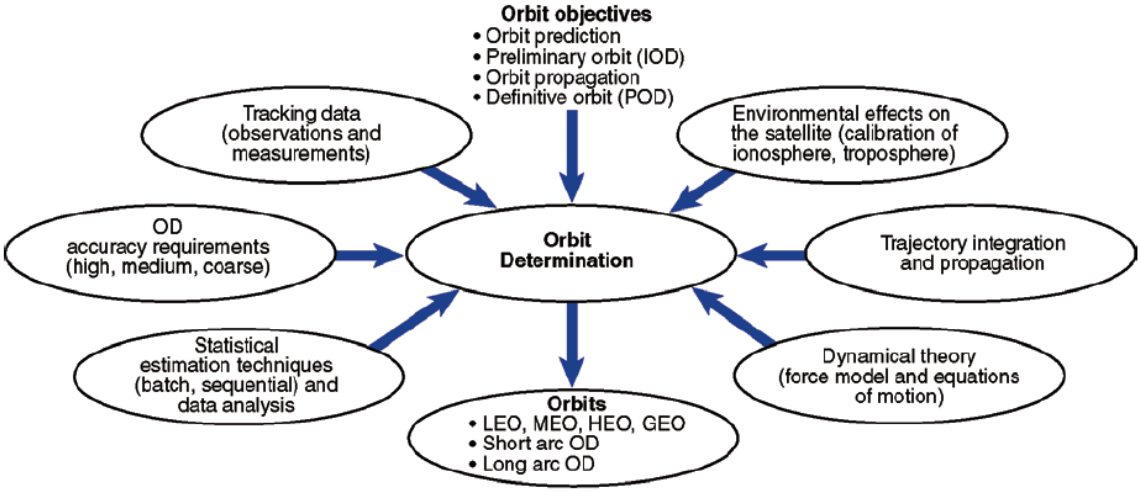

Figure I-1 Orbit determination problem and topics

Modern OD systems, which are the result of methodologies developed over the past 50 years[1], have demonstrated, in the framework of many research programs carried out by DoD, NASA and ESA, the advantage of a generalized Earth orbit determination scheme dealing with a large variety of space missions and orbital regimes (LEO, MEO, GEO, etc.). Their propagation and estimation open architectures allow suitable orbit models to be selected and target state vector rearrangement: it is possible in this way to properly calibrate the model wrt the orbit regime peculiarities by manipulating a list of operating parameters. The capability of handling different kinds as well as different combinations of observables completes the generalized OD paradigm: measurement reconstruction patterns modelling allow optimizing the performance with respect to both random and systematic errors [2].

The possibility to have a configurable OD-based scheme is becoming of high interest also for on-board ON systems, which tries to achieve the same flexibility within the real time constraint. Actually, the modern avionic design driver is the portability and reusability on different platforms (or on different configurations of the same one) of fundamental GNC and AOC functionalities, including orbit determination. TAS-I has been recently promoting several research activity and internal studies [3] aiming to extend the first generation LEO satellite navigation system [4] to the generalized approach ([2],[5]). The target of next years is to make compatible the navigation kernel with novel scenarios as

GNSS based low thrust high orbit transfer and autonomous single and multiple platform orbit control. This issue basically arises from recent advances in avionics. Modern spaceborne GNSS receivers and electric propulsion systems must be considered respectively the navigation and actuation technologies enabling the implementation of an extended altitude steering strategy for next generation platforms.

In this framework, the *multipurpose navigation paradigm*, i.e. the possibility to handle by an integrated solution multiple platform and mission scenarios, still offers a challenging field of research that goes in parallel with advances in space navigation and control requirements.

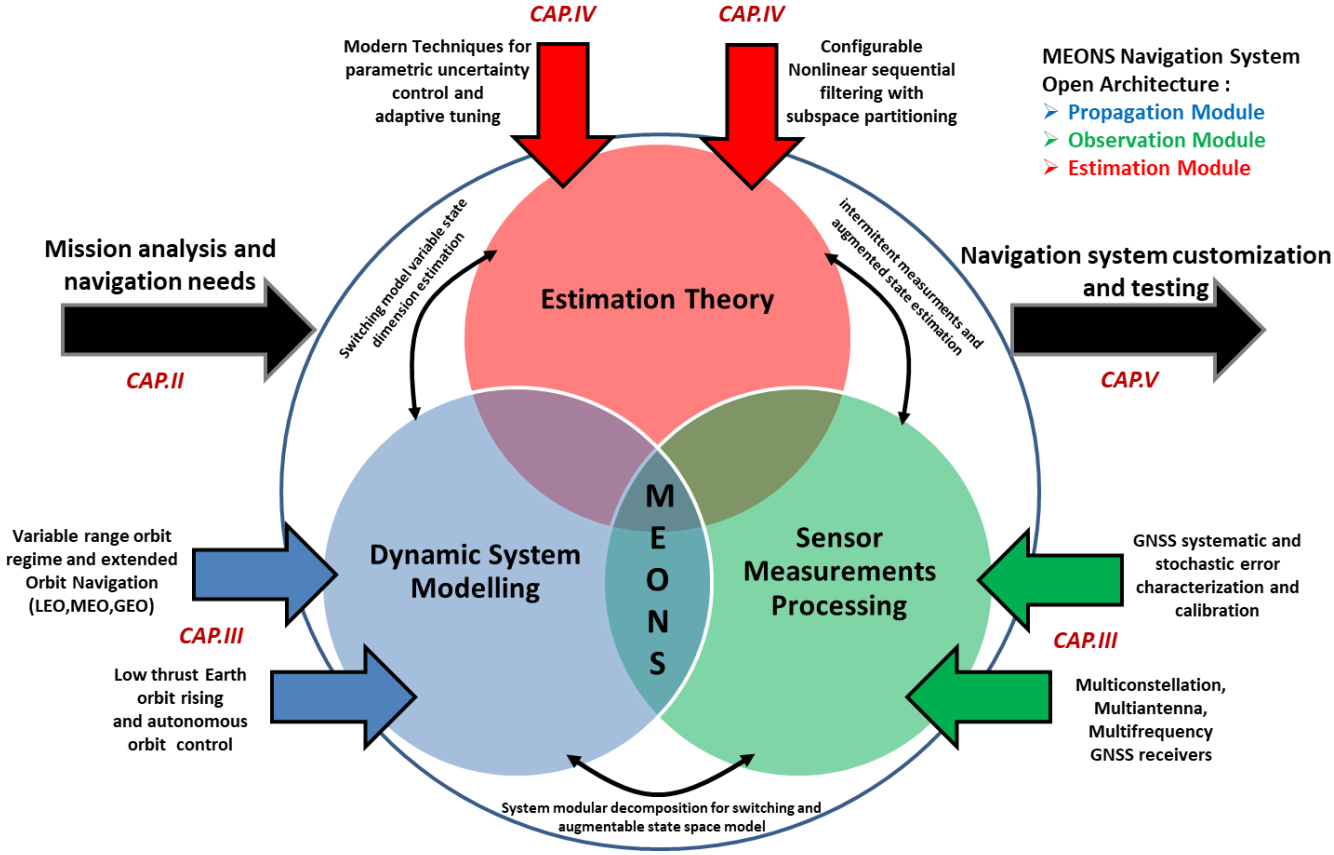

Figure I-2 MEONS system research areas and dissertation drivers

I.2 RESEARCH OBJECTIVE AND CONTRIBUTION

Starting from the analysis of current and planned missions, this research proposes and tests a novel Multi-purpose Earth Orbit Navigation System (MEONS) architecture aimed at improving the standard GNSS based on-board real time orbit determination in accordance to the following fundamental achievements:

- Compatibility with on-board POD for wide range orbit regime (LEO, MEO, GEO, GTO)
- Compatibility with low thrust autonomous transfer (e.g. LEO-MEO) and optimal orbit control
- Compatibility with Multi-antenna, Multi-frequency, Multi-constellation GNSS solutions
- Compatibility with multiple spacecraft missions and small satellite configuration constraints
- Enhanced accuracy and robustness by using advanced sequential filtering solutions
- Enhanced flexibility and reusability in different applications by modular augmentation and system open architecture

The theoretical background, where investigating such navigation system requirements, involves the three fundamental research areas of Estimation Theory, Dynamic System Modelling and Sensor Measurements Processing (Figure I-2).

RESEARCH ACTIVITY	
MEONS TOPIC	**MEONS generalized state space module design**
PROPAGATION TASK	Non-linear state space propagation task integrating: ➢ Extended variational model and state transition matrix computation ➢ Dynamic system decomposition for modular state space structure ➢ Augmented state vector with dynamic rearrangement ➢ Propagation controller for switching model and mode management ➢ Orbit physical perturbation and control modules for high performance prediction
OBSERVATION TASK	Non-linear state space observation task integrating : ➢ Extended variational model and measurement design matrix computation ➢ Observation function decomposition for modular state space model ➢ Observation controller for switching model and intermittent measurement processing ➢ GNSS Multi-constellation/ Multi-frequency /Multi-antenna GNSS raw measurement reconstruction pattern and observable equation models ➢ Measurement combinations (e.g. Differential) and auxiliary information handling (GNSS SVs, C/N0)
MEONS AUXILIARY TOOL	State Space Model Analysis: ➢ Orbit propagation design via incremental perturbation analysis ➢ Dynamic model initial condition and parameter sensitivity tools ➢ Preliminary navigation performance analysis and model information content by linear CRB evaluation

MEONS TOPIC	**MEONS configurable sequential estimation module design**
MODERN ESTIMATION TECNIQUES	Challenging aspects in Kalman Filtering : ➢ Generalized Gaussian Kalman Filtering (GGKF) ➢ Linear Gaussian Subspace Marginalization ➢ Accounting of Parameter uncertainty via Consider Kalman Filtering ➢ Maximum Likelihood Adaptive Filtering ➢ Variable state dimension approach and Reordering Transformation tool

MEONS ESTIMATOR DEVELOPMENT	MEONS estimator implementation : ➢ Filtering problem decomposition via state partition and model substructure identification ➢ Generalized Reordering Process and state variable management ➢ Configurable Sequential Filtering Module software implementation issues ➢ Numerical issues for future real time implementation

MEONS TOPIC	**MEONS system performance analysis and testing wrt challenging navigation scenarios**
ON BOARD POD APPLICATIONS	1) Constrained Single Difference CDGNSS for Formation Flying on board POD : ➢ Mission: Follow up of SABRINA formation flying study ➢ Covered Topics: multiple spacecraft, ambiguity state augmentation, reduced dynamic estimation, variable state dimension tracking filter, differential measurements 2) Adaptive Kalman POD filter for Hardware in the loop (HIL) GNSS data processing ➢ Mission: EO-LEO Copernicus Sentinel-1 ➢ Covered Topics: Maximum Likelihood Adaptive Filtering, Multi-frequency ionofree measurements, HIL pseudorange and Doppler raw data processing
AUTONOMOUS ORBIT RISING AND LOW THRUST STEERING STRATEGY	3) Consider Kalman Filter for LEO-MEO autonomous orbit rising ➢ Mission : Galileo Second Generation autonomous low thrust constellation steering ➢ Features covered: variable range orbit and LEO-MEO autonomous orbit rising, Multi-antenna/Multi-constellation measurement processing in high orbit, Configurable Consider Kalman filter handling parametric uncertainty (low thrust mechanization errors and measurement biases). 4) Integrated navigation system and control for small spacecraft low thrust orbit acquisition ➢ Mission: Next Generation Small Satellites ➢ Features covered: Marginalized filtering, Consider Kalman Filter, closed loop and attitude steering compatibility, low cost configuration by using single frequency/single constellation measurements

Table I-1 Research topics

This dissertation performs a wide spectrum analysis of modern estimation techniques and state space approaches in order to design, develop and implement the MEONS system architecture in accordance to the pursued *multipurpose navigation paradigm*.

In more details, the contributions of this work can be grouped in three main set, relying respectively to the following research activities:

- MEONS generalized state space module design (propagation and observation tasks)
- MEONS configurable optimal sequential filtering module design (estimation task)
- MEONS system performance analysis and testing with respect to challenging navigation scenarios

Each topic has offered the possibility to investigate different methodologies and navigation design issues that are briefly summarized in Table I-1. In particular, some novelties with respect to the reference literature have been introduced. Multi-constellation/Multi-antenna GNSS based navigation for LEO-MEO autonomous orbit transfer [6] and the application of Marginalized and Consider Filtering approaches ([6],[7]) for orbit estimation substructure exploitation can be ranked as relevant contribution. In more general, the study results demonstrate the possibility to handle different navigation scenarios via the same open architecture by augmenting and configuring it in accordance to the mission requirements and platform avionic subsystem peculiarities.

I.3 DISSERTATION ORGANIZATION

The dissertation organization reflects the topic structure and MEONS development phases:

- **CHAPTER II** introduces the GNSS Space Service Volume (SSV) scenario and the recent advances in GNSS receiver's architectures, addressing the technological basis of wide range altitude Orbit Navigation concept. Benefits of GNSS based ON are analysed for different missions and platforms. The analysis generates navigation requirements used to define MEONS high level architecture and interfaces. The general Bayesian estimation scheme is also introduced as mathematical and theoretical framework within addressing the configurable sequential estimation architecture and the cornerstones of *state space based estimation* and *recursive optimal filtering* are discussed.

- **CHAPTER III** defines the mathematical and theoretical state space model used to implement *spacecraft orbit propagation* and *GNSS measurement processing* modules. The augmentation with variational model equations and model decomposition allows optimizing dynamic system update and run time state rearrangement for multiple mode navigation.

- **CHAPTER IV** introduces Generalized Gaussian Kalman Filtering approach (GGKF), selected as fundamental kernel of the MEONS estimation module and investigates advanced techniques aiming to handle specific navigation problem criticalities. *Mixed Nonlinear/Linear Model Marginalization*, *Consider Kalman filtering*, *Maximum Likelihood Adaptive Filter* and *Variable State Dimension filtering* belong to this set. All the proposed Kalman Filtering Class Methods are finally addressed within the modern interpretation of the optimal filtering based on dynamic system substructures. The investigation converges in the definition of the final MEONS navigation module development taking into account software implementation issues.

- **CHAPTER V** includes all relevant test cases and results achieved considering MEONS as platform navigation kernel for different mission scenarios. POD applications as well as the challenging low thrust autonomous orbit rising and control are treated in this section. In case of Sentinel-1 test campaign, it was possible to process raw data generated by a spaceborne receiver. Other applications relies to phase A/B studies, so they are tested by using an high fidelity simulator specifically devised to points out relevant design drivers and criticalities of the target application. Performance assessments are reported for each study case.

CHAPTER II

A NEW PARADIGM FOR SPACECRAFT AUTONOMOUS NAVIGATION

II.1 MODERN GNSS TECHNOLOGY AND EXTENDED ALTITUDE EARTH ORBIT DETERMINATION

This section introduces the technological framework to which multipurpose approach applies. Recent advances in receiver capabilities and feasibility studies [8] on high orbit utilization of Global Navigation Space System (GNSS) devises are arousing an increasing interest in the possibility of using them as main platform navigation sensor for a wide range of missions. Several research programs and studies carried out by NASA [9] and ESA [10] are currently investigating possible GNSS Space Service Volume enhancements as well as hardware improvements of GNSS spaceborne equipment. This work focuses on the novel Multi-constellation/Multi-frequency/Multi-antenna paradigm, introducing also the high sensitivity processing and GNSS aiding techniques to be considered in the next generation navigation context. However, the effectiveness of having additional frequencies, additional constellations and additional antennas mainly depends on space mission peculiarities and real GNSS system status. Actually, the implementations experienced in this study do not span all frequencies, constellations and antenna configuration possibilities, but they are tailored for each study case in accordance to the specific assumptions on GNSS constellation maturity, platform hardware resources and operative scenario constraints. Nevertheless, test cases addressed in CHAPTER V cover all the relevant navigation task design issues introduced by the Multi-constellation/Multi-frequency/Multi-antenna approach. Almost all the results and compatibilities achieved in this thesis can be extended to the enhanced receiver architectures, which consider more frequencies, constellation and antennas.

A. Modern applications of GNSS in space and the GNSS Space Service Volume

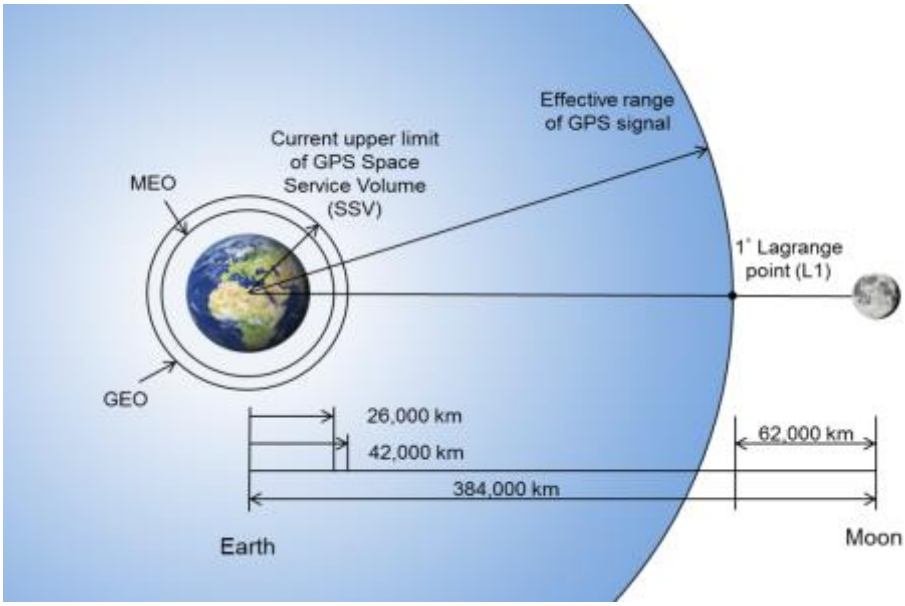

Figure II-1 GPS Space Service Volume and effective range of GPS signal (figure not in scale).

GPS and all other GNSS constellations consist of a core volume of satellites, primarily in MEO, transmitting one-way radio signals that are used to calculate three-dimensional position and time in the terrestrial and near-Earth domain. To achieve this, traditionally at least four GNSS satellites are needed to be within line-of-sight at any given time to enable on-board real-time autonomous navigation [11] through the formation of a point solution.

Continuous availability of at least four signals has become a standard expectation for GNSS users within

the Terrestrial Service Volume (TSV), the regime from the surface of the Earth to 3,000 kilometres altitude, including much of LEO orbits. A LEO mission case is not very dissimilar for a typical user on the Earth surface, apart from dynamic conditions and higher Doppler excursion due to velocity experienced by the receiver. For over two decades, researchers, space users and GNSS service providers have been working to expand the spaceborne use of the GPS and, most recently, to employ the full complement of GNSS constellations (i.e. novel Galileo European Constellation) to increase spacecraft navigation robustness. GNSS use in space is expanding into the whole Space Service Volume (SSV), i.e. the signal environment in the volume surrounding the Earth that should enables real-time raw measurements availability also above altitudes of 3000 km. Actually, GNSS signal extends on a sphere around the Earth with a radius of about 322,000 km (see Figure II-1), so it covers 4/5 of the distance between the Earth and the Moon. This means that GNSS can be theoretically used for all that missions inside this sphere.

Clearly as distance from the GNSS constellation SVs increases, the GNSS signal degrades becomes weaker and the visibility of the satellite constellation reduces due to different geometry. For these reasons different Service Volumes regions (Figure II-2) can be introduced depending on the altitude above the Earth surface:

- TSV, Terrestrial Service Volume, basically the volume of space between the surface of the Earth and an altitude of about 3,000 km, including all LEO.
- MSSV, Mean Space Service Volume for medium altitudes region (3,000 - 8,000 km).
- HSSV, High Space Service Volume for high altitudes (8,000 - 36,000 km).

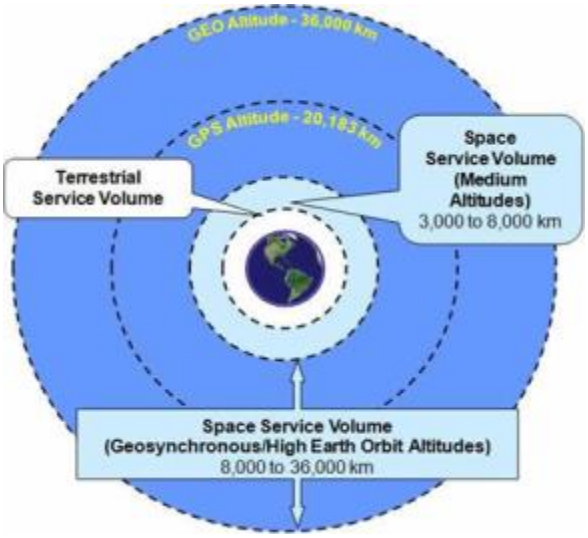

Figure II-2 SSV regions definition

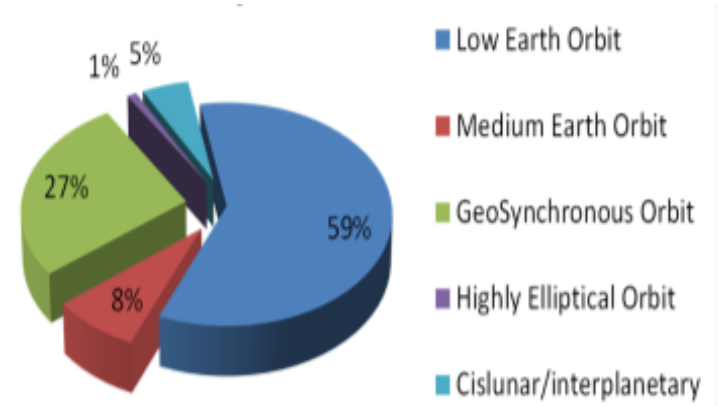

Figure II-3 Space mission trend for the next 20 years worldwide [28]

Observing trends of space missions (Figure II-3) for the next twenty years we can note that approximately 60% of space missions will operate in LEO (less than 3,000 km) and 35% will operate at higher orbits up to 36,000 km. This means that approximately 95% of the space missions will operate not only around the Earth but within the GNSS Space Service Volume. These reasons explain the great importance of the GNSS and the interest in extending the GNSS SSV in order to enable new and better performances in a wide range of applications, extending from LEO missions to GEO-HEO missions.

Nevertheless, further improvements are necessary in order to override scenario criticalities in upper regions of SSV. Let us consider scheme in Figure II-4 that depicts a typical GNSS satellite with its main lobe signal highlighted in dark yellow and its first side lobe signal shown in light yellow. On this graphic a representative spacecraft in an eccentric high Earth orbit is considered to spans low-altitude and high-altitude regimes. As it is evident from this geometry, spacecraft within the high Earth orbit strip relies predominantly on signals that pass over the limb of the Earth. This apply to MEO/GEO/HEO/GTO cases, whose orbit semi-major axis (or its apogee for HEO/GTO) can be very close to or well above the GNSS (i.e. GPS and GALILEO) semi-major axis.

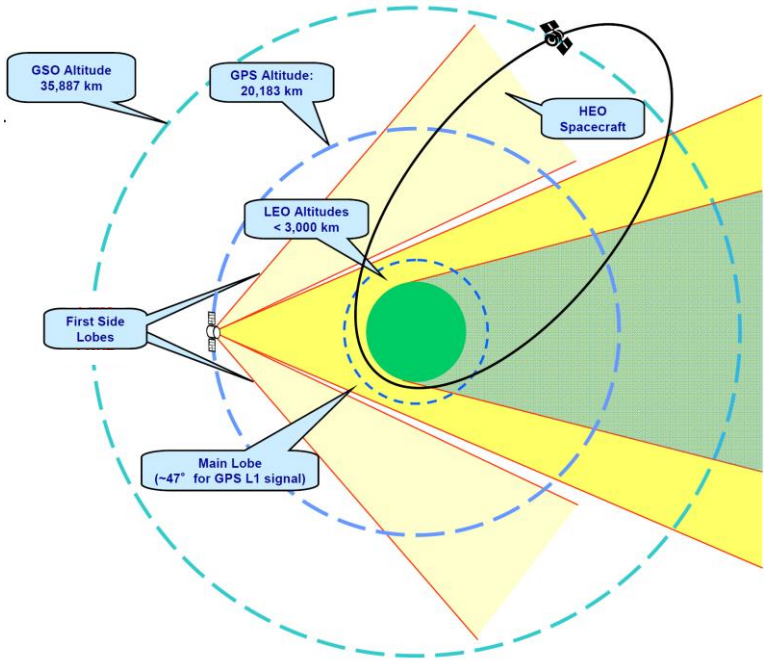

Figure II-4 Reception geometry for GPS signals

The number of visible satellites, in term of geometrical visibility, can be much lower than LEO and periods of complete non-visibility have been experienced in past experimental missions (EQUATOR-S [9]). Actually, the increased distance between GPS satellite and spacecraft impacting the received GNSS signal power modify information distribution, which can be very sparse, if compared with low altitude users. Another constraint to take into account is that the GNSS signals are delayed by the ionosphere in proximity of the Earth. The spacecraft can get full advantage of the navigation signal only when it is on the "far side" of the Earth and the common approach is to ban SVs in the receivers tracking list by satellite masking (see III.2-C).

These issues, summarized in Table II-1 explain why high orbit navigation is a challenging technological area involving all GNSS levels: space segment, ground segment and user segment. It is evident that:

- tracking the main lobe only is not enough for reaching a complete availability of Standard Position Service (SPS) , so both SVs transmitting power and receivers tracking capability (high-sensitivity) shall be improved
- using different GNSS constellation (GPS, Galileo, Glonass, and BeiDou) can be a very effective method to increases satellite availability.

Several initiatives, relying to GPS and European Galileo cooperation, just focus on the employment of aggregate signals (main and side lobes) from both GNSS constellations. Specifically, GNSS providers are involved as concern:

- realization of an effective interoperability between GNSS constellations (i.e. GPS and Galileo)
- improvement of SVs transmitting power and side lobes shaping

while receiver contractors shall:

- develop novel spaceborne receiver architecture integrating different GNSS constellations
- improve receiver sensitivity to low power transmitted signals

The results of these efforts have already proven fruitful: NASA space programs, like SBIRS, GOES-R, MMS [5], showed the possibility to use GPS signal also above the GPS nominal altitude. However, Multi-constellation possibility is not completely investigated and on-board integrated orbit estimation systems for high orbit navigation shall be progressively upgraded in order to follow different receivers' architecture and new mission operative constraints. This thesis introduces the challenging technological issue of using GNSS for Autonomous Earth Orbit Rising (EOR, see II.2-A), which has been recently indicated as an essential capability to accomplish a reliable reduction of the burden and costs of network operations. In this case variable orbit regime and long permanence in different SSV regions shall be considered. Not only conventional LEO applications and routine operations, but also non-operative phases (i.e. the low-thrust target orbit acquisition) and high Earth orbit navigation will be based on GNSS autonomous navigation.

Medium Altitudes SSV (3,000 -8,000 km)	High Altitudes SSV (8,000-36,0000 km)
Four GPS signals available simultaneously a majority of the time	Long periods with no GPS signals available
GPS signals over the limb of the Earth become increasingly important	GPS signals over the limb of the Earth are the only signals available
Conventional Space GPS receivers will have difficulty	
Wide range of received GPS signal strength.	Received power levels weaker than those in TSV or Medium Altitudes SSV
A proper designed integrated GNSS orbit navigation can reach meter order orbit accuracy	A proper designed integrated GNSS orbit can reach accuracies ranging between 10 and 200 meters

Table II-1 Space Service Volume characteristics

B. Spaceborne GNSS receivers novel architecture and high orbit compatibility

The full exploitation of the SSV drastically relies on the possibility to upgrade and improve the current spaceborne receivers' technology (for extended analyses of hardware solution refer to [12] and [13]). This aim shall be balanced by considering other instances as cost, size and power reduction that drives commercial scenarios accessibility and small platform compatibility.

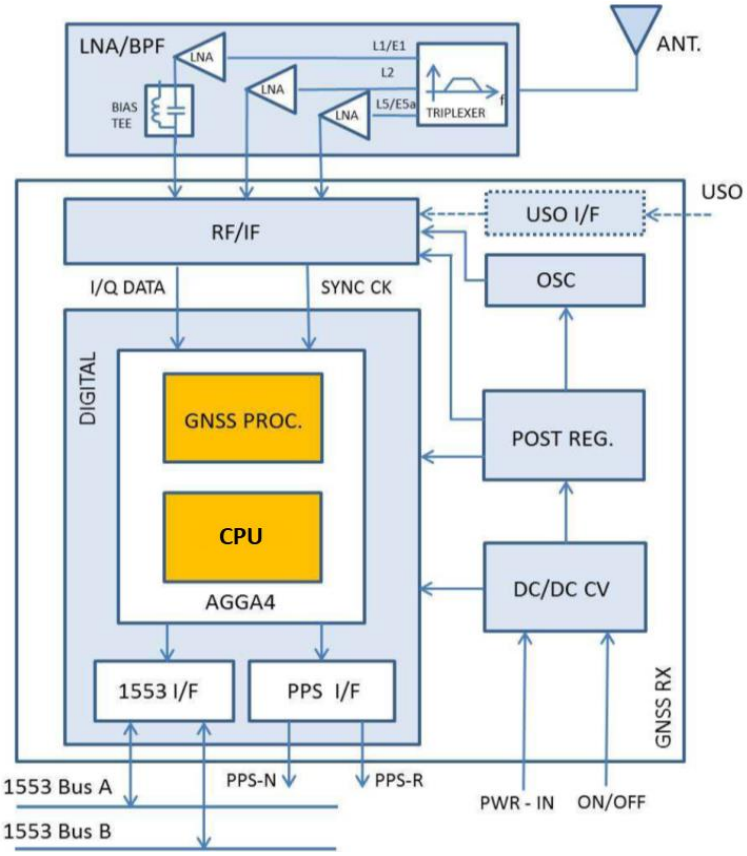

Figure II-5 Multi-frequency / Multi-constellation architecture for spaceborne GNSS receiver based on [12]

Two fundamentals industrial needs can be recognized:

- Development of high performance modular architectures allowing Multi-constellation / Multi-frequency / Multi-antenna customization
- Development of miniaturized and integrated solution for low cost single and distributed small platforms.

This second aspect is considered in the frame of multipurpose orbit estimation topic within the small satellite test case (V.4). Referring to low cost spaceborne receiver solution allows extending dissertation from upper class receivers (i.e. for POD and EOR) to reduced navigation resources case.

All GNSS hardware reference models and trends experienced during this research are hereafter discussed.

- **Modular solution for Multi-frequency / Multi-constellation / Multi-antenna**

Multi-frequency is mandatory for ground based POD applications. It allows compensating atmospheric

path delay [11] and achieving centimetres accuracy by using differential measurements and ground station fiducial network auxiliaries. The GPS L1C/A L1P/L2P [15] compatibility is currently considered the baseline requirement for LEO Earth Observation missions. However, novel frequencies will be made available in the next years for space applications. GPS [16] plans to fully deploy constellation blocks providing enhanced L2C and L5 signals: the first eliminates the issue related to the codeless processing [17] for civil application; the second is designed to allow interoperability with Galileo [18] providing also higher transmitting power [19]. These properties still apply for space application, hence new frequencies shall be considered an attractive alternative for next generation devices. The European Programs spaceborne receivers ([20],[21]) are approaching to single-board architectures using both GPS/GAL signals and exploiting a wide range of frequencies (L1/E1, L2, L5/E5 band). A representative drawing is provided in Figure II-5. In this scheme the fundamental functional blocks and their specification for a Multi-frequency/Multi-constellation solution can be recognized:

- **RFFE**: the RF signal from the antenna is separated in frequency by a Diplexer/Triplexer filter composed by GNSS carrier splitting and signal amplification via Low Noise Amplification (LNA). Filtering stages are present on the signal path, to reduce the out of band unwanted signals (noise, spurious signals). Multiple frequency solution needs different signal path per carrier, thus increasing the number of handled frequencies requires more complex duplexing, filtering and amplification steps in order to minimize the insertion and implementation losses on the signal.

- **RF I/F module**: The RF/IF section encompasses the RF signal conditioning for subsequent sampling and delivery of samples to the correlators (Digital Section). The RF down-conversion chain [11] performance depends also from reference signals provided by LO (generally an OCXO) whose phase's noise and stability affect measurement accuracy (carrier phase). The RF-I/F section performs a super-heterodyne down-conversion scheme generally relying to two steps: signals are first down-converted to an Intermediate Frequency (IF) and then to baseband. This allows reducing signal losses. Basically each carrier needs a correspondent down conversion process with common LO in order to provide signal I/Q components (I in phase, Q in quadrature) to the A/D conversion. This layer defines the transition from the analog processing to the digital one.

- **Digital module:** the digital section is based on DSP or FPGA implementing Code and Carrier acquisition and tracking algorithms. The DLL correletor and PLL/FLL carrier loops (i.e. Costas loop) allows to perform acquisition delay/frequency search and maintains Carrier and Code lock on incoming signals in order to demodulates and decodes navigation data message and provides raw measurements data for each selected satellite [11]. Signal processing works in synergy with the navigation kernel implemented within a spaceborne CPU core that manages channel allocation, tracking list and compute SPS on the basis of GNSS SVs ephemeris and ranging measurements. Basically this module is the most impacted by the Multi-constellation solution, even when RF band is shared (i.e. L1/E1 solution). The processing of a GPS and Galileo subsignals have to be performed separately allocating a dedicated channel of the available processing stack. Increased number of channel is generally requested in order to make effective the enhanced number of simultaneously visible SVs made possible by the Multi-constellation solution.

- **Power and communication module**: the power unit regulates primary power and route all the secondary power line to feed the internal blocks. The communication interface is in charge to dispatch all analogical and digital signals to the external user. Telemetry data (i.e. measurements for avionic navigator) provided on the avionic system bus and important synchronization signals as PPS are included.

As detailed in II.2-A, the structure in Figure II-5 is furthermore complicated considering the EOR space application, which requires Multi-antenna compatibility. Actually, this possibility, generally relying to attitude applications [22], is necessary to cope with navigation during orbit transfer that span low to high

orbit regimes. Taking into account the visibility geometry of high orbits described in Figure II-4, MEO and GEO low thrust acquisition [20], makes necessary to put another receiving antenna pointing towards the Earth. Basically, during transfers at lower orbits the main working direction is the conventional one close to the zenith, but as the altitude increases the geometry changes, the Earth disk becomes smaller and smaller and so GNSS satellites on the other side of the Earth fall in the Field Of View (FOV) of the second antenna (see III.2-C).

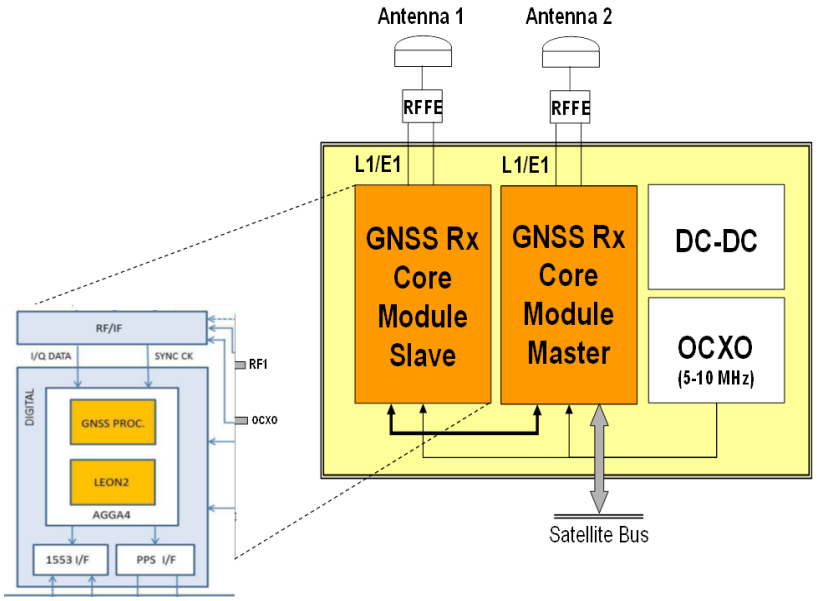

Figure II-6 Double antenna receiver architecture (based on [20])

A representative receiver architecture proposal for a dual antenna configuration is shown in Figure II-6, where can be recognized:

- core modules containing the RF/IF, Digital and signal processing functions
- antennas, RF cables, RFFE for each core module

Core module can include single frequency and single constellation solution as well as Multi-constellation or Multi-frequency chains. It is evident that such schemes rely to a growing complexity and introduction of additional hardware resources.

Actually, the presented overview reveals that enhanced solutions needs increased power consumption, increased hardware realization complexity and, not least, increased cost. The Multi-frequency/Multi-constellation/Multi-antenna possibility shall be intended in a modular fashion. The hardware can be augmented in order to cope with specific application requirements, but the proper trade off shall be investigated with respect to platform available resources. For instance, if high orbit scenario is considered, it is preferable pushing on the Multi-constellation solution instead of double or triple frequency: satellite masking due to ionosphere crossing slightly impact on the final visibility, especially if compared with additional constellation availability (III.2-C). Moreover, some solutions are effective only if the constellation or signals are fully operative. The navigation system testing campaign (CHAPTER V) performed in this study relies on the minimal required ones, i.e. L1/L2 dual frequency and Multi-antenna/Multi-constellation single frequency configurations. The compatibility with the higher complexity receiver architectures can be derived extending the minimal ones.

- **High sensitivity**

The key parameter for a successful navigation message download and GNSS ranging measurements generation is the C/N0 [14]. The carrier-to-noise power ratio is an important factor in all GNSS receiver performances. It is computed as the ratio of recovered power, C, (in Watt) from the desired signal to the noise density N0 (in W/Hz). Several methods for determining C/N0 are provided in [14]. Relevant relation with signal link budget, which drives C, and hardware characteristics, which drive N0, will be detailed in III.2-C. Actually, GNSS signal acquisition is a search and detection process [11] aiming to generate a perfect replication of both the code and the carrier of the target SV in order to demodulate the received signal. Beyond the specific procedure necessary to accomplish two dimensional Code and Phase/Doppler search (see [11] for an extended analysis), during start-up and without a priori information, a receiver perform a sky search (or cold start procedure). All possible PRN codes are sequentially or in parallel spanned in order to associate to the received signal a specific GNSS SV. Some criteria must be established to determine when to terminate the search process for a given SV and select

another candidate. Such detection is a statistical process, whose decision probability function depends on the dimensionless carrier to noise ratio C/N, expressed by:

$$C/N = \left(C/N_0\right)T \tag{2.1}$$

as a function of the signal search time T (or integration time [14]) and of C/N0. Specifically, fixing the searching time T, poorer the expected C/N0, then the lower is the probability to have reasonable success of SVs identification and signal acquisition. Successful detection allows demodulating and decoding the navigation data bits in order to acquire SVs ephemeris, time and auxiliary data necessary to perform SPS solution. However, also navigation frame extraction process [11] is a function of C/N0 since it represents the available signal strength necessary to ensure a low bit error rate for the decoding step. The useful approach is defining a C/N0 threshold allowing performing search, acquisition and demodulation of the signal with high reliability level. Such threshold, also referred as acquisition threshold, represents the receiver sensitivity: a SV can be retained "in view" and exploitable to generate measurements when the associated C/N0 is higher than the selected value. The modernization of spaceborne GNSS receiver technology for high orbit critical scenarios [23] also relies on weak signals mitigation, namely referred as high sensitivity techniques. It is clear that such solutions are put in place in order to improve the receiver sensitivity and increase measurement availability by reducing C/N0 threshold. A careful design of GNSS receiver antenna and low noise front end is the starting point to reduce N0 losses. However, also software solution can be considered in term of advanced signal processing techniques. The trend is to transfer in Space Technology GNSS Indoor positioning techniques, whose needs are typically more demanding with respect to standard positioning. The C/N of eq.(2.1) can be primarily increased by using a longer integration time. Subsequently, higher complexity searching and demodulation solution can be implemented (i.e. Coherent/non coherent Extended Integration [24] , vector tracking [25], half-bit acquisition method and detection techniques based on subspace projection [26]). Drawbacks are present because high sensitivity can introduce increased acquisition time, implementation complexity (in terms of algorithms and needed hardware resources) and interference suppression issues. However, the C/N0 improvements are strongly limited by the constellation message bit decoding threshold. Looking at results provided in [10], [27], the necessary C/N0 is 25.7 and 27 dB-Hz for GALILEO E1 and GPS L1 C/A respectively. In this work a high sensitivity receiver evolution has been considered in the Galileo Second Generation test case (see V.3). Specifically a 34dB/Hz is considered instead of 38 dB/Hz nominal acquisition thresholds, typically selected for target LEO receivers [15]. The receivers latencies introduced by high sensitivity techniques due to and increased acquisition time are considered mitigated by using external data aiding techniques described hereafter.

- **Data-Aiding and hybridization**

Data Aided (DA) defines the aiding of the GNSS receiver with auxiliary information provided externally by the hosting platform. For spaceborne applications, Doppler information, estimated by an orbital Kalman filter is very important when long integration times are necessary to acquire and track signal with low C/N0. In more detail, a priori positioning and attitude can be used respectively to propagate ranging/Doppler measurements and update coherently the SVs tracking list. In this way, Code Phase/Doppler searching space [20] and channel allocation are improved allowing a faster recovery from loss of lock and signal reacquisition. These features generally rely to the concept of hybridization, indicating with this term data-fusion techniques capable to work in closed loop with the receiver. Orbit estimation, attitude aiding, manoeuvre information and auxiliary sensors (i.e. accelerations models, inertial navigation system measurements etc.) can drastically improve propagation performances during and after GNSS outages. The multipurpose solution, which will be introduced in next section (II.2), looks toward DA. It implements raw measurement processing and the orbit estimator interfaces external AOC manoeuvre and attitude data. This allows respectively performing continuous high performance orbit propagation and expected in view SVs list update allowing to trigger fast signal reacquisition and

measurement rearrangement. Another possibility proposed for GNSS SSV critical scenarios is the Assisted GNSS systems (A-GNSS) , which allows to further extend the correlation interval, hence the sensitivity of the receiver. In this case initialization (i.e. cold start blind search) is replaced by warm start procedure by using ground based auxiliary data containing almanacs and timing information. Not requiring navigation message demodulation, receiver performance can be improved in term of increased sensitivity, reduced Time To First Fix (TTFF), computational complexity and power consumption. The main drawback is introduced at the system level: a link between the receiver and the main ground facility providing the data (e.g. over the TT&C link) is necessary for position fixing. This is completely in contrast with spacecraft autonomy objective, so it will be not considered in the following. Only the "Extended ephemeris" approach can be of interest. This solution consist in the idea to make available in the next generation navigation message, SVs ephemeris data whose accuracy degrades in a longer time (28 days) in order to reduce the number of ephemeris data acquisitions. Unfortunately, this capability is not yet available and broadcast ephemeris can be propagated in high orbit scenarios over their validity (4h). The degradation accuracy of SVs positioning with respect to the conventional LEO case shall be properly monitored and considered within the orbit estimation process by tuning the expected raw measurement error (see III.2-D).

- **Integration of the GNSS Receiver within on-board avionic**

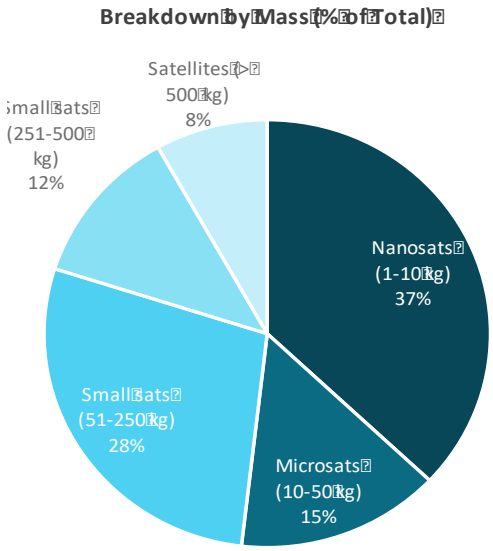

Figure II-7 Forecast of satellites to be launched in the period 2017-2026 [28]

The trend of commercialization of space missions calls for flexible, low-power and low-cost spacecraft's. Subsystems and sensors of these spacecraft shall meet stringent criteria such as low power, small size and reduced mass. A tremendous impact of nano and micro-satellites is expected in the next years (Figure II-7). This aim is not only accomplished by miniaturizing the electronics and minimizing hardware complexity (i.e. for GNSS case single board, single chain version of [15]), but also deeply integrating the navigation function within the avionic subsystem. A possibility could be adapting for small platform the TAS-I architecture proposed in [20] that integrates the receiver module as part of the platform central computer. Specifically, [20] design is targeted on a low-end receiver configuration, which is mainly expressed by a single-frequency open-service receiver to be hosted on the on-board computer of a recurring telecommunication platform.

In that case minimization of the cost and mass is expected coming from the resources sharing with the central computer, which can provide power conversion, clock and bus architecture. The secondary voltages used by the GNSS board are compatible with the output lines of the computer power module. The reference frequency can be derived from a common oscillator, compatible for a GNSS navigation function. More important, the communication with the Computer CPU occurs via a point to point communication avoiding complex routing.

A full data exchange with the avionic kernel can be implemented reducing the "distance" between the navigation sensor and the avionic (Figure II-8) Some receiver functionalities can be moved in the avionic kernel (Figure II-8) in order to realize a deeper synergy with the on-board navigation and control tasks in accordance to the previously discussed hybridization concept. Enhanced orbit determination performances are expected due to the possibility of using other information (control action, attitude information, spacecraft operative modes) and computer computational resources.

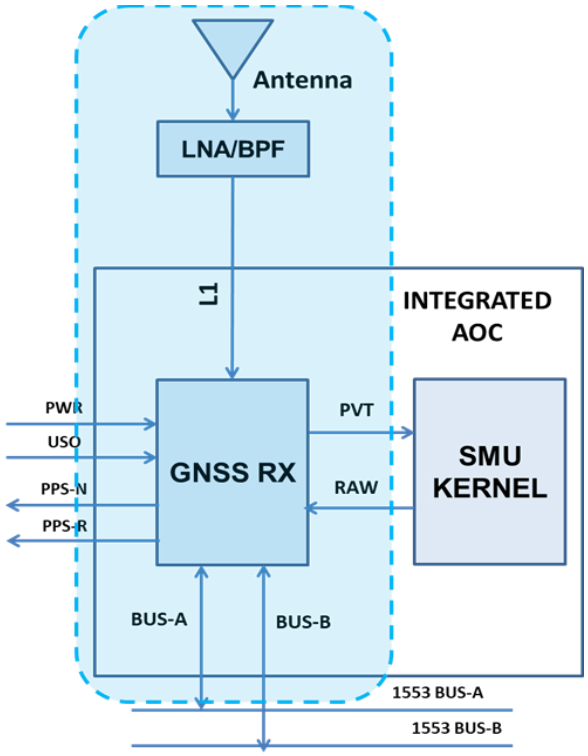

Figure II-8 Integrated Navigation Architecture concept with single chain receiver for small satellite application

Nevertheless, scaling integrated GNSS architecture (Figure II-8) [20] for small platform introduces some relevant navigation issues [7] due to power and reduced complexity constraints. Generally only single antenna, single frequency and single constellation configuration is available in accordance to a reduced number of channels. The performance is inevitably impacted and sensor outage can be more frequent. Using low cost, low complexity GNSS solution and the correspondent drawbacks are taken into account within V.4 . In this case receiver limitation are furthermore stressed by closed loop application where GNSS based navigation supports autonomous low thrust orbit acquisition during LEOP (II.2-A). The possibility to consider GNSS integrated in the avionic kernel will be taken into account by considering orbit navigation and control as a unique software function running on System Management Unit (SMU) CPU and capable to directly interface the receiver as well as all the AOC control modules.

II.2 MULTIPURPOSE EARTH ORBIT NAVIGATION SYSTEM (MEONS)

Multipurpose Earth Orbit Navigation System (MEONS) is the core study proposal for reusable and configurable orbit navigation functionality in different SSV scenarios. System architecture definition starts from the identification of its relevant design drivers. This section provides an analysis of different missions and avionics configurations that benefit of a generalized GNSS based orbit determination scheme in term of automation of critical on-board operations and platform performance. The assessment is mainly devoted to the derivation of the MEONS navigation requirements allowing defining its high level functional and mathematical model. The reviewed programs and studies provide also the background within addressing the specific study cases that will be object of CHAPTER V.

A. Legacy and next generation missions analysis for MEONS design drivers identification

Legacy Earth Observation platform and payload aiding

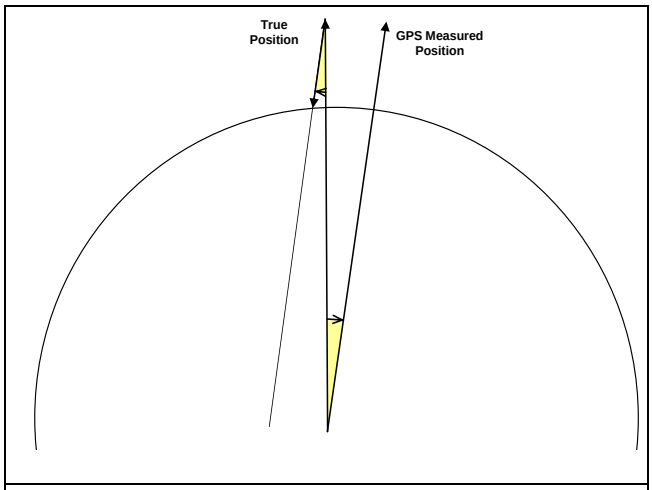

Figure II-9 Orbital error geometrical representation for pointing budget

LEO Earth Observation (EO) applications go from optical payloads exploitation to remote sensing by SAR [29]. Radio occultation and other Earth and space monitoring missions (i.e. reflectometry [30]) also rely on LEO platforms.
Considering such space missions, on board GNSS based orbit and time determination support all primary subsystems performances. The main contribution is to the Attitude and Orbit Control pointing budget. Actually, all stated applications need not only the fine knowledge of the inertial attitude, but also geolocation and tracking of targets located on Earth. The positioning error becomes a pointing accuracy contribution and its effect can be generally evaluated in accordance to simple geometrical schemes. Let us assume the local velocity reference frame defined by the following unit vectors:

$$\underline{u}_X = \frac{\underline{V}_{SC}}{\left|\underline{V}_{SC}\right|} \quad \underline{u}_Y = \frac{\underline{V}_{SC} \times \underline{P}_{SC}}{\left|\underline{V}_{SC} \times \underline{P}_{SC}\right|} \quad \underline{u}_Z = \underline{u}_X \times \underline{u}_Y \qquad (2.2)$$

The following error contribution can be experienced:

- Position Error outside the Orbit Plane induces Roll error (Figure II-9, Scheme 1)
- Velocity Error in the Orbit Plane induces Pitch error (Figure II-9, Scheme 2)
- Velocity Error outside the Orbit Plane induce Yaw error (Figure II-9, Scheme 2)
- Position Error in the Orbit Plane induces Pitch error (Figure II-9, Scheme 3)

For a Position and Velocity error of 10m and 0.01m/s contributions to the attitude performance can be evaluated for a typical LEO S/C as follow:

$$\varepsilon_{Roll} = \frac{\varepsilon_P}{|\underline{P}|} \Rightarrow \varepsilon_{ROLL} = \frac{10m}{6989374.549m} = 1.4307E^{-6}[rad]$$

$$\varepsilon_{Pitch} = \sqrt{\left(\frac{\varepsilon_V}{|\underline{V}|}\right)^2 + \left(\frac{\varepsilon_P}{|\underline{P}|}\right)^2} \Rightarrow 1.9557\text{E}^{-6}[\text{rad}] \qquad (2.3)$$

$$\varepsilon_{Yaw} = \frac{\varepsilon_V}{|\underline{V}|} \Rightarrow \quad \varepsilon_{Yaw} = \frac{0.01m/s}{7500\text{m/s}} = 1.33333\text{E}^{-6}[\text{rad}]$$

The AOC functionalities are also indirectly impacted with respect to attitude sensor processing: the relative position from astronomical objects (Sun, Moon) is necessary for sun sensor and magnetometer attitude algorithms (e.g. TRIAD) and definition of eclipses is used for power supply units and solar arrays management.

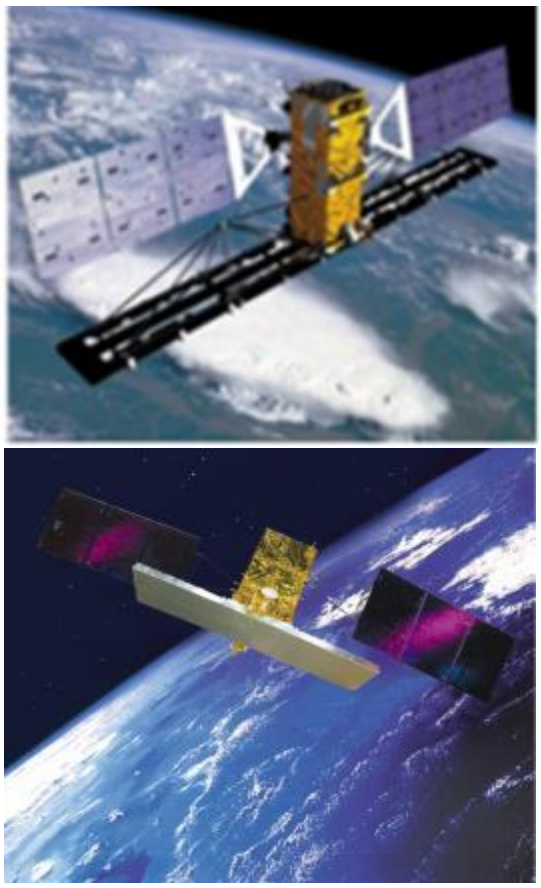

Figure II-10 RADARSAT and CSG EO spacecraft

The second ON contribution is directly related to Ground operations: the on-board determination system feeds position and time tag of telemetry packets during uplink and downlink activities. The orbit and time information are used to correct Time Of Arrival (TOA) for communication antenna signals (generally in S or X bands), which carries payload and platform auxiliary data. Attitude and orbit manoeuvres necessary for target pointing acquisition, trajectory correction or collision avoidance are generally planned on the basis of on-board position and time tags, when postfacto POD and flight dynamic products are not yet available. Indeed, the on-board OD generally collaborates with the ground software POD engines as it provides a "coarse" solution that speed up convergence to the final high accuracy solution. This work relies on LEO SAR applications, for which image processing strictly depends on ground station network POD. However, the on board solution can be used also to generate a "coarse" image product. A resume of the correlation between SAR Interferometric product quality and POD precision is provided in [29] . Referring to different SAR products, it is clarified that Digital Elevation Model (DEM) needs centimetre level accuracy, but monitoring temporal surface changes can be detected with accuracy close to the meter.

All TAS-I mission as COPERNICUS S1, RADARSAT and future programs (Figure II-10) as Cosmo 2nd Generation (CSG) include in the SAR texture geolocation ancillary data generated by the on board POD system. The term POD shall be intended in term of the on board availability of meter order accuracy solution compatible with fast imaging service and alarm detection. Actually, the sequential estimation kernel of first generation POD [4] integrates the single frequency SPS solution (i.e. 4 satellites in view) provided by the GNSS receiver with a high fidelity orbit propagation module. This thesis extend POD navigator to the MEONS one aiming to override its limits. This possibility has been demonstrated in the frame of COPERNICUS S1B Hardware in the Loop test case (V.2), where raw data combination and optimal filtering tuning are used to achieve a sub metric performance.

Ref. Mission	RADARSAT	COPERNICUS	COSMO2G Constellation
Mission Type	Earth Observation	Earth monitoring	Wide Coverage SAR Constellation
Orbit	a = 7176.136 Km e = 0.00052 i = 98.186°	a = 7070.981 Km e = 0.00118 i = 98.186°	a= 7006.433 Km e = 0.00108 i = 97.848°
Altitudes	798km	700km	628km
Propulsion	Chemical	Chemical	Chemical
Attitude /AOCS	Earth Pointing 3 axis stabilized	Earth Pointing 3 axis stabilized	Earth Pointing 3 axis stabilized
GNSS Rx prime sensor	Multi-frequency L1/L2	Multi-frequency L1/L2	Multi-frequency L1/L2

Table II-2 TAS-I EO-SAR mission embarking on-board property POD system

The enhancement of conventional on board LEO satellite orbit estimation function will enables in the future the possibility to provide an improved coarse class of SAR products (generally delivered to the civil user) without passing through the ground segment networking.

High orbit navigation and Earth Orbit Rising (EOR) for next generation MEO and GEO satellites

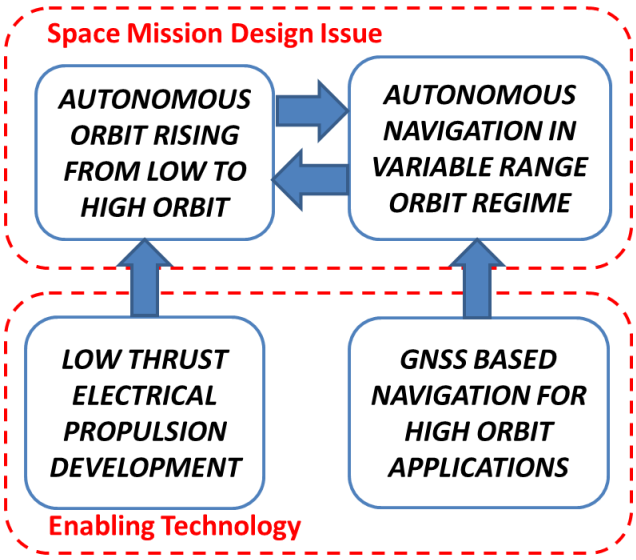

Figure II-11 Autonomous EOR orbit navigation system technology

In line with the current market trends requiring for improved satellite launch costs, it is envisaged in the next future, a high demand of satellite systems based on very efficient propulsion such that the propellant loaded on board of the satellite will be only a small percentage of the mass needed by present systems. Specifically, the envisaged approach for reducing the amount of embarked propellant is the introduction of electrical propulsion that, on one side provide very efficient functionality (the above mentioned reduced propellant consumption) but on the other side, it implies very low level of thrust when compared with chemical propulsion. This concept applies also for efficient steering of MEO and GEO satellites that acquires target position by using low thrust orbit transfers.

From operative point of view, it means that the not-operative phase for transferring the satellite from the launcher release orbit to the operative one (GEO or MEO) can be as long as 8-16 months. During the Earth Orbit Rising (EOR) the satellite transfers from the injection orbit (LEO or GTO) to the final orbit by means of the propulsion S/S and the orbit rising satellite regularly performs attitude manoeuvres during its transfers, to achieve the maximum efficiency concerning rising time or propellant consumption. During this phase, some operations are performed: the electric propulsion is continuously operated and thrust direction during transfer phase is always optimized on the basis of last available positioning. On-board orbit propagation can, in principle, enhance the satellite autonomy and decriticize some operations but nevertheless, this approach would anyhow require for periodic propagator parameters update (i.e. parameter uplink from ground and ranging activity for determining on ground the orbital data). Therefore, GNSS-based satellite navigation and on-board high orbit estimation constitute a good opportunity for enhancing the satellite autonomy and reducing the impacts of a long low-thrust orbit transfer phase (Figure II-11). This scenario, also defined as *Autonomous Low Thrust Earth Orbit Rising* [3], requires the

adoption of advanced navigation system architectures, dealing with a variable range of orbit regimes and GNSS critical visibility conditions. The integrated orbit estimation shall mandatory use GNSS raw measurements (see III.2), since it allows keeping estimation over the kinematic condition loss (satellite in view less than 4) and reduces sensitivity with respect to discontinuous variable number of satellites and high GDOP [31]. A deep synergy with the avionic subsystem shall be accomplished by integrating thrust and attitude auxiliary information, made available by the platform control, with measurements provided by a multi-antenna/multi-constellation receiver configuration. This tightly coupling can be considered a step toward the hybridization concept described in II.1-A because the GNSS navigation collaborates with platform avionics in order to override rising criticalities ([23],[32]).

TAS-I has investigated EOR topic in the frame of two main programs (Table II-4): the next generation platform for Galileo Second Generation (G2G, phase B1 contract on going [3]) and the next generation platform for TLC mission (NEOSAT).

Ref. Mission	Galileo 2nd Generation	GEO – NEOSAT
Mission Type	Navigation	Telecommunication
Final orbit type	LEO-MEO	GTO-GEO
Orbit	a= 29601 km i=56° e=0	a= 42164 km i=0° e=0
Transfer orbit	LEO-MEO LEO- GEO*	GTO-GEO LEO- GEO
Altitudes	1000-22200 km	250 - 35943 km
Propulsion	Electrical	Electrical/Chemical
Attitude during transfer	Variable (Roll steering)	Variable (Roll steering)
AOCS	3 axis stabilized	3 axis stabilized
GNSS Rx prime sensor	Multi-antenna/ Multi-constellation L1/E1	Multi-antenna/ Multi-constellation L1/E1

Table II-3 Navigation Galileo Second Generation and TLC NEOSAT EOR mission data

The GTO, classified as HEO, is the orbit commonly considered for the NEOSAT [20] GEO satellite injection, characterized by a very low perigee and high eccentricity. G2G LEO to MEO transfer relies on a circular spiralling orbit to reach the final (circular) orbit. This work focuses on the G2G satellite low thrust transfer [3]. The idea is to embark electric propulsion in order to enable in the near future efficient constellation updating operations without relying on the launcher upper stage. The multiple launches have been also considered as constellation deployment cost reduction factor. After a waiting period in the injection orbit in order to induce a separation of the orbit planes RAANs by means of the J2 natural drift, the semi-major axis is increased; inclination and eccentricity are adjusted to reach the final orbit in the requested time.

It shall be reminded here that, beyond EOR advantages, both MEO and GEO mission have some further motivation to fly a GNSS receiver and implement an on-board OD system [31]. First, the satellite will rely fully on electrical propulsion thrusters to perform the long lasting station keeping manoeuvres, once that target orbit is acquired. Indeed, the satellite position will be known better on-board than on ground and also in a continuous way, with improved efficiency of the station keeping manoeuvres. The orbit correction could be performed every day, which will remove the weekly full day of free drift, during which the spacecraft position is not controlled. Second, pointing accuracy of payloads antenna improves as for LEO satellite. For instance, the NEOSAT GEO does not use an Earth sensor but a star tracker and just the on-board estimated position to determine the Earth pointing angle. The same applies to MEO spacecraft, so the knowledge of the position has a direct impact on the pointing budget for high orbit satellites.

Autonomous orbit acquisition and agile satellite navigation

The EOR concept can be scaled to LEO case leading to general low thrust autonomous orbit control and

orbit acquisition functionality. The approach becomes attractive during Launch and Early Orbit Phase (LEOP) of all platforms equipped with electrical propulsion. After deployment, the spacecraft could autonomously perform low thrust manoeuvres in order to acquire its target operative orbit by compensating progressively the deviation from the reference trajectory due to launch injection errors. This solution is particularly attractive for small satellite considering complex scenarios as EO and TLC applications based on Low Earth Orbit constellations (Cygnss, Oneweb, Leosat) and single launch multiple satellite deployment. The aim is to perform the Autonomous Acquisition Manoeuvre (AAM) bringing the spacecraft from the initial dispersed position to the target one within a predefined time window and with reduced propellant consumption. From a navigation point of view the needs are similar to what described for EOR, but high dynamic and reduced platform resources shall be considered (single antenna, low cost GNSS equipment). ESA studies as [33], demonstrate the interest for GNSS based autonomous orbit operation. This work relies in V.4 on the possibility of a deeper integration of MEONS solution with AAM optimal control architecture. Similarly to EOR case, MEONS is used to tolerate dynamic stressing conditions, antenna pointing wide excursion and sensor measurements outages. This solution could be reused in the future also to support agile satellite navigation. This term generally indicates LEO platforms that implement actuators capable to inject rapid attitude variations, enhancing optical and SAR payload targeting. In this case the on board estimation shall be capable to keep position continuity against loss of lock in order to implement "hot restart" of the receiver, i.e. very fast signal reacquisition.

Formation flying and network application

Spacecraft formation flying has been considered a technology enabling advanced scientific targets and new space mission concepts. Several studies have already suggested and employed this approach for new applications in observation of the universe [34] , Earth gravity field mapping [35] and Earth remote sensing [36].

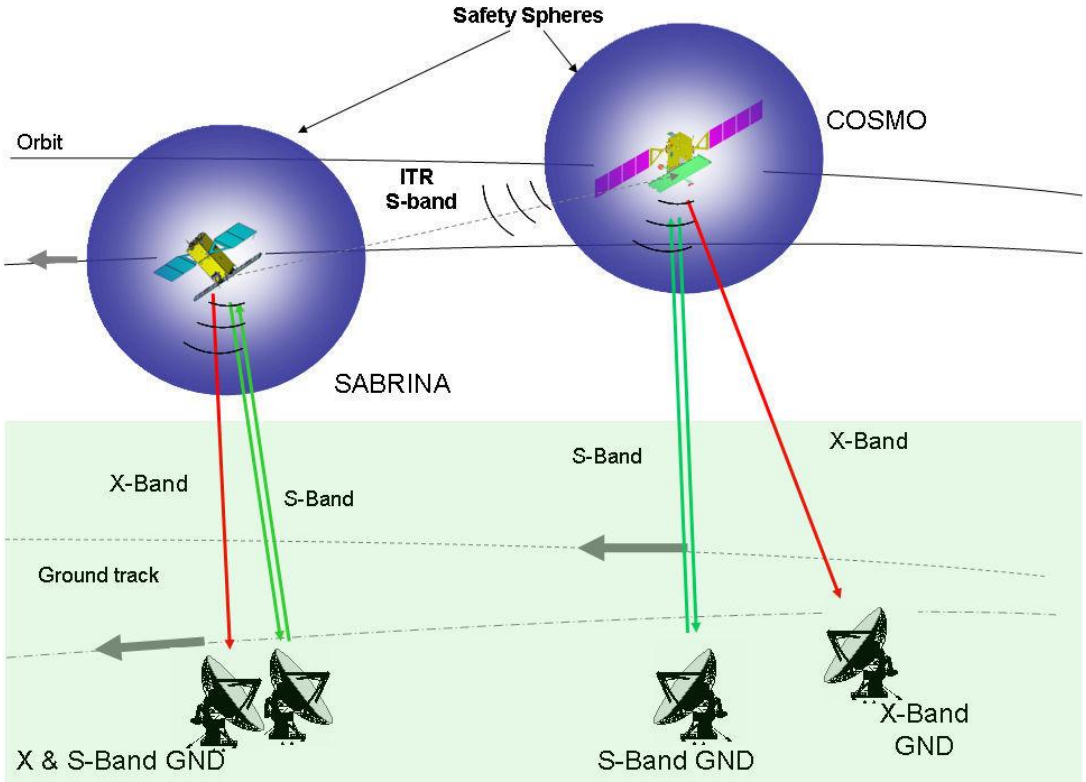

Figure II-12 SABRINA Mission Tandem Formation [41]

Indeed, exploiting a number of co-flying platforms and distributing payload and system functionalities among them allows realizing relative orbital geometries demanded by specific scientific objectives. Simultaneously, it improves the system robustness and flexibility, too. Formation flying poses important

technology challenges with particular concern to autonomous navigation. Specifically many applications enforce the determination of the satellite separations with accuracy at the centimetre level. For determining the relative position among co-flying platforms differential GNSS techniques are preferred with respect to laser interferometry when the platforms operate at a distance higher than e few hundred meters.

Ref. Mission	Cosmo Skymed	BISSAT
Mission Type	Master	Deputy
Final orbit type	EO SAR	Bistatic Companion SAR
Orbit	a=7002.294 e=0.0009648 i=97.878° ω=72.742° Ω=130.110° Ni=137.626°	a=7002.294 e=0.0009648 i=97.878° ω=72.742° Ω=131.790° Ni=137.286
Formation	Reference Orbi	Relative Pendulum
Propulsion	Electrical/Chemical	Electrical/Chemical
Operative Attitude	Earth Pointing (Tx)	Earth Pointing (Rx)
AOCS	3 axis stabilized	3 axis stabilized
GNSS Rx pr me sensor	Multi-frequency L1/L2	Multi-frequency L1/L2

Table II-4 SABRINA formation flying mission data for Cosmo Master Spacecraft and BISSAT Companion

Several studies ([37],[38]) have shown that by processing Single or Double Difference (SD/DD) carrier-phase differential measurements (CDGNSS) it is possible to determine the satellite relative position with the requested precision. Nevertheless, the formation geometry control problem introduces several complications due to on board and real time constraints. The well suited solution is filtering [39] the GNSS differential data in order to provide, without loss of continuity, the estimation of the relative positioning between the elements of the formation. The main issue of the CDGNSS measurement filtering is the determination of the ambiguities [40]. They are the unknown number of integer cycles that must be estimated in order to extract from the measured fractional part the entire ranging information.

When the integer ambiguities are identified, a very high accuracy estimation of relative positioning can be achieved from double difference equations (see III.2-B). The dynamic model of formation shall provide high accuracy propagation compatible with phase measurement resolution and sensor outages conditions. Moreover the hosting receivers' observable shall be shared via a proper communication link in order to perform differential combination and ambiguity bias intermittent tracking. This work specifically deals with follow up of SABRINA (System for Advanced Bistatic and Radar INterferometric Application [41]), that was a phase 0/A mission studied by University of Naples "Federico II", TAS-I and the Italian Space Agency. It consists in a BISSAT (Bistatic and Interferometric Sar SATellite) satellite flying in formation with one of the satellite of COSMO/SkyMed constellation.

Application	Product	AT min baseline
Marine Studies	Current monitoring	28 m
Flood	Flood velocity map	7 m
Flood	Flood extension map	70 m
Traffic	Traffic monitoring	16 m
Fisheries	Ship detecting	36 m
Fisheries	(slow) ship monitoring	400 m

Table II-5 Application and product for ATI techniques

The orbital planning and the formation flying control will allow to realize different observation geometries characterized by inter satellites distances variable from hundreds meters to some hundreds of kilometres. In a so vast scenario, a wide range of bistatic techniques are applicable and testable, ranging from cross and along track interferometry to multichannel techniques and large baseline bistatic observations. In Table II-5 the applications achievable by performing Along Track Interferometry (ATI)

are shown. The BISSAT distance from the COSMO/SkyMed Satellite needs to be precisely known. In this thesis the observation of the formation state is just based on a proper customization of the MEONS for implementing a CDGNSS architecture, which can be used to determine in real time and with high accuracy the relative position of satellites.

B. MEONS requirements and functions definition

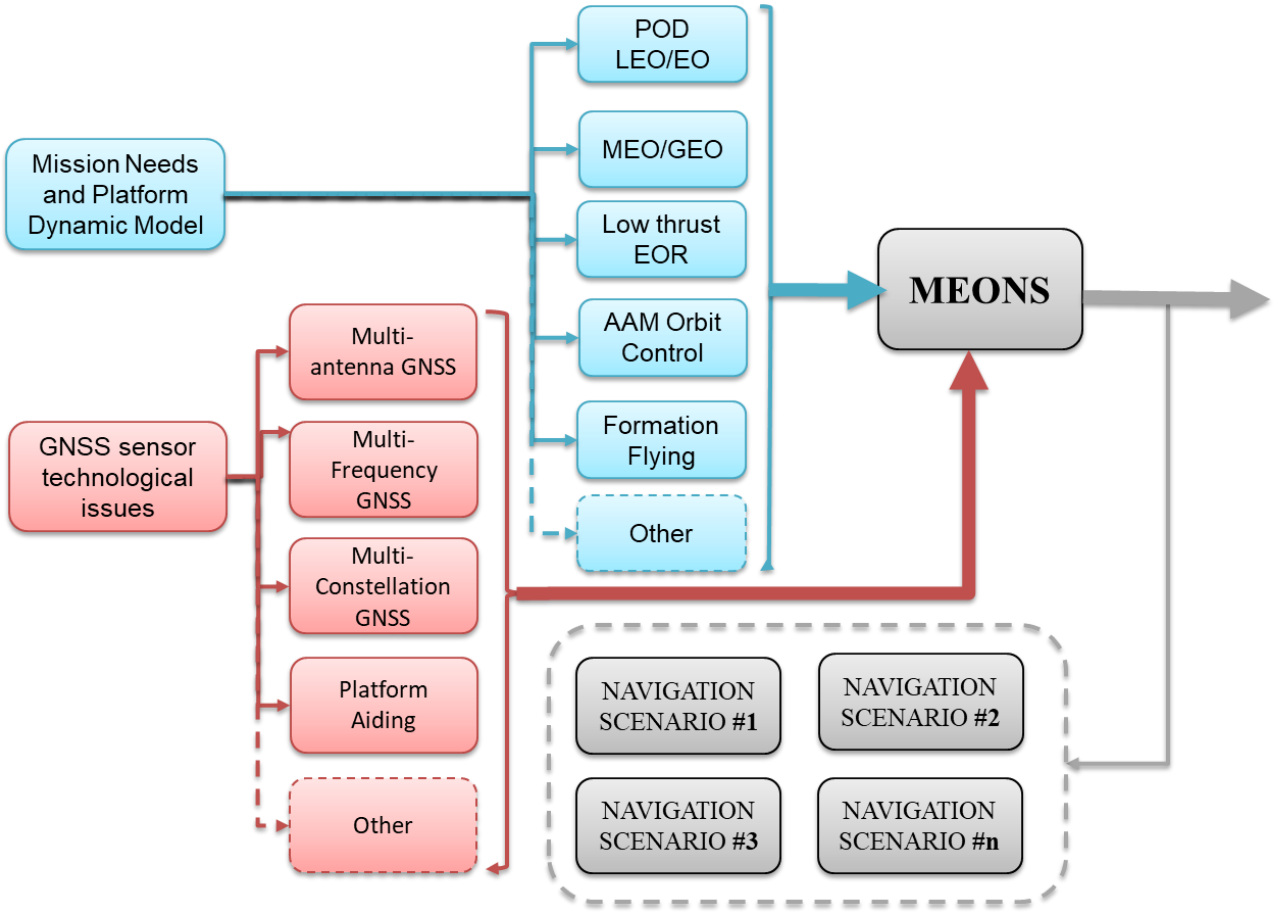

Figure II-13 MEONS design process and application framework

Analysis of the GNSS receiver configurations and missions' operative constraints are used to define the MEONS navigation requirements listed in Table II-6. For each requirement the correspondent enabled capability is reported in Table II-7.

High Level Requirements	
1.	Perform Multispacecraft high performance propagation for different orbit regime
2.	Provide configurable dynamic system and upgradable structure in order to add different orbit perturbation modules and control actions
3.	Multiple modes propagation model and switching solution with dynamic state rearrangement
4.	Possibility to handle tightly coupled approach (i.e. GNSS raw data processing) with intermittent and combined measurements
5.	Configurable and upgradable sensor measurement processing for compatibility with Multi-constellation/ Multi-antenna / Multi-frequency GNSS architectures
6.	Multiple model / Multisensor compatibility
7.	Configurable datapool and interfaces for platform auxiliary data integration, external input acquisition and parameter control (e.g. thruster action and spacecraft physical properties)
8.	Configurable Sequential Estimation Framework implementing modern datafusion and filtering techniques

9.	Configurable Optimal Filtering Kernel handling: a. Nonlinear filtering b. Variable dimension state vector c. Robust error bound and consistency properties d. Model parametric uncertainty, error sources calibration, optimal tuning
10.	Enhanced modularity of functional and mathematical model
11.	Handling of numerical and computational burden optimization
12.	External interfaces management wrt all subsystems that relies on navigation task

Table II-6 MEONS requirement

Benefits	
1.	Compatibility with LEO,MEO,GEO and FF
2.	Compatibility with both extended orbit on board POD and autonomous orbit control
3.	Handling changes in the operative mode, e.g. from controlled (thrust on) to operative (POD)
4.	Enhanced on board POD for fine geolocation in LEO and robustness in high orbit wrt critical visibility conditions (SVs<4)
5.	Handle additional frequencies, constellations and antennas together with their observable combinations
6.	Readiness for future hybridization (inertial and attitude sensor)
7.	Deep synergy with platform orbit and attitude control task with possibility of manipulating a list of operating parameters
8.	Integrate dynamic model and observable in a recursive estimation process that can be customized on the target estimation model
9.	a. Long term outages handling and improved convergence with respect to lost in space conditions b. Dynamic rearrangement and switching models (external control action and intermittent measurement biases, i.e. ambiguities) c. stable performance reacquisition and performance monitoring for autonomous decision making d. control of dynamic model approximation and representative process and measurement error weighting
10.	Scalability and reusability of the orbit function among different applications
11.	Provide software architecture compatible with future real time implementation issues.
12.	Possibility to integrate the system with the AOC, Payload and Data Handling subsystems

Table II-7 MEONS Features

MEONS project corresponds to the realization of a general purpose estimator integrating several GNSS observables with the target mission orbit dynamic in order to perform on-board orbit navigation (Figure II-13).

II.3 MEONS SEQUENTIAL ESTIMATION ARCHITECTURE

Before defining the MEONS detailed architecture, it is worthy to clarify the theoretical background on which it is based. Even considering the possibility to include in the future also deterministic methods [42], the selected operative framework is the *Recursive Bayesian Estimation* and the filtering techniques based on *Stochastic State Space Models*. Widely used for orbit determination, this theory includes several techniques handling non-Gaussian as well as nonlinear estimation problems [43].

This thesis restricts the application field to the (General) Gaussian Nonlinear Kalman Filtering schemes (see IV.1), that following [44], allows incorporating Model Based and Numerical Methods, which approximate the general Bayesian problem. The aim is controlling computational burden and complexity in view of real time implementation, postponing to future work refinement that can deal with the general

case.

Beyond the specific adopted method, the stated assumption allows to derive the two fundamental system architecture cornerstones [43]:

- The Generalized Stochastic State Space Model
- The Recursive Filtering and Prediction-Correction Structure

These theoretical fundamentals are hereafter analysed and then projected in the MEONS high level mathematical and functional model. The achieved representation is very general, allowing extending and reusing the same solution also for next generation navigation system developments. Actually, it can be considered compatible with higher complexity recursive methods (Monte Carlo Solutions, Particle filtering as well as deterministic convex optimization) that could become of interest in accordance to specific needs and spaceborne boards improvements.

A. Recursive Bayesian estimation and state space optimal filtering

For an historical perspective on Bayesian estimation history [45] can be referred. This section aim at deriving relevant tools and schemes used to solve optimal sequential filtering problem.

Filtering identify an operation that involves the extraction of information about a quantity of interest at time t by using data measured up to and including t. Together with prediction and smoothing, which can be seen as the a-priory and a-posterior counterpart, filtering can be addressed as an Inversion Problem [44] aiming of estimating the hidden states $\mathbf{x}_{[0:T]} = (\mathbf{x}_0, ..., \mathbf{x}_T)$ from the observed measurement set $\mathbf{y}_{[0:T]} = (\mathbf{y}_0, ..., \mathbf{y}_T)$. The estimation problem is here handled by using model based methods [46]. The systems under study are dynamic, implying that their mathematical model will mostly be of dynamic nature as well. More specifically, the models are primarily constituted by stochastic differential (or difference) equations. The most commonly used representation is the nonlinear state-space structure and various special cases thereof.

Let us consider the following generic stochastic dynamic system expressed in state-space form [46]:

$$S: \begin{cases} \dot{\mathbf{x}} = \mathbf{f}(\mathbf{x}, \mathbf{p}, \mathbf{u}, \mathbf{w}, t) \\ \mathbf{y} = \mathbf{h}(\mathbf{x}, \mathbf{p}, \mathbf{u}, \mathbf{v}, t) \end{cases} \tag{2.4}$$

where $\mathbf{x}$ denotes the state variable, $\mathbf{u}$ denotes the known input signal, $\mathbf{p}$ denotes the static (or quasi-static) parameters, $\mathbf{y}$ denotes the measurements, $\mathbf{w}$ and $\mathbf{v}$ denote the process and measurement noise, respectively. The system model, first of eq.(2.4), describes the evolution of the state variables over time, while the measurement model, second of eq.(2.4), explains how the measurements relate to the state variables. The dynamic model must describe the essential properties of the underlying system, but it must also be simple enough to make sure that it can be used to devise an efficient estimation algorithm. The mathematical representation of system noises has the same relevance, so they shall be properly modelled in accordance to expected physical uncertainty and the introduced residual approximation. By using proper integration map (see III.1) the problem can be transformed from the continuous-time domain to the canonical discrete-time form:

$$S_k: \begin{cases} \mathbf{X}_{k+1} = \mathbf{f}_d(\mathbf{X}_{k+1}, \mathbf{w}_k, k) \\ \mathbf{Y}_k = \mathbf{h}_d(\mathbf{X}_{k+1}, \mathbf{v}_k, k) \\ \mathbf{X}_k = \{\mathbf{x}_k, \mathbf{p}_k, \mathbf{u}_k\} \end{cases} \qquad \mathbf{w}_k, \mathbf{v}_k: \begin{cases} \mathbf{E}\left[\mathbf{w}_k, \mathbf{w}_k^T\right] = \mathbf{Q}_k \boldsymbol{\delta}_{i,j} \quad \mathbf{E}\left[\mathbf{v}_k, \mathbf{v}_k^T\right] = \mathbf{R}_k \boldsymbol{\delta}_{i,j} \\ \mathbf{E}\left[\mathbf{w}_k, \mathbf{v}_k^T\right] = \mathbf{0} \quad \mathbf{E}\left[\mathbf{x}_0, \mathbf{x}_0^T\right] = \mathbf{P}_0 \end{cases} \tag{2.5}$$

Specifically the stochastic nature of sequences $\mathbf{w}_k$, $\mathbf{v}_k$, generally mapped in discrete time domain as white

random noises with unknown statistics ([47],[48]), leads to a probabilistic state space model that can be furthermore interpreted as sequence of conditional probability distributions:

$$P:\begin{cases}\mathbf{X}_{k+1} \sim p(\mathbf{X}_{k+1} \mid \mathbf{X}_{1:k}, \mathbf{Y}_{1:k}) \\ \mathbf{Y}_k \sim p(\mathbf{Y}_k \mid \mathbf{X}_{1:k}, \mathbf{Y}_{1:k-1})\end{cases} \tag{2.6}$$

In this representation dynamic model describe not only the single realization of the process, but also the stochastic dynamic in term of state transition probability function $p(\mathbf{X}_{k+1} \mid \mathbf{X}_{1:k})$. In the same manner, measurement model allows to define a probability function $p(\mathbf{Y}_k \mid \mathbf{X}_{1:k}, \mathbf{Y}_{1:k-1})$ providing the distribution of measurements given the system state and measurement history. It is clear that the filtering problem objective is the derivation of the posterior density $p(\mathbf{X}_{0:T} \mid \mathbf{Y}_{0:T})$ [44], i.e. the distribution of all the states given the observations up to time T. The Statistical Inverse Problem becomes in essence estimating the posterior density given initial density $p(\mathbf{X}_{0:T})$, transition density $p(\mathbf{X}_{k+1} \mid \mathbf{X}_{1:k})$, and the so called likelihood $p(\mathbf{Y}_{1:T} \mid \mathbf{X}_{0:T})$ of the measurement wrt the states. In Bayesian Statistics [45], such inverse problem can be once more defined by a straightforward application of Bayes' Rule [44]:

$$\begin{aligned} p(\mathbf{X}_{0:T} \mid \mathbf{Y}_{1:T}) &= \frac{p(\mathbf{Y}_{1:T} \mid \mathbf{X}_{0:T})\, p(\mathbf{X}_{0:T})}{p(\mathbf{Y}_{1:T})} \\ p(\mathbf{Y}_{1:T}) &= \int p(\mathbf{Y}_{1:T} \mid \mathbf{X}_{0:T})\, p(\mathbf{X}_{0:T})\, d\mathbf{X}_{0:T} \end{aligned} \tag{2.7}$$

Such rule provides a fundamental relationship that links all relevant probability distributions, considering the proper normalization constant $p(\mathbf{Y}_{1:T})$ of the target a posteriori probability $p(\mathbf{X}_{0:T} \mid \mathbf{Y}_{1:T})$ distribution. Unfortunately, this full posterior formulation has the serious disadvantage that each time it is obtained a new measurement, the full posterior distribution have to be recomputed. Dimensionality increases each step making it prohibitive for dynamic filtering. However, Bayesian approach can solve the estimation issue in a recursive manner. Two additional assumptions shall be introduced in the eq.(2.6) :

- Markov property: this property states that $\mathbf{X}_k$ is a Markov Sequence if given $\mathbf{X}_{k-1}$ is independent of anything that happens before the time step k-1 and the past is independent of the future given the present:

$$\begin{aligned} p(\mathbf{X}_k \mid \mathbf{X}_{1:k-1}, \mathbf{Y}_{1:k-1}) &= p(\mathbf{X}_k \mid \mathbf{X}_{k-1}) \\ p(\mathbf{X}_{k-1} \mid \mathbf{X}_{k:T}, \mathbf{Y}_{k:T}) &= p(\mathbf{X}_{k-1} \mid \mathbf{X}_k) \end{aligned} \tag{2.8}$$

- Conditional independence of measurements: this property states that the current measurement $\mathbf{Y}_k$ given the current state is conditionally independent of the measurement and state histories.

$$p(\mathbf{Y}_k \mid \mathbf{X}_{1:k}, \mathbf{Y}_{1:k-1}) = p(\mathbf{X}_{k-1} \mid \mathbf{X}_k) \tag{2.9}$$

Hypotheses application allows to recursively compute the posterior distribution $p(\mathbf{X}_k \mid \mathbf{Y}_{1:k})$ of the state $\mathbf{X}_k$ at each time step k given the history of the measurement up to the time step k. The fundamental equations of *Bayesian filtering* can be thus derived (for a rigorous demonstration please refers to [44]) as follow:

- Initialization

The recursion starts from the prior distribution

$$p(\mathbf{Y}_k \mid \mathbf{X}_{1:k}, \mathbf{Y}_{1:k-1}) = p(\mathbf{X}_{k-1} \mid \mathbf{X}_k)$$

- Prediction Step

The predictive distribution of the state $\mathbf{X}_k$ at the time step k, given the dynamic model, can be computed by the Chapman–Kolmogorov equation:

$$p(\mathbf{X}_k \mid \mathbf{Y}_{1:k-1}) = \int p(\mathbf{X}_{k-1} \mid \mathbf{X}_k)\, p(\mathbf{X}_{1:k} \mid \mathbf{Y}_{1:k-1}) d\mathbf{X}_{k-1} \tag{2.10}$$

- Update Step (Bayes)

Given the measurement $\mathbf{Y}_k$ at time step k the posterior distribution of the state xk can be computed by Bayes' rule

$$\begin{aligned} p(\mathbf{X}_k \mid \mathbf{Y}_{1:k}) &= \frac{1}{Z_k}\, p(\mathbf{Y}_k \mid \mathbf{X}_k)\, p(\mathbf{X}_k \mid \mathbf{Y}_{1:k-1}) \\ Z_k &= \int p(\mathbf{Y}_k \mid \mathbf{X}_k)\, p(\mathbf{X}_k \mid \mathbf{Y}_{1:k-1}) d\mathbf{X}_k \end{aligned} \tag{2.11}$$

where Z_k is the normalization constant.

It shall be clarified that Bayesian filtering is optimal in a sense that it seeks the posterior distribution which integrates and uses all of available information expressed by probabilities. However, all practical application extracts an estimated system state $\hat{\mathbf{X}}$ from the available distribution on the basis of specific optimal criteria. MMSE and MAP, whose properties and characteristics can be found in ([42],[45]), are the most used ones, allowing also to derive the Kalman filtering declinations used in this work [44].

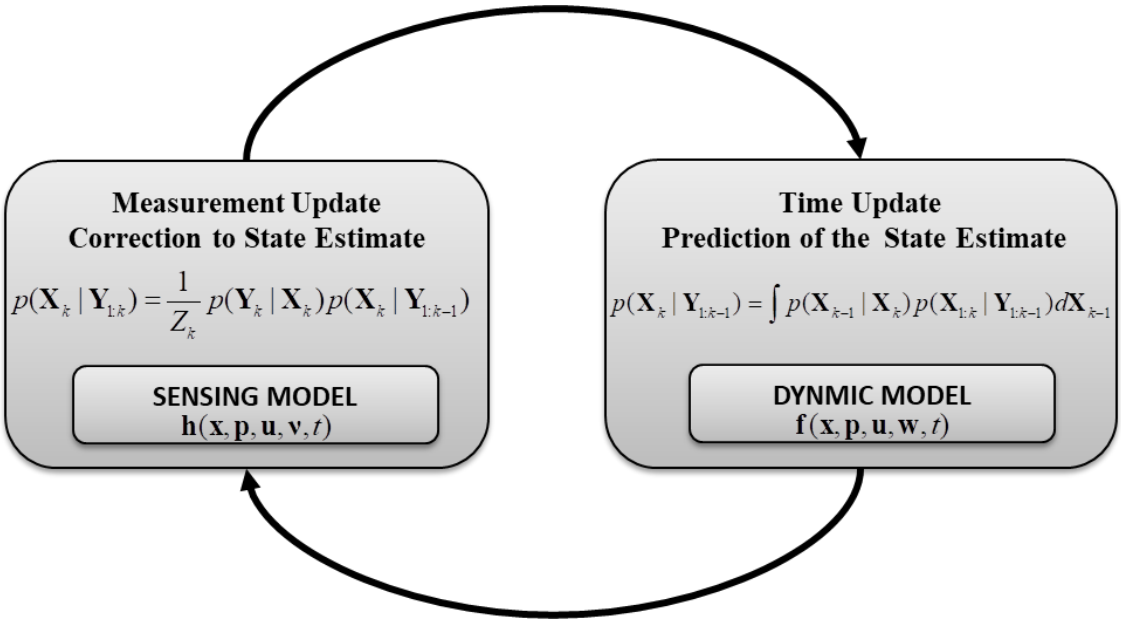

Figure II-14 Prediction-Correction Structure of Recursive Bayesian Estimation and Sequential Filtering

These optimal indexes usually make use of the expectation operator:

$$E[f(\mathbf{X})] = \int f(\mathbf{X}) p(\mathbf{X}) d\mathbf{X}_k \tag{2.12}$$

whose significance depends on the chosen penalty function $f(\mathbf{X})$. Expectation and derived moment integrals [44] have a fundamental part in the definition of specific implementation of sequential filtering methods. Several approaches (i.e. the Kalman Filtering Class) propagate and compute distribution via their moments. Several implementations can be found in accordance to different model and numerical approximations of the moment integrals computation. This issue will be fully addressed in IV.1.

The main result of the described framework is the general *prediction/correction structure* shown in Figure II-14. It shall be noted that for model based approaches, if the mathematical representation does not provide an adequate physical system description, it is impossible to derive an appropriate estimation algorithm. The MEONS navigation system shall reflect Figure II-14 scheme allowing also designing the sensing model and the spacecraft dynamic with respect to the specific application.

B. MEONS navigation system definition

The MEONS architecture proposal can be defined. A complete block diagram description is shown in Figure II-15. The core of the system involves three main parts:

- *Generic Propagator Module ,* $\mathbf{f}(\mathbf{x},\mathbf{p},\mathbf{u},\mathbf{w},t)$

  The propagation module is equipped with a high performance orbit prediction model capable to provide gravitational (gravity, non-spherical gravity, third body) and optionally selectable non-gravitational forces to cope with "sensor-less" conditions. Different configuration of the target estimation state vector $\mathbf{X}_{prop}$, whose arrangement depends on the current platform operative mode (e.g. manoeuvres) and activated sensors shall be supported. The propagator module is designed as an augmented system handling different dynamic modules $\dot{\mathbf{X}}_{prop}$, external information $\mathbf{U}_{prop}$ (e.g. attitude and thrust provided by the platform control) as well as internal structural parameters (spacecraft physical and measurement biases). This block is the engine of MEONS as it continuously updates its internal state until the next estimation reset. Actually, the state propagated by using dynamic model $\mathbf{f}(\mathbf{x},\mathbf{p},\mathbf{u},\mathbf{w},t)$ feeds the observation and estimation tasks that basically return back the estimated solution in accordance to sequential estimation update step. Considering the vectorial nature of the target navigation variable set, the state of propagator shall be intended as the superimposition of tree contributions:

$$\mathbf{X}_{prop} = \mathrm{K}_{prop}\mathbf{X}_{prop} + \mathrm{K}_{est}\hat{\mathbf{X}} + \mathrm{K}_{ext}\mathbf{X}_{ext} \tag{2.13}$$

  where $\mathbf{X}_{prop}, \hat{\mathbf{X}}, \hat{\mathbf{X}}_{ext}$ indicate respectively the propagated, estimated and forced external state. The last one is a useful functionality to reset internal propagation by overwriting it by using more accurate external information. $\mathrm{K}_{prop}, \mathrm{K}_{est}, \mathrm{K}_{ext}$ represent the proper projection matrices allowing combining the propagated state with validated estimation component or externally forced data (eq.(2.13)).

- *Generic Observer Module* $\mathbf{h}(\mathbf{x},\mathbf{p},\mathbf{u},\mathbf{v},t)$

  The observer is in charge to manage GNSS receiver data implementing the general purpose capability of processing different kinds as well as different combinations of primitive measurements.

External data (i.e. SVs ephemeris for GNSS case) are used into observables reconstruction pattern modules **Y** in order to propagate the image of state in the measurement space **Z** by using the observation model.

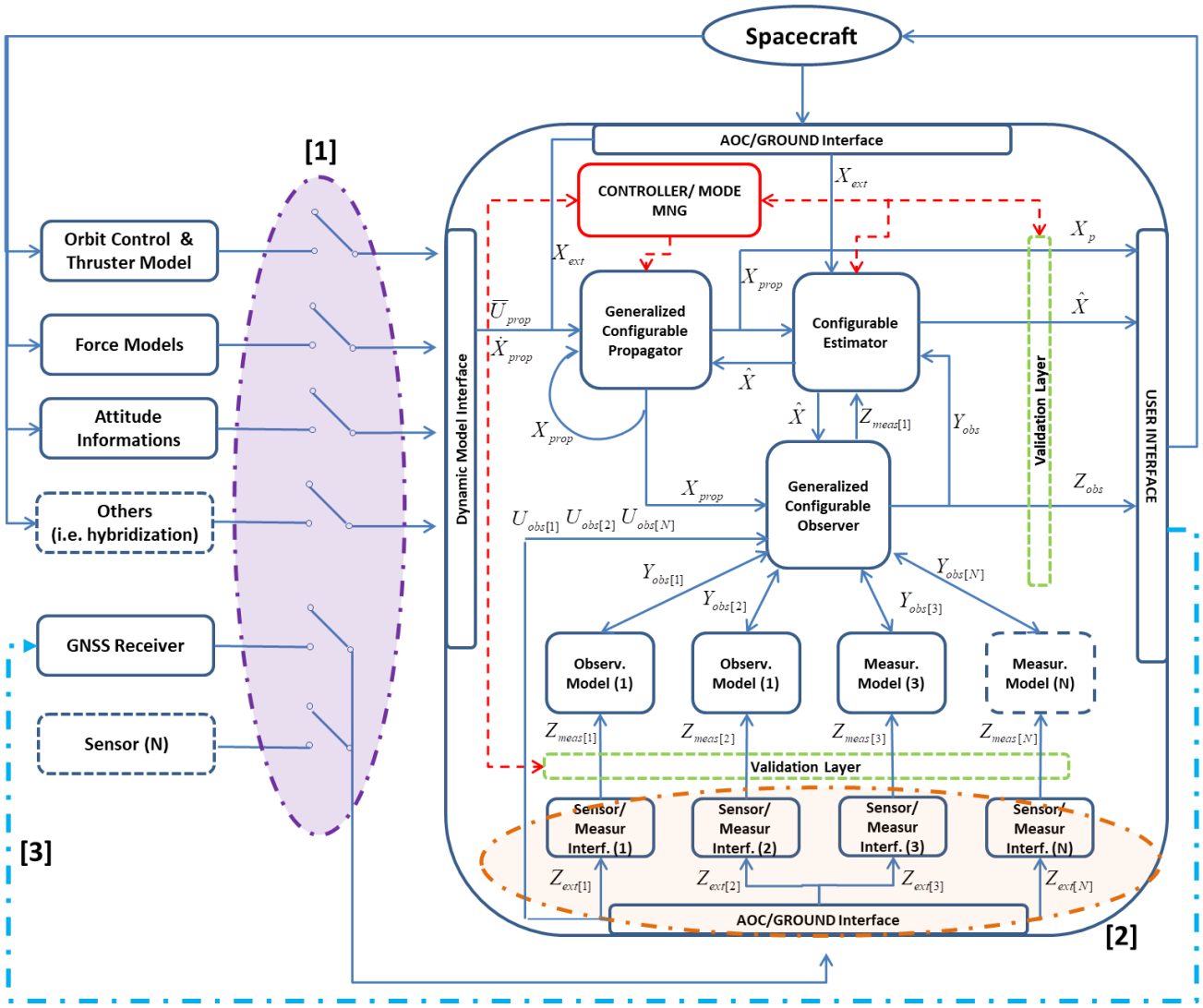

Figure II-15 MEONS architecture block diagram

The module shall be fully scalable wrt different measurement interfaces in order to integrate multi-frequency, multi-constellation and multi-antenna configurations. The functionality expressed by eq.(2.13) is extended to the observable images vectorial space. In this way, the measurement model fed by propagator can be continuously updated also when estimation is disabled. This possibility is very important for future implementation of a data validation layer (Figure II-15) by evaluating consistency of acquired measurements with respect to propagated one (i.e. pseudorange or ephemeris validity checks [49]).

- *Configurable Estimation Kernel,* $\hat{\mathbf{X}}, p(\mathbf{X} \mid \mathbf{Y}_{1:T})$

The configurable estimator integrates in the state space optimal filtering sense all the available information. The complete augmented state vector propagation is exploited for the prediction phase of the estimation process, while observer data are used for the correction one. In this case configurability of the estimator block relies not only on the possibility to select estimation algorithm on the basis of the best trade-off between accuracy and computational burden, but also to integrate a wide class of filtering solutions capable to cope with peculiarities of the specific state space model. It

shall be noted that external data can be used to supersede or correct the process also for the estimation block. $\hat{\mathbf{X}}_{ext}$ and $\mathbf{U}_{est}$. This feature relies to state and input variables used to adjust or reinitialize filter tuning parameters (i.e. process and measurement covariance, see IV.1-E).

The three blocks are managed by a specific MEONS controller function that drives different setting and run time reconfiguration taking into account results of the validation layers.

The system shall include all Figure II-15 interfaces allowing the communication with AOC control modules, Ground Data Aiding and final user output. Actually, the architecture reveals three fundamental peculiarities:

- [1] Possibility to guarantee different but sufficient performances from full optimal data fusion to high performance orbit prediction (sensor-less) with respect to long term propagation period and manoeuvres.

- [2] Possibility to process different GNSS observables in accordance to different platform setting , missions and hardware resources, availability of other sensors

- [3] Possibility to implement a deep synergy with the receiver by feedback/feedforward of platform auxiliary data. For instance, position, attitude and Doppler estimate can be used to eventually initialize receiver and update tracking list for fast performance reacquisition of GNSS SVs.

CHAPTER III

GENERALIZED STATE SPACE MODEL FOR ORBIT NAVIGATION

III.1 PROPAGATION MATHEMATICAL MODEL

This section addresses mathematical and functional architecture of MEONS Generic Propagator Module. Referring to scheme in Figure II-15, this block is in charge of integrating the satellite dynamical system equations and performing state prediction in order to support the sequential estimation kernel. In spite of the simplicity of the task, at least from a theoretical point of view, the module design crosses a wide range of issues going from the implementation of a flexible and augmentable state space structure to the definition of the selectable orbit propagation physical models. The Generic Propagator can work as an independent tool providing precise orbit propagation, so its kernel is used in this section to develop some sensitivity criteria for POD dynamic model and preliminary analyses of the orbit determination scheme.

A. Dynamic and state transition matrix combined integration for variational model update

The most used approach for an Earth Orbit propagation is the Cowell's method [50]. It involves the direct numerical integration of equations of motion with respect to a geocentric inertial reference frame taking into account the Earth central gravity and the sum of all gravitational and non-gravitational perturbation effects:

$$\ddot{\mathbf{r}} = -\frac{\mu_{\oplus}}{r^3}\mathbf{r} + \mathbf{a}_{Pert}(\mathbf{r},\dot{\mathbf{r}}) \qquad \mathbf{a}_{Pert} = \mathbf{a}_G(\mathbf{r},\dot{\mathbf{r}}) + \mathbf{a}_{NG}(\mathbf{r},\dot{\mathbf{r}}) \tag{3.1}$$

where $\mathbf{r}$ is satellite position, r is the Euclidean norm of $\mathbf{r}$, μ is the Earth standard gravitational parameter, the subscripts *G* and *NG* refer to gravitational and non-gravitational perturbations, respectively. When the propagation task is integrated within a navigation system, flexibility needs further improvements. As for reference generalized OD approaches ([1],[2]) an extended state vector $\mathbf{X}$ has to be considered to include any quantities directly affecting the motion of the satellite. These contributions rely to:

- primary states $\mathbf{x}$, representing the target dynamic system variables to be computed (e.g. position, velocity and time)
- auxiliary states $\mathbf{x}_{aux}$ (e.g. attitude, angular velocity, current mass, etc.) that are generally provided as external data. They can be promoted to primary ones in order to propagate information in case of loss of external aiding
- external inputs $\mathbf{u}(t)$ (e.g. manoeuvre activation and thrust data) representing control actions and S/C commands (e.g. operative mode transitions) influencing propagation task
- dynamic model parameters $\mathbf{p}$ (e.g. drag and solar radiation pressure coefficients, thruster errors, unknown stochastic effects etc.) that represent physical properties or model processes slowly varying ($\dot{\mathbf{p}} \cong 0$) with respect to the reference dynamic

This extended system dynamic can be mathematically represented via a standard Ordinary Differential Equation problem (ODE) [51], so the final generalized state space nonlinear model can be expressed by the following set of differential equations:

$$\begin{cases} \dot{\mathbf{X}} = \mathbf{F}(\mathbf{X}) = \mathbf{F}(\mathbf{x}(t), \mathbf{p}, \mathbf{u}, t) \\ \mathbf{X}_0 = \{\mathbf{x}(t_0), \mathbf{u}(t_0), \mathbf{p}, t_0\} \end{cases} = \begin{cases} \dot{\mathbf{x}} = f(\mathbf{x}, \mathbf{p}, \mathbf{u}, t) \rightarrow \mathbf{x}(t) = \{\mathbf{x}(t), \mathbf{x}_{aux}(t)\} \\ \dot{\mathbf{u}} = z(\mathbf{u}, t) \rightarrow \mathbf{u} = \mathbf{u}(t) \\ \dot{\mathbf{p}} = k(\mathbf{p}, t) \rightarrow \dot{\mathbf{p}} \cong 0 \end{cases} \quad (3.2)$$

In eq.(3.2), $\mathbf{F}(\mathbf{X})$ represents the system model as direct function of the extended state vector $\mathbf{X}$, also known as autonomous form [52]. The state trajectory satisfying eq.(3.2) can be expressed in standard integral form as follow:

$$\mathbf{x}(t) = \mathbf{x}(t_0) + \int_{t_0}^{t} \mathbf{f}(\mathbf{x}(\tau), \mathbf{p}, \mathbf{u}(\tau), \tau) \qquad \mathbf{u}(t) = \mathbf{u}(t_0) + \int_{t_0}^{t} \mathbf{z}(\mathbf{u}(\tau), \tau) \qquad \mathbf{p}(t) = \mathbf{p}(t_0) + \int_{t_0}^{t} \mathbf{k}(\mathbf{p}, \tau) \cong \mathbf{p}(t_0) \quad (3.3)$$

Differential equations $\dot{\mathbf{u}} = z(\mathbf{u}, t)$ and $\dot{\mathbf{p}} = k(\mathbf{p}, t)$ are used to address control $\mathbf{u}(t)$ and parameter $\mathbf{p}(t)$ functions within the system autonomous representation. They are decoupled equations with respect to state $\mathbf{X}$, so they can be solved separately. In the following they are invoked only if necessary, underling in the processing of the main state equation $\dot{\mathbf{x}} = f(\mathbf{x}, \mathbf{p}, \mathbf{u}, t)$ the joint update of such auxiliary processes.

The implementation of a step by step numerical integration method (e.g. Runge-Kutta methods [52]) can be used to convert eq.(3.3) In the standard recursive discrete time update of the system equation of motion:

$$\mathbf{x}(t_{k+1}) = \mathbf{x}(t_k) + \int_{t_k}^{t_{k+1}} \mathbf{f}(\mathbf{x}(\tau), \mathbf{p}, \mathbf{u}(\tau), \tau) \quad (3.4)$$

Where $\mathbf{x}(t_k)$ and $\mathbf{x}(t_{k+1})$ indicates respectively the state at time t_k and t_{k+1} defied by the selected integration step. The realization of a specific system trajectory $\mathbf{x}(t)$ relies to the assumed initial state, parameters and input laws, so a reference solution of the eq,(3.3) can be defined as one that obtained considering the nominal set $\mathbf{X}_{ref} = \{\mathbf{x}_{ref}, \mathbf{p}_{ref}, \mathbf{u}_{ref}\}$:

$$\mathbf{x}_{ref}(t_{k+1}) = \mathbf{x}_{ref}(t_k) + \int_{t_k}^{t_{k+1}} \mathbf{f}(\mathbf{x}_{ref}(\tau), \mathbf{p}_{ref}, \mathbf{u}_{ref}(\tau), \tau) \quad (3.5)$$

However, several tasks addressed in this work (i.e. sensitivity analysis in III.3 and Extended Kalman Filtering in IV.1) needs to map the effects of a perturbation of the nominal state and parameter components on the dynamic system trajectory, namely referred as variational approach. In more details, a movement $\mathbf{X}(t)$ can be expressed as a perturbation of the reference one by using a first order approximation of the ODE right hand side [51]:

$$\mathbf{x}(t) \approx \mathbf{x}_{ref}(t_0) + \int_{t_0}^{t} \left(\mathbf{f}(\mathbf{x}_{ref}(\tau), \mathbf{p}_{ref}, \mathbf{u}_{ref}(\tau), \tau) + \left[\frac{\partial \mathbf{f}(\ )}{\partial \mathbf{x}} \right] \delta\mathbf{x} + \left[\frac{\partial \mathbf{f}(\ )}{\partial \mathbf{u}} \right] \delta\mathbf{u} + \left[\frac{\partial \mathbf{f}(\ )}{\partial \mathbf{p}} \right] \delta\mathbf{p} \right) \quad (3.6)$$

where $\delta\mathbf{x}, \delta\mathbf{u}, \delta\mathbf{p}$ are the applied set of extended state $\mathbf{X}$ components variations. The trajectory modification $\delta\mathbf{x}(t)$, i.e. the direct difference between eq.(3.5) and eq.(3.6) can be defined as ones that satisfy the following linear integral equation:

$$\delta\mathbf{x}(t) \approx \delta\mathbf{x}(t_0) + \int_{t_0}^{t} \left([J_A(\tau)]\delta\mathbf{x} + [J_B(\tau)]\delta\mathbf{u} + [J_C(\tau)]\delta\mathbf{p} \right) \qquad with \qquad \delta\mathbf{x}(t) = \mathbf{x}(t) - \mathbf{x}_{ref}(t) \quad (3.7)$$

It is worthy to note that this expression relies on the computation of J_A, J_B, J_C matrices that represent

Jacobians of the dynamic equation (eq.(3.2)) evaluated along the current reference trajectory. Actually, a variation problem always implies a joint integration of the relevant variational equations (eq.(3.7)) with the system reference dynamic (eq.(3.2)). Introducing also effect of $\delta\mathbf{u}, \delta\mathbf{p}$ perturbations with respect to control and parameters reference envelopes, the variation equation set can be completed and expressed in differential form as follow:

$$\delta\dot{\mathbf{x}}(t) \approx \left[J_A(\tau)\right]\delta\mathbf{x} + \left[J_B(\tau)\right]\delta\mathbf{u} + \left[J_C(\tau)\right]\delta\mathbf{p} \qquad \delta\dot{\mathbf{u}} = \left[J_U(\tau)\right]\delta\mathbf{u} \qquad \delta\dot{\mathbf{p}} = \left[J_P(\tau)\right]\delta\mathbf{p} \tag{3.8}$$

where coefficients J_U and J_P are evaluated along nominal $\mathbf{u}_{ref}(t)$ and $\mathbf{p}_{ref}(t)$ functions. It is known from system theory [52] that inner linear time variant structure of eq.(3.8) allows expressing the solution at time t by using matrix operators namely referred as State Transition Matrices (STM):

$$\begin{aligned} &\delta\mathbf{x}(t) \approx \left[\Phi(t,t_0)\right]\delta\mathbf{x}(t_0) + \int_{t_0}^{t}\left[\Phi(t,\tau)\right]\left(\left[J_B(\tau)\right]\delta\mathbf{u} + \left[J_C(\tau)\right]\delta\mathbf{p}\right)d\tau \\ &\delta\mathbf{u}(t) \approx \Upsilon(t,t_0)\delta\mathbf{u}(t_0) \qquad \delta\mathbf{p}(t) \approx \mathrm{K}(t,t_0)\delta\mathbf{p}(t_0) \end{aligned} \tag{3.9}$$

In order to better clarify their meaning, a derivative of eq.(3.7) with respect to the initial variation vector component can be performed:

$$\begin{aligned} \left[\Phi(t,t_0)\right] &= \left[\frac{\partial(\delta\mathbf{x}(t))}{\partial(\delta\mathbf{x}(t_0))}\right] = \left[I_{nxn}\right] + \int_{t_0}^{t}\left[J_A(\tau)\right]\left[\frac{\partial(\delta\mathbf{x}(t))}{\partial(\delta\mathbf{x}(t_0))}\bigg|_{\tau}\right]d\tau \\ \left[\Xi(t,t_0)\right] &= \left[\frac{\partial(\delta\mathbf{x}(t))}{\partial(\delta\mathbf{u}(t_0))}\right] = \left[0_{nxn}\right] + \int_{t_0}^{t}\left[J_A(\tau)\right]\left[\frac{\partial(\delta\mathbf{x}(t))}{\partial(\delta\mathbf{u}(t_0))}\bigg|_{\tau}\right] + \left[J_B(\tau)\right]d\tau \\ \left[\Psi(t,t_0)\right] &= \left[\frac{\partial(\delta\mathbf{x}(t))}{\partial(\delta\mathbf{p}(t_0))}\right] = \left[0_{nxn}\right] + \int_{t_0}^{t}\left[J_A(\tau)\right]\left[\frac{\partial(\delta\mathbf{x}(t))}{\partial(\delta\mathbf{p}(t_0))}\bigg|_{\tau}\right] + \left[J_C(\tau)\right]d\tau \\ \left[\Upsilon(t,t_0)\right] &= \left[\frac{\partial(\delta\mathbf{u}(t))}{\partial(\delta\mathbf{u}(t_0))}\right] = \left[I_{nxn}\right] + \int_{t_0}^{t}\left[J_E(\tau)\right]\left[\frac{\partial(\delta\mathbf{u}(t))}{\partial(\delta\mathbf{u}(t_0))}\bigg|_{\tau}\right]d\tau \\ \left[\mathrm{K}(t,t_0)\right] &= \left[\frac{\partial(\delta\mathbf{p}(t))}{\partial(\delta\mathbf{p}(t_0))}\right] = \left[I_{nxn}\right] + \int_{t_0}^{t}\left[J_F(\tau)\right]\left[\frac{\partial(\delta\mathbf{p}(t))}{\partial(\delta\mathbf{p}(t_0))}\bigg|_{\tau}\right]d\tau \end{aligned} \tag{3.10}$$

Such relations reveal that transition matrices are the linear operators allowing to properly map any variation vector component defined at time t_0 into the target one at time t. The matrices $\Xi(t,t_0)$ and $\Psi(t,t_0)$ are also known as sensitivity matrices. Specifically, they represent cross effects between variation vector components, since they respectively map the effect of control and parameters variation on the primary system state variation. The extended state representation in eq.(3.2) can be used here to rearrange the state transition matrix set (eq.(3.10)) in the compact differential form:

$$\left[\dot{\Phi}_{\mathbf{x}}(t,t_0)\right] = \left[A(\tau)\right]\left[\Phi_{\mathbf{x}}(t,t_0)\right] \qquad \textit{with} \qquad \left[\Phi_{\mathbf{x}}(t,t_0)\right] = \begin{bmatrix} \Phi(t,t_0) & \Xi(t,t_0) & \Psi(t,t_0) \\ 0 & \Upsilon(t,t_0) & 0 \\ 0 & 0 & \mathrm{K}(t,t_0) \end{bmatrix} \tag{3.11}$$

where $\Phi_{\mathbf{x}}(t,t_0)$ will be referred as the generalized STM, including sensitivity blocks. The high interest for state transition matrix computation relies to the possibility to solve in a recursive manner important

estimation and control problems [47] that uses system variational representation. Actually, STM is the fundamental tool used to represent discrete time t_k and t_{k+1} updates of any first order state perturbation component as simple linear transformation:

$$\left[\Phi_{\mathrm{X}}(t_{k+1},t_k)\right]=\left[I_{nxn}\right]+\int_{t_k}^{t_{k+1}}\left[A_{\mathrm{X}}(\tau)\right]\left[\Phi_{\mathrm{X}}(t_{k+1},t_k)\right]d\tau \longrightarrow \delta\mathbf{X}_{k+1}=\left[\Phi_{\mathrm{X}}(t_{k+1},t_k)\right]\delta\mathbf{X}_k \tag{3.12}$$

MEONS navigation and estimation framework considers this complete variational model by mean of a joint numerical integration of the following ODE system:

$$\begin{cases}\dot{\mathbf{X}}=\mathbf{F}(\mathbf{X})=\mathbf{F}(\mathbf{x}(t),\mathbf{p},\mathbf{u},t) & \mathbf{X}_0=\{\mathbf{x}(t_0),\mathbf{u}(t_0),\mathbf{p},t_0\}\\ \left[\dot{\Phi}_{\mathrm{X}}\right]=\left[A(\mathbf{X})\right]\left[\Phi_{\mathrm{X}}\right] & \left[\Phi_{\mathrm{X}}\right]=I_{nxn}\end{cases} \tag{3.13}$$

It shall be noted that in eq.(3.13) variations $\delta(\cdot)$ are not directly computed as they are only handholds virtual variables considered in order to derive the STM update process. Actually, they differs from state deviations $\Delta(\cdot)$ (i.e. ΔCd of the following section III.1-C) that will be used in this work to represent an effective change of the state vector components and treated as additional state, control or parameter variables. In this framework, the MEONS propagation step can be once more reduced to the generalized integration step defined in eq.(3.3) simply considering within the extended state vector $\mathbf{X}$ also state transition matrices columns:

$$\{\mathbf{X}(t),\Phi_1(t,t_k),\Phi_2(t,t_k),....,\Phi_n(t,t_k)\} \tag{3.14}$$

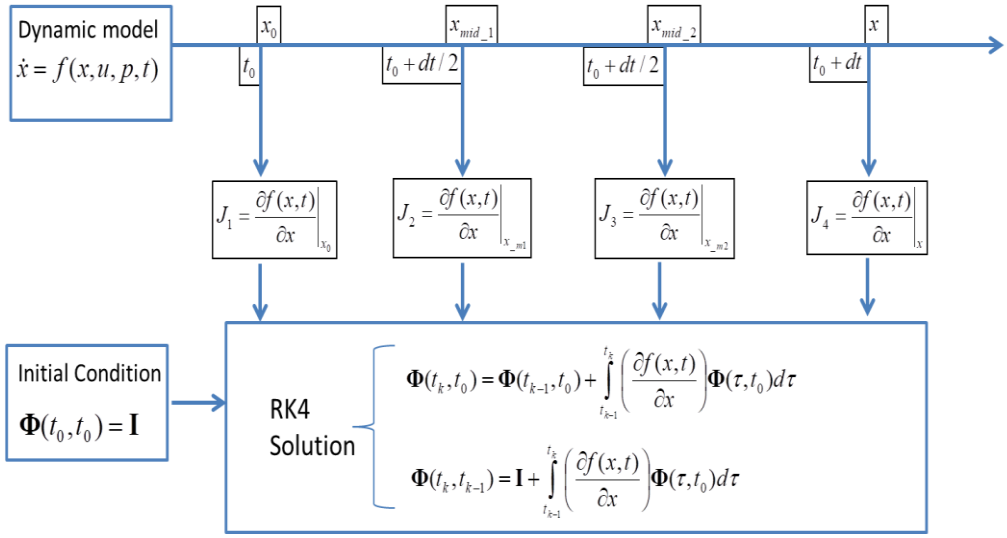

Figure III-1 Joint dynamic and STM equation update

This scheme underlines possibility to exploit STM linearity in order to vectorize the differential matrix equation by solving it per column. In more general, the proposed approach makes the relevant variational joint integration of figure Figure III-1 equivalent to a single propagator integration step. A fourth order Runge Kutta is considered for MEONS propagation task.

The addressed propagation function is implemented aiming at simplifying state rearrangement necessary for the introduction of new states as well as state transition matrix components. Actually, augmentation of eq.(3.2) allows extending propagation step to multiple satellite and multiple realization (or samples) applications [44].

This work deals with formation flying scenarios as well as sigma points nonlinear filtering compatibility. Both problems rely on the possibility to propagate the spacecraft dynamic many times in accordance to the number of spacecraft of the formation or the number of trajectories realization to be evaluated. Basically, the advantage of having simultaneous propagation of multiple systems strictly depends to their coupling. This occurs for formation flying at observation level (e.g. differential measurements in III.2-B) and for nonlinear filters at covariance level within the nonlinear numerical methods synthesis (IV.1-A). In conclusion, the MEONS propagation state can be furthermore extended as follow:

$$\begin{pmatrix} \{\mathbf{X}(t), \Phi_1(t,t_k), \Phi_2(t,t_k), ..., \Phi_n(t,t_k)\}_{Sat\_1} \\ \{\mathbf{X}(t), \Phi_1(t,t_k), \Phi_2(t,t_k), ..., \Phi_n(t,t_k)\}_{Sat\_2} \end{pmatrix} \wedge \{\hat{\mathbf{x}}(t_k), \hat{\boldsymbol{\chi}}_1(t_k), \hat{\boldsymbol{\chi}}_2(t_k,), ..., \hat{\boldsymbol{\chi}}_n(t_k)\} \tag{3.15}$$

in order to handle multiple spacecraft $\{\cdot\}_{Sat\_1}, \{\cdot\}_{Sat\_2}$ and sigma point filtering $\hat{\boldsymbol{\chi}}(t_k)$ (IV.1-A) .

B. Dynamic system modular decomposition

The flexibility of state propagation shall be completed by a modular decomposition of the dynamic model. This approach allows easily introducing a new perturbation, control action or auxiliary process as well as reusing modules for the multiple spacecraft / multiple particles case. In more details, it shall be also possible to run-time activate/deactivate a module contribution in accordance to specific operational phases or requests from sensor processing (e.g. actuation switch off, bias tracking rearrangement etc.). The proposed solution is in line with the widely used paradigm to represent the dynamic system right hand side as a linear combination of non-linear models expressed in function of the extended state vector $\mathbf{X}$. This nonlinear contributions decomposition can be expressed in compact manner by using the following representation:

$$\mathbf{X}_{k+1} = \mathbf{X}_k + \int_{t_k}^{t_{k+1}} \mathbf{F}(\mathbf{X}, \tau) d\tau \rightarrow \begin{cases} \mathbf{F}(\mathbf{X}) = \alpha A \mathbf{X} + \sum_{1...m}^{p} \beta_p B_p M_p(C_p \mathbf{X}_{extend}) \\ \mathbf{X} = \{\mathbf{x}, \mathbf{u}, \mathbf{p}, t\} \qquad \mathbf{X}_{extend} = g_1 \circ g_{2...} \circ g_q(\mathbf{X}_{extend}) \end{cases} \tag{3.16}$$

$$Datapool = s_1 \circ s_{2...} \circ s_r(Datapool) \qquad Datapool_i = \{\mathbf{X}_k, M_{1...m}, \mathbf{X}_{extend}\}$$

The β factor and matrix B_p represent respectively the enabling/disabling factors (i.e. 0/1) and participation coefficient matrix of the model output vector M_p to the system dynamic right hand side. α and A are the linear counterpart of β and B_p introduced to accomplish integrator optimization described in IV.3. C_p is the state participation matrix that maps the components of the vector $\mathbf{X}_{extend}$ to the correspondent model local set. $\mathbf{X}_{extend}$ incorporates not only the internal state $\mathbf{X}$, but also all the information requested by the active models (external data and derived quantities). Actually, functions $g(\cdot), s(\cdot)$ defined in eq.(3.16) represent internal and external interface modules used respectively to cope with:

- additional and transformed variables that $g(\cdot)$ made available in $\mathbf{X}_{extend}$ combining state $\mathbf{X}$ and external data. Modules could not be explicitly dependent on the internal state components but on their transformed version (e.g. reference frame changes)

- Post-processing of updated data in order to made available additional information to the user within the correspondent datapool structure.

As indicated by function composition symbol $\circ$ interfaces can implements series schemes: the interface function $g_i(\cdot), s(\cdot)$ is applied on the transformed data structure provided by the previous one until the end of recursion. In this framework, the overall propagation architecture allows identifying three different functional blocks:

- $M_p(\cdot)$ modules set containing physical models necessary to build the state space derivative
- $g_q(\cdot)$ interface set containing function providing all the inputs for the M_p modules functions

- $s_r(\cdot)$ modules set containing function providing all the outputs required for the user

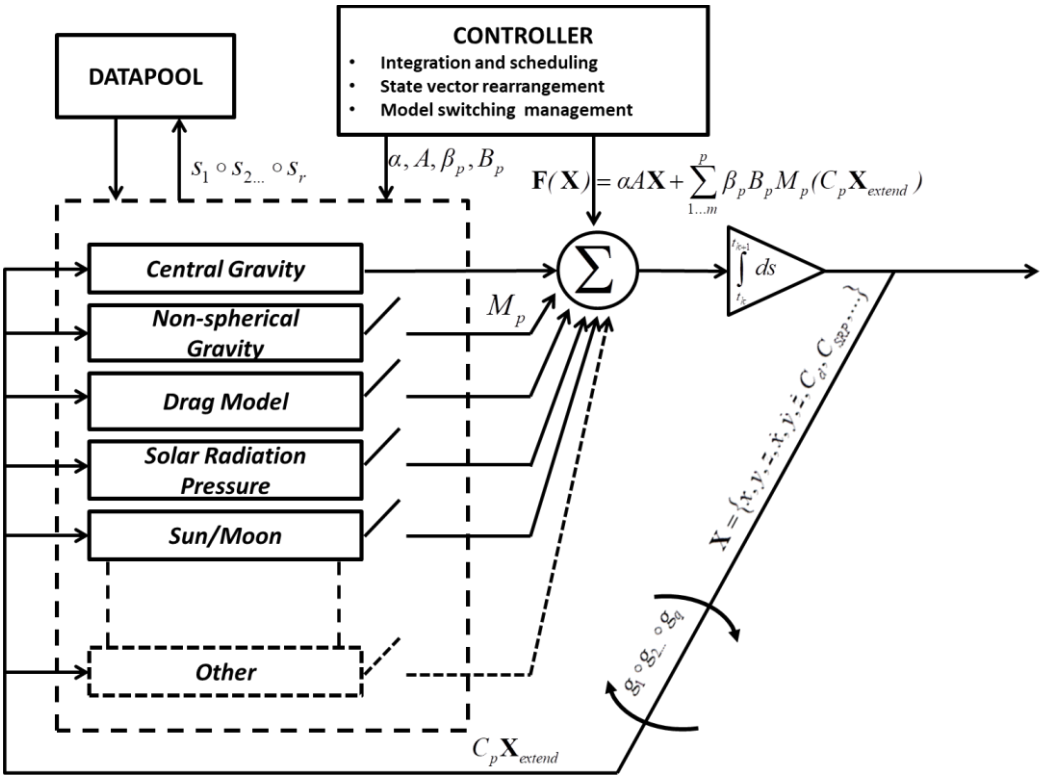

Figure III-2: MEONS Propagation Architecture

The indexes p, q, r allows to cycle on the modules and matrices at each integration step, so the propagation task results in three different processing recursion relying on M_p, $g_q(\cdot)$, $s_r(\cdot)$. The switching and arrangement of each contribution can be managed by a dedicated propagation controller function that set for the current cycles activate/deactivate models and interfaces. Propagation architecture elements can be recognized in the block diagram of Figure III-2, where are also indicated some relevant physical models that will be detailed in the following section. It is worthy to note that internal interfaces $g_q(\cdot)$ are a very useful tool when some auxiliary data are shared by different $M_p(\cdot)$ modules. For instance, transformed position or attitude (e.g. from ECI to ECEF) can be dispatched to several orbit perturbation or control models not repeating the computation for each one. Variational equation terms can also benefit of interface functionality for the evaluation of relevant Jacobians. Actually, the STM can be represented, in accordance to the modular approach, as linear combination of transition matrix component relying to the Jacobian of a specific module M_p:

$$J(\mathbf{X}) = \frac{\partial \mathbf{F}(\mathbf{X})}{\partial \mathbf{X}} = \alpha A + \sum_{1...m}^{p} \beta_p B_p \frac{\partial M_p(\mathbf{X}_{loc})}{\partial(\mathbf{X})} \longrightarrow$$
$$\longrightarrow \dot{\Phi}_{\mathbf{X}} = J(\mathbf{X})\Phi_{\mathbf{X}} = \alpha A \Phi_{\mathbf{X}} + \sum_{1...m}^{p} \beta_p B_p J_p(C_p \mathbf{X}_{extend})\Phi_{\mathbf{X}} = \alpha \dot{\Phi}_A + \sum_{1...m}^{p} \beta_p B_p \dot{\Phi}_p \quad (3.17)$$

This solution interprets the natural necessity of introducing a new transition matrix derivative block $\dot{\Phi}_p$ whenever an RHS module is added to the reference dynamic model equation. Considering the use of interfaces, even if the module $\dot{\Phi}_m$ shall be evaluated once per each STM column, the Jacobian of the target model can be evaluated ones for all transition blocks on the basis of the knowledge of the current integration state (see Figure III-1). These computed Jacobians are also made available via external interfaces to the user (i.e estimation block). $s_r(\cdot)$ includes the collecting function providing to the user not

only updated variables, but also internal state in order to maximize the information sharing.
All described issues results in an open architecture of the MEONS Generic Propagator module, whose functionalities and tasks can be configured with respect to the specific application. The following feature has been finally included:

- The state $\mathbf{x}$, the control action $\mathbf{u}$ and parameter vector $\mathbf{p}$ can be easily augmented and rearranged throughout the system dynamic
- The propagation can handle the complete variational problem as well as multiple spacecraft and multiple realization filtering
- The introduced modular decomposition allows performing contribution switching and sorting, at the same time matrix participation maps allows using matrix projection and permutation operators to accomplish component weighting and rearrangement
- The system complexity can be continuously upgraded by adding a new non-linear term M_m, interface $g_q(\cdot)$, $s_r(\cdot)$ or STM contribution, which become dynamic system modules stored in a proper model database.

This database is the object of the following sections. The use of notation M_p, $g_q(\cdot)$, $s_r(\cdot)$ has been introduced just to address, when necessary, the several contributions within their own functional set.

C. High performance perturbation models for real time POD applications

An accurate POD system relies on modelling orbital perturbations in order to handle fine geolocation during Nominal Pointing Mode (NPM) and payload operational phase (see II.2-A). The MEONS Generic Propagator modules database includes force models well-defined in literature and shared by all currently used legacy POD programs ([1]).

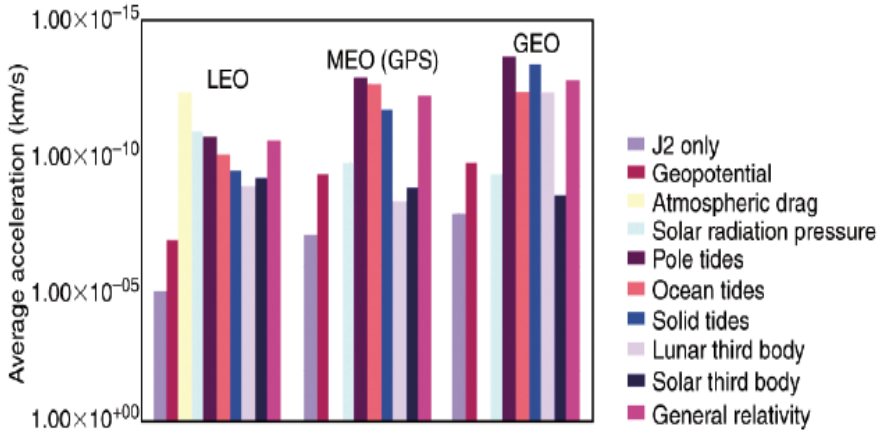

Figure III-3 Avarage perturbation acceleration contribution with respect to target orbit scenario

A summary is reported in Table III-1, where $\mathbf{a}_G$ and $\mathbf{a}_{NG}$ lists respectively gravitational and non-gravitational accelerations used in the Cowell's method in eq.(3). Relevance of these contributions relies on orbital altitude. Figure III-3 illustrates the effect of different force model perturbations on three different orbit regimes from low-Earth orbit (LEO) to geosynchronous Earth orbit (GEO).

This comparison is provided in term of experienced accelerations, but propagation design should investigate also other aspects as perturbation dynamic content and final effects on the trajectory excursion (e.g. dissipative orbit decay or relevant frequency content). A possible analysis method is the object of III.3. At least, the significant contributions shared by all MEONS target orbit scenarios shall be included in order to provide a variable Earth orbit regime compatibility. This work considers the real time POD configuration of Table III-1 as MEONS propagation model baseline (MPMB). The selected non-spherical gravity and drag models have already extensively demonstrated on-flight real time compatibility in several TAS-I LEO mission. The SRP and TRB contributions have been introduced in order to handle high orbit scenarios with a reduced computational cost. The aim is to cope with the OD "pure propagation" accuracy requirement defined by the maximum expected sensor outage. A detailed

mathematical description of real time baseline models is provided in Appendix A. Particular emphasis must be reserved to auxiliary stochastic models, which are the fundamental connection of the propagation task with the estimation one.

Legacy Perturbations	*MEONS Generic Propagator modules*
Gravitational: ($\mathbf{a}_G$) ➢ **NSPH** Non-spherical Earth Gravity Field ➢ **TRB**: third body effect and other attracting bodies ➢ **SET**: solid-Earth tides ➢ **OT**: ocean tides Non-gravitational($\mathbf{a}_{NG}$): ➢ **DRAG**: Atmospheric drag and lift ➢ **SRP** : Effect of Solar-Radiation Pressure ➢ **ALBEDO**: Earth re-radiation ➢ **IF :** infra-red radiation pressure ➢ **RE**: Relativistic effects ➢ **MF**: Magnetic field	**Real time POD configuration** • Non-spherical Earth Gravity Field ,up to 30x30, with selectable EGM96-2008-GM10 models (M_1) • Third Body gravitational force considering Sun, Moon (M_2) • Solar Radiation Pressure: Cannon Ball and cylindrical eclipse model (M_3) • Aerodynamic force Cannon Ball considering relativeatmosphere velocity (M_4) • Auxiliary stochastic models (0^{th} costant bias, 1^{st} and 2^{nd} order Gauss Markov processes etc.) for state augmentation • Atmospheric density computation with Modified Harris Priester (g_1) • NOOA Penticton solar flux and buldge evaluation (g_2) • J2000, ECEF and WGS-84 transformations with IERS bulletin setting (g_3) • Legacy Sun and Moon position computation (g_4) **Higher order models (DSS modules)** • Gravity field up to 120x120, with selectable EGM96-2008-GM10 • Spacecraft Surface Projection and shadowing and spacecraft attitude effect handling • Multi-plate or CAD models for force computation and fine • Atmospheric density computation with MSISE, Jacchia-Roberts • Fine JPL Sun and Moon ephemeris computation • Solid-Earth tides, Ocean tides • Earth albedo and infra-red radiation pressure • Thermal perturbation • Magnetic field Relativistic effects

Table III-1 - MEONS orbit Perturbation Modules

It is worthy to remind that general purpose state space model in eq. (2.4) can consider state variable components as stochastic variables, associating to them a proper probability distribution. The compatibility with the general stochastic model does not rely only on the inclusion of the process noise term $\mathbf{w}$, but also to the proper representation of the degree of uncertainty affecting state, control or internal parameters variables. The proposed approach is in line with the well-known reduced dynamics technique proposed for standard LEO navigation system [53]. The fundamental eq.(3.1) becomes:

$$\begin{cases} \dfrac{d\dot{\mathbf{r}}}{dt} = -\dfrac{\mu_{\oplus}}{r^3}\mathbf{r} + \mathbf{a}_{Pert}(\mathbf{r},\dot{\mathbf{r}},\mathbf{p}_{Pert}) + \mathbf{w}_{\mathbf{a}} \\ \mathbf{p}_{Pert} = k(\mathbf{p}_{Pert},t) \end{cases} \tag{3.18}$$

where $k(\mathbf{p}_{Pert},t)$ represents auxiliary processes defined in eq.(3.2) for the following parameter state augmentation:

$$\mathbf{p}_{Pert} = \{a_R, a_T, a_N, \Delta C_D, \Delta C_R\} \tag{3.19}$$

Eq.(3.19) is the most used reduced dynamic parameter set and it includes $\mathbf{a}_{emp}$, which are the empirical accelerations (subscripts R, T and N stand for radial, tangent and normal components) representative of residual, unmodelled accelerations and $\Delta C_D, \Delta C_R$, which are uncertainty in both spacecraft drag coefficient and SRP coefficient. $k(\mathbf{p}_{Pert}, t)$ are generally modelled by using representative of the Linear Markov family (see Appendix A), whose coefficients rely to the expected parametric uncertainty behaviour (time scale, frequency content) [54]. Due to linearity, these models generally do not require a dedicated module and they can be handled by the term $\alpha A\mathbf{X}$ of the configurable dynamic model eq.(3.16) by properly setting matrix A elements. Conversely, their contribution in $\mathbf{a}_{Pert}$ is properly mapped by the impacted acceleration module. The baseline perturbation model database (Appendix A) is completed by the relevant Jacobians interfaces feeding the state transition modules necessary to update MEONS variational equations eq.(3.17). Some higher order derivative contributions have been neglected when compatible with the target accuracy. An example is the case of non-spherical Earth Gravity Jacobian, whose derivatives are evaluated up to fourth harmonic order. Jacobians depends on the target extended state vector components, so the introduction of new component generally relies to an update of this interface module: best trade-off between accuracy and computational burden shall be pursued during the propagator initial design phase.

For the sake of completeness, Table III-1 also reports higher complexity physical models and secondary perturbation contributions. They will be implicitly referred during navigation testing phase (CHAPTER V), when the GNSS Scenario Simulator (GSS) is used to address navigation performances, Actually, the TAS-I Dynamic Spacecraft Simulator (DSS) block (see Appendix C) exploits higher-accuracy perturbations and higher fidelity models in order to generate the proper spacecraft reference trajectory. Specifically, the DSS module perform integration of complete spacecraft orbit and attitude dynamic [6] taking into account 120 x 120 gravity model based on GEM-10; third body effects based on JPL Development Ephemeris; computation of the atmospheric density up to 2500 km altitude based on Jacchia and Damosso models and solar activity in function of solar radio flux and geomagnetic indexes. This model will be referred as DSS reduced model (R-DSS) in order to distinguish it from the Complete DSS model (C-DSS) developed for the G2G study. In this case high-rate integration, with 0.125s step size has been performed and the cannon ball models are replaced by corresponding external forces and torques evaluated on a triangular mesh of the spacecraft (referred in Table III-1 as CAD model), taking also into account shadowing effects introduced by the attitude dynamics. Generating reliable reference data wrt evaluating navigation performances is fundamental to test by simulation the system architecture and close all design trade off , before implementing any experimental validation.

In accordance the upgradable philosophy of the developed propagator, it shall be reminded that higher order counterpart of perturbation models can be optionally included as MEONS selectable module in order to deal with future applications. For instance, multi-plate model has been proposed for MEO satellites during final operative phase [3] or Solar sail applications, which rely to high accuracy SRP evaluation requirements. These challenging issues are out of scope of the present thesis. However, assumed the compatibility with the target computational constraints, they demonstrate benefits of augmentation capability with respect to different scenarios.

D. Low thrust orbit control and electric propulsion navigation issues

As stated in II.2-B autonomous orbits rising and control scenarios are one of the most challenging technological issues to be handled via GNSS based navigation. Actually, the principal merit of this work is reviewing the on-board orbit estimation strategy to make it compatible with autonomous steering strategy based on low thrust electric propulsion. The management of standard almost-impulsive orbit control (i.e. cold gas) is generally handled in a different manner: high thrust manoeuvre correspond to a brief non-operative phase completely performed under the control of the ground segment. In this scenario the orbit determination performance can be relaxed and manoeuvre plan accomplishment is followed by a

new convergence transient of the navigation system. Considering both open loop (manoeuvre plan uploaded on-board) or closed loop strategies (manoeuvre direct computation from orbit error) autonomous control is in charge to the avionic subsystem. It relies on bounded accuracy of spacecraft positioning, whose constant monitoring is exploited for decision making and manoeuvre scheduling. In addition, differently from the conventional impulsive one, low thrust is a long term continuous action and eventual navigation degradation cannot be side-lined within a brief operative time window. The simplest and most effective solution is the direct thrust information feedforward, which drastically reduces the control actions effects on the orbit estimation task. Performance during long term propagation due to critical GNSS visibility conditions, strictly depends on correct application of the actuation force, whose effect supersede other perturbation as altitude grows. Beyond the possibility to tune the process error at estimation level, MEONS propagator implements a configurable actuation module $\mathbf{a}_{Thrust}$:

$$\dot{\mathbf{x}} = \mathbf{f}(\mathbf{x}, \mathbf{p}_{Pert}, \mathbf{p}_{Thrust}, t) = \begin{cases} \dfrac{d\mathbf{r}}{dt} = \dot{\mathbf{r}} \\ \dfrac{d\dot{\mathbf{r}}}{dt} = -\dfrac{\mu_{\oplus}}{r^3}\mathbf{r} + \mathbf{a}_{Pert}(\mathbf{r}, \dot{\mathbf{r}}, \mathbf{p}_{Pert}, m_p, \mathbf{o}_{att}) + \mathbf{a}_{Thrust}(\mathbf{r}, \dot{\mathbf{r}}, \mathbf{p}_{Thrust}, m_p, \mathbf{T}, \mathbf{o}_{att}) \\ \dfrac{dm_p}{dt} = -\dfrac{\|\mathbf{T}\|}{g_0 ISP} \end{cases} \tag{3.20}$$

that generates thrust acceleration in accordance to three main contributions:

1. attitude quaternion (or Euler angles) and current mass auxiliary information $(\mathbf{o}_{att}, m_p)$
2. spacecraft orbit control law and thrust direction generation $(\mathbf{T}(t))$
3. electric propulsion engine mechanization parameters $(\mathbf{p}_{Thrust})$

The three identified model design drivers extend the problem formulation to other research areas as AOC and platform avionic configuration. Specifically, they correspond to three fundamental topics:

- attitude guidance generation and AOC control architecture
- low thrust optimal control algorithm and integration
- efficiency and mounting issues of Ion (or Hall) based [55] electric propulsion

Even focusing on their navigation problem significance, this section details these issues with respect to achievements and expertize envisaged in the frame of Galileo2G LEO-MEO transfer [6] and small satellite orbit acquisition studies [7].

AOC control architecture and spacecraft roll steering $(m_p, \mathbf{o}_{att})$

Embarking electric propulsion requires taking into account on-board resources constraints due to power and fuel limitation. Specifically, the actuation law shall be designed in order to achieve minimization of either propellant consumption (or transfer time) and maximization of solar panel radiated cross section. The first aim can be handled via on-board implementation of optimization based algorithms for thrust vector generation. The second aim can be pursued by properly generating attitude guidance in such a way that solar array hinge reorientation mechanism maximizes the overall sun exposure. A general scheme of the control architecture is defined in Figure III-4, which provides a general framework to address the EOR or AAM applications. MEONS, in its definitive sequential estimation arrangement, interfaces the following modules:

- The Optimal Thrust Vector Generator (OTVG): this block solve the transfer problem and generate the firing direction by using the MEONS position tag and all auxiliary information in order to solve the target optimal control problem

- The Attitude Profile Generator (APG): this work considers fixed mounting of electric propulsion, so it is necessary to generate a reference attitude guidance reorienting the spacecraft in accordance to the generated firing direction and power supply constraint. For target EOR and AAM study case, assuming the thrust mounted along the x-mechanical axis and solar arrays mounted along the y-mechanical axis, the following Firing Reference Frame (FRF) is defined:

$$\hat{\mathbf{x}}_{FRF} = \hat{\mathbf{U}} \qquad \hat{\mathbf{y}}_{FRF} = \hat{\mathbf{X}}_{est} \wedge \hat{\mathbf{U}} \qquad \hat{\mathbf{z}}_{FRF} = \hat{\mathbf{x}}_{FRF} \wedge \hat{\mathbf{y}}_{FRF} \tag{3.21}$$

This computation exploit MEONS estimated position $\hat{\mathbf{X}}_{est}$ and the thrust unit vectors $\hat{\mathbf{U}}$ generated by OTVG. Specifically, alignment of x-mechanical axis with the FRF x-axis provides the first fundamental condition to determine the attitude guidance. The second one requires that Sunlight vector lies in the spacecraft x-z body plane, which correspond to the Sun exposure maximization considering rotating solar array assembly. The final reference spacecraft orientation can be thus obtained by a roll rotation around the FRF x-axis that continuously preserves the alignment with the firing direction. However, a roll steering law, similarly to that provided in [56], shall be considered to cope with collinearity conditions.

- The Attitude and Orbit Control (AOC) and Attitude Estimation Filter (AEF): MEONS provides auxiliary information (i.e. Sun light knowledge and eclipse occurrence) in order to perform attitude sensor management (Sun sensor, Star tracker) and attitude estimation. Attitude guidance and estimation drives the final Orbit Control Mode (OCM) management. On the other hand the AOC function feeds MEONS with the estimated attitude (with related covariance or error bounds), auxiliary information on propellant mass and diagnostics. For instance if the attitude covariance is above a predefined threshold the thrust feedforward shall not be performed, taking into account the effect of this lack in the sequential estimation.

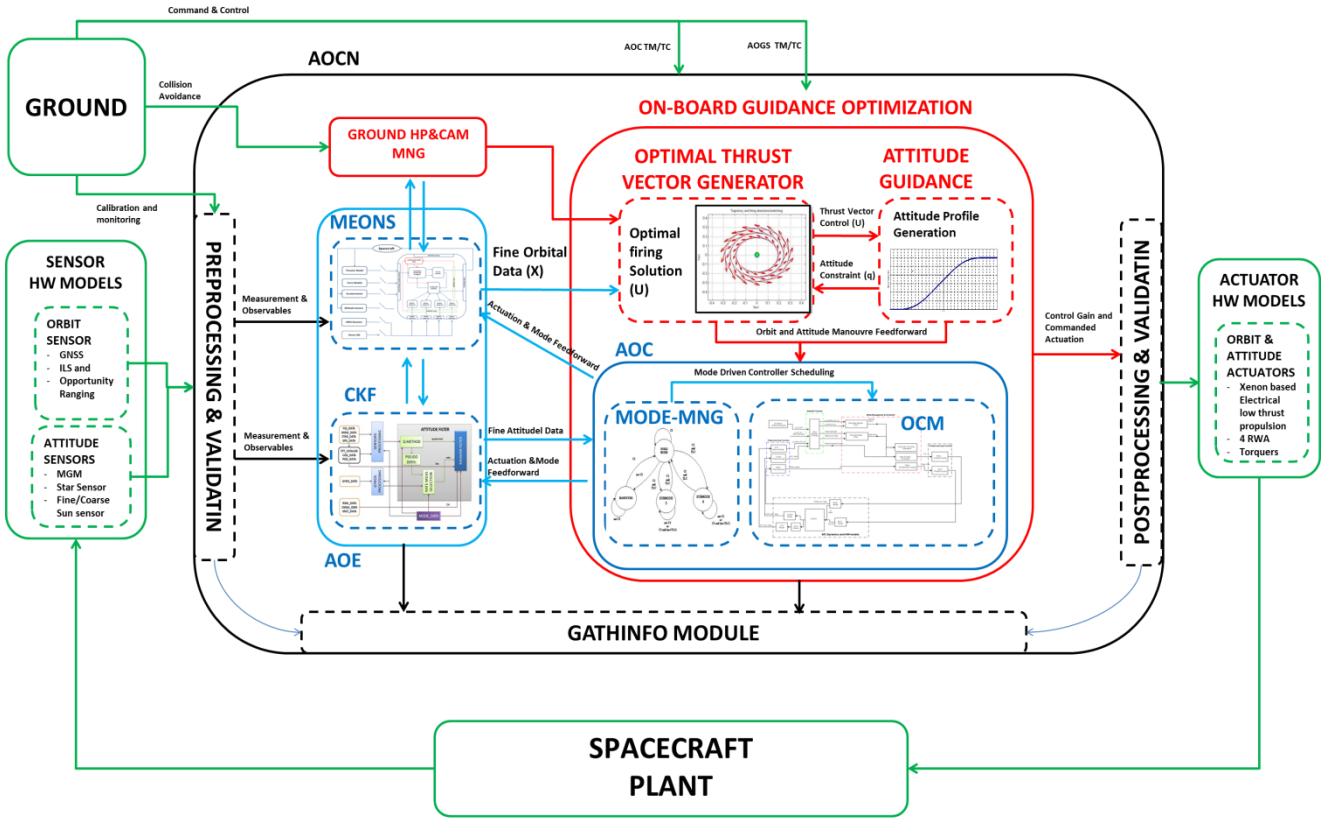

Figure III-4 Next Generation Satellite Low Thrust Autonomous Orbit Control block diagram

Those peculiarities reinforce the idea that an on-board estimation block has an extended significance,

when integrated in orbit control architecture. Attitude quaternion q, angular velocity ω and other variables as current propellant mass m_p shall be managed. In the frame of MEONS variable classification (III.1-A), the best solution is to consider them as auxiliary state $\mathbf{x}_{aux} = \{q, \omega, m_p\}$. When the aiding is provided, $\mathbf{x}_{aux}$ is superseded by the external one in accordance to eq.(2.13). Otherwise, if Zero Order Hold [52] approximation is not allowed (fast dynamic conditions) or there is the necessity to propagate the information before having a new external aiding, the correspondent state update equations are enabled. Augmented propellant mass and kinematic attitude can be used for this aim for the selected auxiliary set:

$$\frac{dm_p}{dt} = -\frac{\|\mathbf{T}\|}{g_0 ISP}; \qquad \frac{dq}{dt} = \left[\tilde{\Omega}(\boldsymbol{\omega})\right] q; \qquad \frac{d\boldsymbol{\omega}}{dt} = f(q, \boldsymbol{\omega}, t) \tag{3.22}$$

It is worthy to remind here that navigation information have to provide together with estimated orbit data, also the associated error bound. The covariance monitoring (II.3, IV.1), is important for the control task: trapping divergent covariance or discard low accuracy navigation data allows to keep stability and avoid closing the loop on a wrong signal error.

Low thrust orbit control (T)

This paragraph aim at providing some highlights on the control laws $\mathbf{T}(t)$ used to feed MEONS thrust model $\mathbf{a}_{Thrust}(\mathbf{r}, \dot{\mathbf{r}}, \mathbf{p}_{Thrust}, m_p, \mathbf{T}, \mathbf{o}_{att})$ in EOR and AAM scenarios. As stated before, firing vector generation can be addressed within the application of Optimal Control Theory to orbital transfer problems. Actually, at theoretical point of view, orbit control optimization techniques can be divided in two branches [57]: direct techniques; indirect techniques. The direct techniques imply the discretization of the problem and the use of standard minimization routines where the dynamic equations and the final desired orbit are considered as constraints. The indirect techniques are based on the Pontryiagin necessary conditions, where a suitable Hamiltonian Flow is defined: the problem is reduced to find the costate that allow to this Hamiltonian flow to reach the final orbital target (see [58],[59]). Considering this work specific setting, the algorithm exploited for EOR and AAM cases results quite different, despite the common indirect methods mathematical framework. Table III-2 compares the two adopted solutions.

Specific application	Algorithm	Optimization Feature	Control scheme	Results
LEO-MEO low thrust autonomous orbit transfer (V.3)	Pontryagin based Non Linear Optimal problem solution [58]	Transformed space Minimum Time solution, orbit perturbations management, intermittent thrust for eclipse constraint handling	Very slow navigation reset (10 days), orbit data smoothing, nearly open loop analysis wrt navigation task	Spiraling, almost constant low-thrust one year LEO-MEO transfer
Small satellite low thrust autonomous orbit acquisition (V.4)	Pontryagin based Linearized Optimal problem solution [60]	Minimum Fuel fixed time window, unperturbed discrete time approximation via virtual satellite approach in Hill coordinates frame, continuous thrust (no eclipse constraint)	Linearized and approximated solution requires fast closed loop update and close synergy with the navigation	High dynamic LEO orbit acquisition with continuous variable thrust magnitude

Table III-2 Orbit Acquisition Control Peculiarities for EOR and AAM cases

For the Galileo 2nd generation LEO-MEO transfer which may last several months, TAS-I has developed an effective optimization routine called SOFTT (Figure III-5) based on the indirect techniques presented in plus the averaging methodology. This allows solving full nonlinear Pontryagin based optimal problem in a proper transformed space taking into account J2 perturbation as well as eclipses constraint. SOFFT [60] is capable to handle different EOR cases and different optimization objective. The target LEO-to-MEO rising has been set in accordance to Galileo Second Generation specific needs. A Minimum Time

orbit transfer from 1221 km altitude parking orbit to the 23813 km altitude target orbit has been selected. The generated trajectory qualifies as a spiralling, one-year long, almost constant tangential low-thrust (0.180 N thrust) rising exploiting J2 effect for RAAN accommodation. Thruster switch off during eclipses is considered to preserve platform power supply in very long scenario experiencing different seasonal phases.

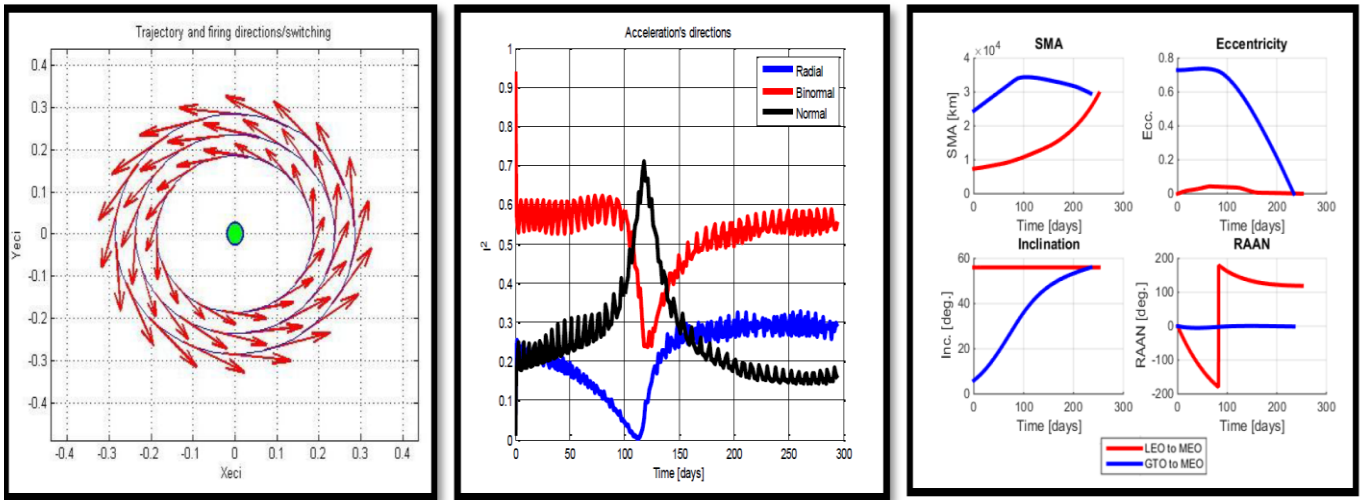

Figure III-5 SOFFT representative results: trajectory, control and Keplerian orbital parameters

Specifically, the configuration of TAS-I proprietary EOR strategy [60] can be described by the following steps:

1. Before launch the optimal transfer solution is calculated by SOFTT as off line optimization in the Ground Segment (GS). The initial optimal database is stored in the satellites computer memory.

2. The satellite uses the stored database to compute the thrust strategy (thrusters switch on/off and firing direction). The On Board Software (OBSW) stores continuously the local position and velocity from the navigation task.

3. After N days (typically 10 days) the database is updated using the stored navigation data in order to define the averaged optimization state vector. The OTGV computes the new optimal transfer solution from the new initial guess to the target operative orbit.

Basically, due to the long time scale of the transfer as well as low rate OTVG reset, such closed loop slightly interact with the orbit estimation performance: assuming one day simulation scale, the thrust can be considered as an open-loop firing sequence planned and triggered to the overall AOC architecture. However, even mitigated by data averaging, the target navigation accuracy shall be guaranteed in so far as it enhances autonomous rising efficiency by absorbing second order perturbations and firing errors within the reset. For G2G V.3 test case, the one year transfer is windowed on 7 orbit rising days (Figure III-6, left) and test are performed on ones that are relevant in term of GNSS visibility conditions [62]. Actually, the main effect on the navigation task relies on in view SVs visibility changes. Figure III-6 (right) depicts the experienced angular velocity of the satellite around the thruster axis due to roll steering and thrust vector tracking. The necessity to use more than one GNSS antenna proposed in III.2-C mitigates such irregular angular velocities from a GNSS receiver tracking point of view.

In case of AAM, a Minimal Fuel problem is considered and the orbit acquisition time window is a configuration parameter that can be set in accordance to actuation saturation limits. Details on the specific implementation are provided in V.4 to better understanding closed loop results. Actually, from a comparative point of view, AAM solution deals with a less sophisticated approach, because the Pontryagin problem passes troughs a linearization and discretion of unperturbed relative equation in

accordance to the virtual spacecraft reference approach [63]. Therefore, compensation of such approximations requires a higher thrust update rate leading to a tighter closed loop between MEONS and OTVG. Improvements in the model (perturbation, calibration), constraints integration (navigation singularities, maximum sovra-elongation, saturation and eclipses) and other control issues are out of scope of this thesis. Nevertheless, the idea is to reduce, in the future, the distance between the control task and the MEONS system in other to share some functionality (i.e. reference orbit and predictive model generation). The aim is developing a complete single and multiple small satellite orbit acquisition and station keeping architecture compatible with the integrated GNSS-AOC architecture presented in II.1-B.

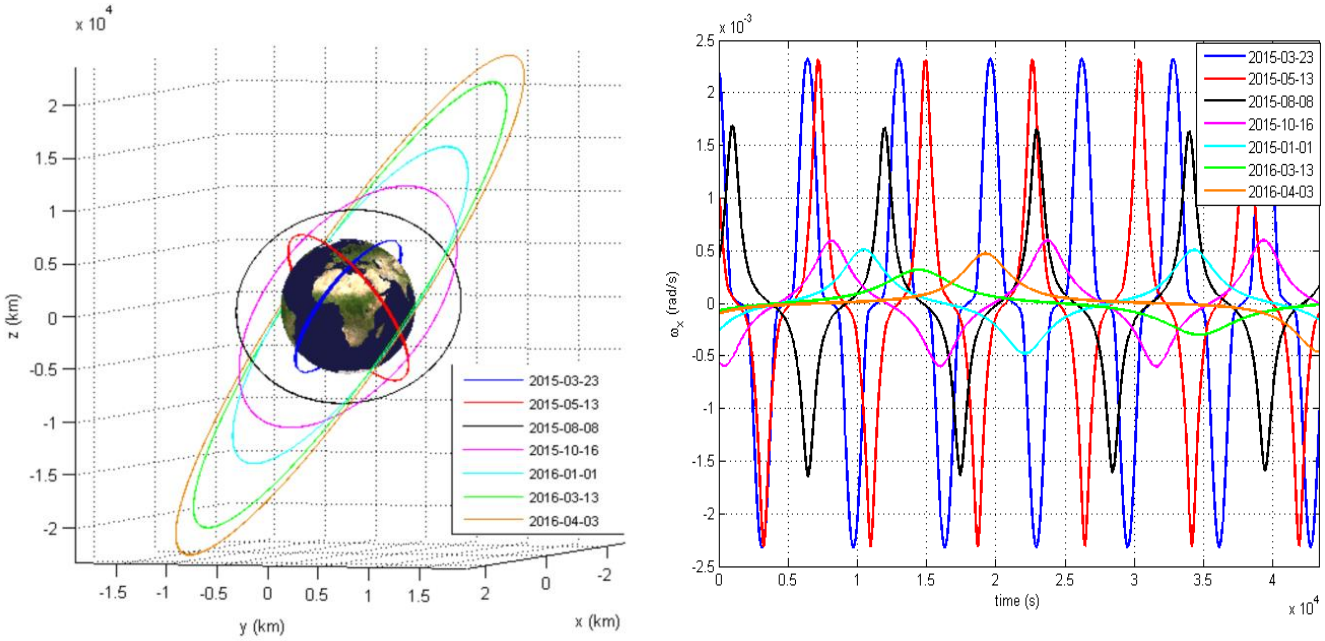

Figure III-6 (left) Seven representative days of the simulated, one-year long, low-thrust transfer (right) satellite angular velocity around the thruster axis during the same days.

The two considered cases deal with different characteristics of $\mathbf{T}(t)$. The first EOR scenario considers a higher magnitude constant thrust with relatively slow direction variation and possible intermittent activations due to eclipse. The second is a small perturbation that rapidly varies in magnitude and direction in a fast closed loop realization.

Actuator mechanization error

It has to be observed that the effective thrust is in general different from the commanded one due to geometrical errors, such as scaling, misalignment ad coupling, but also uncertainty in plume magnitude and direction. In more details, if the commanded thrust is written in spherical coordinates as:

$$\mathbf{T} = \{A, \alpha, \beta\} \tag{3.23}$$

where A is the thruster magnitude and α and β are the angles defining the orientation of the plume in the body reference frame BRF, the true one can be thus expressed as:

$$\tilde{\mathbf{T}} = \left(\mathbf{I} + d\mathbf{K}_{scale} + d\mathbf{C}_{coupl} + d\mathbf{S}_{mis}\right)\mathbf{T}' + \boldsymbol{\nu} \tag{3.24}$$

where $\mathbf{I}$ is the identity matrix, $\boldsymbol{\nu}$ is thrust noise, $\mathbf{T}'$ is the actual thrust expressed by Cartesian coordinates in BRF. The matrixes d$\mathbf{K}$, d$\mathbf{C}$, and d$\mathbf{S}$ represent scaling, coupling, and misalignment errors, respectively:

$$d\mathbf{K}_{scale}=\begin{bmatrix} k_x & 0 & 0 \\ 0 & k_y & 0 \\ 0 & 0 & k_z \end{bmatrix};\quad d\mathbf{S}_{mis}=\begin{bmatrix} 0 & \phi & -\theta \\ -\phi & 0 & \psi \\ \theta & -\psi & 0 \end{bmatrix};\quad d\mathbf{C}_{coupl}=\begin{bmatrix} 0 & \zeta & \eta \\ \zeta & 0 & \xi \\ \eta & \xi & 0 \end{bmatrix}; \tag{3.25}$$

and the parameters defining the matrixes identify the considered propulsion system. The acceleration generated by the effective thrust depends on the current satellite mass and attitude as:

$$\mathbf{a_T}=\frac{1}{\left(m_{dry}+m_p\right)}\mathbf{R}\tilde{\mathbf{T}} \tag{3.26}$$

where $\mathbf{R}$ is the attitude matrix, m_{dry} is the satellite dry mass and m_p is the current propellant mass evaluated on the basis of eq.(3.22). Unfortunately, $\mathbf{a}_T$ deviates from that associated to the commanded thrust because of partial knowledge of all the introduced actuation parameters. Firstly, the actual thrust $\mathbf{T}'(t)$ is affected by bias errors:

$$\mathbf{T}'=\mathbf{T}+\{\Delta A,\Delta\alpha,\Delta\beta\} \tag{3.27}$$

where ΔA, $\Delta\alpha$ and $\Delta\beta$ indicates respectively amplitude and orientation errors in BRF. Moreover, according to eq.(3.25), the effective trust is derived from the actual thrust vector accounting for scaling, coupling and misalignment matrixes. Three independent parameters are associated to each matrix and the knowledge of each of those parameters is in general also biased. Uncertainty in the knowledge of the current satellite mass, represented as a deviation Δm from the nominal value, is another source of error affecting the evaluation of the acceleration generated by the thruster. On the whole, 13 parameters have to be considered to model the deviation of the nominal acceleration from the true one:

$$\mathbf{p}_{thrust}=\left\{\Delta A,\Delta\alpha,\Delta\beta,\Delta k_x,\Delta k_y,\Delta k_z,\Delta\vartheta,\Delta\psi,\Delta\phi,\Delta\xi,\Delta\eta,\Delta\zeta,\Delta m\right\} \tag{3.28}$$

This parameterization assumes small contributions of error in attitude rotation matrix $\mathbf{R}$, which are generally superseded by other mechanization errors. OCM control, except for short transient windows and unexpected plume impingement issues, ensure a high performance tracking (10^{-3} rad error) for almost constant thrust case, which, from a stochastic point of view, can be adsorbed within high frequency estimation noises. However, if necessary, $\Delta\alpha,\Delta\beta$ can be used to eventually map and desensitize (see IV.1-C) such deviation within the propagation and estimation. It is clear that the proposed set in eq.(3.28) is not the minimal representation aiming to cope with any thrust mounting and parameter uncertainty contribution. For instance, when the thrust is aligned to a mechanical axis the effective number of variables reduces to the active set. The focus here is on the possibility of extending and updating the thruster model and its parameterization in accordance to the configuration assumptions. Actually, the representation of thruster efficiency with a bias is very effective in case of almost constant thrust, which is the case of the LEO-MEO EOR. In case of variable AAM thrust, the following representations have been preferred:

$$\tilde{\mathbf{T}}=\left(\mathbf{I}+d\mathbf{K}_{scale}+d\mathbf{C}_{coupl}+d\mathbf{S}_{mis}\right)\mathbf{T}+\mathbf{v}\longrightarrow\mathbf{a_T}=\frac{1-\varepsilon}{\left(m_{dry}+m_p\right)}\mathbf{R}\tilde{\mathbf{T}} \tag{3.29}$$

where efficiency parameter ε is a multiplicative factor. In [7], considering x-axis alignment only the reduced active set has been reported. Regardless the selected specific parameterization, the introduced variable corresponds to a stochastic process augmentation (as for perturbation parameters of eq.(3.29)) where mechanization deviation carries the uncertainty content on the actuation model in the estimation process. They are the fundamental tools to correctly determine our effective knowledge of propagated or estimated orbital error bound in case of controlled applications (II.3-C).

III.2 OBSERVATION MATHEMATICAL MODEL

This section addresses mathematical and functional architecture of MEONS Generic Observer Module. Referring to scheme in Figure II-15, this block is responsible to properly interface all the sensing sources and then process their measurements in accordance to the correspondent reconstruction patterns. Even sharing some features and state space criteria with the propagation task, Observer has been designed as a standalone module, since it copes with a different phase of the general prediction-correction structure (II.3). The application of modular decomposition and selectable model allows managing intermittent raw data acquisition as well as different kind of GNSS measurement combinations.

A. Observation model modular decomposition and intermittent measurement processing

The modular structure of the observation model still follows the approach of decomposing the right hand side as a linear combination of nonlinear models expressed in function of the generalized state vector. The nonlinear contributions decomposition can be expressed, with notation similar to eq.(3.16), by the following representation:

$$\mathbf{Y}_k = \mathbf{H}(\mathbf{X}_k) \rightarrow \begin{cases} \mathbf{H}(\mathbf{X}) = \delta D\mathbf{X} + \sum_{1...m}^{p} \varepsilon_p E_p N_p(F_p \mathbf{X}_{extend}) \\ \mathbf{X} = \{\mathbf{x}, \mathbf{u}, \mathbf{p}, t\} \qquad \mathbf{Y} = \{\mathbf{y}_1, \mathbf{y}_2, ..., \mathbf{y}_i\} \qquad \mathbf{X}_{extend} = h_1 \circ h_{2...} \circ h_q(\mathbf{X}_{extend}) \end{cases} \tag{3.30}$$
$$Datapool = t_1 \circ t_{2...} \circ t_r(Datapool) \qquad Datapool_i = \{\mathbf{Z}_k, L_{1...m}, \mathbf{X}_{extend}\} \qquad \mathbf{Z} = \{\mathbf{z}_1, \mathbf{z}_2, ..., \mathbf{z}_j\}$$

$\mathbf{Y}_k$ represents the image of measurement pattern, while $\mathbf{Z}_k$ refer to the effective sensor data. The ε_p factor and matrix E_p represent respectively the enabling/disabling factors and participation coefficient matrix of the model vector N_p to the system dynamic right hand side. δ and D are the linear counterpart of ε and E , while F is the state participation matrix mapping the components of the augmented state $\mathbf{X}_{extend}$ to the correspondent model local set. Functions $h(\cdot)$ and $t(\cdot)$ defined in eq. (3.30) respectively represent internal and external interface modules: their significance and utilization is the same of the propagation step. Actually, the three different functional blocks of modules $N_p(\cdot)$, internal interfaces $h(\cdot)$ and external interfaces $t(\cdot)$ can be recognized and define the observer update main cycles. Similarly to propagation design, the switching and arrangement of each observable contribution as well as the local state feeding the modules can be managed run time by a dedicated observation controller function that set, for the current cycle, active/inactive models and interfaces.

Nevertheless, beyond those commonalities, some differences can be found in the specific customization of the functions wrt the measurement processing problem. Firstly, the observable equations do not rely with an integration step, so the algebraic equation set in eq.(3.30) can be evaluated once per measurement acquisition cycle. The extended state of the observer can include a contraction of the propagation state and in general incorporates additional data provided by the sensors (Figure II-15). For instance, in case of GNSS raw measurement management, this relies to SVs ephemeris and tuning parameters, i.e. the C/N0, provided by the receiver (see III.2-C).

Focusing on GNSS observables, their processing shall be applied per each SV in view, so a great benefit derives from the reusability of the implemented measurement model $N_p(\cdot)$. Actually, the modular and switching capability of eq.(3.30) deals with the GNSS tracking issue. The observable equations (i.e. pseudorange, carrier phase and Doppler of III.2-B) can be initialized whether on the basis of the full constellation approach or on the basis of effective receiver channels allocation, considering the active model set in accordance to in view SVs indexes (SVID). This thesis implements the first approach [64],

which is very flexible with respect to constellation augmentation to the expense of a superior memory allocation. The second one can be implemented in the proposed architecture in order to reduce the memory allocation, but higher computational load on the controller have to be considered in term of active/inactive model management and auxiliary data dispatching.

A superior involvement of external interfaces shall be considered, since they are used to perform combination of basic measurements as well as computation of the residuals $\mathbf{r = Z - Y}$ for estimation and monitoring purposes (IV.1-C).

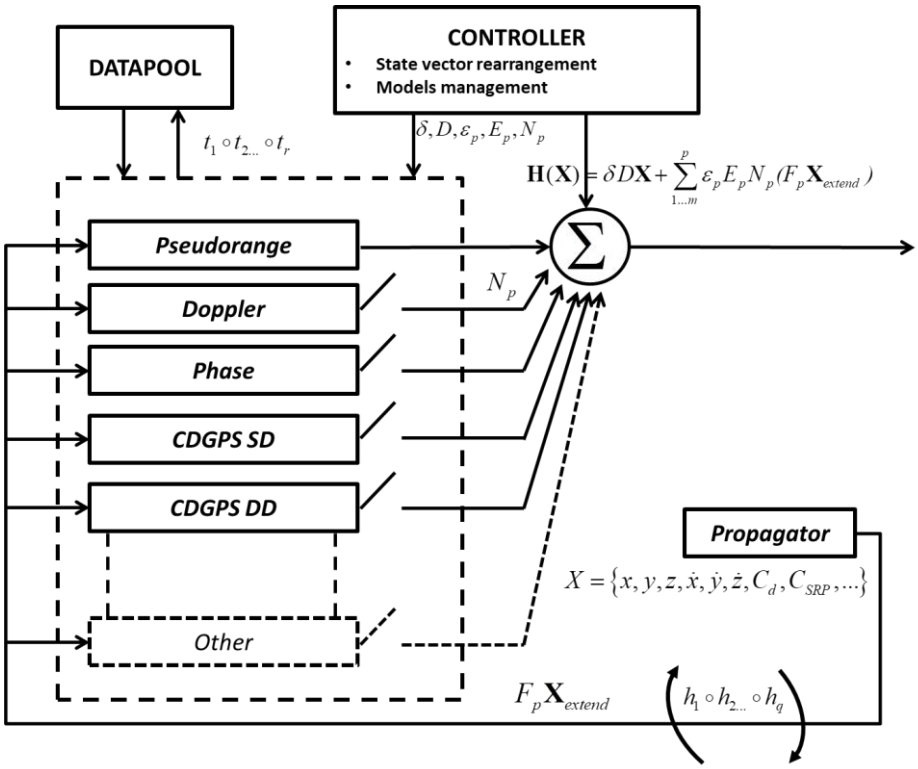

Figure III-7 Generic Observer Block Diagram

Moreover, the observer shall cope with variational approach and model estimation techniques based on Taylor series approximation (II.3):

$$\mathbf{y}(t_k) \approx \mathbf{h}(\mathbf{x}_{ref}(t_k), \mathbf{p}_{ref}, \mathbf{u}_{ref}(t_k), t_k) + \left[\frac{\partial \mathbf{h}(\ )}{\partial \mathbf{x}}\right]\delta\mathbf{x} + \left[\frac{\partial \mathbf{h}(\ )}{\partial \mathbf{u}}\right]\delta\mathbf{u} + \left[\frac{\partial \mathbf{h}(\ )}{\partial \mathbf{p}}\right]\delta\mathbf{p} \tag{3.31}$$

so the online computation of measurement model Jacobians J_D, J_E, J_F shall be performed:

$$J_D = \left[\frac{\partial \mathbf{h}(\ )}{\partial \mathbf{x}}\right], J_E = \left[\frac{\partial \mathbf{h}(\ )}{\partial \mathbf{u}}\right], J_F = \left[\frac{\partial \mathbf{h}(\ )}{\partial \mathbf{p}}\right] \tag{3.32}$$

The same derivative decomposition used for the propagation task can be considered in order to associate each module with the correspondent Jacobian contribution:

$$J_H(\mathbf{X}) = \frac{\partial \mathbf{H}(\mathbf{X})}{\partial \mathbf{X}} = \mathbf{H}(\mathbf{X}) = \delta D + \sum_{1...m}^{p} \varepsilon_p E_p \frac{\partial N_p (F_p \mathbf{X}_{extend})}{\partial (\mathbf{X})} \tag{3.33}$$

Basically, internal interfaces $h(\cdot)$ are used for this aim and Jacobians information is included in the external datapool for estimation purposes.

All described issues results in an open architecture of the MEONS Generic Observer module, whose synthetic representation is provided in Figure III-7. The following features have been included:

- The observer handle the extended state $\mathbf{X}$ as well as auxiliary information necessary to build measurement reconstruction patterns
- As for propagation, Jacobians relative to observable equations are provided for estimation purposes and model linearization
- The introduced modular decomposition allows performing intermittent measurement by switching and sorting state and measurement vectors. The system can be considered compatible with Multisensor or Multiple measurements (e.g. provided by the same sensor or by a distribution/network of sensors) configurations
- The system complexity can be continuously upgraded by adding a new non-linear measurement model $N_p(\cdot)$, interface or Jacobian contribution, which becomes dynamic system modules stored in a proper model database.

This database is the object of the following sections. The use of notation $N_p(\cdot)$, $h(\cdot)$ and $t(\cdot)$ will be used to address, when necessary, all models within their own functional set.

B. Single- and dual-frequency GPS measurements for absolute and relative POD

A summary of the selectable measurement database is provided in table Table III-3 and, similarly to propagation, a mathematical description of the primitive observation equation is postponed in Appendix B. In the same Appendix is also reported the reference notation that will be used hereafter to indicate GNSS systematic and stochastic errors due to legacy timing and signal propagation degradation effects. For the sake of brevity clarification on GNSS theoretical background is omitted and the lecturer can refer to [11], [14], [65], [66], where are addressed signal and geometrical measurement treatment as well as hardware analogical and digital processing issues. Here the focus is on the GNSS measurement combination experienced during the design of the navigation system for the POD applications investigated in CHAPTER V. Navigation solution for Sentinel-1 HIL application (V.2) aims at compensating ionospheric path delay error ΔI_j [11] (Appendix B) by using L1 and L2 GNSS measurements availability. The ionofree linear combination has been adopted for the on-board solution (V.2) in accordance to the follow equations [11]:

$$\begin{aligned}\rho_{FLC} &= \frac{f_1 f_1}{f_1 f_1 - f_2 f_2}\rho_{L1} - \frac{f_2 f_2}{f_1 f_1 - f_2 f_2}\rho_{L2} = \\ &= \frac{f_1 f_1}{f_1 f_1 - f_2 f_2} r_r^s - \frac{f_2 f_2}{f_1 f_1 - f_2 f_2} r_r^s + \frac{f_1 f_1}{f_1 f_1 - f_2 f_2}\eta_1 - \frac{f_2 f_2}{f_1 f_1 - f_2 f_2}\eta_2\end{aligned} \tag{3.34}$$

The MEONS ionofree interface $t(\cdot)$ processes the currently available pseudoranges ρ_{L1}, ρ_{L2} (Appendix B) derived from the same tracked satellite and removes the systematic error by weighting them with the related f_1, f_2 frequencies.

Aiming to achieve CDGPS compatibility for multiple spacecraft navigation (II.2-D), MEONS includes GNSS differential measurement within its observation database (Table III-3) .In more details, a precise baseline (i.e. the tridimensional relative distance) determination can be accomplished by the combination of the measurement of the two available receivers, i.e. one that hosted on the formation elements.

A representation of the involved geometry is provided in Figure III-8 .

MEONS Generic Observer modules	
Absolute and differential measurements	
• Pseudorange for GPS L1/L2 signals (N_1) • Pseudorange for Galileo E1 signals (N_2) • Pseudorange rate/Instantaneous Doppler for GPS L1/L2 signals • Pseudorange rate/Instantaneous Doppler for Galileo E1 signals • Carrier Phase for GPS L1/L2 signals • Carrier Phase for Galileo E1 signals • Legacy Ionofree combination (t_1) • Legacy GPS SVs ephemeris/position and time corrections interface (t_2)	• Legacy Galileo SVs ephemeris/position and time corrections interface • J2000, ECEF and WGS-84 transformations with IERS bulletin setting • Single Difference combination (CDGPS) • Double Difference combination (CDGPS) • Lever arm interface for antenna displacement and phase centre calibration
Optionally selectable modules (currently under development)	
• Legacy Graphic combination • Triple frequency combination (new E5/L5 scenario) • Other ranging (Time Of Arrival) and Doppler measurements (i.e.TDRSS, Satellite Interlink, inverse GPS) • Celestial observations(emergency mode)	

Table III-3 GNSS measurements model database

Under proper assumptions [65], some systematic errors can be considered common to both sensors and deleted by difference wrt the same in view satellite. This feature is immediately perceived deriving the carrier phase Single Difference equations:

$$\begin{aligned} SD_j^{AB}(t) &= \left(\phi_j^A(t) - \phi_j^B(t)\right)\lambda = \\ &= r_j^A(t) - r_j^B(t) + c\left(\Delta t^A(t) - \Delta t^B(t)\right) + mp_j^{AB}(t) + \beta_j^{AB}(t) + A_j^{AB}(t) \end{aligned} \tag{3.35}$$

as the direct difference between absolute phase measurements (Appendix B). referring to the same SV (j index in eq.(3.35)). Ephemeris and constellation errors are removed, but other degradation sources are still present, even though reduced to their not common residuals (i.e. differential receiver time $\Delta t^A(t) - \Delta t^B(t)$). The error contribution can be fatherly reduced differentiating two SD observations with respect to two different SVs (j,k indexes). The following DD equations are obtained:

$$\begin{aligned} DD_{j,k}^{AB} &= SD_j^{AB}(t) - SD_k^{AB}(t) = \left(\left(\phi_j^A(t) - \phi_j^B(t)\right) - \left(\phi_k^A(t) - \phi_k^B(t)\right)\right)\lambda = \\ &= \left(r_j^A(t) - r_j^B(t)\right) - \left(r_k^A(t) - r_k^B(t)\right) + mp_{j,k}^{AB}(t) + \beta_{j,k}^{AB}(t) + A_{j,k}^{AB}(t) \end{aligned} \tag{3.36}$$

In this case the relative receiver clock bias computation is not necessary, avoiding a dedicated compensation procedure. The main issue of the CDGPS observation model relies to the determination of the ambiguities. Considering DD observation, they are the unknown number of integer cycles $A_{j,k}^{AB}(t)$ that must be estimated in order to extract from the measured fractional part the entire ranging information.

When the integer ambiguities are identified, a very high accuracy estimation of relative positioning can be achieved from double difference equations [65]. This variable introduces the issue of considering in the general GNSS tracking problem a variable dimension state vector. Actually, ambiguities shall be handled at propagation and observation level by using auxiliary process augmentation for additional bias tracking (3.36). All the insights on the associated estimation issue are discussed in IV.1-D.

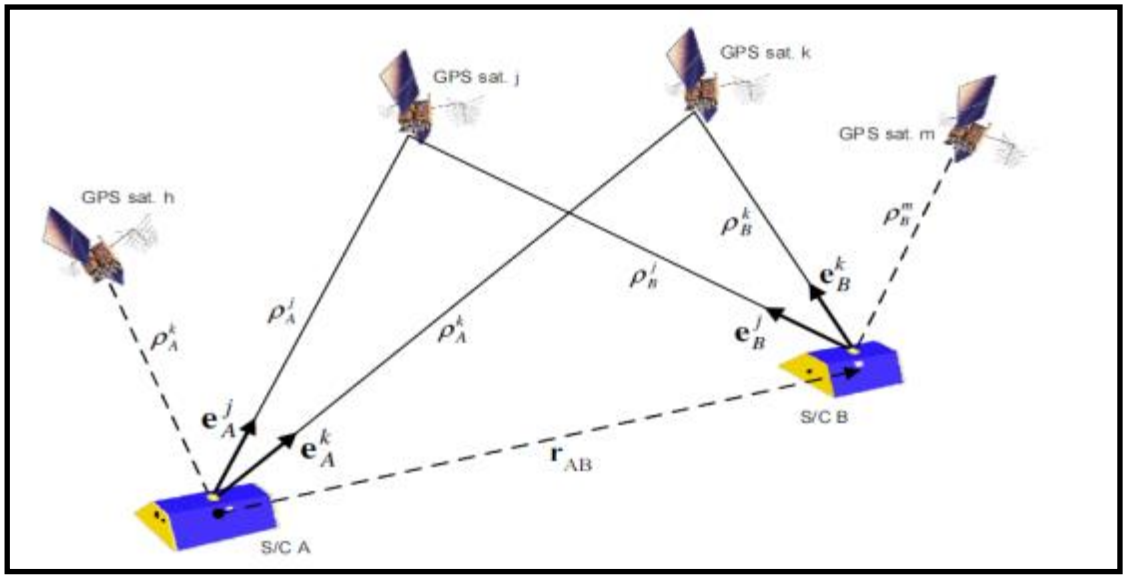

Figure III-8 GNSS differential measurement geometry

It is worthy to note that GRAPHIC [54] solution can do the same ionospheric path delay compensation of ionofree combination with a reduced level noise. However, the use of phases relies on GRAPHIC bias estimation and proper carrier phase data management as for the CDGPS ambiguity tracking. In case of Sentinel-1 HIL data processing the ionofree Pseudorange/Doppler solution has been preferred in term of robustness and lower complexity. GRAPHIC solution is mandatory when high accuracy shall be achieved with single frequency receivers. Nevertheless, also in single frequency applications, the GRAPHIC processing should be viewed as an enhanced possibility that is enabled to refine positioning when it has been already reached a coarse accuracy range with unbiased measurements. During high dynamic and bad visibility conditions pseudoranges and Doppler measurements can offers a robust conservative starting configuration. Alternative GRAPHIC approach, as well as other frequency combination can be considered in future works (Table III-3) and integrated in MEONS solution to cope with high accuracy POD with single frequency devices.

C. Multi-constellation/Multi-antenna measurements and GNSS high orbit peculiarities

Beyond compatibility of the system with conventional POD measurement processing, this work investigates GNSS Multi-constellation/Multi-antenna schemes and high orbit issues introduced by the G2G mission study case (V.3). High orbit peculiarities shall be properly modelled at simulation level as visibility and measurement errors drive MEONS navigation performance in high orbit. Specifically, the receiver model, integrated in the high fidelity GSS simulator (Appendix C), shall generates visibility conditions and raw data in accordance to the high orbit issues allowing to appreciate differences wrt the conventional LEO case. This topic is addressed here, since it influences MEONS GNSS measurements ($\mathbf{Z}$) and observation vector ($\mathbf{Y}$) processing. The analysis focuses on the specific autonomous LEO-MEO rising case and GNSS scenario assumptions relies on G2G mission study case. However, all the arrangements can be extended to other EOR scenarios and SSV orbit regime.

High orbit scenario peculiarities

The low power of GNSS signals at high altitudes has two fundamental effects:

- limits the capability of the GNSS receivers to lock on and track GNSS signals, whose carrier to noise ratio, C/N0 reduces (II.1-A)
- Affect the navigation accuracy: raw measurements noise increase as signal power decrease and other

systematic degradation sources shall be reviewed.

As described in Appendix C, the GSS Geometrical Visibility selection step detect all the GNSS signals coming from the GNSS satellites not overshadowed by the Earth disk and falling into the FOV of the receiving antenna. However, for high orbits, the subset shall be properly refined in accordance to signal power sensitivity, namely defined Electronic Visibility selection. The basic assumption is one that defined in (II.1-A): a GNSS satellite can be tracked when its signal is characterized by a C/N0 value stronger than the receiver acquisition and tracking thresholds (see also [20]). GSS implements such Carrier-to-noise ratio evaluation by using the following link budget for the generic i-th GNSS satellite:

$$\left(C/N_0\right) = P_{Tx}^i + G_{Tx}^i + G_{Rx} - L_{FS} - L_{SVf} - L_{IL} - L_{IMP} - \left(K_B + T_{Sys}\right) \tag{3.37}$$

where dB unit is assumed. In eq.(3.37), P_{Tx}^i is the power transmitted by the i-th GNSS satellite and G_{Tx}^i is the relevant antenna gain in the direction of the GNSS line of sight. G_{Rx} is the half-power receiver antenna gain (i.e hemispherical low-directivity antenna gain with 5° masking angle) whereas L_{FS} indicates free space loss factor:

$$L_{FS}^i = 20\log\left(\lambda/4\pi d^i\right) \tag{3.38}$$

where λ is signal wavelength, i.e. 19 cm for L1 GPS, and d^i is the distance from GNSS satellite to GNSS receiver antennas. The link budget of eq. (3.37) takes into account filtering and modulation loss of the SVs signal L_{SVf} as well as the insertion loss factor L_{IL} due to spacecraft and cable accommodation. The implementation loss factor representative of potential effects of receiver mounting and manufacturing is L_{IMP} . Finally, receiver noise is computed considering Boltzmann's constant, K_B, and a system noise equivalent temperature T_{Sys} [14].

As stated in SSV geometry analysis (II.1-A), a crucial role in high orbit GNSS signal simulation is played by the antenna patterns of GNSS satellites. During high orbit phases, GNSS signal availability is allowed by spillover of signals coming from the opposite side of the Earth, and hence through the side-lobes of transmitting antennas [67]. The legacy (block IIA) and improved gain patterns (block IIR, [68]) are used herein for GPS satellites. This work deals also with Galileo satellite, so a first order approximation of the expected patterns is evaluated from [69]. Figure III-9 shows antenna patterns implemented for GPS block IIA, GPS block IIR and Galileo as single off-boresight angle function by averaging among different satellites and azimuths angles.

At GSS simulation level, standard GNSS measurement models [11], must be reviewed. Let us consider reference pseudorange and Doppler observables (eq.(B.1) and eq.(B.2) in Appendix B). This work relies on [70], where the contribution of using broadcast ephemeris ΔE_i has been refined by considering a non-white error source affecting the knowledge of SVs data. Specifically, the range and range-rate measurement Δr_i and $\Delta \dot{r}_i$ are assumed to be evaluated by the receivers considering GNSS satellite position, $\Delta \mathbf{X}_i$, velocity, $\Delta \mathbf{V}_i$ and clock δa_0^i deviations as:

$$\begin{aligned} \Delta r_i &= \left\| \left(\mathbf{X}_i(t_{Tx}) + \Delta \mathbf{X}_i(t_{Tx})\right) - \mathbf{r}(t_{Rx})_{SC} \right\| \qquad \Delta t_{Tx}^i = \delta a_0^i(t_{oe}) \\ \Delta \dot{r}_i &= \left\langle \mathbf{e}_i(t_{Tx}), \mathbf{V}_i(t_{Tx}) + \Delta \mathbf{V}_i(t_{Tx}) - \dot{\mathbf{r}}(t_R) \right\rangle \end{aligned} \tag{3.39}$$

where t_{Tx} and t_{Tx} are the epochs of signal transmission and reception, respectively and t_{oe} is the current time of ephemeris.

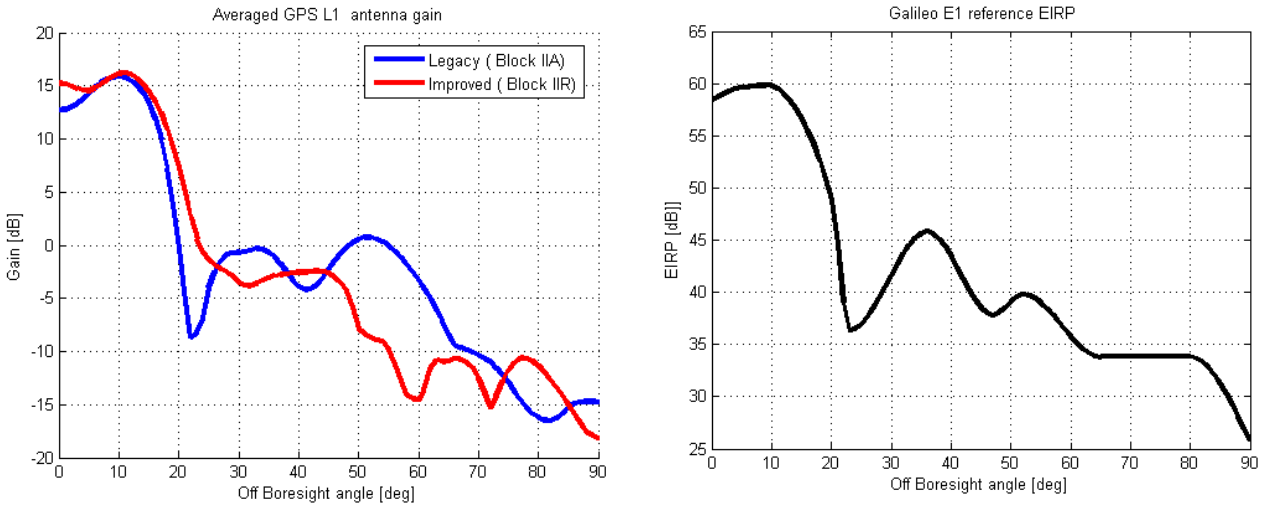

Figure III-9 Antenna directivity for GPS block IIA/GPS block IIR (left), and Galileo satellites (right).

This effect is generally mitigated by the redundancy of navigation data allowing on one sight to have fast SVs ephemeris update and on the other to eventually discard satellite with high SISRE [71].

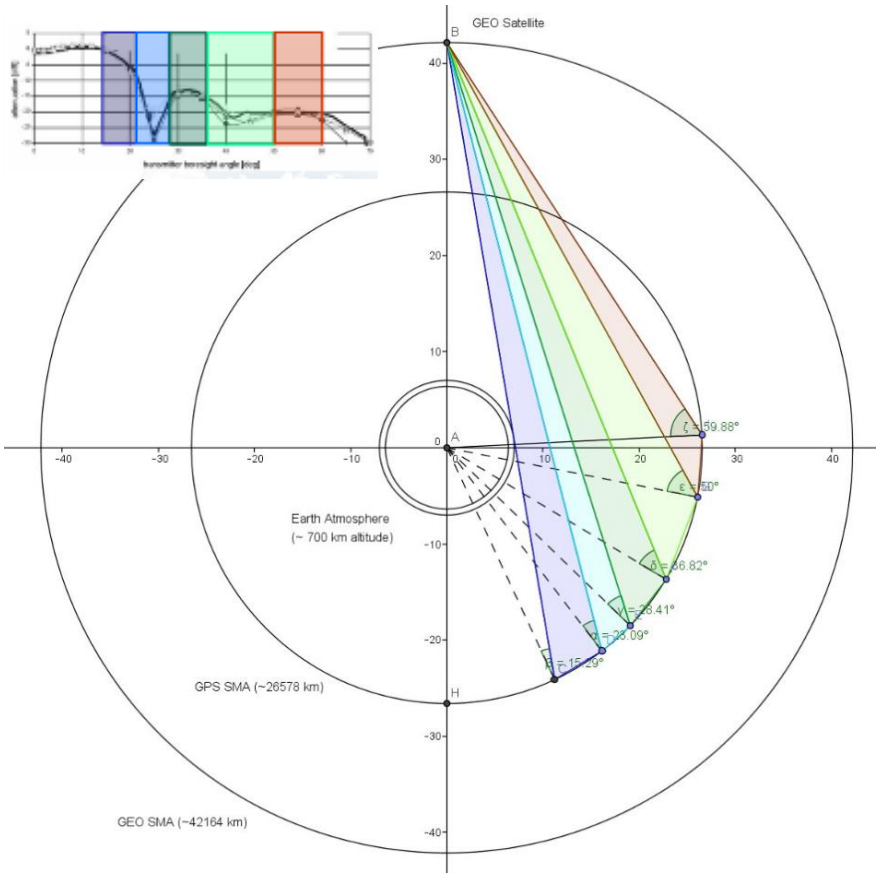

Figure III-10 Complete geometry model, GEO planar case, considering antenna pattern sections and increased Earth disk overshadowing due to ionosphere [20]

In high orbit, an all-in view processing approach is necessary and long ephemeris propagation (II.1-B) can be experienced.

The values of ephemeris $\Delta\mathbf{X}_i$ $\Delta\mathbf{V}_i$ error follow those proposed in [70] but a realization is extracted each two hours from the normal distribution that assumes the error level in [70] as 3σ value. This approach leads to a bias error ranging from 0.1m to 4.5m which is kept constant for a two-hour long window. Since this error source is strongly correlated in time it is expected to jeopardize estimation performance much more than other error sources characterized by equivalent magnitude but not correlated in time, e.g. receiver noise and propagation path error. According to eq.(3.39), only the zero-order term of broadcast clock calibration error δa_0^i , is simulated.

The clock error can be treated as bias term in the same manner as ephemeris bias, but it is herein simulated as a residual random error.

As far as ionospheric delay is concerned, it is important to remark that high orbit scenarios, even considering low to high rising manoeuvre, start above 1000 km altitude, i.e. outside the most significant part of the ionosphere. In this scenario, an ionosphere delay is important only for those signal paths crossing Earth ionosphere. During the LEO phase, this occurs for GNSS satellites characterized by very low, negative elevation angles. During MEO phases, instead, GNSS signals generated by satellites that are very close to Earth disk, as seen from the receiver, can experience strong ionospheric delays. In such conditions, standard ionospheric models, e.g. Klobuchar's [72] or Lear's [73], cannot be applied and specific techniques, such ray tracing or tomography must be used to provide the simulator with an accurate estimate of the ionospheric delay. For scenarios as G2G rising, the number of satellites that is affected by a significant ionospheric delay is, actually, quite low and negligible, so the following strategy is used for the high orbit simulation: Earth mask angle is incremented to include the whole Earth ionosphere (i.e. up to 1000 km altitude). In this way, GNSS satellites with a line of sight crossing Earth ionosphere are masked and the relevant signals are assumed not to be tracked by the receiver. It is important to remark that this solution can be also implemented in real-time by setting GNSS receiver masking angle parameters.

GSS simulator handles unmodeled contributions, as well as residuals of modelled ones (i.e. contribution for which random assumption apply) incorporating them within the User Equivalent Range χ_i (UERE) and Range Rate $\dot{\chi}_i$ Errors (UERRE) term (Appendix B). Residual ionospheric and timing effects ($\tilde{\Delta}t_{Tx}^i$, $\tilde{\Delta}I_i$) and multipath effects (MP_i) are generally taken into account in this term and modelled as additive ranging noise. Also measurement noise v_ρ (i.e. code and phase noises) is simulated as additive random contribution, but it is generated separately in order to take into account GNSS satellite elevation. Actually, in high orbit case, at least pseudorange random noise, which is the most relevant contribution for the considered scenarios, shall be evaluated wrt current C/N0. Referring to [14] and considering the reference target hardware [15] , the delay lock loop (DLL) can be generated by using the following standard deviation :

$$\sigma_{DLL} = \sqrt{\frac{B_n}{2\kappa(C/N_0)}\left(\frac{1}{B_{fe}T_c} + \frac{B_{fe}T_c}{\pi - 1}\left(D - \frac{1}{B_{fe}T_c}\right)^2\right)\left[1 + \frac{2}{T(C/N_0)(2-D)}\right]} \tag{3.40}$$

Where B_n is the noise loop bandwidth, T is the coherent integration time (see II.1-B), set, D is the correlator spacing set , B_{fe} is the front end bandwidth (i.e for L1/E1 24MHz) and T_c is the chip period [14]. Eq.(3.40) can be used for both GPS and Galileo, depending on the value of κ. Specifically, the standard deviation is scaled by a factor of $\kappa = 3$ for Galileo observables following [74].

GPS-Galileo measurements management and double antenna configuration

As stated in II.2 several mitigation solutions can be implemented in order to override high orbits and EOR GNSS visibility criticalities. In the case of G2G mission, the Galileo and GPS Multi-constellation approach and double antenna implementation are put in place in order to respectively cope with increased number of space vehicle and different geometry during rising phases. The Multi-constellation enhancement mainly relies on the simultaneous processing of raw measurements (pseudorange , Doppler) derived from GPS and Galileo constellations. One key goal of Galileo Program is to be fully compatible with the GPS system. Measures are being taken to ensure interoperability between the two systems. Primary interoperability factors being addressed are signal structure (shared bands), geodetic coordinate reference frame, and time reference system [62]. Precise timing is a fundamental part of GNSS like GPS, Glonass and Galileo. Each GPS satellite contains several atomic clocks and continually broadcasts its position and timing corrections relative to a common time scale (GPS Time System). In the same manner, each Galileo satellite contains, also, several atomic clocks and broadcasts its position and timing corrections relative to the internal Galileo System Time (GST) [75]. The main problem is that the two

time systems, GPS System Time and GALILEO System Time (GST), are not perfectly synchronized. The time difference between the two time scales is called GPS-to-GALILEO Time Offset (GGTO). To increase interoperability and compatibility between GPS and GALILEO it was agreed that both GPS and Galileo systems will compute and broadcast the mutual time offset between both system's time scales. This information is available in the Signal-in-Space (SIS) navigation message and enhances users' interoperability achievable with a combined receiver [75]. However, the most effective solution is to compute the GGTO including it in the navigation sequential estimation process, so considering it in the observation model of Galileo raw measurements. For this aim pseudorange and pseudorange-rate shall be referred to a unique reference time. Assuming GPS System Time as the common reference, the GPS and Galileo pseudrange measurement time line can be defined respectively by Figure III-11 and Figure III-12. As shown by relevant time tags defined in Table I-1 , both measurements have the same geometrical content:

$$\tilde{\rho} = c\left[\left(T_u^{'} + t_u\right) - \left(T_s + \delta t\right)\right] = r + c\left(\Delta t_r - \delta t + \delta t_D\right) \tag{3.41}$$

except for the introduced GGTO offset. Assuming the standard notation for signal propagation and timing error affecting the GNSS measurement (Appendix B) GPS and Galileo pseudoranges and pseudorange rate can be expressed in a compact manner as follow:

$$\begin{aligned} \rho_i &= r_i + c\Delta t + \alpha c\Delta t_{GGTO} - c\Delta t_{Tx}^i + I_i + MP_i + v_\rho \\ \dot{\rho}_i &= \dot{r}_i + c\Delta \dot{t} + \alpha c\Delta \dot{t}_{GGTO} - c\Delta \dot{t}_{Tx}^i + \dot{I}_i + \dot{MP}_i + v_{\dot{\rho}} \end{aligned} \tag{3.42}$$

where α is a coefficient corresponding to 1 for Galileo satellites and to zero for GPS ones.

T_s	system time at which the signal leaves the satellite;
t_u	system time at which the signal would have reached the user receiver in he absence of errors;
T_u'	system time at which the signal reaches the user receiver with δt_D
δt,	offset of the satellite clock from the system time
δt_D,	time offset due to the error not related with the satellite and receiver clocks
$t_u = \Delta t_r$,	offset of the receiver clock from the system time
$T_s + \delta t$,	effective satellite clock reading when the signal leaves the satellite
$T_u' + t_u$,	effective user receiver clock reading at which the signal reaches the user
Δt,	geometric range.

Table III-4 Relevant time tags for pseudorange measurement definition

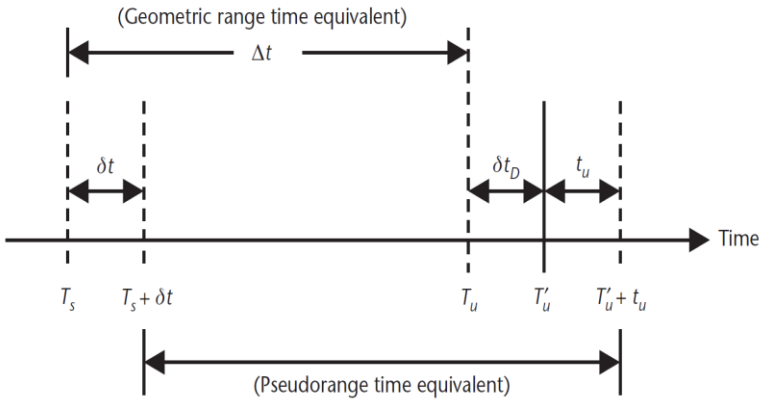

Figure III-11 GPS Time Line wrt GPS Time scale

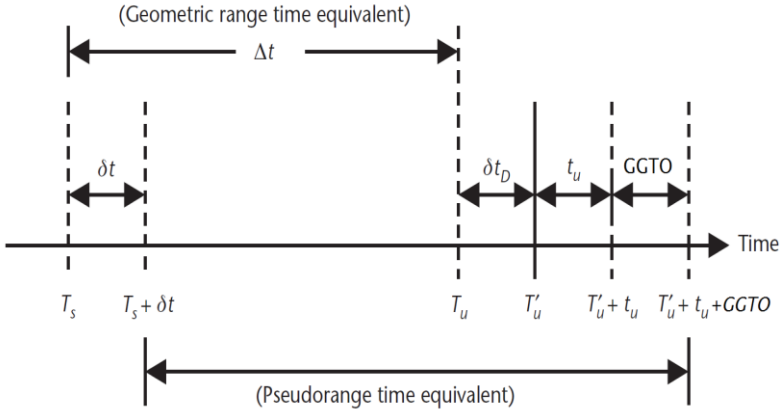

Figure III-12 Galileo Time Line wrt GPS Time scale

The several error sources are indicated with the proper index i as they rely on the specific SV from which signal propagate, hence they shall be considered different among GPS and Galileo measurements.

$$\dot{\mathbf{s}} = \mathbf{f}(\mathbf{s}, \mathbf{p}_{Pert}, \mathbf{p}_{Thrust}, t) = \begin{cases} \dfrac{d\mathbf{r}}{dt} = \dot{\mathbf{r}} \\ \dfrac{d\dot{\mathbf{r}}}{dt} = -\dfrac{\mu_{\oplus}}{r^3}\mathbf{r} + \mathbf{a}_{Pert}(\mathbf{r}, \dot{\mathbf{r}}, \mathbf{p}_{Pert}, m_p, \mathbf{o}_{att}) + \mathbf{a}_{Thrust}(\mathbf{r}, \dot{\mathbf{r}}, \mathbf{p}_{Thrust}, m_p, \mathbf{T}, \mathbf{o}_{att}) + \mathbf{w}_{\mathbf{a}} \\ \dfrac{\mathrm{d}(\Delta t)}{\mathrm{dt}} = \Delta\dot{\mathrm{t}} + \mathrm{w}_{\dot{\mathrm{t}}} \qquad \dfrac{\mathrm{d}(\Delta\dot{\mathrm{t}})}{\mathrm{dt}} = \mathrm{w}_{\ddot{\mathrm{t}}} \\ \dfrac{\mathrm{d}(\Delta t_{\mathrm{GGTO}})}{\mathrm{dt}} = \Delta\dot{t}_{\mathrm{GGTO}} + \mathrm{w}_{\dot{\mathrm{t}}_{\mathrm{GGTO}}} \qquad \dfrac{d(\Delta\dot{t}_{GGTO})}{dt} = w_{\ddot{t}_{GGTO}} \\ \dfrac{dm_p}{dt} = -\dfrac{\|\mathbf{T}\|}{g_0 ISP} \end{cases} \tag{3.43}$$

The extended system in eq. (3.43) is defined by indicating with Δt and $\Delta\dot{t}$ bias and receiver clock drift, as well Δt_{GGTO} and $\Delta\dot{t}_{GGTO}$ as GGTO bias and rate. Handling Multi-constellation raw measurement means considering in the reference propagated and estimated state vector at least 10 scalar variables:

$$\mathbf{x}(t) = \left\{\mathbf{r}, \dot{\mathbf{r}}, \Delta t, \Delta\dot{t}, \Delta t_{GGTO}, \Delta\dot{t}_{GGTO}\right\} \tag{3.44}$$

Although indicating the additional parameter as GGTO, the effective unknown of eq.(3.42) are the bias (A_{0G}) and drift (A_{1G}), which represents only the fractional part of the difference between GPS time and GST. Actually the complete relationship between the two system times is:

$$\begin{aligned} GGTO &= \Delta t_{System} = t_{Gal} - t_{GPS} = A_{0G} + A_{1G}\,\Delta t \\ \Delta t &= \left[TOW - t_{0G} + 604800\left(\left(WN - WN_{0G}\right) \bmod 64\right)\right] \end{aligned} \tag{3.45}$$

where t_{Gal} is the GST, t_{GPS} is the GPS system time;A_{0G} is the constant term of the GGTO;A_{1G} is the rate of change of the GGTO; TOW is the Time of the week; t_{0G} is the reference time for GGTO; WN is the GST Week Number; WN_{0G} is the Week Number of the GGTO reference.

During LEO-MEO orbit rising low/high altitudes GNSS visibility geometrical condition (II.1) does not occur within the same orbit as for GTO, but they are experienced, also for a long time, in different transfer phases. Below the constellation conventional GNSS geometry identifies as main antenna direction the closest one to the zenith; in high orbit the main antenna direction is one that points toward Earth. Even if the effective best mounting directions is an important design issue to be considered also taking into account spacecraft possible envelope [20] , it is clear that at least two opposite antennas is the suitable solution. The needs is opposite wrt formation flying because GNSS antennas shall receive signals from the higher number of uncommon GNSS satellites:

$$\{SV_1, SV_2, ..., SV_n\}_{Ant\_1} \cap \{SV_1, SV_2, ..., SV_n\}_{Ant\_2} = \varnothing \tag{3.46}$$

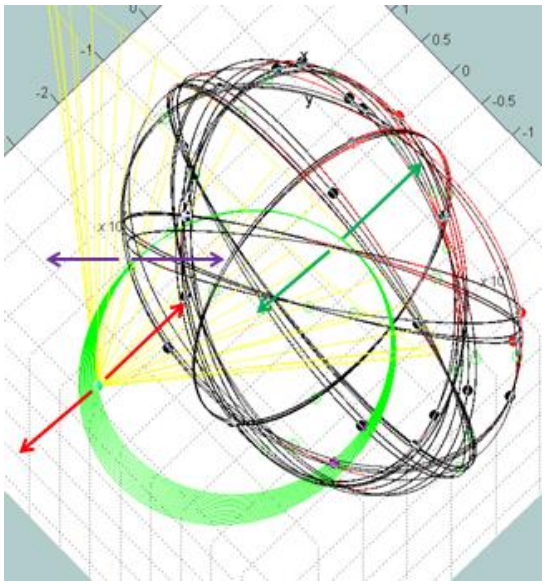

Figure III-13 GSS Double Antenna Geometry Simulation for GTO case

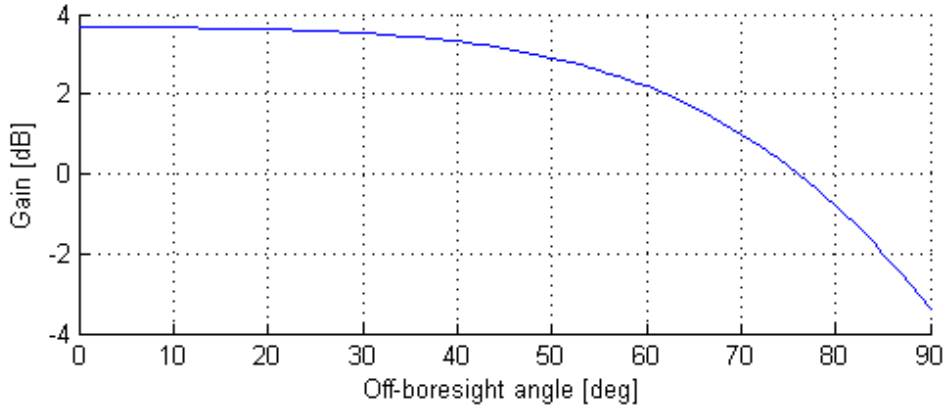

Figure III-14 Receiver antenna with hemispherical pattern

A couple of non-overlapping field of view (FOV) antenna is a robust solution, since they realizes a quasi-spherical FOV (assuming Figure III-14 hemispherical pattern each) less sensitive to attitude excursion. Multi-antenna configuration has some impact on the MEONS task. Managing tracking list with two different sources introduces the necessity to configure observer controller and interfaces. Moreover calibration issues shall be considered for raw measurement processing in accordance to different antennas displacement. Lever arm compensation interface has been introduced to reduce the measurements with respect to the same spacecraft reference point (e.g. CoG):

$$\mathbf{r}(t_{Rx})_{ANT} = \mathbf{r}(t_{Rx})_{SC_{CoG}} + R\left(q_{BRF\,2\,ECI}\right)\mathbf{l} \tag{3.47}$$

This contribution is generally negligible when the error is high, but fine fixing of the position during good visibility condition is positive also for long term propagation start-up. In addition, Multi-antenna solution generally introduces delays due to different cable length and transmission signal path. These ranging errors are compensated by hardware preliminary calibration, but residuals errors can be still present. This contribution can be eventually adsorbed as colored noise affecting pseudorange and Doppler observation models in the same manner of the ranging biases introduced hereafter for constellation errors.

Measurement bias and systematic error handling

It has been shown that several systematic errors can affect the GNSS measurement, whose model, if not properly calibrated, significantly deviates from the assumption of unbiased and uncorrelated observations. Among the different sources that can be considered, this work deals with the contribution of broadcast ephemeris in accordance with what proposed in [70]. In eq.(3.39) $6n$ Independent biases; i.e. 3 positions, 3 velocities for each tracked satellite have been introduced:

$$\left\{\Delta\mathbf{X}_1, \Delta\mathbf{X}_2, ..., \Delta\mathbf{X}_n, \Delta\mathbf{V}_1, \Delta\mathbf{V}_2, ..., \Delta\mathbf{V}_n\right\}_{6nx1} \tag{3.48}$$

Specifically, assuming the maximum expected projection along the line of sight [71] as upper bound of the ephemeris error distribution, the equivalent ranging error corresponding to those biases can be represented as a single variable per measurement, corresponding to $2n$ ranging and ranging rate deviations:

$$\mathbf{p}_{range} = \left\{\Delta\varepsilon_1, \Delta\varepsilon_2, ..., \Delta\varepsilon_n, \Delta\dot{\varepsilon}_1, \Delta\dot{\varepsilon}_2, ..., \Delta\dot{\varepsilon}_n\right\}_{2n} \tag{3.49}$$

This error is the responsible of solution offset in precise absolute navigation positioning. Moreover, such

contribution, due to their time correlation, cannot be easily handled as white noises by the navigation filter. As a result, the measurement error contribution can be easily underestimated within an estimation process. As for propagation internal parameters variables, it shall be possible also for measurement to augment the system via proper processes carrying information on systematic errors uncertainty content [76] . Each observable can be once more formulated as:

$$\mathbf{y} = \mathbf{h}\left(\mathbf{s}, \mathbf{p}_{range}\right) = \begin{cases} \rho_i = \left\| \left(\mathbf{X}_{SV_i} \right) - \mathbf{x}_{SC} \right\| + c\Delta t_R + \alpha c \Delta t_{GGTO} + \Delta\varepsilon_{SV_i} + \chi_i + \nu_{\rho_i} \\ \dot{\rho}_i = \left\langle \mathbf{e}_{\mathbf{x}_{SV_i}}, \mathbf{V}_{SV_i} - v_{SC} \right\rangle + c\Delta t_{_{SV_i}} + \alpha c \Delta \dot{t}_{GGTO} + \Delta\dot{\varepsilon}_{SV_i} + \dot{\chi}_i + \nu_{\dot{\rho}_i} \end{cases} \tag{3.50}$$

where $\Delta\varepsilon_{SV_i}$ and $\Delta\dot{\varepsilon}_{SV_i}$ are the uncertain parameters representing broadcast ephemeris error and $\chi_i, \dot{\chi}_i$ (UERE,UERRE) incorporate the rest of residual stochastic contributions. It is important to note that the introduced parameter set can be generalized for other applications [76], intending them as uncalibrated ranging and range rate errors. Actually, the term $\mathbf{p}_{range}$ represent a useful tool that can be exploited to adsorb several type of unmodeled systematic contributions (i.e. residual ionosphere delay error in single frequency applications or hardware channel biases), which cannot be easily handled by using pseudorange and Doppler measurement random errors $v_\rho, v_{\dot{\rho}}$. However , it shall be reminded that, as for ambiguity bias in the differential model, this vector varies in accordance to current SVs ID set. A reordering issue is present, but differently from ambiguities, it relies on intermittent unmodeled non-white tracking errors.

III.3 AUXILIARY TOOLS FOR DYNAMIC MODEL ANALYSIS

A. Design methods for Precise Orbit Determination and navigation preliminary error budget

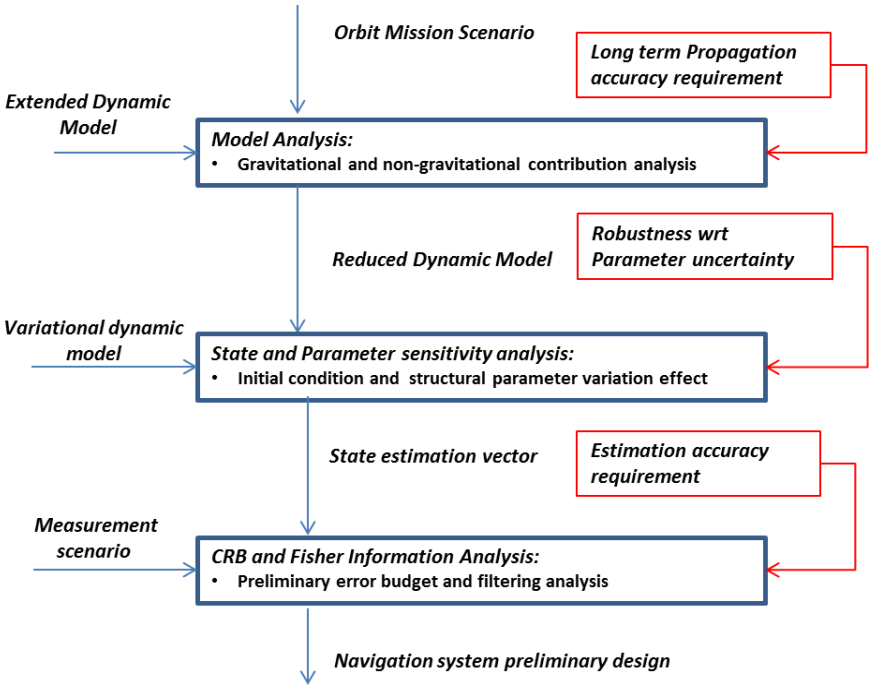

Figure III-15: Orbit Determination system design logic

In the initial project phase of [3], the reconfigurable model architecture of MEONS has been exploited to identify a design work logic [77] capable to support future implementation and tuning in wide range of applications. Specifically, a sensitivity analysis tools has been developed in order to analyse the dynamic process and expected performances in both propagation and estimation tasks taking into account the presence of uncertain parameters. The design logic block diagram is defined in Figure III-15. The following main issues are considered:

1) orbit propagation and dynamic model definition by force model contribution analysis
2) identification and inclusion in the state vector of most influencing parameters via sensitivity analysis
3) preliminary error budget and navigation performance evaluation based on Fisher Information Matrix

The long term propagation accuracy drives the first step of the analysis: the extended force model can be reduced to the suitable one by neglecting or tuning contributions which undergo below a defined propagation error threshold. As described in [78], evaluating a variety of acceleration contributions by enabling/disabling the correspondent propagation module, the gravitational and non-gravitational perturbation ranking can be performed for a wide range of orbit regimes. Second analysis step carries out the proper sensitivity analysis of parameter variations. The force model analysis reduces the critical parameters to the feasible subset (belonging to force model not neglected), the sensitivity analysis investigates the most effective ones. Actually, this kind of assessment points out specific mission phases where the considered parameters are dominant and typically better observable for implementing calibration procedures [79] . Moreover, the sensitivity wrt the initial conditions can be also performed and exploited to assess position accuracy and measurement update criticalities. The selected model and state augmentation are used to perform the last assessment. It provides a preliminary evaluation of the efficiency of the developed propagator, when included within a recursive estimation process. The selected figure merit (Figure III-15) is the Fisher Information Matrix (FIM), which is mostly used to evaluate the maximum achievable performances [80] and inner critical properties of estimation, as inverse representation of the Cramer-Rao Lower Bound. Using the nominal trajectory, the coefficients provided by the variational equation defined in eq.(3.13) can be exploited to evaluate recursively [81] a local

representation of the posterior CRLB. Hereafter a simple High Orbit Determination case is considered. However, the approach can be extended to higher complexity cases in order to confirm expected properties and limits of the adopted propagation and filtering process before implementing it.

B. Orbit perturbation and sensitivity analysis for variable orbit regime

The main output of the force model analysis is to determine if a particular perturbation contributes to the majority of the difference to the overall solution. The analysis is carried out by comparing the baseline two-body orbit propagation with the perturbed one on a defined time window. This comparison, starting from the same initial condition and parameter set, considers the trajectory deviation, defined in term of 3D difference:

$$\Delta_{3D} = \left\| \mathbf{X}_{pert} - \mathbf{x}_{ref} \right\| \tag{3.51}$$

as a measurement of the model truncation error. The choice of the propagation horizon can be critical. It should be at least in agreement with prediction requirements that usually indicate a survival level guaranteeing system safety against sensor failure or ground system outage. In general, a suitable multiple of the orbital period should be selected in order to point out trends and harmonic contents of the injected perturbation. The developed tool provides compact error statistics evaluated on the last propagation period [78]. The force model comparison sequence can be accomplished by the following setups:

1. *Two-body plus different non-central gravity field setting*
2. *Two-body plus atmospheric drag*
3. *Two-body plus solar radiation pressure (SRP)*
4. *Two-body plus third body effects*
5. *Two-body plus albedo and infrared radiation (or other second order perturbations)*

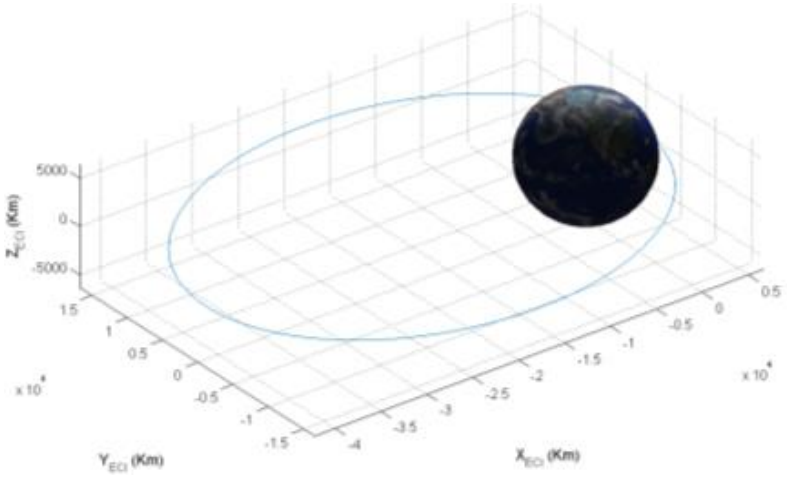

Figure III-16 Highly Elliptical Orbit for telecommunication satellite injection

In the case of gravity-field analysis the comparison with respect to closest considered harmonic is taken into account being more effective than that to the two-body problem. It is worth noting that each test checks a different portion of the problem under consideration. The nominal configuration is provided by erasing force model in such a way that the accuracy and complexity constraints are compliant with mission requirements. The test case considered to show MEONS analysis procedure results is an highly eccentric orbits, i.e. the first injection orbit type selected for NEOSAT and G2G missions (Figure III-16)

In [77] some LEO and GEO examples have been provided, but high elliptical (data setting is defined in Table III-5) are usually among the most difficult orbits to model because they have very high velocities in the atmosphere, enhancing the effect of atmospheric drag, and they spend long periods of time at apogee where the third body and solar radiation pressure forces can influence the orbit. It allows to design propagation for wide range altitude application due to the nonhomogeneous action of force models.

S/C Propagation Setting		
Starting date	y_i, m_{i-},d_i	2015y 06m 21d
Starting eccentricity, RAAN and Inclination	e_i, Ω_i, i_i	0.7292, 0.3°, 6°
Cd and Cr	Cd Cr	2.2,1.
Lateral/Frontal Ballistic coefficient	Al/m, Af/m	0.04, 0.04
Model setting	-	Reduced DSS propagation model

Table III-5 Highly Elliptical Orbit Propagation Data

The output of force model analysis is shown in Figure III-17 and Figure III-18. A period of 2 days has been considered in order to point out the mean motion effect of 38000 seconds. In general, gravity is the largest single perturbation source. The peaks/valleys are associated with atmospheric entry/exit and satellite eclipse/sunlight.

The albedo is very negligible instead of third body effect which is of the order of the lower non-spherical gravitational force. Mean and standard deviation are evaluated over the last period within the one day requirement.

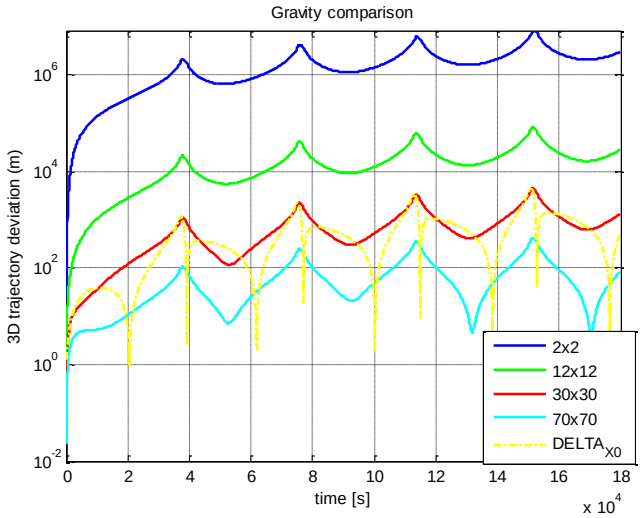

Figure III-17 Gravity order comparison analysis for high elliptical orbit scenario

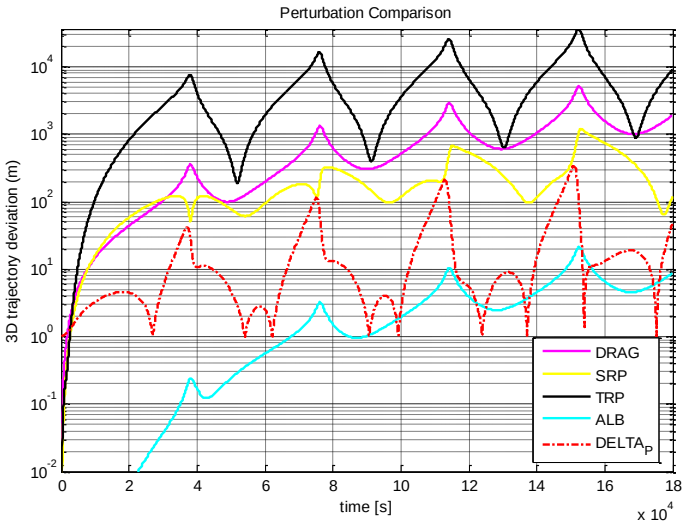

Figure III-18 Perturbation comparison analysis for high elliptical orbit scenario

	Mean for the period 38000s-76000s	Std for the period 38000s-76000s
2x2	1204962.94	727081.49
12x12	11384.91	7596.65
30x30	502.84	446.30
70x70	52.21	51.01
Drag	286.59	240.76
SRP	153.38	38.61
TRB	3561.20	3496.45
ALB	0.66	0.63

Table III-6 Force Model Ranking Analysis

The force model ranking is easily to accomplish by looking at the data reported in Table III-6. It allows one to derive the preliminary navigation dynamic model setting based on the inclusion of the following force models **F** :

- 30x30 Non-spherical Earth Gravity Field order
- Third body motion
- Drag Force Model
- Solar radiation pressure model

70x70 harmonic degree gravitational force can be neglected. In the same manner the albedo effect will not be included.

The trade-off results coincide with MBPM defined in (III.1): the analysis has been just performed aiming to support compatibility of current MEONS propagation setting with extended altitude variable orbit regime. The error budget derived from the dynamic reduction does not consider yet effects due to hypothesis of perfect knowledge of initial condition and force model parameters (e.g. CD, CR, surfaces, etc). Local parametric sensitivity analysis (PSA) [51] can be now performed by using eq.(3.13). framework. Actually, the target coefficients can be expressed as:

$$\partial \mathbf{x}(t)/\partial \mathbf{x}(t_0) \to \Phi(t,t_0) \qquad \partial \mathbf{x}(t)/\partial \mathbf{p}(t_0) \to \Psi(t,t_0) \tag{3.52}$$

that correspond to the relevant blocks of the generalized state transition matrix of eq.(3.11). Multiplying coefficients with the target initial error or parameter deviation in t_0 provides a first order budget of the error due to a persistent variation along the whole time span $[t_0,t]$:

$$\Delta\mathbf{X}(t) = \Phi(t,t_0)\Delta\mathbf{P} \qquad \Delta\mathbf{X}(t) = \Psi(t,t_0)\Delta\mathbf{X}_0 \tag{3.53}$$

If the analysis is restricted to a small finite time windows or within the integration step (i.e. $\Phi(t_k,t_0)$ and $\Psi(t_k,t_0)$). The result for a very small deviation $\Delta\mathbf{X}_0 = 0.17m$ (3D) drastically influences trajectory error Figure III-19 as it defines orbit energetic content. As concern model parameter variation, the C_D and C_R coefficients are the natural candidate to be analysed by the sensitivity tool in order to completely define the weight of Drag and SRP. For $\delta CD = 0.22, \delta CR = 0.13$, which correspond to 10% variation, the sensitivity integral produces trajectory modification higher then neglected force models (Figure III-18) suggesting the necessity to take into account them in the error budget. Sensitivity evaluated on a local time span representative of short time variation points out mission phase peculiarities. Figure III-19 shows 3D trajectory variation due to different parameter deviation for C_D and C_R on low altitude and high altitude orbit arcs. The sensitivity confirms that C_D can be directly related to the density envelope excited by the spacecraft passage at atmosphere lower layer, so its influence is constrained to the low altitude phases. The effect of C_R with respect to altitude is quite constant and it has been verified that it correctly drops to zero during the eclipse.

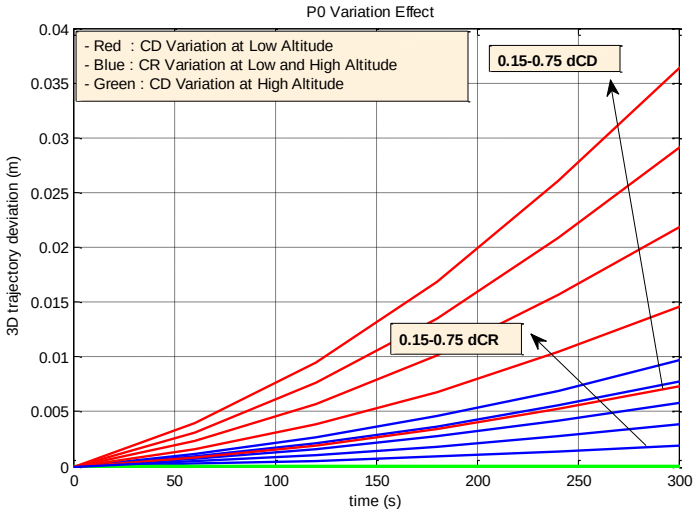

Figure III-19 State trajectory variation $\delta X(t)$ due to different CD and CR deviation (δP)

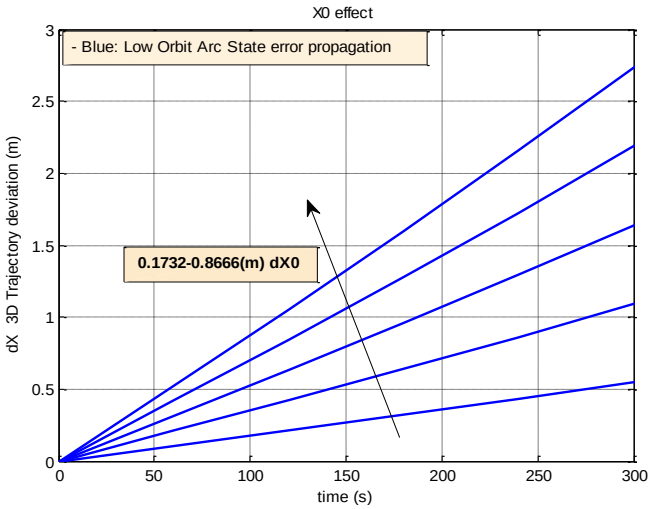

Figure III-20 State trajectory variation $\delta X(t)$ due to different initial state deviation δX_0

The same analysis can be done for state variation. Figure III-20 shows the sensitivity for the low earth orbit phase where the positioning is critical due to the most important change in the gravitational potential energy.

C. The posterior Cramer-Rao Bound utilization for orbit determination performance analysis

For the problem at hand, it is interesting to assess how well a state can be estimated. Concerning this, theoretical performance bounds represent an important design tool. This kind of bounds allows one to evaluate whether target performance specifications are feasible or not. The Cramer-Rao lower bound (CRLB) is a useful metric that can be used to cope with this problem. For time-invariant statistical models, CRLB provides a lower bound on the variance of any unbiased estimator of an unknown constant parameter p of that particular statistical model. Specifically, according to the Cramer-Rao inequality:

$$CRLB = \Im^{-1} < Cov\{p_n, p_m\} \tag{3.54}$$

CRLB can be expressed as inverse of the FIM. Limiting to the second order mean square error (MSE, see [80]), the index can be used as a design tool to predict the best achievable performance even before the system is built. CRLB arises as a valuable analysis tool to assess performance also in case of dynamical estimators. However, as described in [81], it has to be properly derived in its a-posteriori version also known as PCRLB. More general results for the index exist for non-linear non-Gaussian systems and its efficient computation has been provided in [82]in term of recursive evaluation of the FIM. A restriction to non-linear discrete filtering with Gaussian additive noise has been implemented within MEONS software analysis package. It is based on the recursive generation of the CRB following [81] :

$$\begin{aligned} &\Im_k = H_k R_k^{-1} H_k + \left[Q_{k-1} + \Phi_k \Im_{k-1}^{-1} \Phi_k^T \right]^{-1} \\ &\Phi_k = \nabla_{x-1} f(x_{k-1}) \qquad H_k = \nabla_{x_k} h(x_k) \\ &w_k \text{ -} N\left[0, Q_k\right] \qquad \nu_k \text{ -} N\left[0, R_k\right] \end{aligned} \tag{3.55}$$

where the sequential $\Im_k$ (FIM) update correspond to time variant CRLB by inversion of Eq.(3.55). All matrices are computed by using MEONS model and Q_k, R_k are the so called process and measurement noise covariance whose significance will be detailed in the following chapter. Actually, it will be clear in IV.1 that Eq.(3.55), is very close to the information form [48] of linearized Kalman filters (e.g. EKF) but in spite of standard covariance update, the recursive performance estimation has to be evaluated onto the exact state .

In [77] for comparative purposes, a conventional ground based non-autonomous high orbit scenario has been considered. In this case, the on-board propagator is fed by predicted PVT computed on the basis of tracking station observations. The following OD problem has been considered for the target high elliptical orbit:

$$\begin{cases} \dot{\mathbf{x}} = F(\mathbf{x}, \Delta C_D, \Delta C_R, t) + w_x \\ \Delta \dot{C}_D = -\alpha \Delta C_D + w_{CD} \\ \Delta \dot{C}_R = -\alpha \Delta C_R + w_{CR} \\ \qquad y_k = H_k(\mathbf{x}, t) + \nu \end{cases} \tag{3.56}$$

F is the model selected by the previous analysis steps, the parameter processes are set as first order Gauss-Markov process with time constant assessed at nominal orbital periods, the spectral density matrix Q(s) are set in order to obtain via procedure described in IV.3 the expected discrete variances Q_{k-1}:

$$Q(\tau)=\left\{q_{Vel}=5\cdot10^{-7}\,{}^{m^2}\!/_{s^3}\qquad q_{CD}=0.22(1-e^{-2\alpha_{CD}})\qquad q_{CR}=0.13(1-e^{-2\alpha_{CD}})\right\} \tag{3.57}$$

The matrix H is representative of the ground station observation comparable to a set of predicted Orbit State Vectors set allowing to update S/C PVT at 60s. The following accuracy is considered:

$$H=\begin{bmatrix} I_{6x6} & 0_{6x2} \\ 0_{2x6} & 0_{2x2} \end{bmatrix} \qquad R_k=\begin{bmatrix} \sigma_x^2 I_{3x3} & 0 \\ 0 & \sigma_{\dot{x}}^2 I_{3x3} \end{bmatrix} \qquad \sigma_x=45\,m \qquad \sigma_{\dot{x}}=0.3\,m/s \tag{3.58}$$

The recursive application of eq.(3.55) with initial state covariance starting $\sigma_x=10\,m, \sigma_{\dot{x}}=0.01\,m/s$, leads to the OD 3D error shown in Figure III-21 . It shall be reminded that this curve indicates the maximum achievable performance of the OD system under the stated assumption, so an estimation process based on the same dynamic model and measurement assumption could perform at most with a 10 meter order accuracy. Further improvements rely on technological and operative issues as observation accuracy and update rate enhancement as well as flight model parameter calibration. Actually, a degradation of such contribution determines a variation of the bound that shall be controlled in accordance to the accuracy requirement.

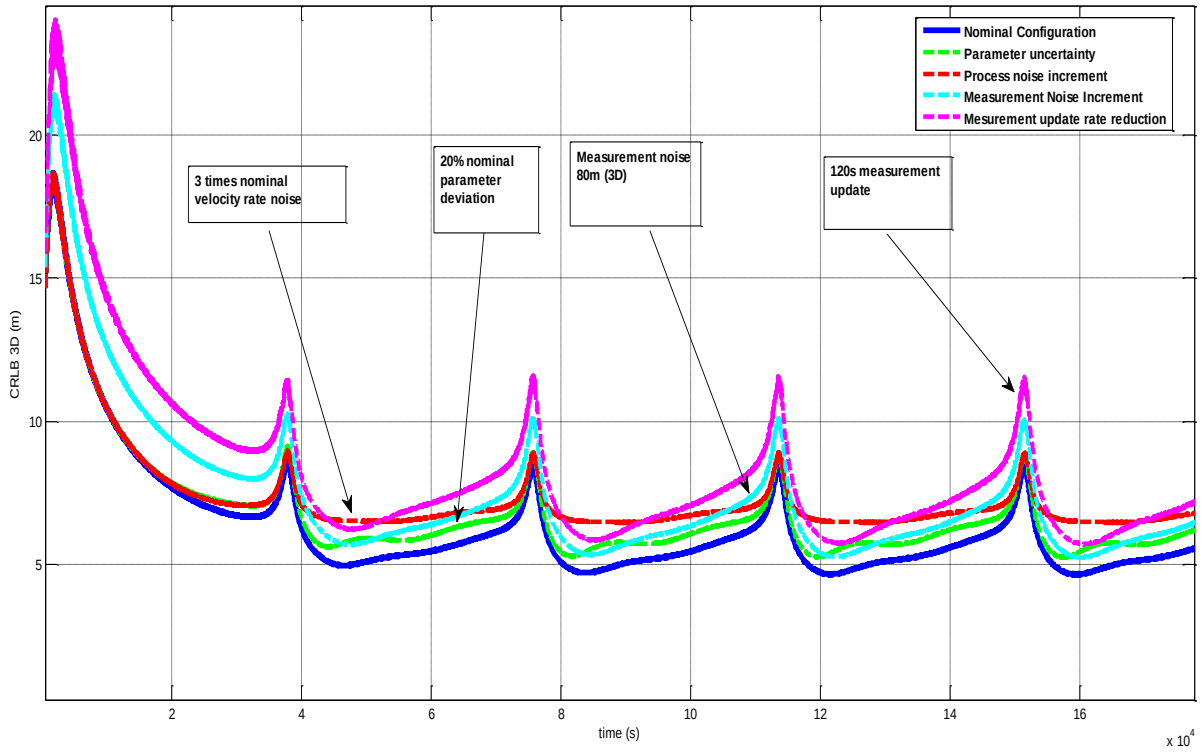

Figure III-21 Time Variant 3D CRB for High Elliptical Orbit OD problem

For the target case, the dynamics correctly map the highest state error at low orbit in accordance to sensitivity analysis. Basically, the most critical effect is certainly the measurement update rate: intermittent measurement can be critical for the estimation performance; so ON approach based on GNSS can be very advantageous in this sense (1Hz update). In conclusion dynamic model sensitivity analysis and preliminary CRB evaluation provides a useful method to define a preliminary error budget supporting the design of MEONS for OD and ON applications.

CHAPTER IV

ADVANCED TECHNIQUES AND CHALLENGING ASPECTS IN MODERN STATE ESTIMATION

IV.1 ADVANCED METHODS IN KALMAN FILTERING

Moving to the effective navigation filtering kernel development, the Bayesian system state estimate (II.3) procedure must correspond to an operational implementation of prediction and update integrals by using analytic or numerical approximation. Many authors have investigated this issue providing a wide range of approaches [45]. The MEONS current implementation deals with Kalman Filter Class Techniques, which are integrated within the Configurable Estimation Kernel. Specifically, the modern General Gaussian Kalman Filtering [44] (GGKF), is proposed as possible unified framework. Actually, Kalman filtering techniques still offers a wide range area of research: advanced solutions can be investigated and implemented in order to deal with specific orbit navigation issues.

As typically experienced in satellite GNSS-based navigation, non-linearity arises from both satellite dynamics and GNSS observation equations [66]. In the framework of GGKF toolset, at least, an Extended Kalman Filtering (EKF) solution has to be selected to deal with problem nonlinearity. Actually, EKF, demonstrating its compatibility with real time constraints, has been selected as MEONS baseline setting in continuity with first generation on-board LEO navigation systems [4]. However, this work try to override some limits of the conventional approach taking into account two main issues:

- the necessity to introduce filtering scheme improvements in order to properly handle further peculiarities introduced by the investigated scenarios (i.e. model parametric uncertainty, filter tuning)
- the possibility of mixing higher order solution and linearized one (i.e. EKF) on the basis of dynamic model nonlinear/linear substructure

Specifically, this section addresses four possible enhancements of [4]:

1) Marginalized Kalman Filtering for improved nonlinearities mitigation within competitive computational cost
2) Configurable Consider Filtering and State Augmentation for model uncertain parameter handling and error shaping
3) Maximum Likelihood Adaptive Filtering for autonomous covariance tuning
4) Variable State Dimension filtering for active/quiescent states and online model rearrangement

A. The General Gaussian Nonlinear Kalman Filtering solution for real time applications

The fundamental hypothesis introduced by the GGKF in the general Bayesian framework [44] is approximating filtering distributions as Gaussian:

$$p(\mathbf{X}_k \mid \mathbf{Y}_{1:k}) \simeq N(\mathbf{X}_k \mid \mathbf{m}_k, \mathbf{P}_k) \tag{4.1}$$

Computation of mean $\mathbf{m}_k$ and covariance $\mathbf{P}_k$ via moment matching allows reducing prediction-correction Bayesian procedure to computation of Gaussian integrals via numerical and closed form approximations. Actually, the recursive schemes provided in Table IV-1 can be obtained by using marginalization and conditioning properties for Gaussian distribution and nonlinear discrete state representation defined in

eq.(2.5). A rigorous demonstration of the Table IV-1 optimal estimation steps can be found in [44] for both not additive and additive noises. Here, the focus is on the possibility of using the GGKF paradigm for MEONS sequential filtering kernel design without referring to a specific implementation.

GGKF (additive noise)	GGKF (not additive noise)
Prediction:	**Prediction:**
$\mathbf{m}_k^- = \int \mathbf{f}_k(\mathbf{X}_{k-1}, t) N(\mathbf{X}_{k-1} \mid \mathbf{m}_{k-1}, \mathbf{P}_{k-1}) d\mathbf{X}_{k-1}$ $\mathbf{P}_k^- = \int \left(\mathbf{f}_k(\mathbf{X}_{k-1}, t) - \mathbf{m}_k^-\right)\left(\mathbf{f}_k(\mathbf{X}_{k-1}, t) - \mathbf{m}_k^-\right)^T \times N(\mathbf{X}_k \mid \mathbf{m}_{k-1}, \mathbf{P}_{k-1}) d\mathbf{X}_{k-1} + Q_k$	$\mathbf{m}_k^- = \int \mathbf{f}_k(\mathbf{X}_{k-1}, \mathbf{q}_{k-1}) N(\mathbf{X}_{k-1} \mid \mathbf{m}_{k-1}, \mathbf{P}_{k-1}) \times N(\mathbf{X}_k \mid \mathbf{m}_{k-1}, \mathbf{P}_{k-1}) N(\mathbf{X}_{k-1} \mid 0, \mathbf{Q}_{k-1}) d\mathbf{X}_{k-1} d\mathbf{q}_{k-1}$ $\mathbf{P}_k^- = \int \left(\mathbf{f}_k(\mathbf{X}_{k-1}, \mathbf{q}_{k-1}) - \mathbf{m}_k^-\right)\left(\mathbf{f}_k(\mathbf{X}_{k-1}, \mathbf{q}_{k-1}) - \mathbf{m}_k^-\right)^T \times N(\mathbf{X}_k \mid \mathbf{m}_{k-1}, \mathbf{P}_{k-1}) N(\mathbf{X}_{k-1} \mid 0, \mathbf{Q}_{k-1}) d\mathbf{X}_{k-1} d\mathbf{q}_{k-1}$
Update:	**Update:**
$\mu_k = \int \mathbf{h}_k(\mathbf{X}_k, t) N(\mathbf{X}_k \mid \mathbf{m}_k, \mathbf{P}_k) d\mathbf{X}_{k-1}$ $\mathbf{S}_k = \int \left(\mathbf{h}_k(\mathbf{X}_k, t) - \mu_k\right)\left(\mathbf{h}_k(\mathbf{X}_k, t) - \mu_k\right)^T \times N(\mathbf{X}_k \mid \mathbf{m}_k^-, \mathbf{P}_k^-) d\mathbf{X}_k + \mathbf{R}_k$ $\mathbf{C}_k = \int \left(\mathbf{f}_k(\mathbf{X}_{k-1}, t) - \mathbf{m}_k^-\right)\left(\mathbf{h}_k(\mathbf{X}_k, t) - \mu_k\right)^T \times N(\mathbf{X}_k \mid \mathbf{m}_k^-, \mathbf{P}_k^-) d\mathbf{X}_k$ $K_k = \mathbf{C}_k \mathbf{S}_k^{-1}$ $\mathbf{m}_k = \mathbf{m}_k^- + K_k(\mathbf{Y} - \boldsymbol{\mu}_k)$ $\mathbf{P}_k^+ = \mathbf{P}_k^- - K_k \mathbf{S}_k K_k$	$\mu_k = \int \mathbf{h}_k(\mathbf{X}_k, \mathbf{r}_k) \times N(\mathbf{X}_k \mid \mathbf{m}_{k-1}, \mathbf{P}_{k-1}) N(\mathbf{X}_{k-1} \mid 0, \mathbf{R}_{k-1}) d\mathbf{X}_k d\mathbf{r}_k$ $\mathbf{S}_k = \int \left(\mathbf{h}_k(\mathbf{X}_k, \mathbf{r}_k) - \mu_k\right)\left(\mathbf{h}_k(\mathbf{X}_{k-1}, \mathbf{r}_k) - \mu_k\right)^T \times N(\mathbf{X}_k \mid \mathbf{m}_{k-1}, \mathbf{P}_{k-1}) N(\mathbf{X}_{k-1} \mid 0, \mathbf{R}_{k-1}) d\mathbf{X}_k d\mathbf{r}_k$ $\mathbf{C}_k = \int \left(\mathbf{f}_k(\mathbf{X}_k, \mathbf{q}_{k-1}) - \mathbf{m}_k^-\right)\left(\mathbf{h}_k(\mathbf{X}_k, \mathbf{r}_k) - \mu_k\right)^T \times N(\mathbf{X}_k \mid \mathbf{m}_{k-1}, \mathbf{P}_{k-1}) N(\mathbf{X}_{k-1} \mid 0, \mathbf{R}_{k-1}) d\mathbf{X}_k d\mathbf{r}_k$ $K_k = \mathbf{C}_k \mathbf{S}_k^{-1}$ $\mathbf{m}_k = \mathbf{m}_k^- + K_k(\mathbf{Y} - \boldsymbol{\mu}_k)$ $\mathbf{P}_k^+ = \mathbf{P}_k^- - K_k \mathbf{S}_k K_k$

Table IV-1 General Gaussian Kalman Filtering schemes for optimal estimation [44]

Indeed, as stated in [44], the selected representation includes the following approaches:

- The Taylor series expansion methods that approximates the non-linear measurement and dynamic models by forming a Taylor series expansion at the nominal solution: Extended Kalman Filter (EKF) , Second Order Extended Kalman Filter (SOEKF) and higher-order linearization

- The numerical approximation method handling prediction and update integrals via numerical schemes : Cubature Kalman Filter (CUBKF), Unscented Kalman Filter (UKF), GHKF (Gauss Hermite Kalman Filter)

The GGKF analysis aims at pointing out MEONS state space model compatibility with both Taylor series and numerical approximation solutions. Actually, considering eq.(3.15), the augmentable state space model can provide both state transition matrix (together with correspondent Jacobians) and sigma points feeding respectively the linearized analytical solutions and the numerical integration methods. This thesis envisages EKF and UKF implementations (considering additive noise case). However, SOEKF, CKF and GHKF can be seen as other representative that can be optionally analysed in future trade-off. EKF and UKF final equations are reported in Table IV-2 together with hypothesis that must be introduced in order to address them within the general schemes of Table IV-1. The extended derivation of stochastic model linearization and Unscented Transformation (UT) peculiarities can be found in [44].

Hypothesis EKF

$$\mathbf{g}:\begin{cases}\mathbf{f}_k(\mathbf{X}_{k-1})\\ \mathbf{h}_k(\mathbf{X}_k)\end{cases}$$

$$\mathbf{X}\simeq\mathbf{m}\ +\delta\mathbf{X}\qquad \delta\mathbf{X}\sim N(0,\mathbf{P})$$

$$\mathbf{g}(\mathbf{X})=\mathbf{g}\ (\mathbf{m}\ +\delta\mathbf{X}\ )+G_{\mathbf{X}}(\mathbf{m}\ )\delta\mathbf{X}\ +o\ (\delta\mathbf{X}^T\delta\mathbf{X})$$

$$G_{\mathbf{X}}=\left.\frac{\partial\mathbf{g}(\mathbf{X})}{\partial\mathbf{X}}\right|_{\mathbf{X}=\mathbf{m}}\qquad E\left[\mathbf{g}(\mathbf{X})\right]\simeq\mathbf{g}(\mathbf{m})$$

$$E\left[\left(\mathbf{g}(\mathbf{X})-E\left[\mathbf{g}(\mathbf{X})\right]\right)\left(\mathbf{g}(\mathbf{X})-E\left[\mathbf{g}(\mathbf{X})\right]\right)^T\right]\simeq$$

$$\simeq G_{\mathbf{X}}E\left[\delta\mathbf{X}\delta\mathbf{X}^T\right]G_{\mathbf{X}}^T$$

Filtering Scheme

$$\mathbf{m}_k^-=\mathbf{f}_k(\mathbf{m}_{k-1},t)$$

$$\mathbf{P}_k^-=\Phi_{k-1}\mathbf{P}_{k-1}^+\Phi_{k-1}^T+\mathbf{Q}_{k-1}$$

$$\boldsymbol{\mu}_k=\mathbf{Y}_k-\mathbf{h}_k(\mathbf{X}_k,t)$$

$$\mathbf{C}_k=\mathbf{P}_k^-\mathbf{H}_k^T\qquad \mathbf{S}_k^{-1}=\mathbf{H}_k\mathbf{P}_k^-\mathbf{H}_k^T+\mathbf{R}_k$$

$$\Phi_{k-1}=\left.\frac{\partial\mathbf{f}_k(\mathbf{X})}{\partial\mathbf{X}}\right|_{\mathbf{X}=\mathbf{m}_{k-1}^+}$$

$$H_k=\left.\frac{\partial\mathbf{h}_k(\mathbf{X})}{\partial\mathbf{X}}\right|_{\mathbf{X}=\mathbf{m}_{k-1}^-}$$

$$K_k=\mathbf{C}_k\mathbf{S}_k^{-1}$$

$$\mathbf{m}_k=\mathbf{m}_k^-+K_k(\mathbf{Y}-\boldsymbol{\mu}_k)$$

$$\mathbf{P}_k^+=\mathbf{P}_k^--K_k\mathbf{S}_kK_k$$

Hypothesis EKF

$$\mathbf{g}:\begin{cases}\mathbf{f}_k(\mathbf{X}_{k-1})\\ \mathbf{h}_k(\mathbf{X}_k)\end{cases}\qquad \xi^{(i)}=\mathbf{g}(\chi^{(j)})$$

$$\chi^{(j)}=\mathbf{m}+K^{(j)}\sqrt{\mathbf{P}^{(j)}}\quad j=0....i+n$$

$$E\left[\mathbf{g}(\mathbf{X})\right]\simeq\sum_{i=0}^{2n}W_i\ \xi^{(i)}$$

$$Cov[\ ]=\sum_{i=0}^{2n}W_i\ \left[\left(\xi^{(i)}-E\left[\mathbf{g}(\mathbf{X})\right]\right)\left(\xi^{(i)}-E\left[\mathbf{g}(\mathbf{X})\right]\right)^T\right]$$

$$W_i=\frac{\kappa}{n+\kappa}\quad W_i=\frac{\kappa}{2(n+\lambda)}\quad W_{i+n}=-\frac{\kappa}{2(n+\lambda)}$$

$$K^{(0)}=0\quad K^{(i)}=\sqrt{n+\kappa}\quad K^{(i+n)}=\sqrt{n+\kappa}\qquad i=1...n$$

Filtering Scheme

$$\mathbf{m}_k^-=\sum_{i=0}^{2n}W_i\ \xi_k^{(i)}\qquad \xi_k^{(i)}=\mathbf{f}_k(\chi_{k-1}^{(i)},t)$$

$$\mathbf{P}_k^-=\sum_{i=0}^{2n}W_i\ \left(\mathbf{f}_k(\chi_{k-1}^{(i)},t)-\mathbf{m}_k^-\right)\left(\mathbf{f}_k(\chi_{k-1}^{(i)},t)-\mathbf{m}_k^-\right)^T+Q_{k-1}$$

$$\chi_k^{(j)}=\mathbf{m}_k^-+K^{(j)}\sqrt{\mathbf{P}_k^{(j)}}\quad j=0....i+n$$

$$\mu_k=\sum_{i=0}^{2n}W_i\ \zeta_k^{(i)}\qquad \zeta_k^{(i)}=\mathbf{h}_k(\chi_k^{(i)},t)$$

$$\mathbf{S}_k=\sum_{i=0}^{2n}W_i\ \left(\mathbf{h}_k(\chi_k^{(i)},t)-\mathbf{m}_k^-\right)\left(\mathbf{h}_k(\chi_k^{(i)},t)-\mathbf{m}_k^-\right)^T+R_k$$

$$\mathbf{C}_k=\sum_{i=0}^{2n}W_i\ \left(\mathbf{f}_k(\chi_{k-1}^{(i)},t)-\mathbf{m}_k^-\right)\left(\mathbf{h}_k(\xi_k^{(i)},t)-\mathbf{m}_k^-\right)^T$$

$$K_k=\mathbf{C}_k\mathbf{S}_k^{-1}\qquad \mathbf{m}_k=\mathbf{m}_k^-+K_k(\mathbf{Y}-\boldsymbol{\mu}_k)\quad \mathbf{P}_k^+=\mathbf{P}_k^--K_k\mathbf{S}_kK_k$$

Table IV-2 EKF and UKF scheme and relevant hypothesis for their derivation in the GGKF framework [44]

Beyond application of the filtering class within the orbit estimation and navigation applications of CHAPTER V, it is useful to provide additional insight and compare algorithms peculiarities by testing them on a simplified study case. Specifically, except for minor modification, the stochastic dynamic system, which will be considered for the rest of this chapter, is the following:

$$system1\ :\begin{cases}\dot{\mathbf{X}}=A\mathbf{X}+B\mathbf{U}+\mathbf{w}\\ y=h(\mathbf{X})+\mathbf{v}\\ \mathbf{X}_0=\begin{Bmatrix}X_0^1 & X_0^2\end{Bmatrix}^T\\ \mathbf{U}=\begin{Bmatrix}0 & a\cdot\bar{u}(t)\end{Bmatrix}^T\end{cases}\rightarrow\begin{cases}A_{2x2}=\begin{bmatrix}\sigma & \omega\\ -\omega & \sigma\end{bmatrix}\qquad B=I_{2x2}\\ h(\mathbf{X})=\left(X^1\right)^2+\left(X^2\right)\end{cases}\tag{4.2}$$

The dynamic model, also referred as System 1, is a second order oscillator [47] with complex conjugate eigenvalues fed by a step input of magnitude a. Measurement equation is designed in order to introduce

nonlinear effects on the first state component.

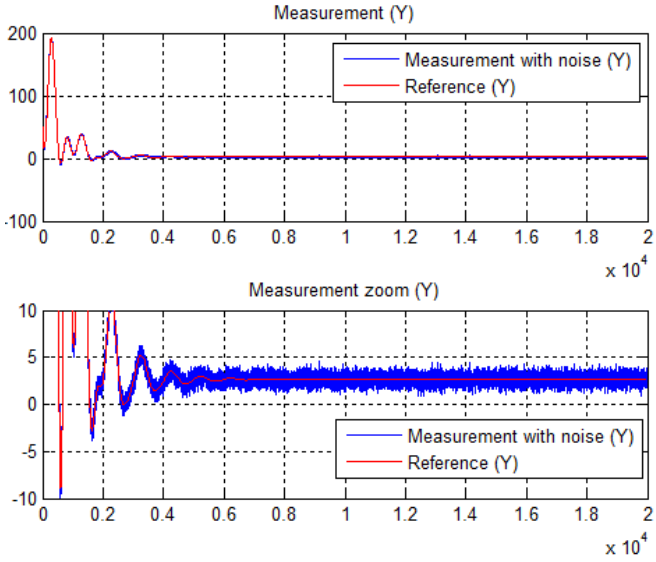

Figure IV-1 2D Simulated dynamic system noisy observation

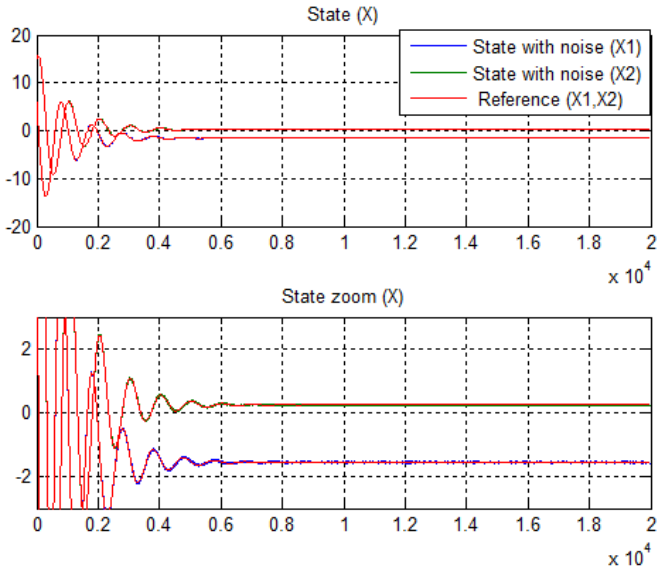

Figure IV-2 Simulated dynamic system state trajectory

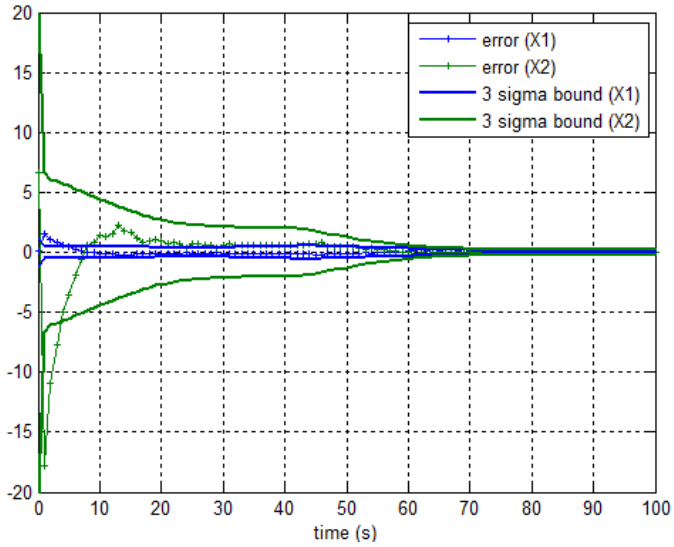

Figure IV-3 Transient Error of EKF approach for 2D state estimation example

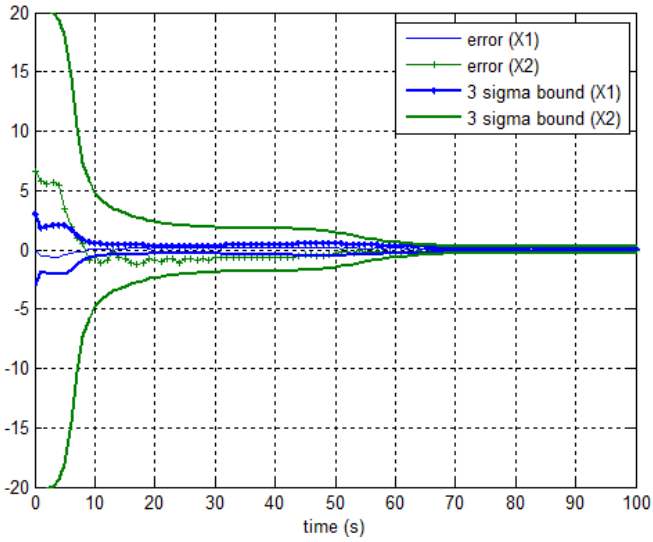

Figure IV-4 Transient Error of UKF approach for 2D state estimation example

The noises are generated in accordance to the Kalman filtering hypothesis as uncorrelated white noises with Gaussian random distribution:

$$E\{\mathbf{w}_k, \mathbf{w}_j^T\} = Q_k \delta_{kj} \qquad \mathbf{w}_k \sim N(\mathbf{0}, Q_k) \qquad \mathbf{v}_k \sim N(\mathbf{0}, R_k)$$
$$E\{\mathbf{v}_k, \mathbf{v}_j^T\} = R_k \delta_{kj} \qquad E\{\mathbf{w}_k, \mathbf{v}_k^T\} = 0 \qquad \forall k \tag{4.3}$$

A realization of the system is provided in Figure IV-1 and Figure IV-2 considering reference parameters defined in Table IV-3. A first use of simplified System 1 model is the comparison between the EKF and UKF approaches. A wide description of UKF properties can be found in [43]. Generally two main peculiarities are appreciated:

- Nonlinearities rise especially during the transient as long as the initial condition is far from the correct one or an ill posed initial covariance is set. Nonlinear approach generally avoids divergence and improves transient convergence properties.

- The covariance bound of nonlinear filter generally shows a higher consistency wrt the effective error allowing to better control the effective performance of the estimation.

An underestimated initial covariance $P_0 = diag\{9,49\}$ has been considered for problem in eq.(4.2) to better point out these issues. Figure IV-3 and Figure IV-4 confirm the expectations: even if the linearized approach converges, the transient of the EKF exhibit an overshoot and inconsistent result. Conversely the UKF covariance is able to properly represent the estimation error. As pointed out in [83] these properties can be useful for orbit estimation in critical initialization phases and during low rate measurement update conditions. However, this advantage shall be evaluated against increased computational cost that can be prohibitive. A trade off solution, the Marginalized approach, will be presented in the next section aiming at providing higher flexibility with respect to nonlinearities handling.

2D system data	
Parameter	**Symbol**
Dynamic and noises	$eig(A_{2x2}) = \begin{Bmatrix} -0.0010 + 0.0063i \\ -0.0010 + 0.0063i \end{Bmatrix}$ $\mathbf{w}_k \sim N(\mathbf{0}, Q_{11} = Q_{22} = 0.01^2)$ $\mathbf{v}_k \sim N(\mathbf{0}, R_{11} = 0.5^2)$
Initial Conditions and initial error (worst and best)	$\mathbf{X}_0 = \{6 \quad 15\}^T$
	$\delta\mathbf{X}_0^{worst} = 0.5\mathbf{X}_0$ $P_0 \rightarrow diag\{9,60\}$ $\delta\mathbf{X}_0^{best} = 0.1\mathbf{X}_0$ $P_0 \rightarrow diag\{0.36,2.25\}$
Input Data	$a = 0.01$
Relevant Covariance	$Q_k \rightarrow diag\{0.001,0.001\}$ $R_k \rightarrow \{0.5\}$

Table IV-3 2D test parameter setting

B. Conditionally linear substructure marginalization in nonlinear Kalman filtering

It is often advantageous, in mathematics, to exploit certain structures present in the problem under investigation. For instance, in the framework of Sequential Monte Carlo (SMC) methods, the Rao-Blackwellization technique [44], was proposed to fully exploit the availability of a linear, Gaussian sub-structure in the model equations. As deeply investigated in [46] the method is based on the marginalization principle. Its application on relevant moment integrals allows handling the solution applying Kalman filter for the linear state variables and a particle filter for the nonlinear state variables. The result valid for the SMC can be basically specialized also for GGKF with clear advantage in term of complexity reduction for high dimension system state vector. The attention is here focused on the possibility of combining model based and numerical approximations for nonlinear/linear (or nonlinear/linearized) mixed problems. For MEONS estimator, this corresponds on the possibility of combining Taylor series approximation and numerical integration methods in accordance to the target navigation model. This work deals with UKF/EKF combination, although other combination has been proposed within GGKF methods [84]. Specifically, this thesis refers to Marginalized Unscented Kalman Filter (MUKF) scheme proposed in [85]: this solution is very compact since it jointly calculates the mean and covariance of the corresponding nonlinear and linear subspaces. Utilization for navigation purposes can be found in the test case (V.4), but in general it is here proposed as possible future upgrade for all tightly coupled GNSS based solutions. The fundamental starting point to exploit such techniques is the possibility to identify within the general stochastic state space model of eq.(2.5) the following conditionally linear substructure:

$$\mathbf{X} \longrightarrow \begin{Bmatrix} \mathbf{x}_k^{nl} \\ \mathbf{x}_k^{l} \end{Bmatrix} \longrightarrow \begin{cases} \mathbf{x}_k = \mathbf{f}_k^{nl}(\mathbf{x}_{k-1}^{nl}) + F_k^{nl}(\mathbf{x}_{k-1}^{nl})\mathbf{x}_{k-1}^{l} + G_k^{nl}\mathbf{w}_k \\ \mathbf{x}_k^{l} = \mathbf{f}_k^{l}(\mathbf{x}_{k-1}^{nl}) + F_k^{l}(\mathbf{x}_{k-1}^{nl})\mathbf{x}_{k-1}^{l} + G_k^{l}\mathbf{w}_k \\ \mathbf{y}_k = \mathbf{h}_k(\mathbf{x}_k^{nl}) + H_k(\mathbf{x}_k^{nl})\mathbf{x}_k^{l} + V_k\,\mathbf{v}_k \end{cases} \tag{4.4}$$

Eq.(4.4) is generated by partitioning the state $\mathbf{X}$ in two sub-components $\mathbf{x}_k^{nl}$ and $\mathbf{x}_k^{l}$ representing the

state variables associated to model nonlinear and linear content. Actually, the linear substructure can be one that generated for Taylor Series Approaches (i.e. EKF) by linearizing along the estimated trajectory. Matrices F_k, G_k, H_k, V_k refers to STM operators and time derivative obtained in the frame of the discretized variational model generated by MEONS propagation and observation tools (III.1). Eq.(4.4) relies on first scheme of Table IV-1, but moving noise variable as augmented nonlinear states the hypothesis of additive noise can be removed. For the majority of the considered navigation problems, the full conditionally linear model generally applies and reduces in a further simplified form, namely referred as triangular model:

$$\mathbf{X} \longrightarrow \begin{Bmatrix} \mathbf{x}_k^{nl} \\ \mathbf{x}_k^{l} \end{Bmatrix} \longrightarrow \begin{cases} \mathbf{x}_k = \mathbf{f}_k^{nl}(\mathbf{x}_{k-1}^{nl}) + F_k^{nl}(\mathbf{x}_{k-1}^{nl})\mathbf{x}_{k-1}^{l} + G_k^{nl}\mathbf{w}_k \\ \mathbf{x}_k^{l} = F_k^{l}(\mathbf{x}_{k-1}^{nl})\mathbf{x}_{k-1}^{l} + G_k^{l}\mathbf{w}_k \\ \mathbf{y}_k = \mathbf{h}_k(\mathbf{x}_k^{nl}) + H_k(\mathbf{x}_k^{nl})\mathbf{x}_k^{l} + V_k\,\mathbf{v}_k \end{cases} \tag{4.5}$$

in addition, a further simplification can be generally introduced considering $F_k^{l}(\mathbf{x}_{k-1}^{nl}) = F_k^{l}$ not explicitly dependent by $\mathbf{x}_{k-1}^{nl}$ (i.e. control and parameter auxiliary processes in the MEONS eq.(3.2)) .This structure is compatible with the MUKF derivation of [85]: the triangular structure allows focusing marginalization criteria on the first equation considering the second as auxiliary. The key tools allowing passing from conventional UKF implementation to MUKF is the substitution in the reference scheme of Table IV-2 of UT with Marginalized Unscented Transformation (MUT). Let us incorporate the dynamic and observation equation of eq.(4.5) via the following general expression:

$$\mathbf{y} = g(\mathbf{x}) = \psi(\mathbf{x}^{nl}) + \gamma(\mathbf{x}^{nl})\mathbf{x}^{l} \qquad \psi = [f_k, h_k] \qquad \gamma = [F_k, H_k] \quad \mathbf{y} = [\mathbf{x}_{k+1}^{nl} \quad or \quad \mathbf{y}_k] \tag{4.6}$$

where the mean and covariance of the state can be also partitioned in the linear and nonlinear counterparts:

$$N\left(\mathbf{X}_k \mid \hat{\mathbf{X}} = \begin{Bmatrix} \hat{\mathbf{x}}_k^{nl} \\ \hat{\mathbf{x}}_k^{l} \end{Bmatrix}, \mathbf{P}_{\mathbf{x}} = \left[\begin{array}{c|c} \mathbf{P}^{nlnl} & \mathbf{P}^{nll} \\ \hline \mathbf{P}^{lnl} & \mathbf{P}^{ll} \end{array}\right]\right) \xrightarrow{\psi,\gamma} N\left(\mathbf{x}_k, \mathbf{y}_k \mid \mu = \begin{Bmatrix} \hat{\mathbf{X}}_k \\ \hat{\mathbf{Y}}_k \end{Bmatrix}, \mathbf{P}_{(\mathbf{X},\mathbf{Y})} = \left[\begin{array}{c|c} \mathbf{P}_{\mathbf{XX}} & \mathbf{P}_{\mathbf{XY}} \\ \hline \mathbf{P}_{\mathbf{YX}} & \mathbf{P}_{\mathbf{YY}} \end{array}\right]\right) \tag{4.7}$$

As for the UT transformation under joint Gaussian assumption the objective is to derive the mean and covariance of the transformed variable $\mathbf{y}$. The relevant moment integrals are defined in eq.(4.8). For the sake of simplicity, the demonstration is referred in [85]. However, applying marginalization wrt $\mathbf{x}_k^{l}$ the final solution for MUT can be obtained as reported in Table IV-4. Given that the MUT step is the same for propagation and correction steps, the approach reduces the number of requested sigma points $i = 1...n_{(nl)}$ in accordance to dimension of linear and nonlinear state partitions. The general marginalization principle does not introduce modification of the analytical problem, but the solution results can be different due to the different number of sigma points [85].

$$\begin{aligned}
\hat{\mathbf{Y}}_k &= \iint (\psi(\mathbf{x}^{nl}) + \gamma(\mathbf{x}^{nl})\mathbf{x}^{l}) N\left((\mathbf{x}^{l} \mid \mathbf{x}^{nl}) \mid \mathbf{m}_{\mathbf{x}^{l}|\mathbf{x}^{nl}}, \mathbf{P}_{\mathbf{x}^{l}|\mathbf{x}^{nl}}\right) \times N(\mathbf{x}^{nl} \mid \mathbf{m}_{\mathbf{x}^{nl}}, \mathbf{P}_{\mathbf{x}^{nl}}) d\mathbf{x}^{l}\, d\mathbf{x}^{nl} \\
\mathbf{P}_{YY}^{-} &= \iint \left(\psi(\mathbf{x}^{nl}) + \gamma(\mathbf{x}^{nl}) - \hat{\mathbf{Y}}_k^{-}\right)\left(\psi(\mathbf{x}^{nl}) + \gamma(\mathbf{x}^{nl}) - \hat{\mathbf{Y}}_k^{-}\right)^{T} \times N\left((\mathbf{x}^{l} \mid \mathbf{x}^{nl}) \mid \mathbf{m}_{\mathbf{x}^{l}|\mathbf{x}^{nl}}, \mathbf{P}_{\mathbf{x}^{l}|\mathbf{x}^{nl}}\right) N(\mathbf{x}^{nl} \mid \mathbf{m}_{\mathbf{x}^{nl}}, \mathbf{P}_{\mathbf{x}^{nl}}) d\mathbf{x}^{l}\, d\mathbf{x}^{nl} \\
\mathbf{P}_{XY} &= \iint \left(\begin{bmatrix} \mathbf{x}^{nl} \\ \mathbf{x}^{l} \end{bmatrix} - \hat{\mathbf{X}}_k^{-}\right)\left(\psi(\mathbf{x}^{nl}) + \gamma(\mathbf{x}^{nl}) - \hat{\mathbf{Y}}_k^{-}\right)^{T} \times N\left((\mathbf{x}^{l} \mid \mathbf{x}^{nl}) \mid \mathbf{m}_{\mathbf{x}^{l}|\mathbf{x}^{nl}}, \mathbf{P}_{\mathbf{x}^{l}|\mathbf{x}^{nl}}\right) N(\mathbf{x}^{nl} \mid \mathbf{m}_{\mathbf{x}^{nl}}, \mathbf{P}_{\mathbf{x}^{nl}}) d\mathbf{x}^{l}\, d\mathbf{x}^{nl}
\end{aligned} \tag{4.8}$$

However, this approximation is generally less significant with respect to the EKF one and it is more realistic as the conditionally structure approximate the complete nonlinear model.

MUT transformation	Nonlinear trasformed mean and covariances
$\left(\xi_k^{(i)}\right)_{nl} = \mathbf{g}_k(\chi_k^{(i)}, t) \qquad i = 1...n_{(nl)}$ $\left(\xi_k^{(i)}\right)_{l} = F_k^{l}\mathbf{b}$ $\chi_k^{(j)} = \left(\mathbf{m}_k^{-}\right)_{nl} + K^{(j)}\sqrt{\left(\mathbf{P}_k^{nl}\right)^{(j)}} \qquad j = 0....i + n_{(nl)}$ $\left(\mathbf{b}_k^{(i)}\right)_{l} = x_k^{l} + \left(\mathbf{P}_k^{lnl}\right)\left(\mathbf{P}_k^{nl}\right)^{-1}\left(\chi_k^{(i)} - \mathbf{m}_k^{-}\right)$ $K^{(0)} = 0 \quad K^{(i)} = \sqrt{n+\kappa} \quad K^{(i+n)} = \sqrt{n+\kappa}$	$\mu_k = \sum_{i=0}^{2n} W_i\, \xi_k^{(i)} \qquad \xi_k^{(i)} = \left\{\left(\xi_k^{(i)}\right)_{nl}, \left(\xi_k^{(i)}\right)_{l}\right\} \qquad i = 1...n_{(nl)}$ $\mathbf{S}_k = \sum_{i=0}^{2n} W_i \left(\xi_k^{(i)} - \mu_k\right)\left(\xi_k^{(i)} - \mu_k\right)^T + R_k$ $\varsigma = \left\{\chi_k^{(j)}, b\left(\chi_k^{(j)}\right)\right\}$ $\mathbf{C}_k = \sum_{i=0}^{2n} W_i \left(\varsigma - \mathbf{m}_k^{-}\right)\left(\xi_k^{(i)} - \mu_k\right)^T$

Table IV-4 MUT transformation and MUKF moments evaluations [85]

The MUKF has been tested on the System 1 and compared with UKF.

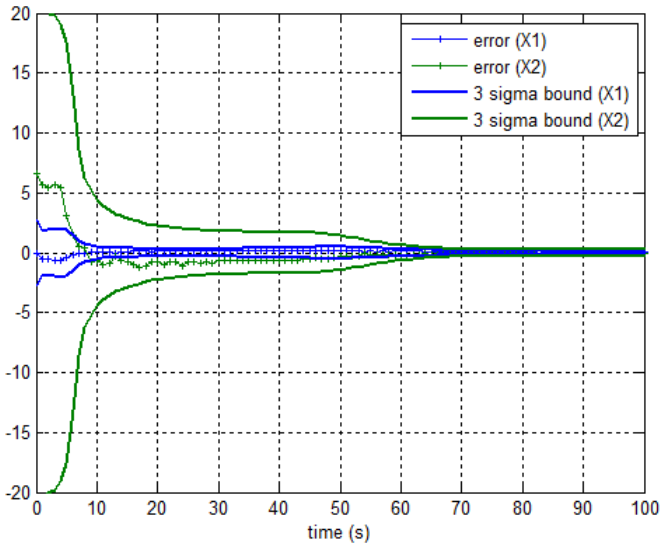

Figure IV-5 Transient Error of MUKF approach for 2D state estimation example

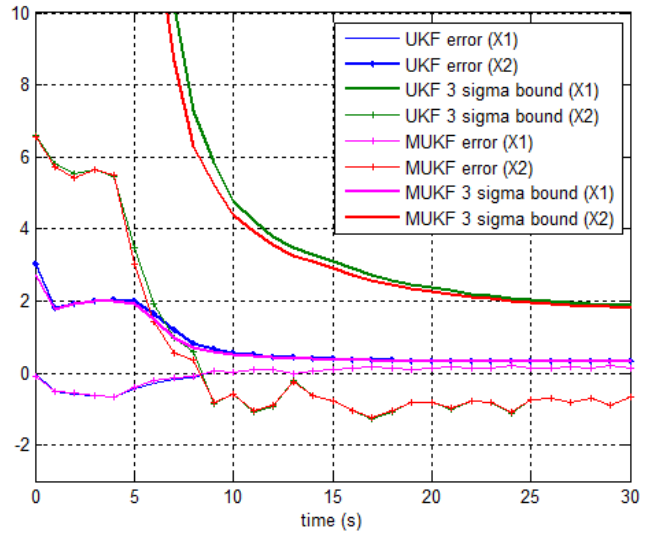

Figure IV-6 Transient Error MUKF-UKF comparison (2D state estimation example)

As shown from results the MUKF exhibit the same capability to handle wrong initialization and converge with the same consistency of the UKF Figure IV-5. The difference (Figure IV-6) can be appreciated only in the early phase and it is negligible for the proposed example (<10%).

C. Accounting for parameter uncertainty: a configurable Consider-Augmented Kalman Filtering approach

Incorrect initial covariance estimates and sparse measurements (or long term propagation time span) are generally handled via higher order filtering and, as described hitherto, one possibility is focusing numerical approximations on the relevant nonlinear part of the model. However, convergence problem as well as biased state and covariance estimates can occur due to other issues. Neglecting system model parameters uncertainty or presence of unmodeled uncertainty sources can jeopardize the accuracy and consistency of the filtering estimate more than neglecting nonlinearities. The simplest mitigation action would rely on omitting all these parameters and on increasing both measurement and process noises [86]. This approach introduces large bias errors since the neglected parameters and effects can be quite far from being white noise processes. Actually, model uncertainty issue does not include only the presence of physical parameters, whose real values are not perfectly known, but also those degradation sources that cannot be handled as simple uncorrelated white noises. Shaping techniques ([86],[87]) allow to include such contribution within the Kalman framework by using auxiliary variables that represent biases as well

as coloured noises affecting propagation and measurement equations.

The most logical solution, reducing errors caused by parametric uncertainty, is to augment the state vector by including such parameters as states. Many applications not only benefit in term of state estimates, but also improve the accuracy and precision of the parameters themselves. This approach, also known as Augmented Kalman Filtering (AGKF), has been widely indicated [88] as the natural solution of a wide range of problem relying to the research area of joint state and parameter estimation [45]. Although, these approaches requires further conditions in order to be effective. Actually, not all filters benefit from this augmentation due to computational restrictions or because the parameters are poorly observable. In general the computational load is increased and a parameter with low observability may not acquire enough measurements along a particular trajectory to improve its accuracy. In many cases, the additional degrees of freedom are a challenge for the numerical calculations causing detrimental effects on the performance and error bound control: covariance can reduce even estimate remain biased or not consistent [89].

A possible alternative is to “consider" the parameters. This method [92] , also called Consider Kalman Filtering (CKF) allows shrinking the dimension of the state augmentation and minimizing the effect of model reduction on the estimation performance. The basic idea is that the uncertain parameters are not directly estimated, but the cross-correlation between the states and the uncertain parameters are brought into the covariance matrix of the state estimate errors in order to take into account their stochastic effect. The approach becomes advantageous in term of filter design simplification, computational cost and provides higher robustness since it bypass observability and tuning assessments [91] usually required by efficient full order process augmentation.

Developed by S.F. Schmidt in the 1960s [92] and widely used for bias mitigation in tracking problems [93], CKF has recently raised a greatest interest in space navigation systems [94]. As pointed out for the LEO precise orbit determination case [95], the CKF implementation is considered an interesting trade-off between the full-order state augmentation and conventional solutions that completely neglect parameter uncertainty, limiting also the computational burden and the level of complexity for the on board implementation. This advantage is all the more true than the number of parameter sources increase. Therefore, it becomes particularly attractive for the novel G2G orbit transfer scenario that needs to handle a huge amount of uncertain parameters, namely related to control action and GNSS systematic biases. This study, for the first time, exploits the CKF approach [6] as suitable solution to override rising estimation criticalities and select CKF as baseline MEONS arrangement for GNSS based autonomous electrical steering applications (V.3). In CHAPTER III additional errors concerning thruster actuation, eq.(3.28), inaccuracies of spacecraft dynamic models, eq.(3.19), and measurement systematic errors affecting the GNSS information, eq.(3.49), have been addressed as uncertainty sources, whose effect on the estimation have been represented by a set of unknown parameters. For the G2G test case (V.3), according to [6], more than 30 parameters can be required to evaluate a navigation solution using an AGKF. The CKF allows desensitizing estimation [96] wrt both dynamics and measurement model unknowns’ without the necessity to perform full order estimation.

In more detail, the state $\mathbf{X}$ is partitioned in two sub-components: $\mathbf{x}$, representing the true state to evaluate, and $\mathbf{p}$, including all the parameters and effects that are not really estimated but only considered as potential error sources affecting $\mathbf{x}$ [90]. In orbit steering strategy experiments (V.2,V.3), $\mathbf{x}$ is the vector introduced in eq.(3.43) and $\mathbf{p} = \{\mathbf{p}_{Pert}, \mathbf{p}_{Thrust}, \mathbf{p}_{range}\}$ is the vector consisting perturbation parameters, thruster actuation errors and measurement biases. Based on the standard state space formulation of discrete-time stochastic model and Gaussian filtering assumption, the partition of the state can be also applied to the relevant covariance matrix $\mathbf{P}_{xx}$:

$$\mathbf{X} = \{\mathbf{x}, \mathbf{p}\} \rightarrow N\left(\mathbf{X} \mid \hat{\mathbf{X}} = \begin{Bmatrix} \mathbf{x} \\ \mathbf{p} \end{Bmatrix}, \mathbf{P}_{\mathbf{x}} = \begin{bmatrix} \mathbf{P}_{\mathbf{xx}} & \mathbf{P}_{\mathbf{xp}} \\ \mathbf{P}_{\mathbf{px}} & \mathbf{P}_{\mathbf{pp}} \end{bmatrix} \right) \tag{4.9}$$

Assuming Consider Extended Kalman Filter (CEKF) implementation (i.e. the Taylor series approximation case), the general variational model in eq.(2.5) can be specialized in:

$$\begin{cases} \dot{\mathbf{x}} = \mathbf{f}_{\mathbf{x}}(\mathbf{x}, \mathbf{p}, t) \\ \dot{\mathbf{p}} = \mathbf{f}_{\mathbf{p}}(\mathbf{p}, t) \simeq 0 \end{cases} \qquad \boldsymbol{\Phi}_k = \begin{bmatrix} \boldsymbol{\Phi}_{\mathbf{xx},k} & \boldsymbol{\Phi}_{\mathbf{x}p,k} \\ 0 & \simeq \mathbf{I} \end{bmatrix} \tag{4.10}$$

If parameters are assumed constant with respect to estimation prediction step, the CEKF covariance propagation can be ones more specialized in state and cross covariance update equations:

$$\begin{aligned} \mathbf{P}^{-}_{\mathbf{xx},k+1} &= \boldsymbol{\Phi}_{\mathbf{xx},k} \mathbf{P}^{+}_{\mathbf{xx},k} \boldsymbol{\Phi}^{T}_{\mathbf{xx},k} + \boldsymbol{\Phi}_{\mathbf{xx},k} \mathbf{P}^{+}_{\mathbf{xp},k} \boldsymbol{\Phi}^{T}_{\mathbf{xp},k} + \boldsymbol{\Phi}_{\mathbf{xp},k} \mathbf{P}^{+}_{\mathbf{pp},k} \boldsymbol{\Phi}^{T}_{\mathbf{xp},k} + \mathbf{Q}_{\mathbf{xx},k} \\ \mathbf{P}^{-}_{\mathbf{xp},k+1} &= \boldsymbol{\Phi}_{\mathbf{xx},k} \mathbf{P}^{+}_{\mathbf{xp},k} + \boldsymbol{\Phi}_{\mathbf{xp},k} \mathbf{P}^{+}_{\mathbf{pp},k} \end{aligned} \tag{4.11}$$

At this point, considering the measurement design matrix (i.e. MEONS observer Jacobians) partition $\mathbf{H} = \left[\mathbf{H}_{\mathbf{x}}, \mathbf{H}_{\mathbf{p}} \right]$ as one that generated by state and observation model parameter splitting, the Kalman filter correction step can be reduced to the following expression:

$$\begin{aligned} \mathbf{K}_{\mathbf{x}} &= \left(\mathbf{P}^{-}_{\mathbf{xx},k} \mathbf{H}^{T}_{\mathbf{x},k} + \mathbf{P}^{-}_{\mathbf{xp},k} \mathbf{H}^{T}_{\mathbf{p},k} \right) \left(\mathbf{H}_{\mathbf{x},k} \mathbf{P}^{-}_{\mathbf{xx},k} \mathbf{H}^{T}_{\mathbf{x},k} + \mathbf{H}_{\mathbf{x},k} \mathbf{P}^{-}_{\mathbf{xp},k} \mathbf{H}^{T}_{\mathbf{p},k} + \mathbf{H}^{T}_{\mathbf{p},k} \mathbf{P}^{-}_{\mathbf{ps},k} \mathbf{H}^{T}_{\mathbf{x},k} + \mathbf{H}_{\mathbf{p},k} \mathbf{P}^{-}_{\mathbf{pp},k} \mathbf{H}^{T}_{\mathbf{p},k} + \mathbf{R} \right)^{-1} \\ \mathbf{x}^{+}_{k} &= \mathbf{x}^{-}_{k} + \mathbf{K}_{\mathbf{x}} \left(\mathbf{y}^{+}_{k} - \mathbf{h}(\mathbf{x}^{-}_{k}, \mathbf{p}^{-}_{k}) \right) \\ \mathbf{P}^{+}_{\mathbf{xx},k} &= \left(\mathbf{I} - \mathbf{K}_{\mathbf{x}} \mathbf{H}_{\mathbf{x},k} \right) \mathbf{P}^{-}_{\mathbf{ss},k} - \mathbf{K}_{\mathbf{x}} \mathbf{H}_{\mathbf{p},k} \mathbf{P}^{-}_{\mathbf{xp},k} \\ \mathbf{P}^{+}_{\mathbf{xp},k} &= \left(\mathbf{I} - \mathbf{K}_{\mathbf{x}} \mathbf{H}_{\mathbf{x},k} \right) \mathbf{P}^{-}_{\mathbf{xp},k} - \mathbf{K}_{\mathbf{x}} \mathbf{H}_{\mathbf{p},k} \mathbf{P}^{-}_{\mathbf{pp},k} \end{aligned} \tag{4.12}$$

where the CEKF constraints has been considered as for [90]:

$$\begin{aligned} \mathbf{p}^{+}_{k} &= \mathbf{p}^{-}_{k} = \mathbf{p}_0 \\ \mathbf{P}^{+}_{\mathbf{pp}} &= \mathbf{P}^{-}_{\mathbf{pp}} = \mathbf{P}^{0}_{\mathbf{pp}} \end{aligned} \tag{4.13}$$

with $\mathbf{p}_0$ and $\mathbf{P}^{0}_{\mathbf{pp}}$ being, respectively, the initial vector of parameters and the initial covariance matrix of the parameters. It is worthy to remind some CKF peculiarities wrt other Kalman filter class techniques.

Firstly, CKF can be also ranked within the desensitized approach class [96]. It coincides, at least in the linear case, with the Desensitized Approach. In [97], it has been demonstrated that consider filter is one that minimizes the simplified sensitivity robust objective function:

$$\begin{aligned} &\min \left\{ J = Tr\left(\mathbf{P}^{+}_{\mathbf{xx}} \right)_k + Tr\left(\mathbf{S}^{+} \mathbf{W} \mathbf{S}^{+T} \right)_k \right\} \longrightarrow \mathbf{K}_{\mathbf{x}} \\ &\mathbf{S}^{-}_{k} = \left(\boldsymbol{\Phi}_{\mathbf{xx},k} \mathbf{S}^{+}_{k} + \boldsymbol{\Phi}_{\mathbf{xp},k} \right) \qquad \mathbf{S}^{+}_{k} = \mathbf{S}^{-}_{k} - \mathbf{K}_{\mathbf{x}} \left(\mathbf{H}_{\mathbf{s},k} \mathbf{S}^{-}_{k} \mathbf{H}^{T}_{\mathbf{p},k} \right) \end{aligned} \tag{4.14}$$

when the weighting matrix $\mathbf{W}$ is selected in accordance to the parametric uncertainty covariance $\mathbf{P}^{0}_{\mathbf{pp}}$. This points out that the CKF is not a minimum variance filter with respect to both state and parameter variable [90]. However, $\mathbf{K}_{\mathbf{x}}$ in eq.(4.12), even though sub-optimal with respect to the estimation of the entire vector $\mathbf{X}$, preserves its consistency wrt the vector $\mathbf{x}$ and make estimation robust by proper

modulating increment of the covariance in accordance to the parameter sensitivity [98].

Secondly, CKF is also considered a model reduction method [87] allowing one to reduce the computational cost. With reference to CEKF eq.(17)-(22), covariance blocks update dimension reduces in accordance to the ratio between consider and state variable partition dimension. Further improvements can be obtained via Triangular Covariance Factorization (also known as UDU factorization [99]) implementation, detailed in IV.3.

The Consider Filter is tested on System 1. A parametric error due to the input partial knowledge is considered. A wrong input amplitude $\tilde{a} = 0.004$ is applied (true one is $\bar{a} = 0.01$) and the filter is desensitized wrt this parameter considering a parametric consider variable $\mathbf{p} = \{a\}$. This correspond to the extended consider state $\mathbf{X} = \{X^1, X^2, a\}$ and the introduction of the consider covariance block $\mathbf{P}_{\mathbf{pp}}^0 = 0.001$. The comparison with EKF solution is performed following the approach proposed in [90]. The reference EKF is defined as the one that processing the same CEKF state vector defined as $\mathbf{x} = \{X^1, X^2\}$ and accounting for the unmodeled effects simply increasing both process and measurement noise.

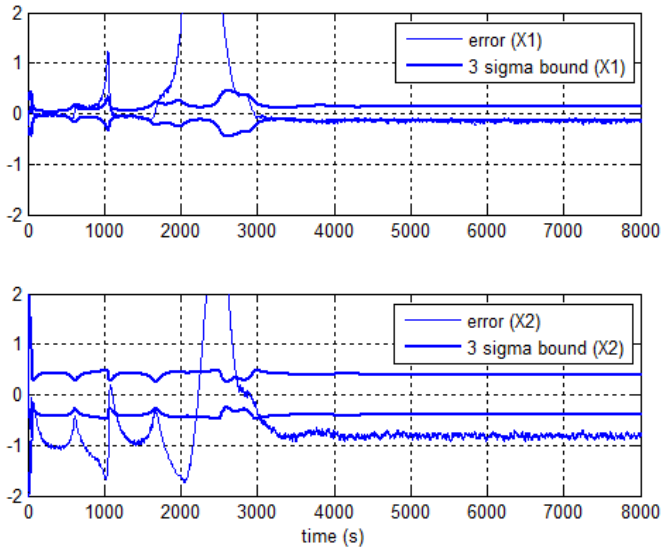

Figure IV-7 EKF error , considering $\tilde{\mathbf{Q}}_{\mathbf{xx},k}$

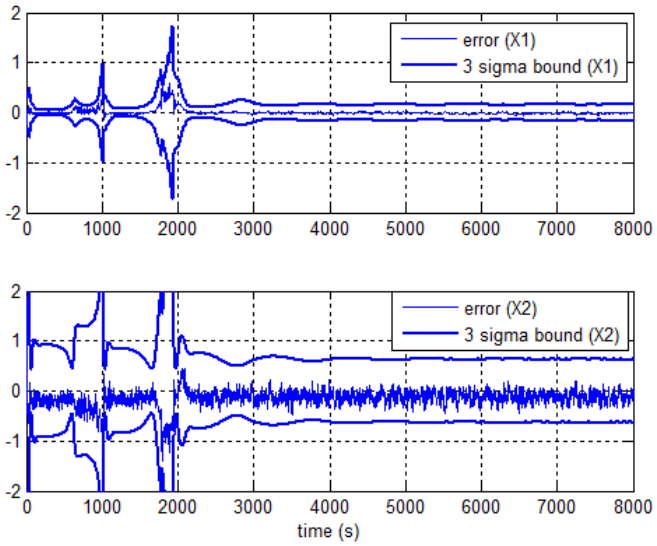

Figure IV-8 CEKF error and covariance bound

The latter EKF solution maps the parameter uncertainty directly via sensitivity matrices as simple additive contribution:

$$\begin{aligned} \tilde{\mathbf{R}} &= \mathbf{H}_{\mathbf{p}}\mathbf{P}_{\mathbf{pp}}\mathbf{H}_{\mathbf{p}}^{\mathbf{T}} + \mathbf{R} \qquad & \tilde{\mathbf{Q}}_{\mathbf{xx},k} &= \boldsymbol{\Psi}_{\mathbf{xp}}\mathbf{P}_{\mathbf{pp}}\boldsymbol{\Psi}_{\mathbf{p}} + \mathbf{Q}_{\mathbf{xx},k} \\ \tilde{\mathbf{R}} &= \mathbf{H}_{\mathbf{p}}\mathbf{P}_{\mathbf{pp}}\mathbf{H}_{\mathbf{p}}^{\mathbf{T}} + \mathbf{R} \qquad & \tilde{\mathbf{Q}}_{\mathbf{ss},k} &= \boldsymbol{\Psi}_{\mathbf{sp}}\mathbf{P}_{\mathbf{pp}}\boldsymbol{\Psi}_{\mathbf{ps}} + \mathbf{Q}_{\mathbf{ss},k} \end{aligned} \tag{4.15}$$

neglecting the cross-correlation terms that are, instead, considered in the CEKF covariance update. With specific reference to Eq. (4.15), it is important to remark that EKF matrices are set to be representative of the same error levels (both noise and bias affecting Q and R) as modelled in the CEKF. The most important difference is that the error addition in EKF cannot take into account the cross correlation terms that CEKF is able to manage during covariance update [90]. Setting and tuning parameters for both filters are ones that provided in in Table IV-3 and the initial state condition is affected by the same error in accordance to the best initial state condition.

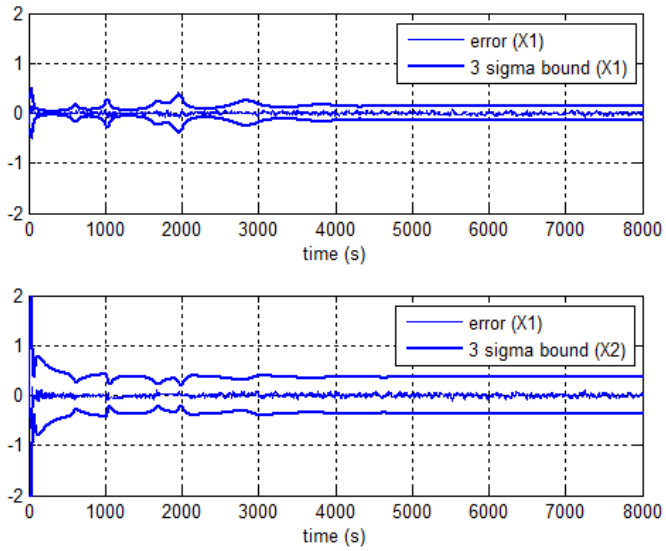

Figure IV-9 AGKF performances

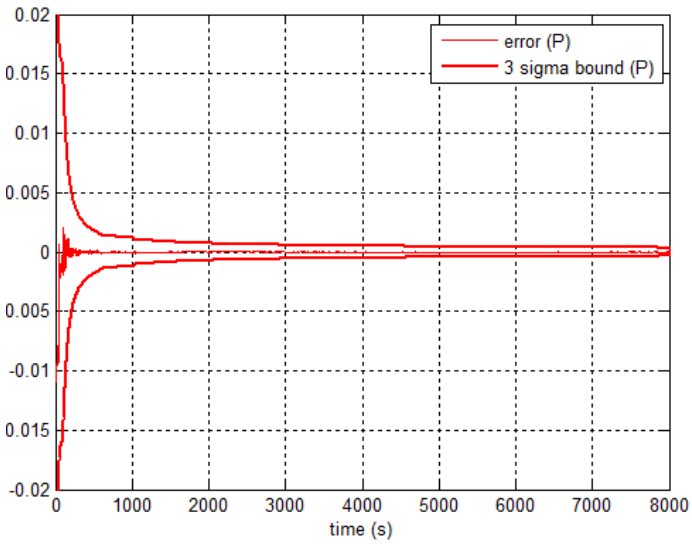

Figure IV-10 AGKF parameter $\{a\}$ direct estimation

Results provided in Figure IV-7 and Figure IV-8 confirm that CEKF incorporating the statistics of the uncertain parameters into the state estimate can achieve an improved performance by properly mapping stochastic parameter effects. The CEKF can result noisier than EKF, but it is more precise providing an unbiased estimation. More important, as expected, the covariance bounds are consistent with respect to the effective filter estimation error [90]. This corresponds to superior real time robustness, because the covariance bound can be safely used for on-board decision making and quality control . As shown in Figure IV-9, the optimal AGKF solution. i.e. one that directly estimates parameter $\{a\}$ outperforms the suboptimal CEKF. The parameter via a random constant auxiliary process is observable: it is highly correlated in time providing a continuous acquisition of the information along the trajectory (Figure IV-10). However, in case of low observability degree [100], stability margin can be critical generating wrong estimation for critical initialization condition and noise magnitude.

In the framework of MEONS design, CEKF implementation at navigation level in V.3 has been considered not as an AGKF exclusive alternative, but in a collaborative manner. Basically, this research identifies the CKF filter as the minimal conservative solution to be enabled in presence of parameter uncertainty for EOR. However, other possibilities can be investigated and an efficient state augmentation strategy, which selects estimated and considered parameters, could represent the suitable approach. The following consideration must be taken into account:

- At least in the linear case, promoting a consider p_1 variable into the augmented one correspond to perform the following rearrangement on the state and parameter subspaces :

$$\mathbf{x}' = \{\mathbf{x}, p_1\} \qquad \mathbf{p}' = \{p_2, p_3, \ldots . p_n\} \tag{4.16}$$

- The change of Consider/Augmented subset can be performed runtime by using switching matrices (see IV.2) that select within the extended state vector the augmented state and consider partition.

The idea is providing the algorithm with possibility of selecting which parameter is used to reduce system model errors sensitivity and which conversely is promoted within the augmented state vector to improve the navigation accuracy. MEONS current design is compatible with such Configurable State Augmentation Paradigm described in Figure IV-11 (IV.3-D). Propagation/observation controllers can be used in order to rearrange the target state vector and perform activation/deactivation of correspondent auxiliary processes.

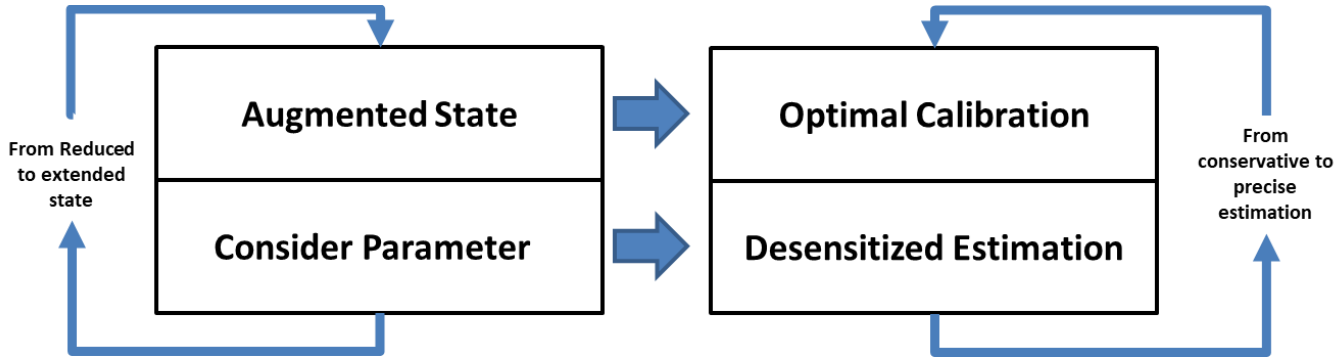

Figure IV-11 Configurable State Augmentation Paradigm

The CKF is always considered as the default starting configuration for all parameters, whose initial variances is selected in accordance to the expected upper bound. Activating a state depends on the specific operative phase and on stability/consistency issues. The variance and error of such parameter is then improved till the optimal one. It shall be noted that in order to reduce computational burden, it is better to select the subset of parameter that run time can be promoted and one that are static consider parameters: this allows applying an effective model reduction for static consider parameters for computational cost reduction. This functionality is verified at navigation level in V.3-E.

D. Innovation based Adaptive Filtering for process covariance tuning

Kalman filtering performance does not depend only on the accuracy of state space equation and parameter uncertainty handling. Filter optimality relies also on the knowledge of the noise level represented by process covariance matrix Q and the measurements noise covariance matrix R [101], whose exact statistical description is not always available.

They represent distance between mathematical representation and the real physical system, but take also into account unexpected events and error level changes. Carful characterization of degradation source via considers parameters and/or augmentation techniques can effectively restrict residual error to a set of white stochastic processes $\mathbf{w}_k, \mathbf{v}_k$. However, covariance choice became a critical procedure, also known as filtering tuning, that can determine severe performance degradation in term of filter stability, tracking and accuracy. The possibility to readjust noise strengths on the basis of internal model information is often termed as adaptive or self-tuning estimation algorithm [47]. The innovation $\boldsymbol{\upsilon}_j$ or the residuals $\mathbf{r}_j$, obtained in real time from measurement becoming available, are the key element for adaptation:

$$\begin{aligned} &\boldsymbol{\upsilon}_j = \mathbf{Z}_j - \mathbf{Y}_j \qquad \mathbf{Y}_k = \mathbf{h}_d(\mathbf{X}_{k+1}, \mathbf{v}_k, k) \qquad A_{\boldsymbol{\upsilon}\boldsymbol{\upsilon}} = Cov\{\boldsymbol{\upsilon}_j, \boldsymbol{\upsilon}_j^T\} \\ &\mathbf{r}_j = \mathbf{X}_k^+ - \mathbf{X}_k^- \qquad \mathbf{X}_k^+ = \mathbf{m}_k^+ \qquad \mathbf{X}_k^- = \mathbf{m}_k^- \qquad A_{\mathbf{rr}} = Cov\{\mathbf{r}_j, \mathbf{r}_j^T\} \end{aligned} \tag{4.17}$$

Consistent mismatch between actual measurements and best measurement predictions ($\boldsymbol{\upsilon}_j$) or a priori and a posteriori estimations ($\mathbf{r}_j$) indicate erroneous model formulation. Particular characteristics of such mismatch can be exploited to perform the necessary adaptation. The two major techniques for adaptive Kalman filtering are the multiple model adaptive estimation (MMAE) and the innovation-based adaptive estimation (IAE). The MMAE is time-consuming and takes heavy computation burden, so IAE is generally considered compatible with real time applications. The first assumes the system obeys one of a finite number of models [102] that are weighted wrt squared measurement of residuals. The second directly exploit innovation sequence mismatch in order to derive target noise matrices. Mayback categorized innovation based solutions in Maximum likelihood, Bayesian, correlation based methods and covariance matching methods [47]. This research focuses on the first solution, whose relevant results for POD purpose will be presented in V.2.

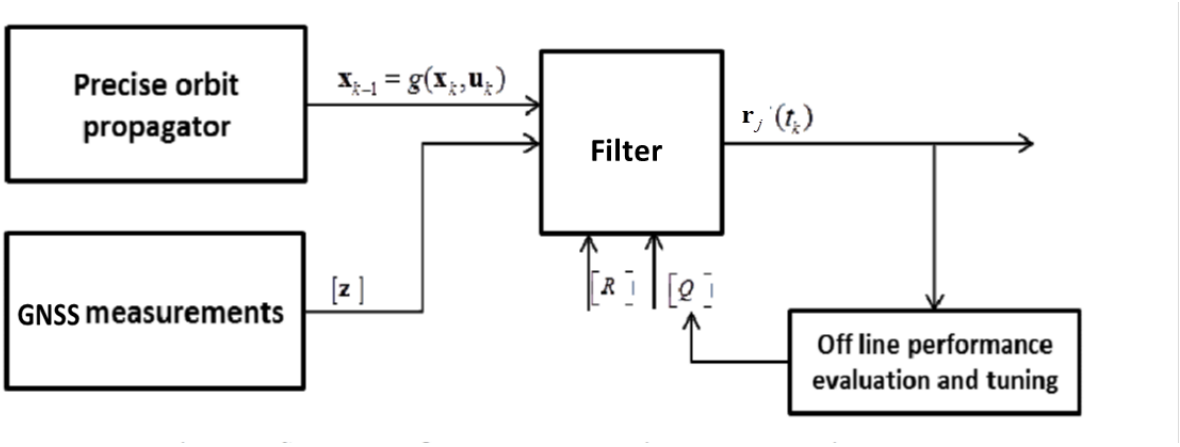

Figure IV-12 IAE Self-tuning Approach for GNSS navigation

The full scale ML dynamic estimator [47] is generally prohibitive. Therefore, the underlying approximations [101] of the ML adaptive Kalman filtering problem are:

- The filter states $\mathbf{X}$, filter dynamic and measurement function (as well as transition matrix and the measurement design matrix) are independent of the adaptive parameters α
- the innovation/residual covariance matrix $A_{\mathbf{vv}}$ (or $A_{\mathbf{rr}}$) is the key to adaptation and hence is the key α dependent function. Specifically innovation sequence is assumed a white and ergodic sequence within the estimation
- It is assumed that the process and measurement unknown set of parameters are constant-over-N-steps

Under these approximations, one can state the following approximated ML minimization problem (see [101]) :

$$\begin{aligned} &\min\left\{ J_{ML} = \ln\left|A_{\mathbf{vv}}(t_j)\right| + \mathbf{v}_j^T \left(A_{\mathbf{vv}}^T(t_j)\right)^{-1} \mathbf{v}_j \right\} \\ &A_{\mathbf{vv}}(t_j) = \left[H(t_j) P_k^-(t_j) H(t_j) + R_k(t_j) \right] \end{aligned} \tag{4.18}$$

which can be handled via finite length window methods proposed in ([47],[101]), achieving the following parameter adaptation equation:

$$\sum_{j=j_0}^{n} tr\left\{ \left[A_{\mathbf{vv}}(t_j)^{-1} + A_{\mathbf{vv}}(t_j)^{-1} \nu_j \nu_j^T A_{\mathbf{vv}}(t_j)^{-1} \right] \frac{\partial A_{\mathbf{vv}}(t_j)}{\partial \alpha_{kk}} \right\} = 0 \tag{4.19}$$

$A(t_j)$ is also known as the model based innovation covariance matrix and α_{kk} can be selected among element of process or measurement covariance. For a complete derivation of eq.(4.21) [47] and [101] can be referred. Putting respectively $\alpha_{ij} = \sigma_{w_{ij}}$, $\alpha_{ij} = \sigma_{w_{ij}}$, the final expressions for the explicit suboptimal Q and R estimators can be obtained:

$$\hat{Q} = \frac{1}{N} \sum_{j=j_0}^{k} \mathbf{r}_j \mathbf{r}_j^T + P_j^+ - (P_j^- - Q_j) \qquad \hat{R} = \frac{1}{N} \sum_{j=j_0}^{k} \mathbf{v}_j \mathbf{v}_j^T - \left(H(t_j) P_k^-(t_j) H(t_j) \right) \tag{4.20}$$

Adaptation of both covariance can be very dangerous because could cause divergence [101] without well-posed conditions. In this work the Q adaptation Figure IV-12 is implemented because, for orbit estimation purposes, the knowledge of the sensor noise is usually higher than the process noise wrt real environmental conditions. The eq.(4.20) cannot be applied as is, but it needs same modifications. Actually, many applications [103] simplify it considering the predicted residual covariance negligible, but the non-stationary variation of gain and covariance in nonlinear approaches does not allow using the

reduced formula. It introduces other difficulties because the complete estimator has the potential limitation to not guarantee the process noise estimate to be positive definite [101]. Finally, the adaptation needs proper dynamic condition for convergence, so it is generally not performed before the filter works around the nominal trajectory (convergence transient extinction). The reference scheme hereafter exploited can be expressed as follow

$$\hat{Q}_{k>K_{ss}} : \begin{cases} Q^* = \dfrac{1}{N}\sum_{j=j_0}^{k} \mathbf{r}_j \mathbf{r}_j^T + P_j^+ - (P_j^- - Q_j), & Q^* > 0 \\ Q_{k-1}, & Q^* \le 0 \end{cases} \tag{4.21}$$

It considers only diagonal element, starts after steady state achievement (K_{ss}) and stop adaptation if the current estimation Q* is not definite positive in order to avoid divergence issues. Other schemes are possible and alternatives have been investigated in [104] . A fading function can be also selected:

$$\hat{Q}_k = Q_k + 1/L_{smooth}\,(Q^* - Q_k) \tag{4.22}$$

in order to smooth the Q data even using small windows [104]. It is worthy to note that $\hat{Q}$ represents the estimation of process noise covariance at t_j . This value is propagated at next step by using the procedure described in IV.3 considering $Q(s) = \hat{Q}/\Delta t$. The approach has been applied to System 1 within an EKF structure. The standard EKF result for optimal Q matrix tuning ($diag(Q) = 0.01$) are shown in Figure IV-13). Performance results for adaptive solution (N=10, L=10) are reported in Figure IV-14 respectively considering $10^2 \cdot Q_{in}$. The superimposition of the optimal solution confirms the capacity to converge to the right performance. $0.1^2 \cdot Q_{in}$ initialization test case has not been reported, but convergence properties are preserved. Basically, the adaptive error and covariance bound show a high variability as the tuning is fed by residuals. Actually square root of Q_{11}, Q_{22} elements estimation, shown in Figure IV-15, fluctuates around the optimal values. Some overshoot are experienced due to time varying problem. However, this not jeopardizes the adaptive benefit of modifying a too wrong tuning setting in accordance with the current data.

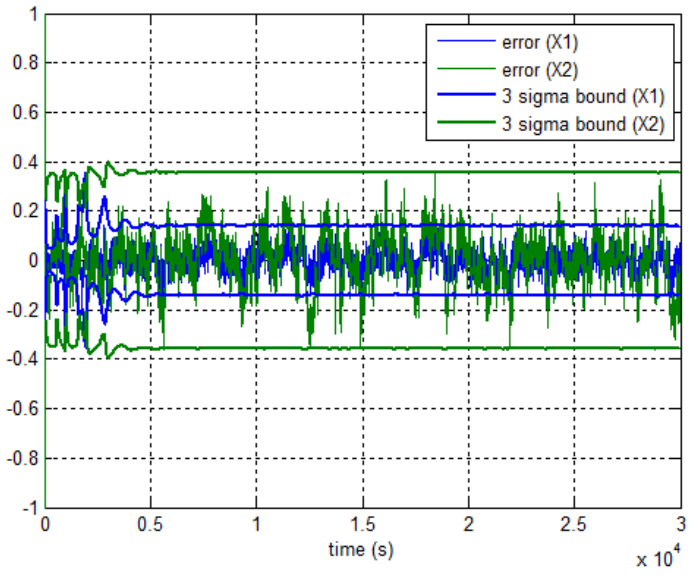

Figure IV-13 Optimally tuned EKF performance

For on-line constant-over-N-steps ML based approximation, the length of finite window (as well as fading function) can be used to balance reactivity and smoothness of adaptation [101]. Some insight on this issue are provided in [104] wrt GNSS navigation application (V.2). For the sake of brevity, results for N=20 and L=10 are not reported, but even reducing parameter estimation variability convergence values and general performance apply. A too wide window is not always the best solution because the memory of wrong values can introduces long convergence issues and worse tracking capability.

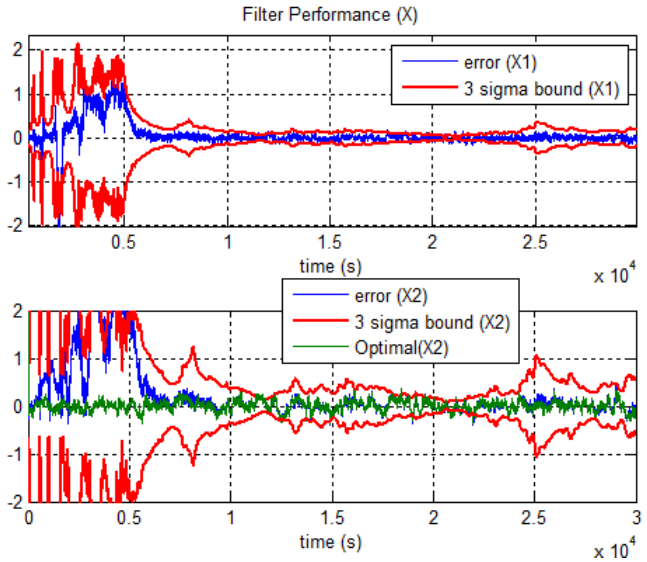

Figure IV-14 ML Adaptive Filter Performance

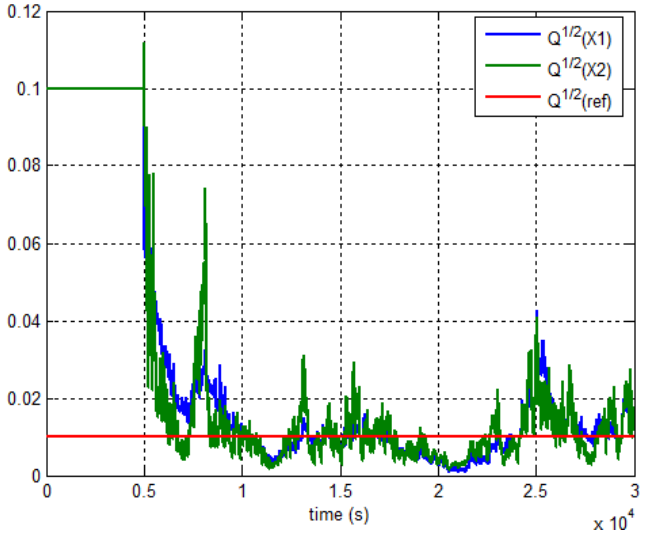

Figure IV-15 ML process noise covariance estimation

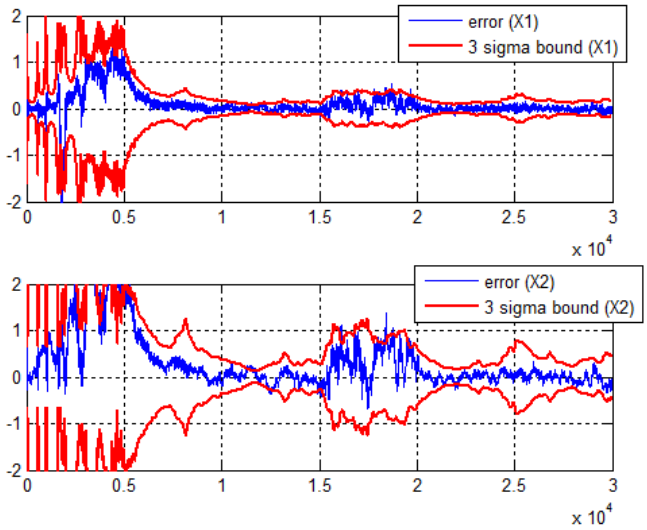

Figure IV-16 Adaptive Filter Performance in case of unexpected covariance change

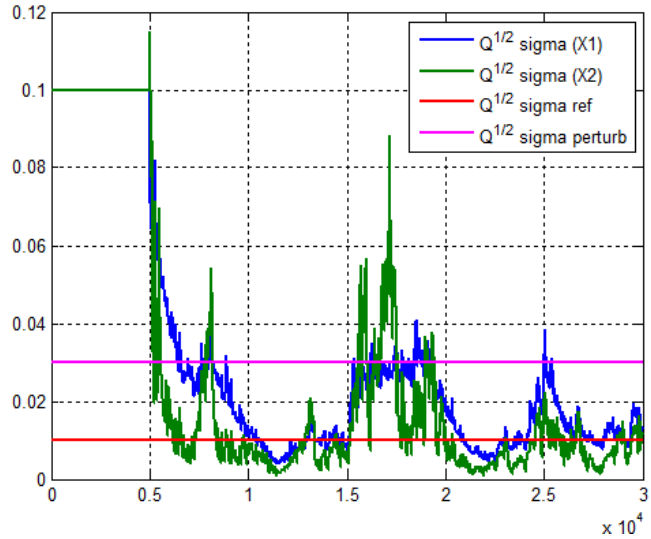

Figure IV-17 ML process noise covariance estimation in case of unexpected covariance change

The adaptive approach can be also used for unexpected error magnitude increment. An increased noise level has been simulated for System 1 within the 15000-20000s time windows. Figure IV-16 and Figure IV-17 confirms that the covariance term estimation is sensitive to such variation.

The example makes clear that the introduction of an adaptive processing block can be very useful, especially in case of covariance initialization far from the effective one. Nevertheless, in case of IAE approximated methods some arrangements have to be considered. Actually, overshoot in parameter estimation experienced during nonstationary and critical condition can have detrimental effect on stability of the process. Covariance threshold (i.e. minimum and maximum possible Q) must be introduced and a logic enabling or disabling the adaptation is usually considered in order to process only valid innovation samples. Moreover blunders detection and other diagnostics (i.e. whiteness tests [101]) can be considered as validation layers. Further investigations are necessary in this sense to fully enable adaptive methods within the MEONS kernel. Switching between different static level of uncertain parameters and noise can offer a more robust solution in critical applications. Adaptive scheme inclusion in MEONS framework looks toward future enhancement of self-tuning capability and adaptive issues shall be considered for next MEONS research activities.

E. Variable state dimension approach and Reordering Procedure

An important feature considered in the frame of MEONS estimation module design is the compatibility with online state rearrangement and model switching. This capability mainly refers to two well suited techniques:

- Variable State Dimension (VSD) filtering [86]
- State Vector Reordering [54]

The VSD filter has been widely used for tracking problems with manoeuvring targets. Actually it involves a quiescent lower-order model and an augmented one [86] that switches in accordance to change detection criteria. Several activation function have been developed for autonomous detection, activation and reverting of the models. However, this approach is basically applicable also in case of commanded transitions, generally triggered by a mode operative change. This is the case of thruster model switch on / switch off in the LEO to MEO EOR case. Actually, the activation of the specific stochastic contribution, i.e. the consider parameters exploited in the MEONS model of V.3, involves the transition from a shorter to a larger state vector and covariance. Specifically, the following partition of the state can be considered:

$$\mathbf{X} = \left\{ \mathbf{x}_{inactive}, \mathbf{x}_{active} \right\} \rightarrow \begin{cases} \mathbf{x}_{ac} = \pi_{ac} R\mathbf{X} = \left[I, 0 \right] R\mathbf{X} \\ \mathbf{x}_{in} = \pi_{in} R\mathbf{X} = \left[0, I \right] R\mathbf{X} \end{cases} \tag{4.23}$$

Where $\mathbf{x}_{ac}$ indicates the A*ctive Variables* (with respect to the stochastic problem) and $\mathbf{x}_{in}$ are the *Inactive variables* (with respect to the stochastic problem) set. Active and inactive substate in eq.(4.23) can be intended as a full state projection by mean π_{ac}, π_{in} matrices. In the Gaussian filtering framework the well-known mean and covariance transformation rules can be applied [105]:

$$\begin{aligned} &\mathbf{m}_{ac} = \pi_{ac} R\, \mathbf{m}_{\mathbf{X}} \qquad \mathbf{P}_{x_{ac}} = \pi_{ac} R \mathbf{P}_{\mathbf{XX}} R^T \pi_{ac}^T = \left[\begin{array}{c|c} \mathbf{P}_{x_{ac}} & 0 \\ \hline 0 & 0 \end{array} \right] \\ &\mathbf{m}_{in} = \pi_{in} R\mathbf{m} \qquad \mathbf{P}_{x_{in}\, in} = \pi_{in} R \mathbf{P}_{\mathbf{XX}} R^T \pi_{in}^T = \left[\begin{array}{c|c} 0 & 0 \\ \hline 0 & \mathbf{P}_{x_{in}} \end{array} \right] \end{aligned} \tag{4.24}$$

Where R is a matrix allowing to reorder the extended state in accordance to the active/inactive state set. After projection the state and covariance can be rearranged again as follow:

$$\mathbf{X} = \left\{ \mathbf{x}_{inactive}, \mathbf{x}_{active} \right\} \rightarrow \mathbf{P}_{\mathbf{XX}} = \left[\begin{array}{c|c} \mathbf{P}_{x_{ac}} & 0 \\ \hline 0 & \mathbf{P}_{x_{in}} \end{array} \right] \tag{4.25}$$

that fixes the two systems as uncorrelated and separated, the active and quiescent one. The quiescent part is transparent to the Kalman filtering processing, but it can be used to keep in memory inactive covariance used to reset or update the process when the target variable became active. Actually, run time promotion of inactive variable to the active set can be easily performed by repeating the procedure and changing the R matrix in order to consider the new state partition. During transition $\mathbf{P}_{x_{in}}$ element moves to the $\mathbf{P}_{x_{in}}$ block in order to participate to filtering process starting from a current or reset value. It is worthy to remind that activation is intended in stochastic sense, so MEONS model implicitly consider in the inactive space also all the deterministic auxiliary variable which are not defined by a statistic distribution. Specifically, the following distinction has been put in place within $\mathbf{x}_{inactive}$:

- *Inactive propagated variables*: the state variables that are not active and can be promoted in active part considering a quiescent state and covariance that are updated even not used
- *Inactive static variables:* the state variables that are not active and can be promoted in active part considering reset values (initialization from a reference value)
- *Null* variables, the state variables that cannot be promoted in the stochastic model, so they are only support deterministic variables for the propagation and observation steps. They can be removed and not used within the estimation process.

This solution makes $\mathbf{P}_{x_{in}}$ a block diagonal matrix $\mathbf{P}_{x_{in}} = diag\left\{\mathbf{P}_{x_{prop}} \quad \mathbf{P}_{x_{static}} \quad 0_{x_{null}}\right\}$ whose element are the covariance matrices of the correspondent variable subset.

The Reordering Problem requested by tracking problem with intermittent measurement biases deals with the same issue. At navigation level reordering is a prerogative of CDGPS ambiguity estimation eq.(3.35)-(3.36), but also the consider ranging bias management of eq.(3.49) can be considered as an intermittent contribution depending on the current satellite tracking list (V.3). It uses the Inactive/Active state procedure, but permutation matrix R deals with the necessity to sort the state variables on the basis of a proper indexing criterion. In case of CDGPS if the memory of the previous ambiguity estimation was lost, it could be exhibited a continuous re-initialization of the filter state and covariance at each visibility scenario change. Considering the CDGPS LEO application in V.3, this change could be rapid (the visibility condition changes with a short mean time) not allowing the convergence of the integer searching and the demanded continuity of the baseline estimation. In this case the projection in active and inactive subspaces due to entry and exit of visible SVs is combined with a proper permutation matrix allowing to associate position in the stack with the SV index. In case of GNSS tracking problem the maps builder is based on a rational organization of satellites ID (e.g. in an ascending order). For the sake of clarity, the following transition of the in view satellite set:

$$\begin{matrix} t_k^+ \to [1;2;5;7;15;22;27] \\ t_{k+1}^+ \to [1;2;5;15;22;27] \end{matrix} \qquad \pi_{ac}R = \begin{bmatrix} 1 & 0 & 0 & 0 & 0 & 0 & 0 & 0 \\ 0 & 1 & 0 & 0 & 0 & 0 & 0 & 0 \\ 0 & 0 & 1 & 0 & 0 & 0 & 0 & 0 \\ 0 & 0 & 0 & 0 & 1 & 0 & 0 & 0 \\ 0 & 0 & 0 & 0 & 0 & 1 & 0 & 0 \\ 0 & 0 & 0 & 0 & 0 & 0 & 0 & 1 \end{bmatrix} \tag{4.26}$$

correspond to the eq.(4.26) $\pi_{ac}R$ matrix. The inactive unknowns relying on the SV ID-7 is moved to the active part and the order is preserved. The reordering and projection in inactive subspaces is a very powerful tool for run time estimation configurability. The next chapter is devoted to the Generalized Reordering and Subspace Partitioning Controller that allows incorporating in a unified framework all the methods hereto described.

IV.2 ESTIMATION PROBLEM DECOMPOSITION AND RELEVANT SUBSPACE IDENTIFICATION

Beyond their incorporation within the MEONS estimation kernel, this work considers a rationalization of the proposed techniques by using the Optimal Estimation paradigm based on Dynamic Model Substructures (DMS). Referring to Schon, Gustaffsson[106] and Sarkka [44], this approach is representative of the modern interpretation of the optimal estimation. The idea is to generalize the sequential filtering framework (i.e. via the Bayesian approach) in order to customize or expand it with respect to the specific application. MEONS refers to the research carried out by Nilson [107]. The aim is to provide a Configurable Sequential Filtering Architecture (CSFA) that should be easily manipulated to

exploit state space model peculiarities and stochastic state variable characteristics. DMS is based on two fundamental tools:

- The subspace and system substructure identification, mainly related to estimation state projection and partitions
- The reduction of moment integrals based on correspondent model subspace assumptions (e.g. Gaussian-Linear, Active/Inactive)

The subspace projection matrices used in [107] are exploited to formalize the MEONS Partitioning and Reordering Function, which is the proposed tool to manage system substructures.

A. Filtering problem decomposition using model substructures

Similarly to one that described in IV.1-B, marginalization techniques can be used within Bayesian filtering in order to derive closed form expressions of the posterior means and covariance in terms of subspace projection matrices, subsystem models, and explicit marginal moment integrals for a set of sequentially more constraining state space model assumptions. Specifically, the following class of problem are considered in [107]:

a) Dynamic active subspace

Considering general state space model in eq.(2.5) there are matrices A_k, B_k, C_k, D_k and corresponding function $\mathbf{f}_k^{a)}(\cdot,\cdot)$, $\mathbf{h}_k^{a)}(\cdot,\cdot)$ such that:

$$\begin{cases} S_k\mathbf{X}_k = \left[\mathbf{f}_k^{a)}(A_k\mathbf{X}_k, \mathbf{w}_k); B_k\mathbf{X}_k\right] \\ T_k\mathbf{y}_k = \left[\mathbf{h}_k^{a)}(C_k\mathbf{X}_k, \boldsymbol{\nu}_k); D_k\mathbf{X}_k\right] \end{cases} \tag{4.27}$$

where $S_k = [A_k; B_k]$ and $T_k = [C_k; D_k]$ are the subspace projection matrices that select the state currently active in model $(\bullet)_k^{a)}$

b) Conditionally linear subspaces

Stated assumption a) and model in eq.(2.5), there are matrices $A_k = \left[A_k^{nl}, A_k^{l}\right], A_k^{l}$ and $C_k = \left[C_k^{nl}, C_k^{l}\right]$ $F_k = [F_k^{nl}, F_k^{l}]$, $H_k = [H_k^{nl}, H_k^{l}], G_k = [G_k^{nl}, G_k^{l}]$, $V_k = [V_k^{nl}, V_k^{l}]$ and corresponding function $\mathbf{f}_k = [\mathbf{f}_k^{nl}(\cdot,\cdot), \mathbf{f}_k^{l}(\cdot,\cdot)]$ $\mathbf{h}_k = [\mathbf{h}_k^{nl}(\cdot,\cdot), \mathbf{h}_k^{l}(\cdot,\cdot)]$ such that:

$$\begin{cases} A_k^{nl}\mathbf{X}_k = \mathbf{f}_k^{nl}(A_k^{nl}\mathbf{X}_{k-1}) + F_k^{nl}(A_k^{nl}\mathbf{X}_{k-1})A_k^{l}\mathbf{X}_{k-1} + G_k^{nl}\mathbf{w}_k \\ A_k^{l}\mathbf{X}_k = \mathbf{f}_k^{l}(A_k^{nl}\mathbf{X}_{k-1}) + F_k^{l}(A_k^{nl}\mathbf{X}_{k-1})A_k^{l}\mathbf{X}_{k-1} + G_k^{l}\mathbf{w}_k \\ C_k^{nl}\mathbf{y}_k = \mathbf{h}_k^{nl}(C_k^{nl}\mathbf{X}_k) + H_k^{nl}(C_k^{nl}\mathbf{X}_k)C_k^{l}\mathbf{X}_k + V_k\boldsymbol{\nu}_k \\ C_k^{l}\mathbf{y}_k = \mathbf{h}_k^{l}(C_k^{nl}\mathbf{X}_k^{nl}) + H_k^{l}(C_k^{nl}\mathbf{X}_k)C_k^{l}\mathbf{X}_k + V_k\boldsymbol{\nu}_k \end{cases} \tag{4.28}$$

c) Conditionally linearized subspaces

The structure is the same of b) considering relevant linear subspace matrices as generated by a linearization process:

$$F_k^{nl} = \left.\frac{\partial \mathbf{f}_k^{nl}(\mathbf{X})}{\partial A_k^l \mathbf{X}_{k-1}}\right|_{\mathbf{X}=A_k^{nl}\mathbf{X}_{k-1}} \qquad F_k^{l} = \left.\frac{\partial \mathbf{f}_k^{l}(\mathbf{X})}{\partial A_k^l \mathbf{X}_{k-1}}\right|_{\mathbf{X}=A_k^{nl}\mathbf{X}_{k-1}}$$
$$H_k^{nl} = \left.\frac{\partial \mathbf{h}_k^{nl}(\mathbf{X})}{\partial A_k^l \mathbf{X}_{k-1}}\right|_{\mathbf{X}=A_k^{nl}\mathbf{X}_{k-1}} \qquad H_k^{l} = \left.\frac{\partial \mathbf{h}_k^{l}(\mathbf{X})}{\partial A_k^l \mathbf{X}_{k-1}}\right|_{\mathbf{X}=A_k^{nl}\mathbf{X}_{k-1}} \tag{4.29}$$

For each assumption explicit marginal moment integrals expression are derived in [107]. Actually the results are too general and rely to procedure defined in Figure IV-18:

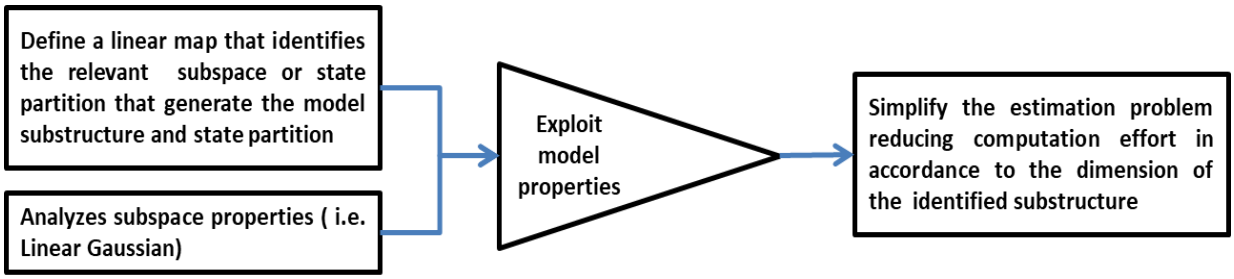

Figure IV-18 Dynamic Model Substructure Paradigm

Beyond the obtained mathematical tools, the interest for [107] is on the identification of a correspondence between filtering capabilities and defined substructure:

a') Handling structure a) corresponds to the capability referred as *decoupling modelling and system composition*. A system model is composed of submodels. At least, as for the decomposed state space description of MEONS eq.(3.2), it is composed of a state model and an output model that incorporate multiple submodels of different states and outputs. Assume submodels:

$$\begin{cases} \mathbf{x}_i = \mathbf{f}_{i,k}(\mathbf{x}_i, \mathbf{w}_k) \\ \mathbf{y}_j = \mathbf{h}_{i,k}(\mathbf{x}_j, \mathbf{w}_k) \end{cases} \qquad i, j = 1, 2...n \tag{4.30}$$

where $\mathbf{x}_i$ and $\mathbf{x}_j$ are states of the properties determining the subsystem dynamics and the subsystem outputs, respectively. The system state $\mathbf{X}$ spans the properties of $\mathbf{X} = \{\mathbf{x}_i, \mathbf{x}_j\}$. The properties of $\{\mathbf{x}_i, \mathbf{x}_j\}$ overlap but individual model states will often not coincide with $\mathbf{X}$ and different models may use different ordering and units of the states. This creates coupling between modelling and system composition, creating dynamic subspace structures. Using assumption a), the composition can be performed by constructing $S_k = [A_k; B_k]$ and $T_k = [C_k; D_k]$ such that $\mathbf{x}_i = A_k\mathbf{X}$ and $\mathbf{x}_j = C_k\mathbf{X}$. The A_k C_k will include scaling (unit transformations) and state selection but may also include further linear transformations. In this case, marginalization can be used to decouple the subsystem modelling and the system composition such that they can be performed separately by marginalizing out the "inactive subspace":

$$f : \mathbf{X} \xrightarrow{S_{[A_k,B_k]}} \begin{matrix} \mathbf{x}_{A_k} = A_k\mathbf{X} \\ \mathbf{x}_{B_k} = B_k\mathbf{X} \end{matrix} \qquad h : \mathbf{X} \xrightarrow{S_{[C_k,D_k]}} \begin{matrix} \mathbf{x}_{C_k} = C_k\mathbf{X} \\ \mathbf{x}_{D_k} = D_k\mathbf{X} \end{matrix} \tag{4.31}$$

b') Handling structure b) corresponds to the capability referred as *focusing numerical approximations capability*: only sub dimensions of the integrals are intractable, thereby focusing the numerical approximation techniques. The main result is that the partition $\mathbf{x}^{nl}$ and $\mathbf{x}^{l}$ of model b):

$$f:\mathbf{X}\xrightarrow{S_{[A_k^{nl},A_k^{l}]}}\begin{matrix}\mathbf{x}_{A_k^{nl}}=A_k^{nl}\mathbf{X}\\ \mathbf{x}_{A_k^{l}}=A_k^{l}\mathbf{X}\end{matrix}\qquad h:\mathbf{X}\xrightarrow{S_{[A_k^{nl},A_k^{l}]}}\begin{matrix}\mathbf{x}_{A_k^{nl}}=C_k^{nl}\mathbf{X}\\ \mathbf{x}_{A_k^{ll}}=C_k^{l}\mathbf{X}\end{matrix} \tag{4.32}$$

can be intended as a projection of the whole state on the relevant components that can be processed differently and then combined.

c') Handling structure c) corresponds to the capability of *combining model and numerical approximations*. Linearizing or making a Gaussian approximation of a part of a model is just a way of introducing related linear and Gaussian subspaces as for b) enabling combination of approach based on sigma points and Taylor series.

The performed general overview allows addressing MEONS methodologies of IV.1 as a DMS capability by recognizing that:

- ***Variable state dimension and switching model filtering*** falls in application of a). Actually an Active/Inactive state partition has been introduced in order to manage intermittent MEONS models :

$$\mathbf{X}\xrightarrow{S_{[A_k,B_k]}}\begin{matrix}\mathbf{x}_{A_k}=A_k\mathbf{X}\\ \mathbf{x}_{B_k}=B_k\mathbf{X}\end{matrix}\qquad A_k=\pi_{ac}R\qquad B_k=\pi_{in}R \tag{4.33}$$

- ***Marginalized mixed nonlinear/nonlinear filtering***, as MUKF, clearly falls under assumption c) and can be considered a specification of the procedure that marginalize out the subspace of Linear Gaussian state component and noises.

- ***Linear/linearized Consider Kalman Filtering*** falls in conditionally linear structure c) assuming :

$$f:\mathbf{X}\xrightarrow{S_{[A_k^{ap},A_k^{cp}]}}\begin{matrix}\mathbf{x}_{A_k^{e}}=A_k^{e}\mathbf{X}\\ \mathbf{p}=\mathbf{x}_{A_k^{cp}}=A_k^{cp}\mathbf{X}\end{matrix}\qquad h:\mathbf{X}\xrightarrow{S_{[C_k^{ap},C_k^{cp}]}}\begin{matrix}\mathbf{x}_{A_k^{nl,l}}=C_k^{e}\mathbf{X}\\ \mathbf{p}=\mathbf{x}_{A_k^{cp}}=C_k^{cp}\mathbf{X}\end{matrix} \tag{4.34}$$

where A_k^e include nonlinear/linear states that are directly estimated and A_k^{cp} identifies the linear consider subset. In more details, the possibility to see consider filter as procedure that marginalize out the subspace of Linear Gaussian Parameters is provided in [108], where Consider algorithm is derived just marginalizing the moment integrals wrt the linear consider parameters subspace. The fundamental difference with conventional linear marginalization is in the application of the Consider constraint during the update step that modifies the gain and covariance evaluation in accordance to the Consider approach. It shall be noted that this thesis consider only the case of linear consider parameters $A_k^{cp}\mathbf{X}\subseteq A_k^{l}\mathbf{X}$, so when integrated in a mixed Nonlinear/linear approach consider partition can be handled as a linear state estimation component during filtering time and measurement update step. Conversely, during consider constraint application, the matrix of estimated parameter refers to both estimated nonlinear/linear i.e $A_k^e=[A_k^{nl},A_k^{l}]$ and A_k^{cp} focuses on the consider block. This is applicable to the V.4 navigation scenario and possibility to have nonlinear consider parameter [109] will be addressed in future researches.

- ***Adaptive filtering*** does not falls in a specific model but the introduced structures can be used in order to handle the adaptive variables wrt the stochastic model. For instance, ML restricts the adaptive parameter set to the inactive state partition, as they are deterministic parameters. Other approaches (i.e. Bayesian [47]) needs to promote them within the estimated part.

The possibility to consider the generation of the model structure and partition of state by liner operators is exploited hereafter for different approach management.

B. State variable classification and estimation problem partitioning via Generalized Reordering

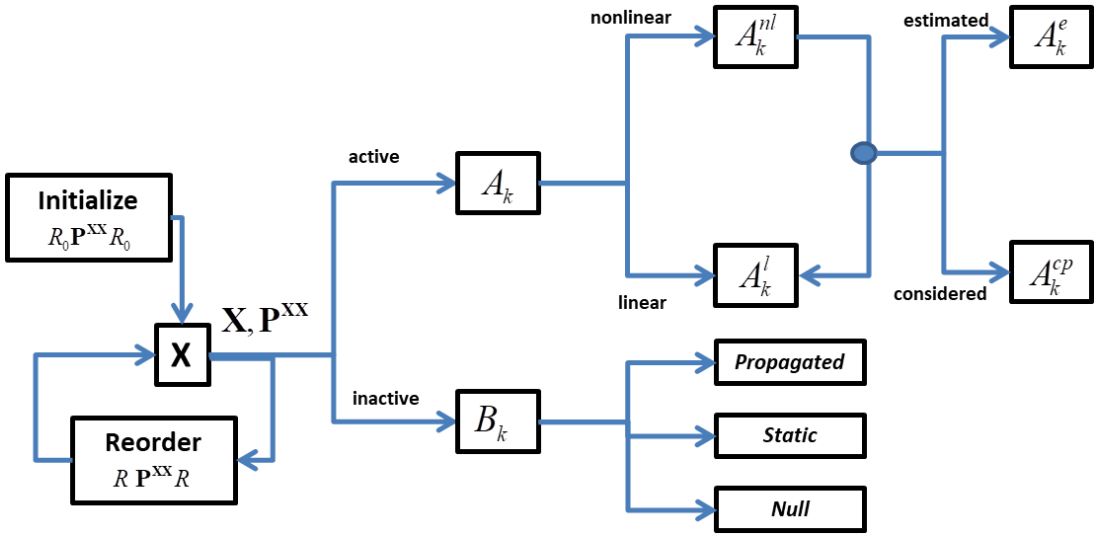

Figure IV-19 MEONS dynamic model substructure management

Figure IV-19 provide the scheme of the operation that can be performed on the extended state vector in order to fully exploit the navigation problem substructures. The procedure can be traduced in a unified solution, namely called Generalized Reordering Procedure, whose main steps are hereafter listed:

- **Initial setting**

At first, MEONS filtering model is arranged in order to set the initial state and model substructures. The extended state $\mathbf{X}$ is reordered by using a proper initialization matrix R_0. As for eq. (4.23), R_0 main function is to sort the physical state in order to have a partitioned state vector:

$$\mathbf{X} = \left\{ \mathbf{x}_{A_k^{nl}}, \mathbf{x}_{A_k^{l}}, \mathbf{x}_{A_k^{cp}}, \mathbf{x}_{B_k} \right\} \tag{4.35}$$

such that all partitions are consistent with the current DMS matrices dimension and correspondent covariance matrix blocks:

$$R_0 \mathbf{X} = \begin{Bmatrix} \mathbf{x}_{A_k^{nl}} \\ \mathbf{x}_{A_k^{l}} \\ \mathbf{x}_{A_k^{cp}} \\ \mathbf{x}_{B_k} \end{Bmatrix} \qquad R_0 \mathbf{P}_{xx} R_0 = \begin{bmatrix} \mathbf{P}_{\mathbf{x}_{A_k^{nl}} \mathbf{x}_{A_k^{nl}}} & \mathbf{P}_{\mathbf{x}_{A_k^{nl}} \mathbf{x}_{A_k^{l}}} & \mathbf{P}_{\mathbf{x}_{A_k^{nl}} \mathbf{x}_{A_k^{cp}}} & 0 \\ \mathbf{P}_{\mathbf{x}_{A_k^{l}} \mathbf{x}_{A_k^{nl}}} & \mathbf{P}_{\mathbf{x}_{A_k^{l}} \mathbf{x}_{A_k^{l}}} & \mathbf{P}_{\mathbf{x}_{A_k^{l}} \mathbf{x}_{A_k^{cp}}} & 0 \\ \mathbf{P}_{\mathbf{x}_{A_k^{cp}} \mathbf{x}_{A_k^{nl}}} & \mathbf{P}_{\mathbf{x}_{A_k^{cp}} \mathbf{x}_{A_k^{l}}} & \mathbf{P}_{\mathbf{x}_{A_k^{cp}} \mathbf{x}_{A_k^{cp}}} & 0 \\ 0 & 0 & 0 & \mathbf{P}_{\mathbf{x}_{B_k} \mathbf{x}_{B_k}} \end{bmatrix} \tag{4.36}$$

In this framework, all the approaches that insist on a target estimation vector and covariance subset can be applied in accordance to the selected Kalman filtering technique. The projection matrices are the tool that mathematically represent extraction procedure to perform active, nonlinear (if present) and considered variable processing:

$$\mathbf{X} \xrightarrow{S,R_0} \begin{cases} \mathbf{x}_{A_k^{nl}} = A_k^{nl} R_0 \mathbf{X} \\ \mathbf{x}_{A_k^{AP}} = A_k^{l} R_0 \mathbf{X} \\ \mathbf{x}_{A_k^{CP}} = A_k^{CP} R_0 \mathbf{X} \\ \mathbf{x}_{B_k} = B_k R_0 \mathbf{X} \end{cases} \qquad \mathbf{P}^{\mathbf{xx}} \xrightarrow{S,R_0} \begin{cases} \mathbf{P}_{\mathbf{x}_{A_k}\mathbf{x}_{A_k}} = A_k R_0 \mathbf{P}_{\mathbf{xx}} R_0 A_k \longrightarrow \begin{cases} \mathbf{P}_{\mathbf{x}_{A_k^{nl}}\mathbf{x}_{A_k^{nl}}} = A_k^{nl} R_0 \mathbf{P}_{\mathbf{xx}} R_0^T A_k^{nlT} \\ \mathbf{P}_{\mathbf{x}_{A_k^{l}}\mathbf{x}_{A_k^{l}}} = A_k^{l} R_0 \mathbf{P}_{\mathbf{xx}} R_0^T A_k^{lT} \\ \mathbf{P}_{\mathbf{x}_{A_k^{e}}\mathbf{x}_{A_k^{e}}} = A_k^{e} R_0 \mathbf{P}_{\mathbf{xx}} R_0 A_k^{e} \\ \mathbf{P}_{\mathbf{x}_{A_k^{cp}}\mathbf{x}_{A_k^{cp}}} = A_k^{cp} R_0 \mathbf{P}_{\mathbf{xx}} R_0 A_k^{CP} \\ A_k = diag(A_k^{nl}, A_k^{l}, A_k^{cp}) \\ A_k^{e} = diag(A_k^{nl}, A_k^{l}) \end{cases} \\ \mathbf{P}_{\mathbf{x}_{B_k}\mathbf{x}_{B_k}} = B_k R_0 \mathbf{P}_{\mathbf{xx}} R_0 B \end{cases} \tag{4.37}$$

It is worthy to note that even if A_k operator is diagonal, the covariance block is fully populated, since cross correlation terms are fulfilled during filtering processing and properly transferred during sequential application of the methods. Actually, MEONS setting applies the following processing sequence:

1) The inactive/active state are projected and rearranged following eq.(4.33) allowing to separate active and inactive subset:

$$\mathbf{P}_{x_{ac}} = \left[\begin{array}{c|c|c} \mathbf{P}_{\mathbf{x}_{A_k^{nl}}\mathbf{x}_{A_k^{nl}}} & \mathbf{P}_{\mathbf{x}_{A_k^{nl}}\mathbf{x}_{A_k^{l}}} & \mathbf{P}_{\mathbf{x}_{A_k^{nl}}\mathbf{x}_{A_k^{l}}} \\ \hline \mathbf{P}_{\mathbf{x}_{A_k^{l}}\mathbf{x}_{A_k^{nl}}} & \mathbf{P}_{\mathbf{x}_{A_k^{l}}\mathbf{x}_{A_k^{l}}} & \mathbf{P}_{\mathbf{x}_{A_k^{l}}\mathbf{x}_{A_k^{cp}}} \\ \hline \mathbf{P}_{\mathbf{x}_{A_k^{cp}}\mathbf{x}_{A_k^{nl}}} & \mathbf{P}_{\mathbf{x}_{A_k^{cp}}\mathbf{x}_{A_k^{l}}} & \mathbf{P}_{\mathbf{x}_{A_k^{cp}}\mathbf{x}_{A_k^{cp}}} \end{array}\right] \qquad \mathbf{P}_{x_{in}} = \mathbf{P}_{\mathbf{x}_{B_k}\mathbf{x}_{B_k}} \tag{4.38}$$

This substantially cancels inactive row and column of the covariance matrix $\mathbf{P}_k^B$

2) The marginalization of linear part, eq. (4.32) is performed to apply MUKF :

$$\mathbf{P}_{MUKF}^{nl} = \mathbf{P}_{\mathbf{x}_{A_k^{nl}}\mathbf{x}_{A_k^{nl}}} \qquad \mathbf{P}_{MUKF}^{nll} = [\mathbf{P}_{\mathbf{x}_{A_k^{nl}}\mathbf{x}_{A_k^{l}}}, \mathbf{P}_{\mathbf{x}_{A_k^{nl}}\mathbf{x}_{A_k^{l}}}] \qquad \mathbf{P}_{MUKF}^{ll} = \left[\begin{array}{c|c} \mathbf{P}_{\mathbf{x}_{A_k^{l}}\mathbf{x}_{A_k^{l}}} & \mathbf{P}_{\mathbf{x}_{A_k^{l}}\mathbf{x}_{A_k^{cp}}} \\ \hline \mathbf{P}_{\mathbf{x}_{A_k^{cp}}\mathbf{x}_{A_k^{l}}} & \mathbf{P}_{\mathbf{x}_{A_k^{cp}}\mathbf{x}_{A_k^{cp}}} \end{array}\right] \tag{4.39}$$

as stated before, at this level the linear consider subset is part of the linear partition.

3) During update step, when all key covariance are available, the consider partition becomes relevant and consider constraint can be applied :

$$\mathbf{P}^{+} = \begin{bmatrix} \mathbf{P}^{-}_{\mathbf{x}_{A_k^{e}}\mathbf{x}_{A_k^{e}}} - \mathbf{K}_{\mathbf{x}_{A_k^{e}}} \mathbf{S}_{\mathbf{YY}} \mathbf{K}^{T}_{\mathbf{x}_{A_k^{e}}} & \mathbf{P}^{-}_{\mathbf{x}_{A_k^{e}},\mathbf{x}_{A_k^{cp}}} - \mathbf{C}_{\mathbf{x}_{A_k^{e}}\mathbf{Y}} \mathbf{S}^{-1}_{\mathbf{YY}} \\ \mathbf{P}^{-}_{Cp,[nl,l]} - \mathbf{C}_{\mathbf{x}_{A_k^{cp}}\mathbf{Y}} \mathbf{S}^{-1}_{\mathbf{YY}} & \mathbf{P}^{-}_{\mathbf{x}_{A_k^{cp}}\mathbf{x}_{A_k^{cp}}} \end{bmatrix} \tag{4.40}$$

$$\mathbf{C}_{\mathbf{X}\,\mathbf{Y}} = [\mathbf{C}_{\mathbf{x}_{A_k^{e}}\mathbf{Y}}, \mathbf{C}_{\mathbf{x}_{A_k^{cp}}\mathbf{Y}}] \qquad \mathbf{K}_{\mathbf{x}_{A_k^{e}}} = \mathbf{C}_{\mathbf{x}_{A_k^{e}}\mathbf{Y}} \mathbf{S}^{-1}$$

Where $\mathbf{C}_{\mathbf{X}\,\mathbf{Y}}\,\mathbf{S}^{-1}_{\mathbf{YY}}$ are the generalized GGKF matrices (i.e. one that computed by EKF,UKF or MUKF during correction step).

Basically the step 1 and 2 has been defined in tem of propagation model $\mathbf{f}$, since only prediction step

matrices are used. The third step relies on correction, so equations should be expressed in term of $C_k = \left[C_k^{nl}, C_k^{l}, C_k^{Cp} \right], D_k$. However, the partition does not change between prediction/correction for the navigation cases considered in this thesis. The operators can be assumed the same, so the procedure and notation of 1 and 2 still apply on observation. However, in order to cope with such particular cases the reordering procedure is repeated in the MEONS software at prediction and correction steps and referred respectively as *Reordering Minus* and *Reordering Plus*.

- **Run time changes**

  As for eq. (4.23) when a state is promoted from a partition to another, the same information transfer rule can be used as it applies in Gaussian framework. Actually, the run time reordering operation is not only used for the inactive space but also to rearrange the nonlinear, augmented and consider partition as follow:

$$R_k \mathbf{X} = \begin{Bmatrix} \mathbf{x}_{A_k^{nl}} \\ \mathbf{x}_{A_k^{AP}} \\ \mathbf{x}_{A_k^{CP}} \\ \mathbf{x}_{B_k} \end{Bmatrix}_k \qquad R_k \mathbf{P}^{\mathbf{xx}} R_k = \left[\begin{array}{c|c|c|c} \mathbf{P}_{\mathbf{x}_{A_k^{nl}} \mathbf{x}_{A_k^{nl}}} & \mathbf{P}_{\mathbf{x}_{A_k^{nl}} \mathbf{x}_{A_k^{l}}} & \mathbf{P}_{\mathbf{x}_{A_k^{nl}} \mathbf{x}_{A_k^{cp}}} & 0 \\ \hline \mathbf{P}_{\mathbf{x}_{A_k^{l}} \mathbf{x}_{A_k^{nl}}} & \mathbf{P}_{\mathbf{x}_{A_k^{l}} \mathbf{x}_{A_k^{l}}} & \mathbf{P}_{\mathbf{x}_{A_k^{l}} \mathbf{x}_{A_k^{cp}}} & 0 \\ \hline \mathbf{P}_{\mathbf{x}_{A_k^{cp}} \mathbf{x}_{A_k^{nl}}} & \mathbf{P}_{\mathbf{x}_{A_k^{cp}} \mathbf{x}_{A_k^{l}}} & \mathbf{P}_{\mathbf{x}_{A_k^{cp}} \mathbf{x}_{A_k^{cp}}} & 0 \\ \hline 0 & 0 & 0 & \mathbf{P}_{\mathbf{x}_{B_k} \mathbf{x}_{B_k}} \end{array} \right]_k \tag{4.41}$$

  The new generated partition and rearrangement make state and covariance ready for application of model substructure decomposition described in the initialization procedure, thus for the application of the Kalman filters class solutions selected for the current cycle.

The proposed approach allows considering the implemented techniques as selectable and the estimation kernel can be reconfigured also run time, defining a proper operative mode of MEONS Controller (Figure II-15). However, not all potentialities have been fully exploited and further investigations are necessary. The run time change of linear/nonlinear partition, even theoretically possible, does not find application in this work that initialize only MUKF at start up in V.4. In general, nonlinear/linear switching partition involves run time augmentation of the MEONS model in order to generate different number of sigma point, so it shall be selected only if necessary. Conversely, active/inactive and augmented/consider can be easily dynamically handled. This active/inactive feature is stressed at navigation level as concern the intermittent measurement bias rearrangement (V.1 and V.3). A Mixed AGKF/CKF example has been provided in V.3 as possible filtering improvement for actuation errors compensation. A mixed MUKF/CKF example, referred as Consider Marginalized Unscented Kalman Filer (CMUKF) is provided in V.4.

It can be concluded that MEONS architecture has been designed in order to change in real-time the filter operative mode and handle by state partition assignment several kind of state vector component:

- Stochastic and deterministic components
- Non-linear and linear components
- State and parameter augmentation
- Systematic errors and colored noises
- adaptive filtering parameters (as external or internal variables)

The baseline notation for the extended state vector decomposition in MEONS navigation study cases $\mathbf{X}$ can be finally defined as $\mathbf{X}^{\mathbf{x}}_{\mathbf{A}^{(\cdot)}}$: the subscript relies on MEONS filter significance , the apex relies on its classification in the state space dynamic model.

IV.3 NUMERICAL IMPLEMENTATION ISSUES

Actually MEONS SW has been designed, developed and tested at high level architectural layer by implementing algorithm and solutions within the MATLAB/Simulink® environment. However, the system functional model looks toward future real time implementation. Some numerical optimizations are described in this section and final filtering cycle is provided as design driver for the on-board integration of the AOC function.

A. Numerical issues and computational cost reduction for real time implementation

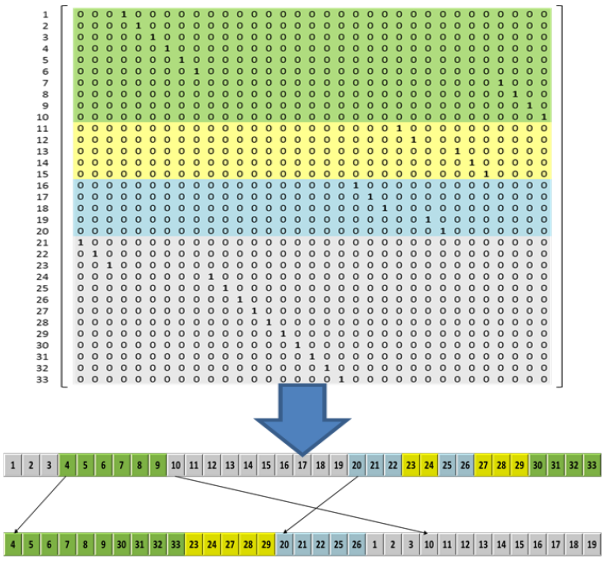

Figure IV-20 Indexing generation from MEONS model participation matrices

Propagator and Observation module optimization

Let us consider the Generic Propagator main mathematical representation i.e. eq. (3.16). Beyond the possibility to manage system configuration by using the propagation controller, the dynamic system maximum realization is always defined by key matrices initialization in eq. (3.16). Actually, it shall be noted that participation matrices representation is a very powerful tool to recognize the state-models relations and problem substructures, at cost of a huge number of matrix elements when a large dimension state vector is considered. This is the case of extended state vector $\mathbf{X}$, which can include STM component as well as generated sigma points

However, these matrices generally show a very sparse structure, so the propagation step, during the initialization phase, can use the sparsity to minimize the dimension of the numerical integration problem, which is reduced to non-null elements. This approach has to be intended as a general aim of minimizing the computational effort without increasing the complexity of the propagation model design and augmentation. In more details, the identification of the effective number of operation to build the right hand side vector $\mathbf{F}(\mathbf{X})$ starting from the computed modules output is independent from the selected matrix representation and it can be mapped in the on-board implementations. The sparse reduction corresponds analytically to the generation of the minimal indexing requested in a real time software framework to perform the algebraic computation $\mathbf{F}(\mathbf{X})$ from M_p (Figure IV-20). The Generic Observer inherit all the propagation design issues, hence the same consideration on matrix representation, sparsity and indexing for real time application can be extended. Beside the optimization of the model right hand side computation, numerical integration step computational burden is mitigated by considering the following fundamentals properties:

1) STM sensitivity component reveals a triangular substructure of the differential problem in eq.(3.11). This structure is preserved during integration, so it is possible to arrange the STM column in order to solve numerically only non-zero term of matrix:

$$\left\{\ldots,\left[\boldsymbol{\Phi}_{\mathbf{S}1}\right]_{sx1},\left[\boldsymbol{\Phi}_{\mathbf{S}2}\right]_{sx1},\ldots,\left[\boldsymbol{\Phi}_{\mathbf{S}n}\right]_{sx1},\left[\boldsymbol{\Psi}_{1}\right]_{sx1},\ldots,\left[\boldsymbol{\Psi}_{n}\right]_{sx1},\left[\boldsymbol{\Phi}_{\mathbf{P}1}\right]_{px1},\left[\boldsymbol{\Phi}_{\mathbf{P}2}\right]_{px1},\ldots,\left[\boldsymbol{\Phi}_{\mathbf{P}n}\right]_{px1}\right\} \quad (4.42)$$

This solution corresponds to separate the state and sensitivity component of extended STM matrix and solve the following differential equation:

$$\begin{aligned}\left[\dot{\Phi}(t,t_0)\right] &= \left[A(\tau)\right]\left[\Phi(t,t_0)\right] \\ \left[\Psi(t,t_0)\right] &= \left[A(\tau)\right]\left[\Psi(t,t_0)\right] + \left[C(\tau)\right] \\ \left[\dot{\mathrm{K}}(t,t_0)\right] &= \left[A(\tau)\right]\left[\mathrm{K}(t,t_0)\right]\end{aligned} \tag{4.43}$$

In addition matrix $\mathrm{K}(t,t_0)$ (and similarly $\Upsilon(t,t_0)$) are independent from state and almost diagonal, so the subsequent statement ((4.44)) can be applied.

2) The extended state can be rearranged in order to point out a triangular substructure also of the dynamic system equations:

$$\dot{\mathbf{X}} = \mathbf{F}(\mathbf{X}) = \begin{cases} \dot{\mathbf{X}}_{NL} = \mathbf{F}_{NL}(\mathbf{X}_{NL}, \mathbf{X}_{LTI}) \\ \dot{\mathbf{X}}_{LTI} = \mathbf{F}_{LTI}\mathbf{X}_{LTI} \end{cases} \tag{4.44}$$

Actually the equations order can be sorted in order to define a lower block subproblem including only linear time invariant part (linear discrete processes can be treated in the same manner). Considering parametric augmentation, common in the considered tracking problems, this partition can be the highest dimensional one. However, the solution for the $\mathbf{F}_{LTI}$ subproblem can be computed analytically by using:

$$\mathbf{\Phi}(\tau,t) = e^{\mathbf{F}_{LTI}(\tau-t)} \longrightarrow x(t_{k+1}) = e^{\mathbf{F}_{LTI}\Delta t}x(t_k) \tag{4.45}$$

where $\Delta t = \mathrm{t_k} - \mathrm{t_{k-1}}$. MEONS manage this issue as the state is ordered in such a way there is a right handside partition depending only by the A matrix. Basically, this procedure introduces a constant, or Zero Order Hold, approximation on lower block linear variables with respect to the numerical integration. However, such approach applies for slowly varying auxiliary parameters. The selection of the linear time invariant partition is in charge to the designer that should trade-off computational load and the introduction of a ZOH approximation of the auxiliary processes.

Configurable Filter optimization

Independently from the specific technique MEONS filter consider as possible computational improvement the optimization of the update step by using sequential processing, namely called scalar update [86]. This approach is widely used to avoid innovation covariance inversion and to extend the solution to a multisensory scenario [86].. This approach fits two MEONS peculiarities:

- The open architecture shall be augmentable with different sensors, as for high level architecture in Figure II-15 . Measurement provided by different sensors are generally considered uncorrelated
- GNSS observables are generally considered uncorrelated and measurement derived from different SVs can be seen as observation provided by a “single” sensor

Actually, except for particular scenarios (differential combinations or channel coupling), the GNSS measurement covariance for absolute navigation can be represented by a diagonal matrix:

$$\mathbf{R}_k = \begin{bmatrix} \sigma^2_{UERE,1} & 0 & 0 & 0 & 0 & 0 \\ 0 & \ddots & 0 & 0 & 0 & 0 \\ 0 & 0 & \sigma^2_{UERE,n_{vis}} & 0 & 0 & 0 \\ 0 & 0 & 0 & \sigma^2_{UERRE} & 0 & 0 \\ 0 & 0 & 0 & 0 & \ddots & 0 \\ 0 & 0 & 0 & 0 & 0 & \sigma^2_{UERRE} \end{bmatrix} \tag{4.46}$$

This copes with the fundamental hypothesis of the serial processing. The uncorellatedness of a measurement batch $\left[\mathbf{z}_1, \mathbf{z}_2, ...\mathbf{z}_N\right]_k$ allows the use of the Kalman filter update sequentially for each "scalar" measurement because it implies whiteness for the scalar measurement noise sequence [86].This approach is actually considered in the MEONS design by introducing an iteration step (see IV.3-B) that allows to repeat cyclically the correction step. It shall be noted that sequential update is a prerogative of the Kalman Filtering Class, and a possible extension to the nonlinear numerical approximation is provided in [110]. A linear transformation can be found in order to project measurement space and obtain diagonal measurement covariance matrix [86]. However, this procedure called whitening can be complex in accordance to the application and baseline MEONS batch update can be preferred.

The natural improvement of sequential processing is the UDU [48] formulation, which is a common strategy to implement covariance processing in real-time flight software. It exploits the symmetric semi-definite property of the covariance matrix, which can be decomposed as $P = UDU^T$ where U is an upper triangular matrix with ones on the main diagonal, and D is a diagonal matrix. As square root methods, this decomposition also improves numerical properties allowing preserving symmetric semi-definite property of the covariance matrix during the computation. Sequential approach is used to efficiently update U and D with measurements defining the so-called rankone update [111] that can be expressed as follow:

$$P^+ = P^- - P^- H^T S^{-1} H P^- \xrightarrow{\textbf{rank one}} U^+ D\, U^{+T} = U^- D^- U^{-T} + c\mathbf{a}\mathbf{a}^T \tag{4.47}$$

where $c = 1/S$ is a scalar in accordance to the sequential update and $\mathbf{a} = D^- U^{-T} H^T$. For CEKF application in [6], UDU implementation has been referred as the best candidate for MEONS solution on-board implementation taking into account the reviewed version of [111] customized for the Consider approach. UDU implementation can be also extended to sigma point solutions by considering results provided in [112]. However further activities shall be carried out in order to implement those numerical optimization in MEONS that in synergy with other filtering complexity reduction methods (CKF,MUKF) will allow an on-flight application.

Due to its importance for the POD application, a dedicated procedure has been implemented in the MEONS recursive kernel in order to handle a proper discretization of the process covariance matrix when it is derived from a continuous time model. For equivalence at the sampling instants, the matrix Q_k must account for the integrated effect of **w**(t) by the system dynamics over each sampling period. With the assumption that **w**(t) is a white noise process [48] it is possible to derive Q_k computing :

$$\mathbf{Q}_k = \int_{t_k}^{t_{k+1}} \mathbf{\Phi}(t_{k+1}, s)\mathbf{G}(s)\mathbf{Q}(s)\mathbf{G}^T(s)\mathbf{\Phi}(t_{k+1}, s)^T\, ds \tag{4.48}$$

A common approximate solution to eq.(4.49) is:

$$Q_k \approx GQG^T T \tag{4.49}$$

which is accurate only when the eigenvalues of **F** are very small relative to the sampling period T. It is preferred to solve (4.48)via a better approach represented by Von Loan Matrix Exponentials and Taylor series. This approach widely agreed in reduced dynamic community [54] for precise stochastic orbit propagation is implemented in order to generate a fully populated process noise covariance matrix starting from the effective error expectation on the residual acceleration term. The Von Loan method [113], which is used in the MEONS algorithm, exploits the availability of the STM in order to compute:

$$\mathrm{M} = e^{\Xi} = \begin{bmatrix} -D & \Phi^{-1}Q_w \\ 0 & \Phi^T \end{bmatrix} \qquad \Xi = \begin{bmatrix} -F & GQG^T \\ 0 & F^T \end{bmatrix} T \tag{4.50}$$

Based on the expressions in the second column of the eq.(4.50), it can be obtained:

$$\Phi = \mathrm{M}\left[(n+1:2n),\ (n+1):2n\right]^T \qquad Q_k = \Phi \mathrm{Y}\left[(1:n),(n+1):2n\right] \tag{4.51}$$

Basically the procedure focuses on the main state variables (i.e. position velocity and time), since for parameters or linear auxiliary process the calculation of can be performed by using (4.49).

B. MEONS Software Model and prediction-correction general cycle

This research looks toward on-board SW development also providing a preliminary MEONS Object-Oriented (OO) style architecture, using Unified Modelling Language notation. This includes a Class Diagram (logical model in Figure IV-21, a State Diagram (state machine behaviour in Figure IV-22), and a Sequence Diagrams (Flowchart model, Figure IV-23). The Class Diagram is designed in order to be integrated within Generic Object Software Paradigm (GOSP) developed by TAS-I for its on-board systems[114].

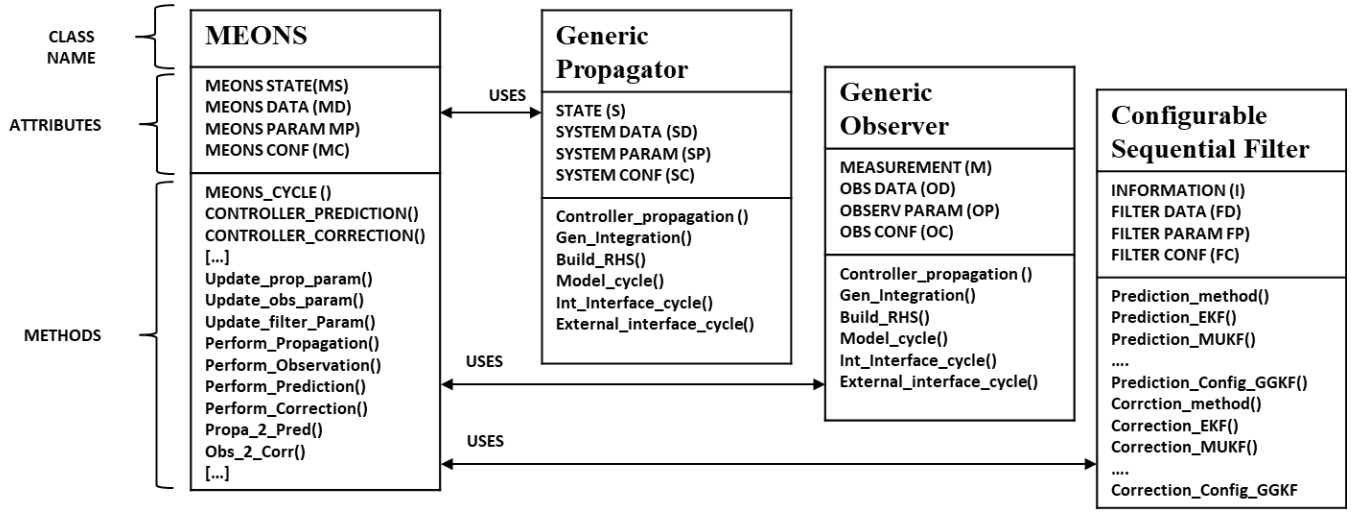

Figure IV-21 Class model

Actually, the proposed architecture for Generic Propagator and Generic Observer model can be seen as a proper declination of GOSP fundamental methods (X, U, Y) which are furthermore decomposed by dynamic, internal and external module in order to improve navigation model scalability.

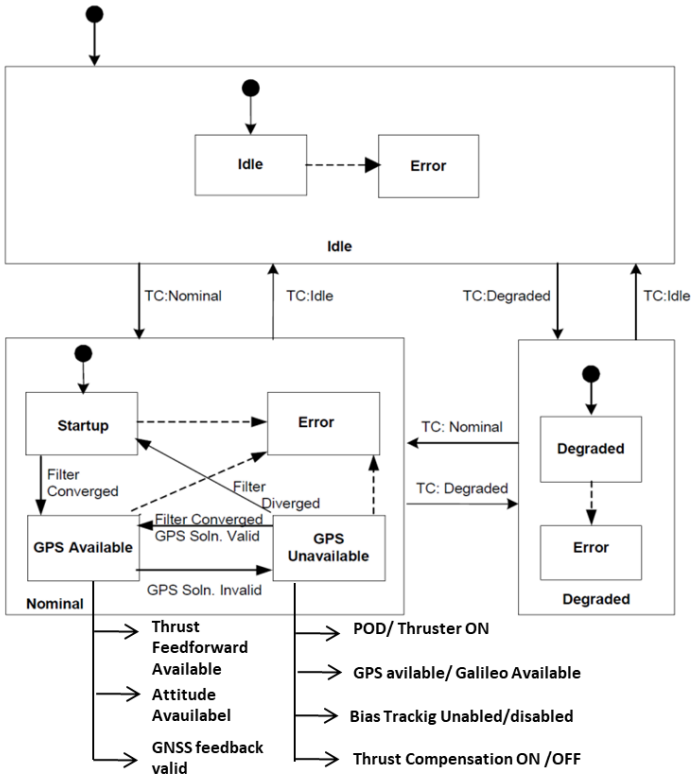

Figure IV-22 state machine

The algorithm is abstracted wrt the specific implementation by generic methods and data structures Figure. State machine in Figure IV-22 define MEONS operative mode transition. Several status and transitions are inherited by the first generation POD system, but new submodes are introduced following low thrust and control management, external platform aiding and Multi-constellation/Multi-antenna solutions. Moreover different internal state can be considered in accordance to the selected filtering scheme (augmented, desensitized, adaptive). A MEONS system mode triggers prediction and correction controllers that set propagation, observation and filtering methods valid for the current MEONS cycle. The cycle is just the sequence of operation necessary to provide a valid a navigation solution. Each block can implement different specific methods (i.e. perform prediction is detailed as MUKF prediction) stated the compatibility with the GGKF framework.

Relevant blocks of Sequence Diagram in Figure IV-23 are hereafter provided in order to complete the SW functional description:

1) Initialize MEONS cycle

The MEONS state machine and the active/inactive cycle block are initialized. Specifically a target MEONS operative mode drives a correspondent setting of Propagation, Observation and Filter Modes. Moreover, all the external data feeding the SW function are dispatched to the proper External Datapool to be acquired by the navigation system.

2) Acquisition

External Datapool reading is performed including:

- Get Measurement:
  - Raw measurement data (Pseudorange,Pseudorange rate)
  - Tracking list management and measurement validation

- Update propagation data:

  - Orbit Propagation and Trasformation Data (physical parameter, Earth rotation coefficients)
  - Control data (Attitude and thruster acceleration)
  - External state and command to force propagation step

- Update Observation data :

  - ID and total number of visible satellites
  - position and velocity of the GNSS visible satellites (or broadcast ephemeris) at transmission time
  - Auxiliary data and constellation correction parameter (i.e. clock corrections)

- Signal to noise ratio C/N_0 for each visible satellite
- External state and command to force observation step

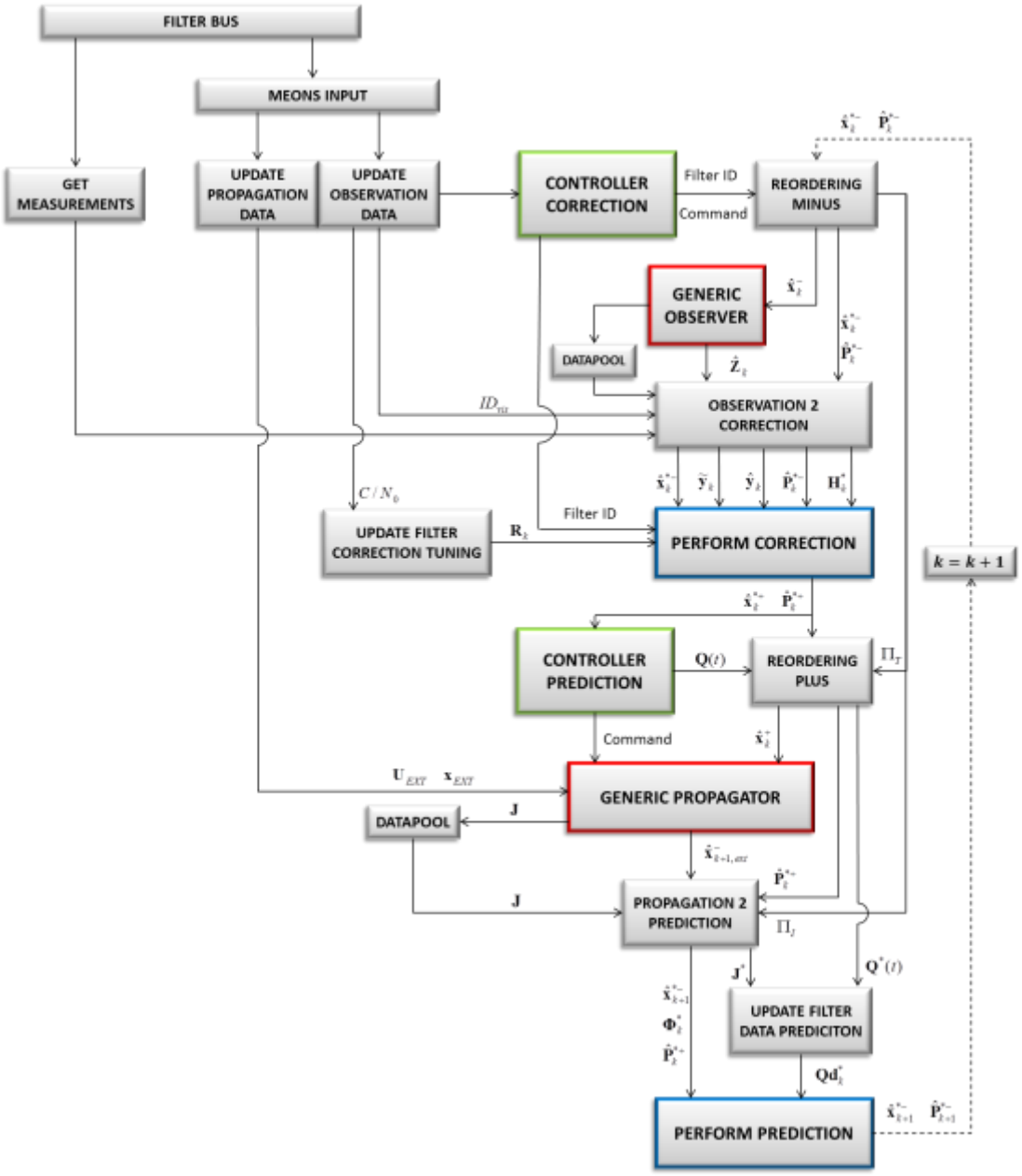

Figure IV-23 MEONS CYCLE Sequence Diagram

➢ Update filter Data

- Full initial state covariance with all MEONS and reset values
- Relevant partition indexing information and initial process and noise covariance
- Covariance thresholds for convergence/divergence or mode transition
- External state and command to force filtering step (i.e. disable correction)

3) Correction

➢ Validation layer

This step has been implemented in order to eventually perform a validation process of the

available solution wrt the current available data. This step works in conjunction with the Controller Correction as it trigger possible autonomous transition.

- Controller Correction

  Controller Correction block is the control unit of the Observation/Correction step. In this block are defined and arranged all the information allowing implementing a MEONS Operative Mode. An operative mode is characterized by the definition of the current partitioning (estimated, consider etc.) and of enable/disable modules of the Generic Observer.

- Reordering Minus

  On the basis of the operative mode defined by the Controller Correction function, the Reordering Minus function performs the reordering of all the variables of the filter in accordance to the procedure described in IV.2. . The Reordering Minus block performs the reorder of the estimated state $\hat{\mathbf{x}}_k^-$ prior the correction and the predicted covariance matrix $\widehat{\mathbf{P}}_k^-$ prior the correction.

- Perform Generic Observer

  Controller Correction manage active measurement reconstruction pattern (i.e. one that associated to a space vehicle) in order to command Observer Controller. All extended measurement equations are here computed in order to fill observation vector and observer datapool (i.e. Jacobians).

- Observation to Correction

  The Observation to Correction block has the function to prepare all the data necessary for the correction phase of the filtering process. This block reads the outputs of the Generic Observer function and rearranges Jacobians and/or sigma points in accordance to the selected Kalman filtering method. All this information takes into account the reordering process in order to project in the proper mode all the relevant filter matrices (i.e Jacobians etc.).

- Update Filter Correction Tuning

  This block computes the measurement noise covariance matrix and computes all the noise level parameters. For instance in V.3 and V.4 the GNSS hardware noise component is modulated in accordance to the eq.(3.40) from the available C/N0. This step is also allocated in order to eventually manage or interface adaptive tuning algorithms applicable on measurement covariance (IV-1-D) and set the correspondent matrix element. In general, this method is designed to handle all the function that act on specific filter method tuning parameters and not on the state and state covariance.

- Perform Correction

  This block performs the correction phase in accordance to the selected filtering configuration. In this phase the different state partition becomes effective if DSM method is considered to merge the different solutions.

- Iterate Observation/Correction

  This block is simply a re-initialization of all data allowing repeating Observation/Correction Sub-cycle in order to eventually perform update sequential approach or recursive observation model computation.

- Diagnostic and preprocessing

  All the statistics and quality indexes are here computed from all available information. If necessary, an additional processing of observation data and a posteriori estimate is used in order to make them compatible with the subsequent prediction step (i.e. different extended state for prediction and correction)

4) Prediction

- Validation layer

  A validation process is performed on a posteriori data eventually on the basis of external aiding or internal threshold. At this step also decision on autonomous transition can be performed in conjunction with the Controller Prediction.

- Controller Prediction

  Controller Prediction block is the control unit of the Propagation/Prediction step. MEONS Operative Mode define partitioning (estimated, consider etc.) and of enable/disable modules of the Generic Propagator.

- Reordering Plus

  On the basis of the operative mode defined by the Controller Prediction function, the Reordering plus block performs the reorder of the estimated state $\hat{\mathbf{x}}_k^+$ posterior the correction and the corrected covariance matrix $\widehat{\mathbf{P}}_k^+$ prior the correction in accordance to the procedure described in IV.2. ..

- Perform Generic Propagator

  All extended dynamic modules are enabled/disabled in accordance to Prediction Controller commands. The computed state update, state transition component and Jacobians fill prediction state vector and datapool.

- Propagation to Prediction

  The Propagation to Prediction block has the function to prepare all the data necessary for the prediction phase of the filtering process. This block reads the outputs of the Generic Observer function and rearranges STM and/or sigma points in accordance to the selected Kalman filtering method, taking into account the reordering process

- Update Filter Prediction Tuning

  This block computes the process noise covariance matrix and computes all the noise level parameters. The procedure described in (4.50) is here performed. This step manages the adaptive tuning algorithms, as one that presented in IV-1-D and set the correspondent covariance element. As for correspondent correction step this methods is designed to handle all the function that act on specific filter tuning parameters.

- Perform Correction

  This block performs the prediction phase in accordance to the selected filtering configuration. This step trigger the selected method of the Kalman filter Class. DSM method is considered to eventually merge the different solutions.

- Iterate Observation/Correction

  A re-initialization step used to repeat Propagation/Prediction subcycle allows to consider higher rate propagation between filter prediction cycle or prediction step between corrections.

CHAPTER V

PERFORMANCE ANALYSIS AND TESTING FOR MEONS APPLICATION IN DIFFERENT MISSION SCENARIOS

V.1 CONSTRAINED SINGLE DIFFERENCE CDGPS FOR SABRINA FORMATION POD

A. Mission scenario: Follow up of SABRINA formation flying study

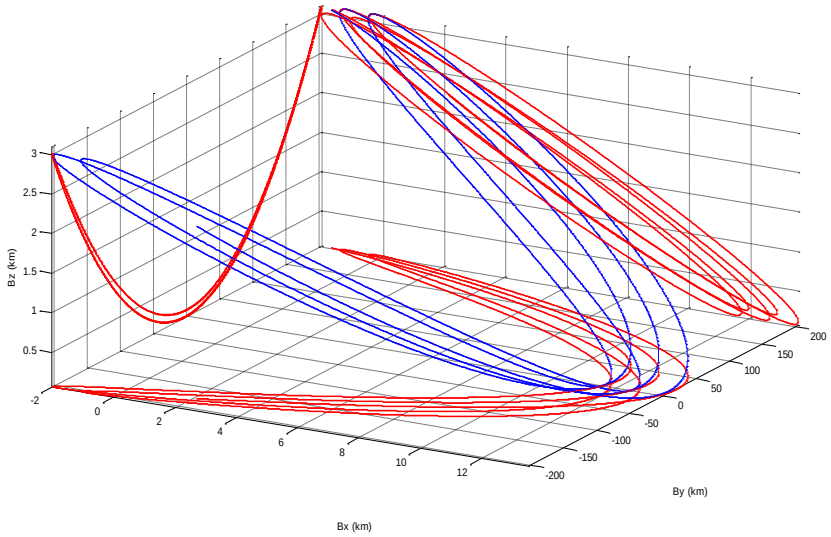

Figure V-1 Pendulum Formation 3D baseline in ORF reference frame (blue) with planar projection (red)

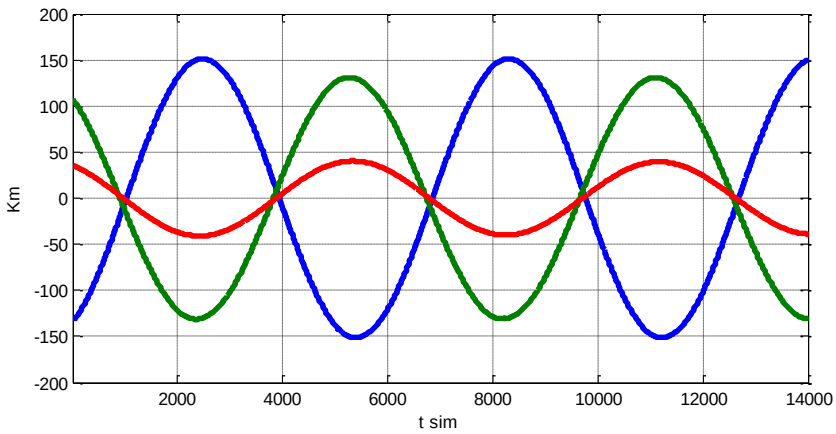

Figure V-2 Δx^{AB} (blue) Δy^{AB} (green) Δz^{AB} (red) Pendulum Formation baseline components in ECI reference frame

MEONS has been designed in order to handle on board CDGPS relative navigation envisaged in the frame of TAS-I SABRINA research program [41]. Even the relative navigation results refers to MEONS embrional version, the performed numerical test gives evidence of MEONS compatibility with Formation Flying Applications [37] and modern solution proposed for dynamic filtering of CDGNSS measurements (II.2-A). Orbital data defined in Table II-4 has been used in the GSS environment in order to generate formation dynamic as well as correspondent GNSS scenario.

Selected Cosmo Skymed Master S/C-A and BISSAT Slave S/C-B formation allows covering a wide range of baseline excursion from a few kilometres to almost 200Km. This can be appreciated in Figure V-1 and Figure V-2, which represent respectively relative motion in the Master Orbital Reference Frame (ORF) and baseline ECI components. A nominal Bistatic imaging observation scenario is considered, so orbital free motion and stable Right/Left looking attitude are assumed in order to perform observation geometry.

The GSS modules, simulating hosted dual frequency L1/L2 GPS receivers, generate 1Hz pseudoranges and carrier phase measurements for the in view SVs. Receiver measurement and auxiliaries data (i.e. SVs ephemeris) feeds the relative navigation architecture provided in Figure V-3, whose main steps can be summarized as follow:

- The Precise Orbit Determination algorithm processes the Master GNSS measurements and propagates the master spacecraft PVT (Position, Velocity and Time) in order to provide the reference for the relative navigation filter
- The Master navigation unit receives the Slave GNSS measurements through the inter-satellite communication channel and processes them in order to build Single Difference observables selecting common in view SVs
- The SD measurements (III.2-B) are arranged and processed by the Relative Filter in order to obtain the relative state and the float SD ambiguities estimate
- The float estimation is rearranged to form the DD ambiguities (III.2-B) to feed the LAMBDA method searching algorithm that fix the target integer value
- The fixed and validated ambiguities are used to constraint the relative navigation solution

S/C Dynamic model (Reduced DSS)			
Parameter	**Symbol**	**Value S/C A**	**Value S/C B**
Starting date	yi, mi-,di	2011/06/21	2011/06/21
mass (kg)	mass (kg)	1870	1320
drag coefficient	CD and Area	2.25, 5.44m^2	2.25, 4.6m^2
Solar Radiation Coefficient	CR and Area	1.3, 32m^2	1.3, 26m^2
Reference orbit Sentinel LEO solar-synchronous orbit	$\{a, e, i, \Omega, \omega, \nu\}$	Table II-4	Table II-4
Operative attitude conditions	$\{q, \omega\}$	The satellite is controlled on the three axis for nadir pointing	The satellite is controlled on the three axis for nadir pointing

GNSS Scenario Simulator			
GSS Module	**Simulation Approach**	**Parameter**	**Value**
Constellation	GPS legacy	N° SVs	24
Visibility analysis	Geometrical selection	FOV Rx (half angle) FOV Tx (half angle)	85° 26°
Measurements	P_{L_1} P_{L_2} L_1 L_2	Rate	1Hz

GNSS Error budget and Filtering				
GNSS error source	**Simulation Approach**	**Pseudoranges 1σ**	**Phase 1σ**	**Estimation/calibration approach (Relative)**
Receiver clock bias and drift	Discrete-time model with colored noise	Residuals Negligible	Residuals Negligible	On line estimation
Satellite Ephemeris and Clock Correction	Low level GNSS data deviations	<0.5m	<0.5m	Compensated by SD combination in relative navigation
Ionospheric delay	VTEC file interpolation	5-12m	5-12m	Calibrated using Ionofree combination and VTEC
Ambiguity	Random Constant Model	-	10^4 cycles	On line estimation
Multipath	Normally distributed random error included in (χ_i)	1m	0.002m	included as equivalent ranging error by filter measurement noise covariance matrix
Measurement noise	Random noise with nominal performance	0.5m	0.005m	

Table V-1 Bissat Test Case Simulation Setting

All the simulation parameters concerning both dynamic and measurement error generation have been summarized in Table V-1. GNSS constellation errors are removed by SD combination so they do not impact baseline estimation. Constellation errors affect absolute reference estimation, but a low level error is introduced considering good visibility and high update rate of navigation data. Conversely, high level ionospheric path delay has been simulated by using GSS error model (Appendix C), since its effect can be relevant for large baseline estimation [115].

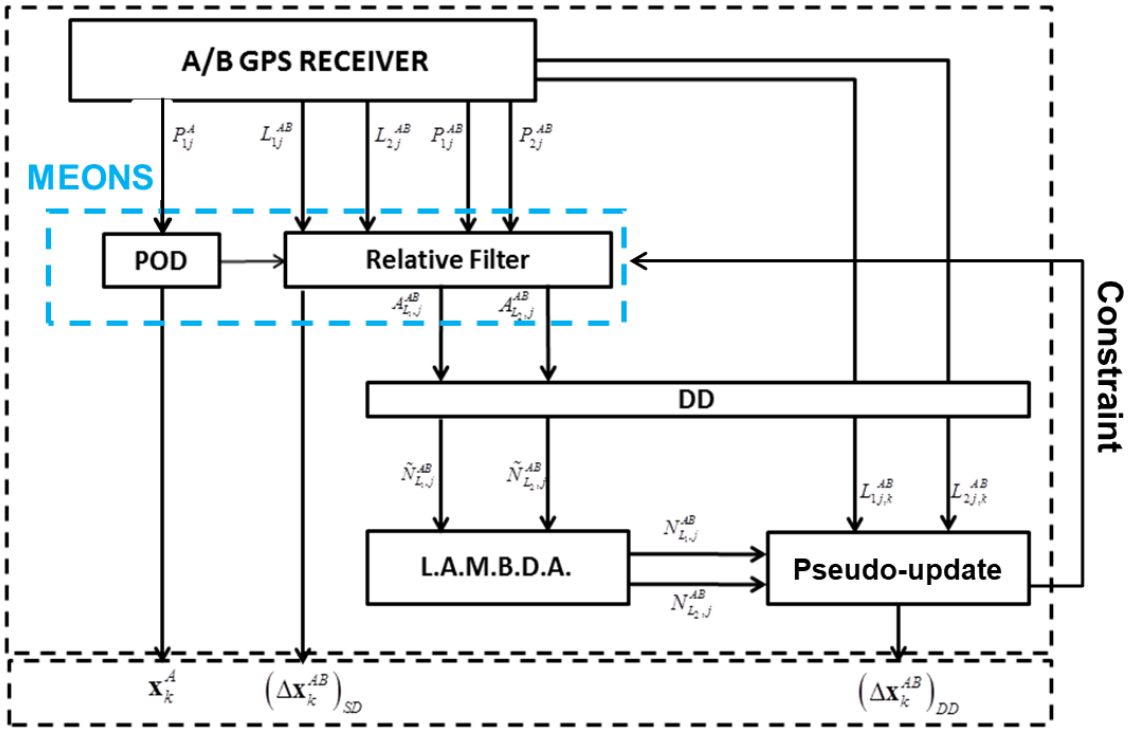

Figure V-3 Relative Navigation Architecture for Formation Flying Application

B. MEONS filter configuration

MEONS filter accomplishes the precise orbit determination of the Master satellite and the implementation of the CDGPS based relative filter within the same prediction/correction cycle. The selected approach relies on [65] integrating within an EKF framework the direct difference between the single spacecraft propagation and the SD differential corrections. However, a modification is introduced by implementing the calibration procedure proposed in [40] in order to handle large baseline ionospheric errors.

Considering eq.(3.16) the relative EKF variational model can be represented as follow:

$$\begin{cases} \left(\mathbf{X}_{k+1}^{A}\right)^{-} = \mathbf{f}_{k}^{A}\left(\mathbf{X}_{k}^{A}, t_k\right) \\ \left(\Delta\mathbf{X}_{k+1}^{AB}\right)^{-} = \mathbf{f}_{k}^{B}\left(\left(\mathbf{X}_{k}^{A} + \Delta\mathbf{X}_{k+1}^{AB}\right), t_k\right) - f_{k}^{A}\left(\mathbf{x}_{k}^{A}, t_k\right) \end{cases} \rightarrow A = \begin{bmatrix} A^{A} & 0 \\ 0 & A^{AB} \end{bmatrix} \qquad B_{1\ldots M} = \begin{bmatrix} B^{A} & 0 \\ B^{A} & B^{B} \end{bmatrix}$$

$$\begin{cases} \left(\mathbf{Y}_{k}^{A}\right)^{-} = \mathbf{h}_{k}^{A}\left(\mathbf{X}_{k}^{A}, t_k\right) \\ \left(\mathbf{Y}_{k}^{AB}\right)^{-} = \mathbf{h}_{k}^{AB}\left(\mathbf{X}_{k}^{A}, \Delta\mathbf{X}_{k}^{AB}, t_k\right) \end{cases} \rightarrow E_{1\ldots M} = \begin{bmatrix} E^{A} & 0 \\ 0 & E^{AB} \end{bmatrix} \qquad (5.1)$$

$$\mathbf{X}_{k}^{A} = \{\mathbf{x}_{k}^{A}, \mathbf{p}_{k}^{A}, \mathbf{u}_{k}^{A}, \Phi_{1}^{A}, \Phi_{2}^{A}, \ldots, \Phi_{n}^{A}\} \qquad \mathbf{X}_{k}^{AB} = \{\mathbf{x}_{k+1}^{AB}, \mathbf{p}_{k+1}^{AB}, \mathbf{u}_{k+1}^{AB}, \Phi_{1}^{B}, \Phi_{2}^{B}, \ldots, \Phi_{n}^{B}\} \qquad \mathbf{X}_{k}^{B} = \mathbf{X}_{k}^{A} + \Delta\mathbf{X}_{k}^{AB}$$

$$\mathbf{Y}_{k}^{A} = \{\mathbf{y}_{k}^{A}, H_{1}^{A}, H_{2}^{A}, \ldots, H_{n}^{A}\} \qquad \mathbf{Y}_{k}^{AB} = \{\mathbf{y}_{k}^{AB}, H_{1}^{B}, H_{2}^{B}, \ldots, H_{n}^{B}\}$$

Where $\mathbf{f}_k^A$ and $\mathbf{f}_k^B$ are baseline MEONS orbit propagation model (Table III-1) for the Master and Slave S/C, $\mathbf{h}_k^A$ represent the ionofree Pseudorange/Doppler measurement model used for absolute navigation, $\mathbf{h}_k^{AB}$ represents the linearized SD relative observation model derived from eq. (3.35), $\Phi_i^A, \Phi_i^B, H_i^B, H_i^B$ are the dynamic STM and observation Jacobians matrices evaluated considering $\mathbf{X}_k^A$ and $\mathbf{X}_k^B$ trajectories. It shall be noted that relative motion is coupled with Master state positioning, which is used as reference trajectory to update the position and STM of the slave starting from the propagated or estimated baseline $\Delta\mathbf{X}_k^{AB}$. This coupling introduces on the relative accuracy a maximum error of 0.02 cm, which corresponds to 1% of the expected 2m on board absolute POD performance [65]. Actually, the absolute filter block is the same used in the next section, so the budget assume ionofree combination, low level constellation error (Table V-1.) and proper filter tuning. The performance analysis hereafter provided focuses on the MEONS relative EKF, whose filtering setting is summarized in Table V-2 .

MEONS Sequential Filtering	
KF class method	Standard EKF is augmented with an ambiguity constraint step by using exact measurement observation method described in [38]
Extended State and Covariance Partition	The extended state $\mathbf{X}$ is partitioned in : ➢ Reference state $\mathbf{X}_{A^e}^{\mathbf{x}} \rightarrow \mathbf{x}^{AB}(t) = \left\{\mathbf{r}^{AB}, \dot{\mathbf{r}}^{AB}, , \Delta t^{AB}, \Delta \dot{t}^{AB}\right\}$ ➢ Augmented parameters $\mathbf{X}_{A^e}^{\mathbf{p}} \rightarrow \begin{cases} \mathbf{p}_{Pert}^{AB} = \left\{\Delta C_D^{AB}, \Delta C_R^{AB}, a_R^{AB}, a_T^{AB}, a_N^{AB}\right\} \\ \mathbf{p}_{iono}^{AB} = \left\{VTEC_A, VTEC_B\right\} \\ \mathbf{p}_{Amb}^{AB} = \left\{A_{L_1,1}^{AB}, A_{L_1,2}^{AB}, ..., A_{L_1,j}^{AB}, A_{L_2,1}^{AB}, A_{L_2,2}^{AB}, ..., A_{L_2,j}^{AB}\right\} \end{cases}$ The correspondent filter covariance $P_{\mathbf{XX}}$ is: $P_{\mathbf{XX}} = \begin{bmatrix} P_{\mathbf{X}_{A^e}^{\mathbf{x}}\mathbf{X}_{A^e}^{\mathbf{x}}} & P_{\mathbf{X}_{A^e}^{\mathbf{x}}\mathbf{X}_{A^e}^{\mathbf{p}}} & 0 \\ P_{\mathbf{X}_{A^e}^{\mathbf{p}}\mathbf{X}_{A^e}^{\mathbf{x}}} & P_{\mathbf{X}_{A^e}^{\mathbf{x}}\mathbf{X}_{A^e}^{\mathbf{p}}} & 0 \\ 0 & 0 & P_{\mathbf{X}_B\mathbf{X}_B} \end{bmatrix}$ $P_{\mathbf{X}_{A^e}^{\mathbf{p}}\mathbf{X}_{A^e}^{\mathbf{p}}} = diag\left(P_{\mathbf{p}_{Pert}^{AB}\mathbf{p}_{Pert}^{AB}}, P_{\mathbf{p}_{iono}^{AB}\mathbf{p}_{iono}^{AB}}, P_{\mathbf{p}_{Amb}^{AB}\mathbf{p}_{Amb}^{AB}}\right)$ $P_{\mathbf{X}_B\mathbf{X}_B} = P_{\mathbf{p}_{Amb,j+1}^{AB}\mathbf{p}_{Amb,j+1}^{AB}}$
Stochastic model peculiarities	Variable State Dimension with inactive variable set: $\mathbf{X}_B = \left\{A_{L_1,j+1}^{AB}, A_{L_1,j+2}^{AB}, ..., A_{L_1,j+N}^{AB}, A_{L_2,j+1}^{AB}, A_{L_2,j+2}^{AB}, ..., A_{L_2,j+N}^{AB}\right\}$
Special topics and remarks	The ambiguities are considered inactive static variables, so their covariance will be reset when the target SV is in tracking. However, reordering procedure guarantees the continuity and information transfer of already converged ambiguities

Table V-2 MEONS Relative EKF configuration

The large state vector augmentation (Table V-2) is devoted to handle the following baseline determination peculiarities:

1) The validity of the differential approach for very long baselines needs specific solutions due to different experienced GNSS propagation pattern. The selected technique [40] includes the Vertical Total Electron Content (VTEC) parameter in the state vector (Random Walk processes [105]). This allows to run time estimate the ionospheric differential path delay $I_j = J_j^B(E_j^B)VTEC_B - J_j^A(E_j^A)VTEC_A$ affecting the following SD observation model:

$$\mathbf{z} = \mathbf{h}(\mathbf{x}(t), t) => \begin{cases} P_{1j}^{AB} = r^{AB}{}_j + \Delta t^{AB} + (J_j^B(E_j^B)VTEC_B - J_j^A(E_j^A)VTEC_A) + v_{j,P1}^{AB} \\ P_{2j}^{AB} = r^{AB}{}_j + \Delta t^{AB} + \frac{f_{L1}^2}{f_{L2}^2}(J_j^B(E_j^B)VTEC_B - J_j^A(E_j^A)VTEC_A) + v_{j,P2}^{AB} \\ L_{1j}^{AB} = r^{AB}{}_j + \Delta t^{AB} - (J_j^B(E_j^B)VTEC_B - J_j^A(E_j^A)VTEC_A) + \lambda_{L1} A_{L1,j}^{AB} + v_{j,L1}^{AB} \\ L_{2j}^{AB} = r^{AB}{}_j + \Delta t^{AB} - \frac{f_{L1}^2}{f_{L2}^2}(J_j^B(E_j^B)VTEC_B - J_j^B(E_j^B)VTEC_A) + \lambda_{L2} A_{L2,j}^{AB} + v_{j,L2}^{AB} \end{cases} \quad (5.2)$$

Notation of eq.(5.2) observation model are provided in Appendix B.

2) It is assumed that no orbit control actions are present and the dynamic is in steady state condition. The relative perturbations deviation becomes the relevant tuning dynamic parameters coping with the reduced dynamic paradigm. The S/C $\Delta C_D^{AB}, \Delta C_R^{AB}$ are modelled as random constant processes, while empirical acceleration $a_R^{AB}, a_T^{AB}, a_N^{AB}$ are implemented as GM-1 (Appendix A).

3) The SD float ambiguity state variables are updated in accordance to variable state dimension filtering overriding intermittent SVs signal tracking (IV.1-E). When the L.A.M.B.D.A integer search [116] converges, the Relative Extended Kalman Filter applies the available DD integer ambiguity fix as solution algebraic constraint. Actually, the following virtual correction step is introduced :

$$\left(\hat{\mathbf{x}}_k^+\right)_{vinc} = \hat{\mathbf{x}}_k^+ + P_k^+ H_k^T \left(H_k P_k^+ H_k^T\right)\left(H_k \hat{\mathbf{x}}_k^+ - d\right) \quad (5.3)$$

Specifically, the exact measurements d are the available integers N_{DD} and the relevant observation equations are defined by the difference operator leading from SD to DD equations:

$$\begin{cases} d = \left[N_{DD_{L1}}, N_{DD_{L2}}\right] \\ H_k = \left[0_{2n-2x2n}, T_{DD,2n-2x2n}\right] \end{cases} \qquad T_{DD} = \begin{pmatrix} -1 & 1 & 0 & 0 & 0 \\ -1 & 0 & 1 & 0 & 0 \\ \vdots & \vdots & \vdots & \ddots & 0 \\ -1 & 0 & 0 & 0 & 1 \end{pmatrix} \quad (5.4)$$

Considering DD integers as state variable can be more accurate, since it does not require clock model information and tuning, but higher complexity pivoting procedure is required in order to handle the tracking update [40]. The constrained solution [65], allowing to return into the SD filter the information of the integer nature of the ambiguity, is here presented as low complexity alternative wrt the direct DD solution. The DD direct approach of [40] will be considered as MEONS extension in the future.

L.A.M.B.D.A method used for integer search is a legacy solution in real time GNSS applications. Its detailed description is out of scope of this work and a complete analysis can be found in [116]. Here, the focus is on the MEONS navigation filter contribution. Actually the integer search minimization objective is expressed as:

$$\min_{n_{LS} \in Z^n} \left\| \hat{a} - n_{LS} \right\|_{Q_a}^2 \Rightarrow \min_{n_{LS} \in Z^n} \left(\hat{a} - n_{LS}\right)^t Q_{\hat{a}}^{-1} \left(\hat{a} - n_{LS}\right) \quad (5.5)$$

where $\hat{a}$ and Q_a are provided by relative EKF as they respectively correspond to the float ambiguity

$A^{AB}_{L_1,1}, A^{AB}_{L_2,1}$ estimation and to the correspondent covariance $P_{\mathbf{p}^{AB}_{Amb}\mathbf{p}^{AB}_{Amb}}$. This means that a high accuracy estimation process can speed up the convergence by reducing the dimension of the integer solution search space defined by $A^{AB}_{L_1,1}, A^{AB}_{L_2,1}$ and $P_{\mathbf{p}^{AB}_{Amb}\mathbf{p}^{AB}_{Amb}}$.

Filter covariance setting	
State initial covariance $\mathbf{P}^0_{xx}$	$P^0_{\mathbf{x}^x_{A^e}\mathbf{x}^x_{A^e}} = \begin{cases} \sigma^0_{\mathbf{r}^{AB}} = 2_{[m]} \quad \sigma_{\dot{\mathbf{r}}^{AB}} = 0.01_{[m/s]} \\ \sigma^0_{\Delta t^{AB}} = 50_{[m]} \quad \sigma^0_{\Delta \dot{t}^{AB}} = 1_{[m/s]} \end{cases}$
auxiliary state and parmaters covariance $\mathbf{P}_{x\mathbf{p}}$	$P^0_{\mathbf{x}^x_{A^e}\mathbf{x}^p_{A^e}} = \begin{cases} \sigma^0_{\Delta C_D} = 0.013 \quad \sigma^0_{\Delta C_R} = 0.013 \quad \sigma^0_{\mathbf{a}_{R,T,N}} = 5\cdot 10^{-8}{}_{[m/s^2]} \\ \sigma^0_{VTEC^A} = 20_{[TECU]} \sigma^0_{VTEC^B} = 20_{[TECU]} \quad \sigma_{A^{AB}_{L_1,2}} = \sigma_{A^{AB}_{L_2,2}} = 10^4{}_{[cycles]} \end{cases}$
Process noise covariance $\mathbf{Q}$ and	$\sigma_{p_1^{AB}} = \left(10^{-7}\frac{m}{s^2}\right) \quad \sigma_{p_2^{AB}} = \left(10^{-7}\frac{m}{s^2}\right) \quad \sigma_{p_3^{AB}} = \left(10^{-7}\frac{m}{s^2}\right) \quad \alpha_{p^{AB}_{i=1,2,3}} = 0.01$ $\sigma_{\Delta t^{AB}} = (100\ m) \quad \sigma_{VTEC^A} = (1\ TECU) \quad \sigma_{VTEC^B} = (1\ TECU)$
measurement noise covariance $\mathbf{R}$	$\sigma_{P_1^{AB}} = \sqrt{2}(0.5m) \quad \sigma_{P_2^{AB}} = \sqrt{2}(0.5m)$ $\sigma_{L_1^{AB}} = \sqrt{2}(0.005m) \quad \sigma_{L_2^{AB}} = \sqrt{2}(0.005m)$

Table V-3 Relative EKF Initialization setting

The tuning of the relative EKF have been carried out by properly setting the process and measurement covariance matrices on the basis of the expected size of the dynamic unmodelled terms. The setting to be considered hereafter is summarized in Table V-3 . The $\sqrt{2}$ scale factor, applied on raw measurement noise, takes into account linear combination of absolute measurement

C. Results

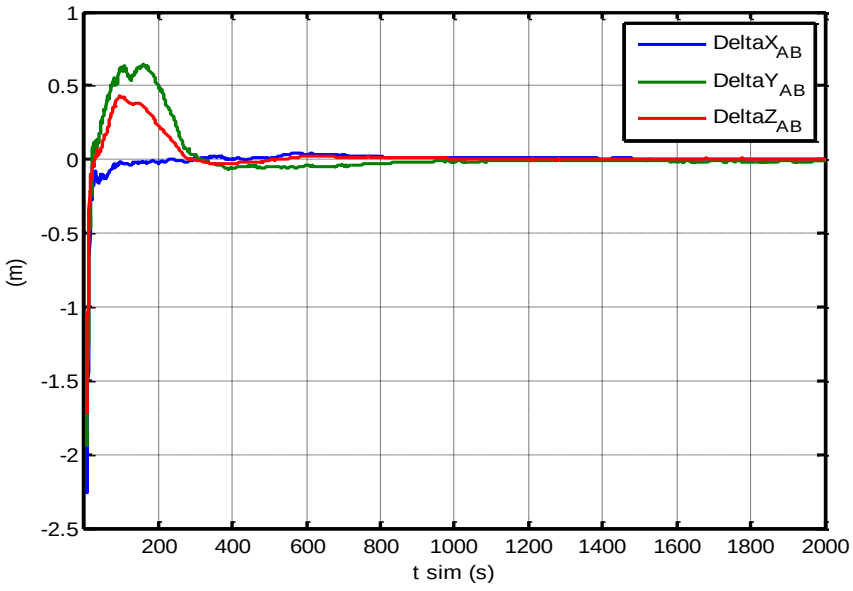

Figure V-4 Relative filter error (ECI) transient

After 2000s the relative filter reaches its nominal performance Figure V-4 Relative filter error (ECI) transient. Accuracy at steady state is provided from Figure V-5 to Figure V-7. Specifically, the relative position and velocity errors are plot together with their numerical mean (blue line) and three σ values (red line) reported in Table V-4. The target centimetre performance is achieved for the most of the two orbit duration. The performance degrades only when the number of satellite is very low Figure V-8. As expected the number of common satellite in view follows the satellite baseline oscillation increasing when the S/C come close.

However, the algorithm demonstrates a good robustness wrt zone where the geometrical condition varies rapidly guaranteeing a real time continuous update of the state estimation.

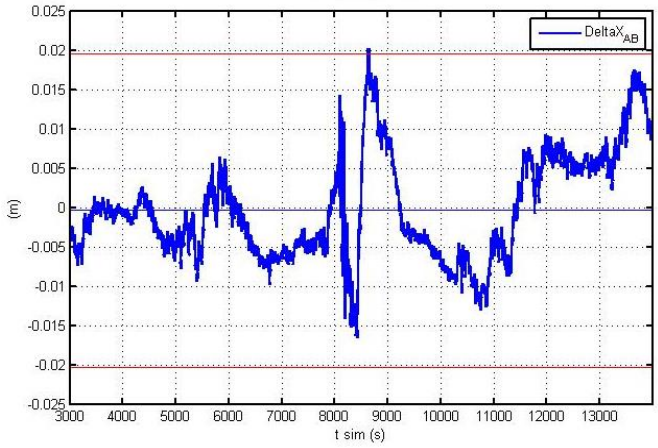

Figure V-5 Baseline error x^{AB} (ECI)

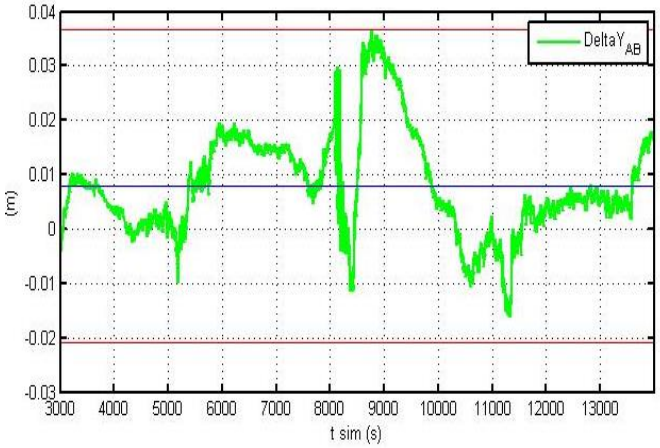

Figure V-6 Baseline error y^{AB} (ECI)

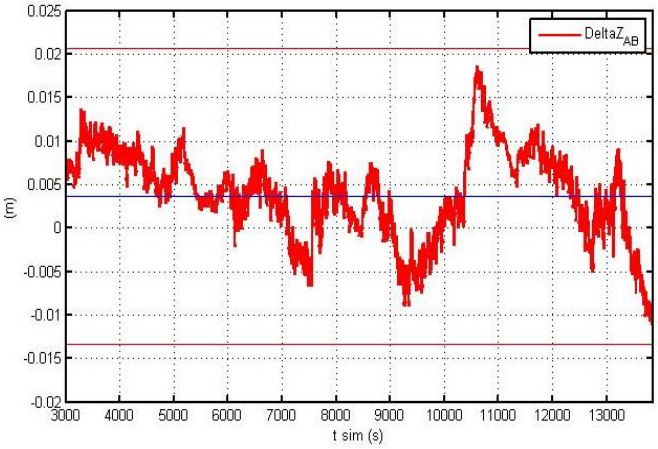

Figure V-7 Baseline error z^{AB} (ECI)

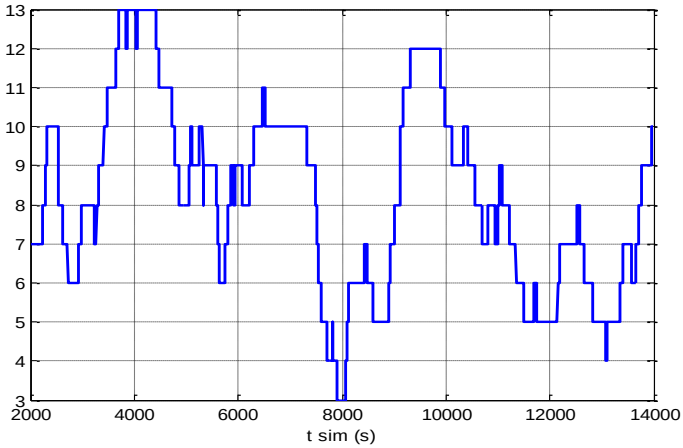

Figure V-8 Number of common in view SVs

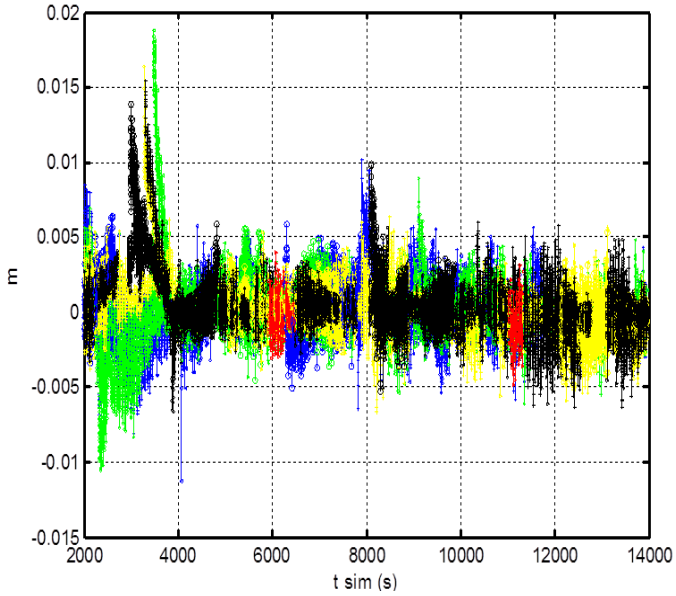

Figure V-9 I_j ionospheric path delay : different colors relies to different tracked SVs

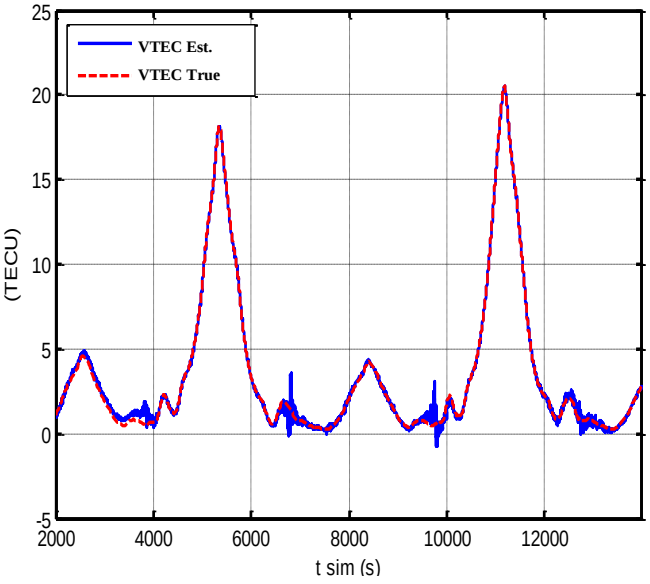

Figure V-10 Estimated VS true VTEC (Master S/C A)

The use of VTEC has provided a successfully result in the estimation of ionospheric differential delay (Figure V-9). It varies with the position along the orbit and exhibits the expected maxima and minima crossing geomagnetic equator. The model seems slightly efficient (Figure V-10) only in points where the baseline achieves the minimum: this condition seems generated by critical geometrical condition for J_j^A, J_j^B factors, but it does not have relevant impact on the overall ionospheric differential delay estimation.

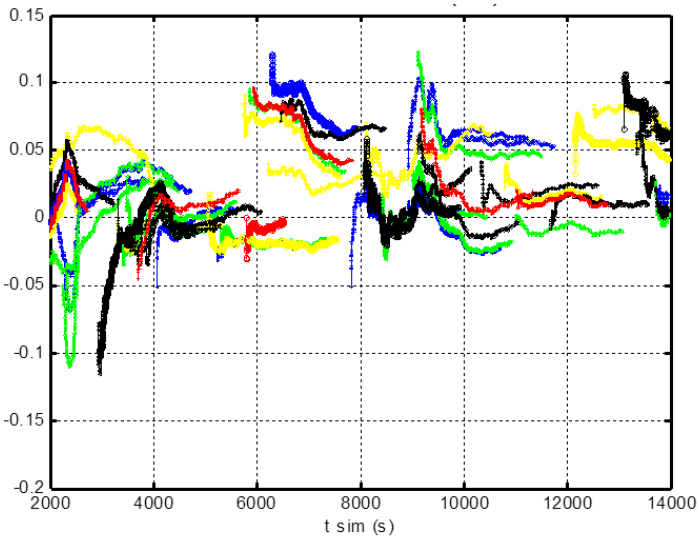

Figure V-11 Float Ambiguity Error, different colours relies to different tracked SVs

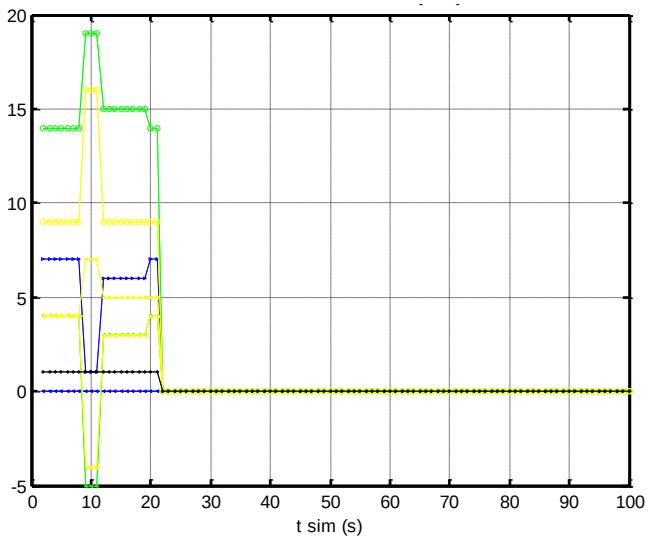

Figure V-12 Integer Ambiguity Error different colours relies to different tracked SVs

The most important result of the entire relative navigation algorithm is the estimation of the float ambiguities. Actually the error wrt correct values (Figure V-11) confirms not only the reaching of the target performance, but also the capacity to continuously transfer the estimated ambiguities and their covariance wrt the changing in the satellite in view set. The LAMBDA reaches in a short time the correct value of the integer double difference ambiguities due to float accuracy inferior than one cycle.

No jumps are experienced after transient phase due to float accuracy after convergence. Basically this simulation does not model other issues (i.e. cycle slip) therefore some issue can be raised in effective hardware applications. However, the COSMO-BISSAT numerical analysis confirms MEONS compatibility with CDGPS precise baseline determination for formation flying applications.

MEONS CDGPS PERFORMANCE		
State Variable	$\mathbf{x}^{AB}\ \mathbf{y}^{AB}\ \mathbf{z}^{AB}$ **(mm)**	$\mathbf{x}^{AB}\ \mathbf{y}^{AB}\ \mathbf{z}^{AB}$ **(μm)**
Mean	**0.131** **-5.875** **-3.091**	**1.153** **0.144** **-1.121**
Standard deviation	**19.312** **-24.317** **13.701**	**173.103** **188.206** **175.708**

Table V-4 Relative position and velocity performances

V.2 ADAPTIVE KALMAN FILTERING ON HIL GENERATED GPS RECEIVER DATA

A. Mission scenario: Copernicus Sentinel-1 test bench

Figure V-13 Copernicus Sentinel-1 Spacecraft

The real time applicability of the adaptive criteria discussed in IV.1-C has been investigated in [104]. The analysis exploits MEONS absolute orbit navigation configuration in order to process Hardware In the Loop GPS data. The main scope of the test is validating MEONS real time adaptive filtering solution verifying also the possibility to achieve on-board sub-metrical geo-location accuracy for improved Fast SAR Imaging Products II.2-A. Target hardware is the 8 channel Engineering Qualified Model (EQM) GPS receiver, available on the Avionics Test Bench (ATB) for Sentinel-1B program. Specifically, the ATB is in charge of providing the required facilities to support testing and maintenance activities from a functional point of view.

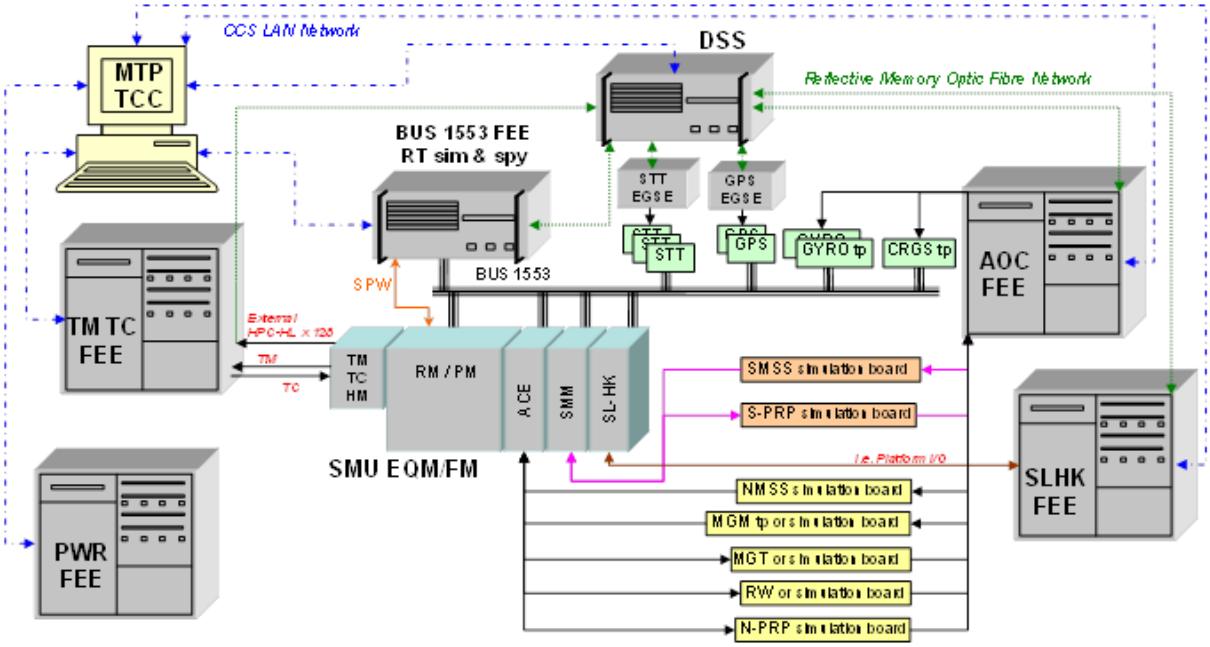

Figure V-14. Avionics Test Bench block diagram (TAS-I intellectual property)

The main functions performed by the Avionics Test Bench are:

- providing the facility to support the real-time simulation of satellite dynamics (DSS)
- providing the simulation of the Telemetry/Telecommand link (TM/TC FE)
- providing the I/F for the external HIL command acquisition (AVS FE)
- providing the simulation of all the external HW I/F (Standard I/O)
- providing the necessary power (PWFE)
- providing the real-time closed loop simulation capability at BUS 1553 level
- providing a Central Checkout System (TCC) in charge of handling:
  - the external I/F with on-board
  - the data-item extraction from packets
  - the parameter monitoring and distribution
  - the test sequences and simulation program preparation, maintenance and execution

- the event logging
- the human interface to operate the ATB
- test data archiving

Figure V-15. Avionic Test Bench Spirent 4760

The Avionics Test Bench includes also the additional EGSE for the test of the GPS receiver and navigation data processing. A Spirent 4760 GPS multi-channel emulator, connected to the GPS-R RF input, is integrated in the ATB through the LAN network. The Spirent and its host computer application SW SimGen (right picture) are in charge of feeding the GPS-R RF input with the signals of the GPS constellation for each space vehicles in the field of view of the receiver's antenna.

Epoch by epoch. the real-time chain "Dynamics Simulation SW – GPS EGSE – GPS Receiver" works according to the following logic flow:

- the DSS provides through an Ethernet connection the following data to the computer hosting the SimGen application @8 Hz: time stamp, motion command, vehicle (hosting the GPS receiver) identifier, CoG vehicle position (x, y, z), CoG vehicle velocity (x, y, z), CoG vehicle acceleration (x, y, z), CoG vehicle jerk (x, y, z), vehicle attitude (heading, elevation, bank), vehicle angular rate (x, y, z), vehicle angular acceleration (x, y, z), vehicle angular jerk (x, y, z)
- the SW SimGen propagates the GPS constellation to the current epoch and, on the basis of the position, velocity, attitude and angular rate of the s/c hosting the GPS receiver, computes the L1 and L2 signals to be synthesized by the Spirent 4760
- the Spirent synthetizes the RF signals according to the SimGen command and feeds the GPS receiver input (antenna)
- the dual frequency L1-L2 receiver GPS receiver telemetry output is sent (through the Bus 1553) to the on board computer (SMU) for the real time AOC purposes (Precise Orbit Determination) and to the Master Test Processor (through the TM/TC FEE)
- The received GPS receiver telemetry and the SimGen commanded orbit are then post processed in order to provide the GPS-R measurements in engineering units and the satellite "true"(from dynamics) orbit (ECEF spacecraft position and velocity, antenna geometric centre position and velocity in ECEF) and attitude.

Sentinel-1 HIL data are generated spanning 9680s. They refer to the orbit scenario summarized in Table V-5 simulated at 2011/06/21 01:16:00 (UTC time). Figure V-16 shows the SPS solution obtained by processing GPS receiver pseudoranges. The ionofree combination is considered in order to compensate the ionospheric path delay, so eq.(3.34) specializes for L1/L2 configuration in:

$$\rho_{IF} = 2.54\rho_{L1} - 1.54\rho_{L2} \tag{5.6}$$

3D error of 2.60m with a mean GDOP of 3 is experienced in this dataset: double frequency and very low ephemeris error (<0.3) allows to achieve high kinematic performance, but filtering can furthermore improve this accuracy.

B. MEONS filter configuration

The developed orbit determination filter is based on the MEONS baseline propagation model (MPMB) and it acquires GPS pseudoranges in order to form the same ionofree combination of eq.(5.6). As for SPS solution, pseudorange rate reconstruction pattern (or Instantaneous Doppler), derived from the L1 and L2 carrier-phase measurements, are also considered as observable in order to have information on spacecraft velocity. The use of such raw data does not require SPS availability ($SVs \geq 4$) so tightly coupled approach can work in critical GNSS visibility conditions. The filter operating cycle is 1s in order to process 1Hz pseudoranges and Doppler measurements. The MEONS filtering setting (Table V-6) relies on the ML adaptive EKF discussed IV.1-D and dealing with online process noise covariance tuning. The diagonal components of Q are selected for adaptation and, specifically, ones that represent velocity errors.

DSS (reduced)		
Parameter	**Symbol**	**Value**
mass (kg)	mass (kg)	$2139Kg$
drag coefficient	CD,Area	2.25, 5.44m^2
Solar Radiation Coefficient	CR,area	1.3, 32m^2
Rising starting date	yi, mi-,di	2011/06/21
Reference orbit Sentinel LEO solar-synchronous orbit	$\{a, e, i, \Omega, \omega, \nu\}$	7080147.3480 0.0012 98.1123 249.6649 68.9302
Operative condition	$\{q, \omega\}$	The satellite is controlled on the three axis at nadir pointing

Table V-5 Simulation parameters

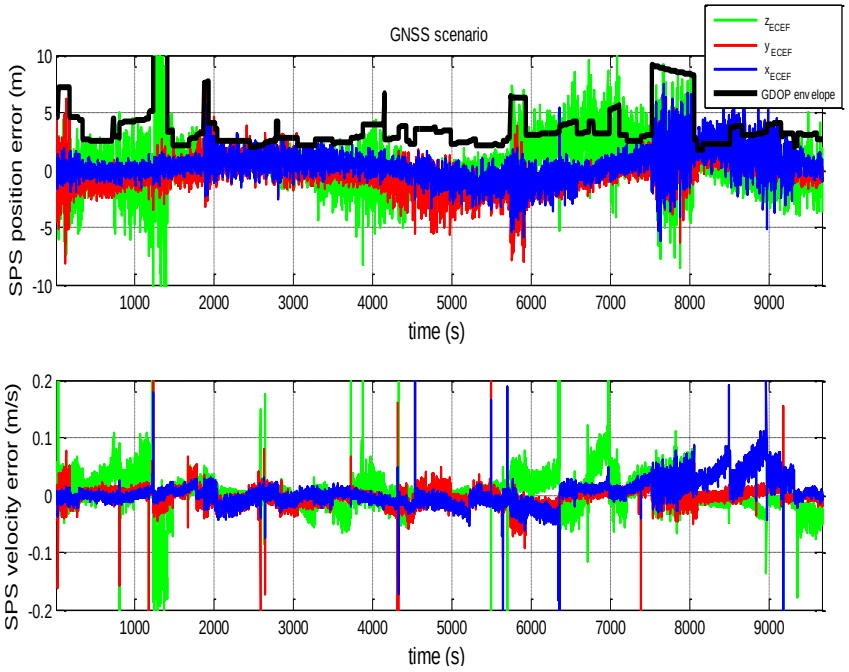

Figure V-16. GPS PVT performance for the 1th GNSS dataset

MEONS Sequential Filtering	
KF class method	EKF supported by ML adaptive step described in (IV.1-D) and referred as AKF
Extended State Partition	The extended state $\mathbf{X}$ can be partitioned in : ➢ Reference state $\mathbf{X}_{A^{nl,l}} \rightarrow \mathbf{x}(t) = \{\mathbf{r}, \dot{\mathbf{r}}, , \Delta t, \Delta \dot{t}, \Delta C_D, \Delta C_R\}$
Stochastic model peculiarities	➢ Adaptive process noise components $\vartheta_{adapt} = Q\{\sigma^2_{\mathbf{w}_{\dot{x}}}, \sigma^2_{\mathbf{w}_{\dot{y}}}, \sigma^2_{\mathbf{w}_{\dot{z}}}\}$
Special topics and remarks	The scheme in eq.(4.21) [104] shall be considered for the implementation. The adaptation can be enabled/disabled in accordance to regime phases and singularity occurrence. In the specific case the adaptive solution has been activated after 2000s transient

Table V-6 MEONS Adaptive Filter Configuration

Clock noise is kept constant and not included in adaptive set. Actually, in the adaptive tightly-coupled approach with real data, it is suitable to avoid the "washing-out" effect induced by the clock noise on the vehicle dynamics uncertainty estimation. Several tests have demonstrated the capacity of the developed

adaptive filter to estimate also clock bias and drift model noise covariance's, but some problem has been occurred when the first guess values and conditions have been considered far from the optimal one. Hold one between dynamic or time partition of Q at constant results in a more robust configuration. Moreover, time parameters are derivable from the receiver characteristics and from the expected measurement bias, so velocity unmodeled residual are usually considered the best candidate [117]. It shall be also noted that reduced perturbation parameters set are considered in Table V-6. However, they are limited to random constant physical coefficients that changes slower than the covariance parameters. This makes more effective the adaptation contribution.

The filter noise reference values are provided in Table V-7. They shall be considered for Q as overestimated initialization, whereas measurement noise covariance R are fixed in order to have a well posed Q adaptation (IV.1-D). It shall be noted that the value of the measurement noise results conservative with respect to the receiver nominal performances and values generally used in simulation case. It takes into account unmodeled errors due to test bench real data processing and velocity high error pointed out by SPS analysis in correspondence of SVs changes (Figure V-16) .

Filter covariance setting	
State initial covariance $\mathbf{P}_{xx}^{0}$	$\sigma_x^2 = 100(m^2/s^2) \quad \left(\sigma_{\dot{x}}^2\right) = 0.5(m^2/s^2) \quad \sigma_{\Delta C_D}^0 = 0.013 \quad \sigma_{\Delta C_R}^0 = 0.013$
Process noise covariance $\mathbf{Q}_{ss}$	$\sigma_{\mathbf{w}_r}^2 = 0.1(m^2/s^2)$
Measurement noise covariance $\mathbf{R}$	$\sigma^2_{v_{\tilde{\rho}_j}} = 0.5(m^2), \quad \sigma^2_{v_{\dot{\tilde{\rho}}_j}} = 0.008(m^2/s^2) \quad j = 1\ldots m$

Table V-7 Relevant Covariance Initialization

C. Results

The canonical and adaptive Kalman filters are compared. The adaptive Kalman filter is started after residual convergence transient exhaustion occurring at t=2000s. a window length of N=10 is selected for adaptation. The EKF vs. AKF comparison relies on the following procedure. The EKF and the AKF are executed within a loop on the α parameter, which defines the first guess variance value for the AKF and the constant variance value for the EKF:

- $-10 \le \log_{10}(\alpha_i) \le 0$
- $\sigma_i^2 = \alpha_i \cdot \sigma_0^2$

Each run of the AEKF and EKF for a fixed value of α provides a vector with position and velocity error components. Figure IV-17 and Figure IV-18 show the position and velocity errors of the EKF and AEKF filters for a fixed value of the α parameter ($\alpha^{1/2}$=0.02), which provide an over-estimated first guess. It is noticeable that the AEKF error is (as expected) by far less that the EKF error. Figure V-19 shows the standard deviation of the two filtering methods vs. the α parameter value. It is noticeable that the AEKF performance is almost flat all over the α values range. The EKF performance is instead highly sensitive to the α parameter value: it achieves the best performance in a narrow range of the α parameter (variance setting). The best performance achieved by the AEKF is almost tangent to the EKF minimal standard deviation error (optimal tuning). This means that in POD application filter tuning is very important to achieve improved (submeter) performance aiming to find the best way to work far from the optimal value

All the results are in line with the simplified experiment accomplished in IV.1-D: the high noise level, correspondent to the conservative setting of the covariance component, is mitigated by the adaptation that tunes the filter in accordance to the ML solution. An important parameter for adaptation process is the window length. A large window size could reduce the biasness of the estimates but may cause the adaptive filter losing the ability of adaptation.

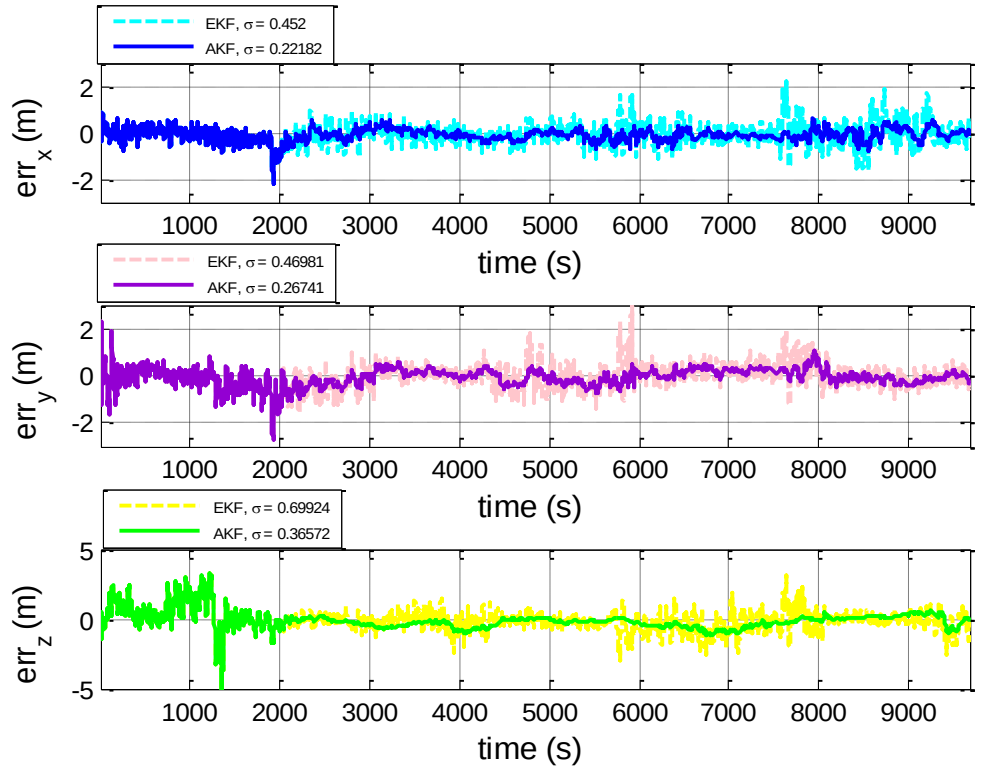

Figure V-17 ECEF position error for EKF and AEKF computed with $\alpha^{1/2}$=0.02 (1th scenario)

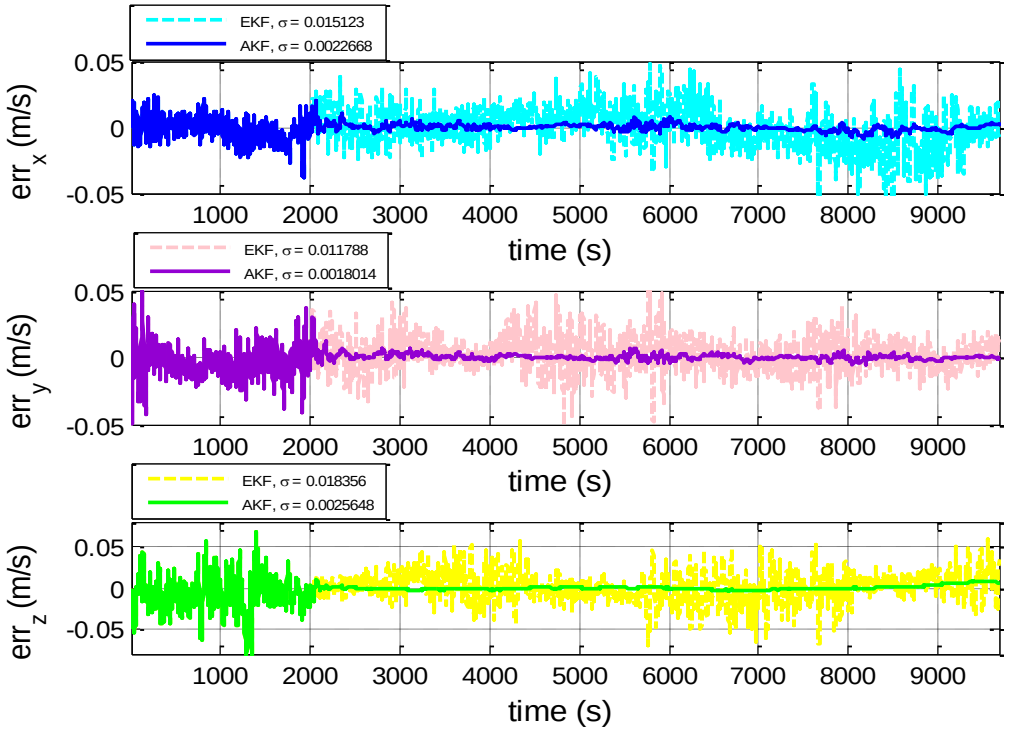

Figure V-18 ECEF velocity error for EKF and AEKF computed with $\alpha^{1/2}$=0.02 (1th scenario)

Figure V-20 shows the variation of the adaptive filtering error (standard deviation) with respect to the length of the window for the fixed $\alpha^{1/2}$=0.02 value . The first two degree of freedom results slightly influenced by the window length, so the N=10 chosen length does not introduce relevant performance modification. The third error component seems highly impacted by the window length. A reduction improves the performance but it is limited by N=5, where the error increase.

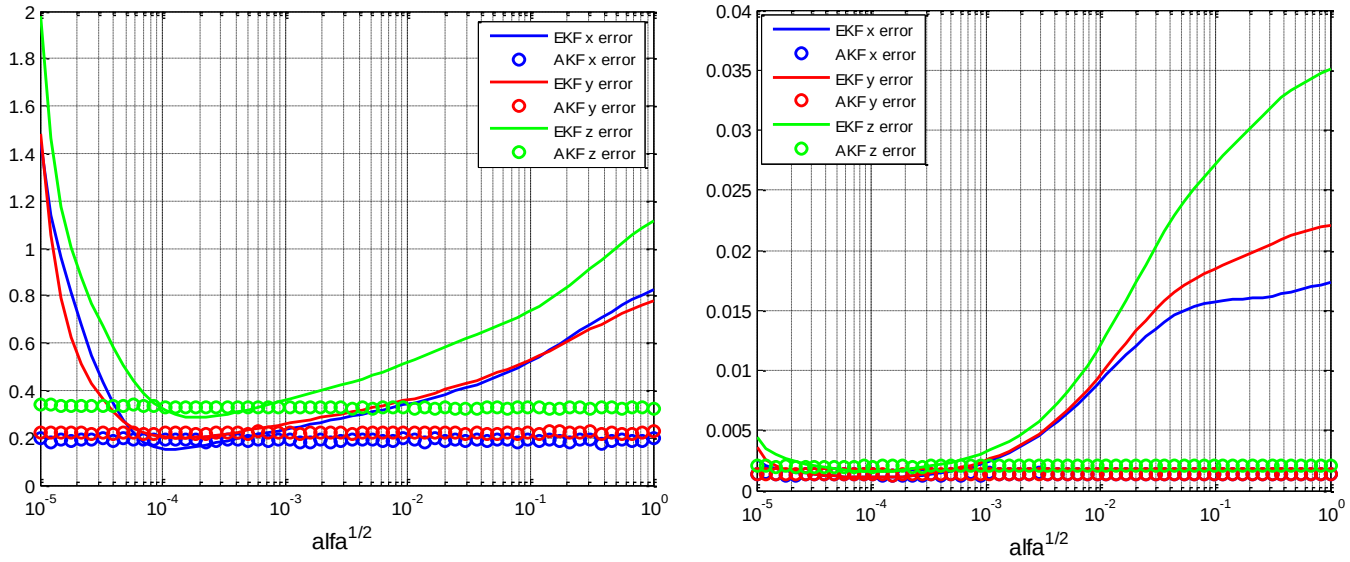

Figure V-19 EKF/AKF position error standard deviation comparison vs $\alpha^{1/2}$ value (first guess setting)

In general, even if the window length influences the final filter performance, it seems no critical because the achieved error results are always better than the standard EKF, when it works at process noise sigma far from the optimal one.

Filter (alfa=0.02)		EKF	AKF
Mean Error	Position (m)	**0.095 0.097 -0.284**	**0.054 0.057 -0.107**
	Velocity (mm/s)	**-0.337 -0.485 0.083**	**-0.057 -0.063 0.056**
Std Error	Position (m)	**0.452 0.469 0.699**	**0.221 0.267 0.365**
	Velocity (mm/s)	**15.123 11.788 18.356**	**2.266 1.801 2.564**

Table V-8 EKF/AKF performance statistics comparison

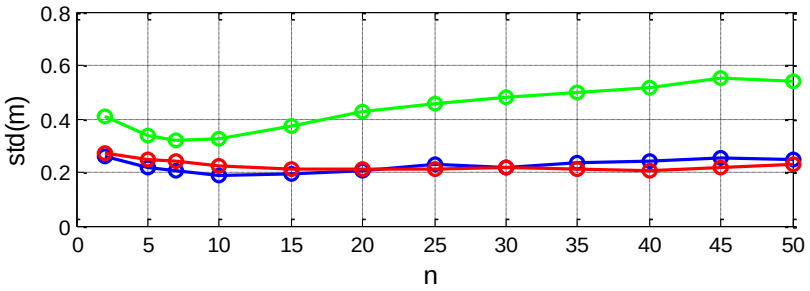

Figure V-20 Position standard deviation VS adaptive filter windows length

V.3 CONSIDER KALMAN FILTER FOR LOW THRUST LEO-MEO AUTONOMOUS ORBIT RISING

A. Mission scenario: Autonomous Low Thrust Orbit Rising for Galileo Second Generation S/C

For the G2G mission the target spacecraft concept is shown in Figure V-21 . The architecture reflects the design of a navigation platform exploiting recent electrical propulsion achievements in order to withstand mission scenario requirement defined in II.2-A. The optimal rising is once that defined in III.1-D .The constant amplitude thrust of 0.180 N is provided by a high impulse Xenon based ion thruster with specific impulse (ISP) of 3829 m/s. The actuator is mounted in such a way the nominal thrust is aligned with the mechanical x-axis. Inertial and physical properties of the analysed satellite are listed in Table V-9.

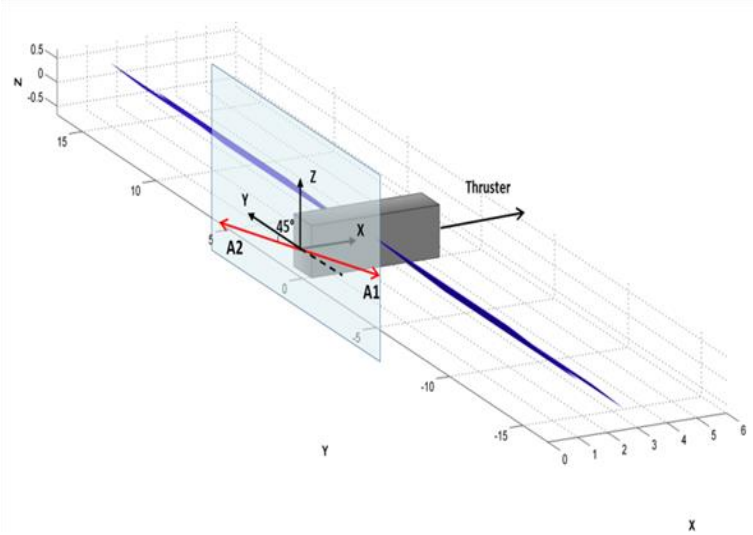

Figure V-21 Illustration of the selected spacecraft

S/C Physical model		
Parameter		**Value**
mass (kg)		1625
Rotational Inertia (kg m^2)		I_{xx}=12640 I_{yy}=2380 I_{zz}=14800
solar panel	absorption coefficients	0.91 (front) 0.92 (back)
	specular reflection coefficients	0.08 (front) 0.00 (back)
	diffuse reflection coefficients	0.01 (front) 0.08 (back)
satellite main body	absorption coefficients	0.20
	specular reflection coefficients	0.60
	diffuse reflection coefficients	0.20
drag coefficient		2.25

Table V-9 Spacecraft inertial and physical properties

Relatively wide solar arrays (dark blue wings in Figure V-21) are required to generate the electric power able to support the electric propulsion and the attitude control, which is based on three-axis reaction wheels. Solar panels can be reoriented by a hinge mechanism in order to improve the overall sun exposure (III.1-D). Nonetheless, the current design assumes that the ion thruster is turned off during solar eclipses. C-DSS (III.1-B) is used for generating transfer reference considering setting. All parametric uncertainty sources discussed in III.1 and III.2 are considered within the propagated spacecraft dynamics.

The applied level of physical model and thrust errors are generated in accordance to Table V-9. For navigation purposes, the satellite is supposed to embark a space qualified GNSS receiver [15] able to track up to 12 GNSS satellites and to work with the dual-antenna configuration. Considering S/C envelope the III.2-C opposite boresight approach is applied by mounting GNSS antennas (A1 and A2) at 45° in the y-z plane (i.e. in the plane orthogonal to the axis of the thruster). The basic assumption is that the embarked GNSS receiver is able to deliver single-frequency, GPS and Galileo, pseudorange and Doppler observables. GSS has been set in order to delivers such observables at 1Hz.

Specifically, a complete GPS constellation with 32 satellites (SVs ID 1-32) is simulated together with a partially deployed, i.e. 10 satellites, Galileo constellation (SVs ID 33-42). At each time epoch both constellations are propagated using the relevant two-line elements (TLE) file data (Appendix C). The link budget parameters (eq.(3.37)) and tracking threshold assumed values are reported in Table V-9. As stated in II.1-B, C/N0 reference value is mitigated to the 34dbHz tracking threshold in order to take into account high sensitivity solutions. The GNSS observables error budget has been defined in Table V-9 taking into

account assumption discussed in III.2-C. The noise level generation considers for eq.(3.39) the characteristics of the selected hardware by setting B_n = 0.9Hz, T=0.020s, D =0.05 chips, B_{fe} = 24MHz . in Table V-9 reports the correspondent expected error dynamic range.

Complete DSS model		
Parameter	**Symbol**	**Value**
Rising starting date	y_i, m_{i-}, d_i	2015, 03, 23
Rising ending date	y_f m_f d_f	2016, 04, 03
Starting altitude	h_i	1221 km
Ending altitude	h_f	23813 km
Starting eccentricity, RAAN and Inclination	e_i, Ω_i, i_i	0.012, 0°, 56°
Ending eccentricity, RAAN and Inclination	e_i, Ω_i, i_i	0.0145,270°,56°
Cd and Cr Uncertainity levels	Cd Cr	0.15, 0.15
Nominal Thrust Magnitude	A,ISP	0.18 N , 3829 m/s
Thrust Magnitude Bias	ΔA	5% of A
Thrust Orientation Erros	$\Delta\alpha, \Delta\beta$	0°, fixed thrust vector with negligible attitude errors (<10-3)
Thrust Magnitude Noise	ν_x, ν_y, ν_z	Normally distributed N(0,10-9 m/s2)
Delta Mass	Δm	0.5Kg (1 day)
Scaling errors	$\Delta k_x, \Delta k_y, \Delta k_z$	10-3
Coupling errors	$\Delta\vartheta, \Delta\psi, \Delta\varphi$	10-3

GNSS Scenario Simulator			
GSS settting	**Simulation Approach**	**Parameter**	**Value**
Constellation	GPS (32 SVs) + Galileo (10 SVs)	TLE	-
Visibility analysis	Geometrical selection	FOV Rx (Half cone) FOV Tx (Half cone)	85° 85°
	Elcetronic Visibility	Acquisition Threshold	34dbHz
		λ L1/E1 , L_{SVf} , L_{IL} , L_{IMP} T_{Sys}	19 cm 1dB 2.5dB, 2.5dB,220K
Measurements	P_L1/P_E1 DL1/D_E1	Rate	1Hz

GNSS Error budget and Filtering				
GNSS error source	**Simulation Approach**	**UERE 1σ (m)**	**UERRE 1σ (m/s)**	**Estimation/calibration approach**
Receiver clock bias and drift	Discrete-time model of colored noise	Negligible	Negligible	On line estimation
GGTO and GGTO rate	Time offset update equations	Negligible	Negligible	On line estimation
Satellite Ephemeris	High level Perturbed GNSS satellite positions and velocity error per axis	1m-4m	0.001-0.004	Neither estimation nor calibration but modeled as considered parameters
Satellite Clock Correction	Perturbed clock correction included in (χ_i)	0.2	0.0005	Neither estimation nor calibration, but included as equivalent ranging error
Ionospheric delay	Earth disk augmentation and residual random delay included in (χ_i)	2.0	0.030	
Multipath	Normally distributed random error included in (χ_i)	1.0	0.010	
Measurement noise	Random noise with standard deviation accounting for C/N0	σ_{DLL} (0.2-0.9)	0.010	

Table V-10 G2G Test Case Simulation Setting

B. G2G GNSS scenario analysis

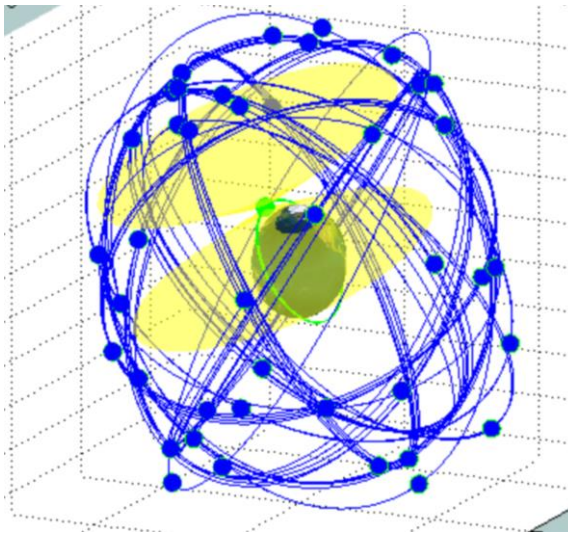

Figure V-22 Low orbit phase Multi-constellation scenario (1221Km)

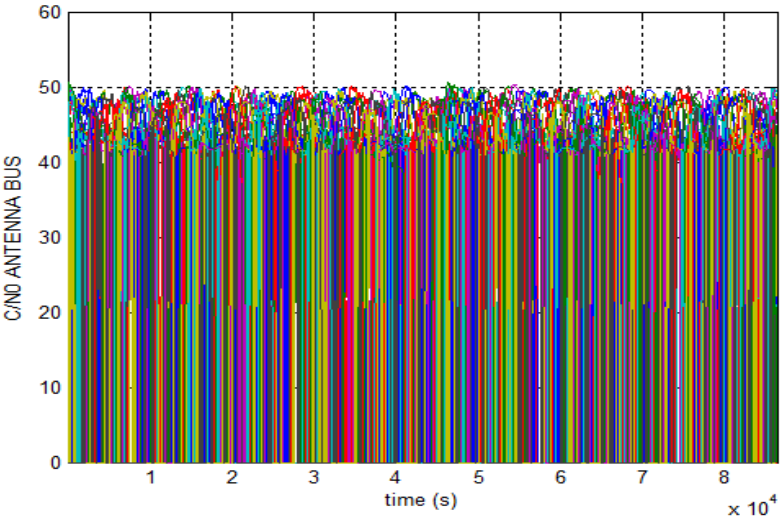

Figure V-23 Low orbit phase C/N0 evaluation for SVs electronic visibility selection

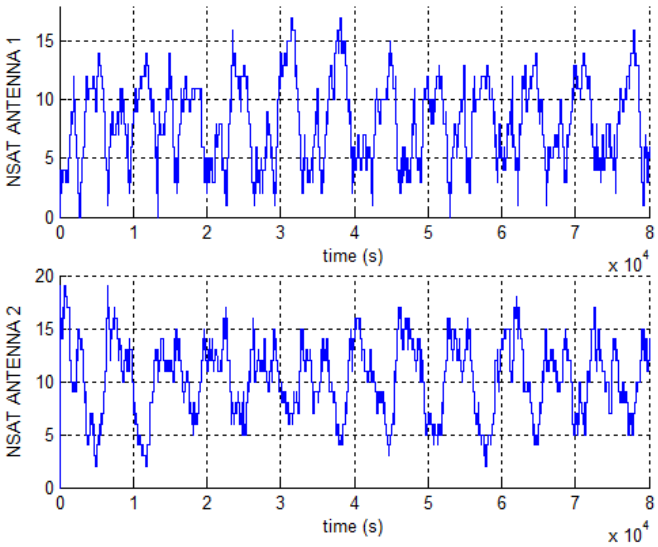

Figure V-24 In view SVs number for GNSS receiver double antenna configuration (1221Km)

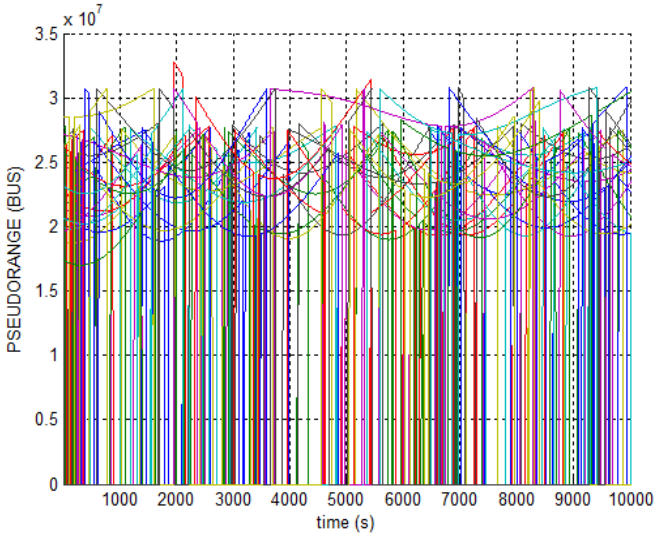

Figure V-25 GNSS receiver raw measurement generation , Pseudorange Antenna Bus (1221Km)

This research has performed a wide range analysis of the GNSS scenario for the LEO-MEO transfer by using the GSS functionality. Preliminary results have been presented in [62] on G2G first guess trajectory, whereas they have been definitively refined in [6] considering the final G2G orbit transfer data set. As result, three different portions of the rising can be considered relevant for the G2G Multi-antenna architecture analysis:

- Low orbit phase, with initial orbital altitude of 1221 km.
- Intermediate orbit phase, with initial orbital altitude of 11860 km.
- High orbit phase, with initial orbital altitude of 21813 km

Figure V-22 to Figure V-33 show all the relevant GSS output for the selected one day extracts. Generally, considering attitude variation due to platform thrust and power optimization, a best antenna cannot be identified. However, single antenna visibility plots allow recognizing the difference between the extreme cases and the intermediate one.

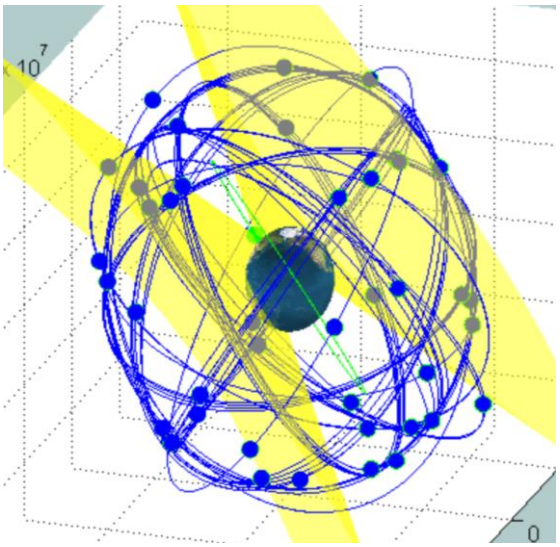

Figure V-26 Intermediate orbit phase Multi-constellation scenario (11860 km)

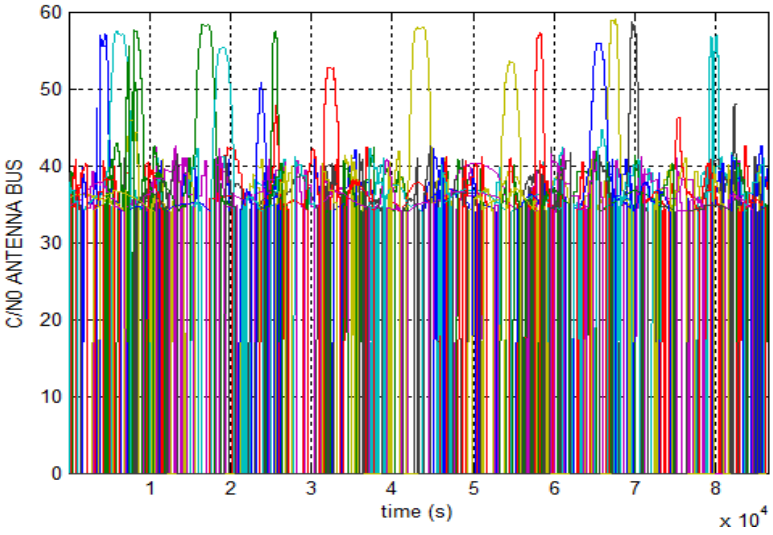

Figure V-27 Intermediate orbit phase C/N0 evaluation for SVs electronic visibility selection

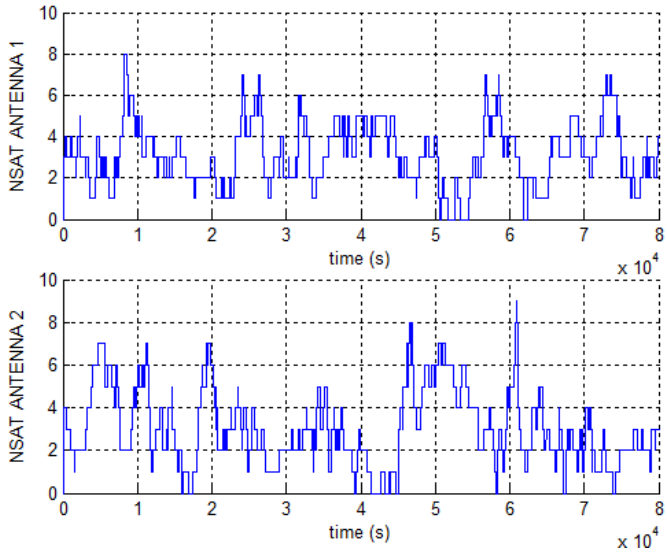

Figure V-28 In view SVs number for GNSS receiver double antenna configuration (11860 km)

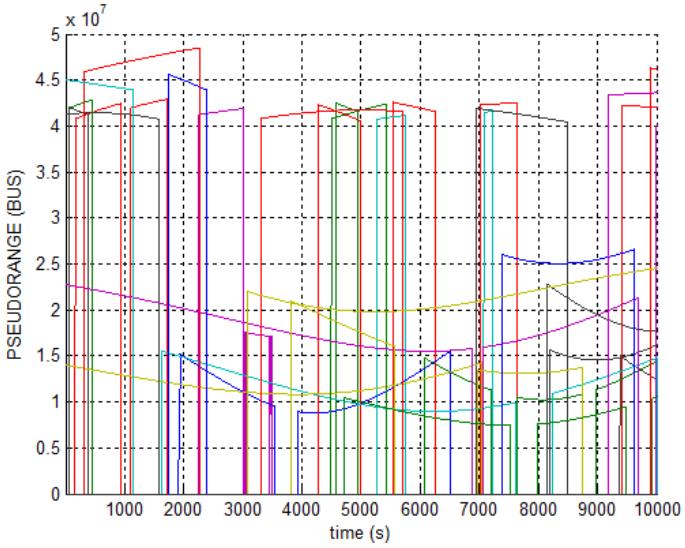

Figure V-29 GNSS receiver raw measurement generation, Pseudorange Antenna Bus (11860 km)

Beyond their difference in term of total in view satellite number, low and high orbit cases show windows where one antenna is predominant wrt the other.

In the 1221 km case, satellite number picks occurring on the Antenna 1 satellite number corresponds to the minimum of the Antenna 2. Similarly 21813 test case shows "active" antenna turnover: window of visibility relies on which one points toward the Earth. This is also confirmed by pseudorange measurements, whose line of sight (LOS), except for SVs proximity occurrences, are close to distance limit defined by the Earth cone (56500 Km). In the intermediate phase a very dominant antenna cannot be identified and the final results strictly depend on the specific operative condition (constellation status at date, attitude, etc).

The performed simulation agrees with the expected signal power degradation as pointed out from C/N0 plots. Almost all geometrically visible signals are acquired in the final orbit phase thanks to the selected tracking threshold. The main effect of the lower signal level is that the visibility time span is shorter due to a narrow compatible elevation interval. GNSS scenario transfer phase's peculiarities are summarized by Figure V-34 and Figure V-35 that provide relevant distribution of combined antennas satellite number.

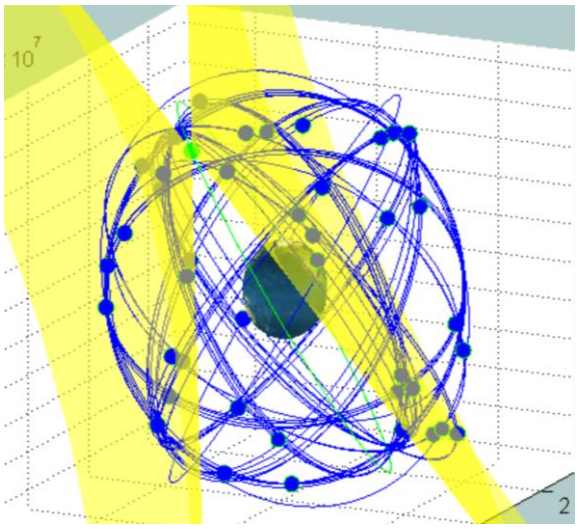

Figure V-30 High orbit phase Multi-constellation scenario (21813 km)

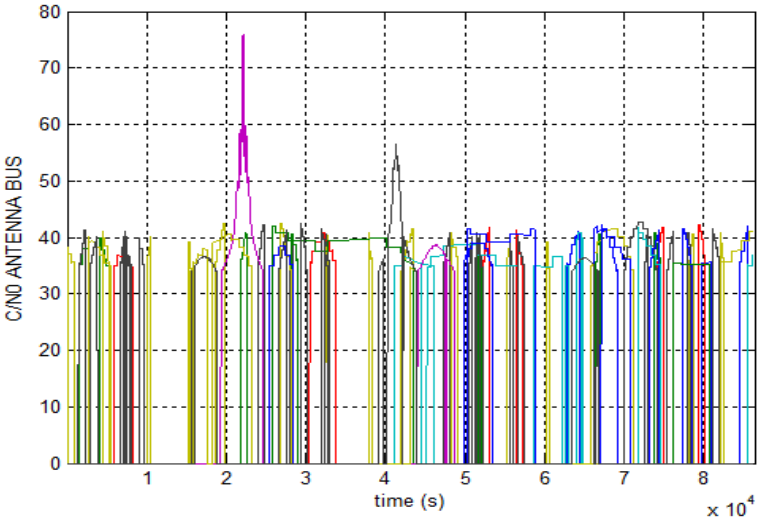

Figure V-31 Intermediate orbit phase C/N0 evaluation for SVs electronic visibility selection

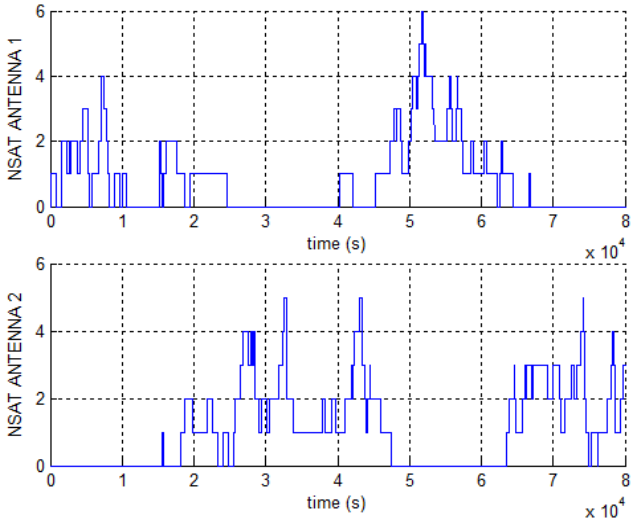

Figure V-32 In view SVs number for GNSS receiver double antenna configuration (21813 km)

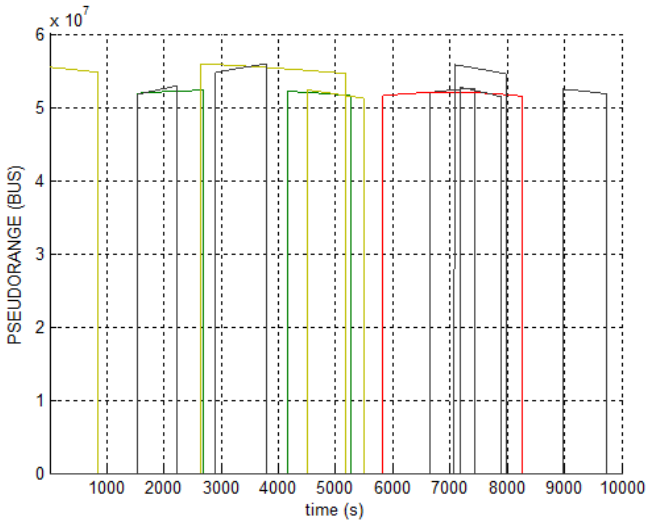

Figure V-33 GNSS receiver raw measurement generation, Pseudorange Antenna Bus (21813 km)

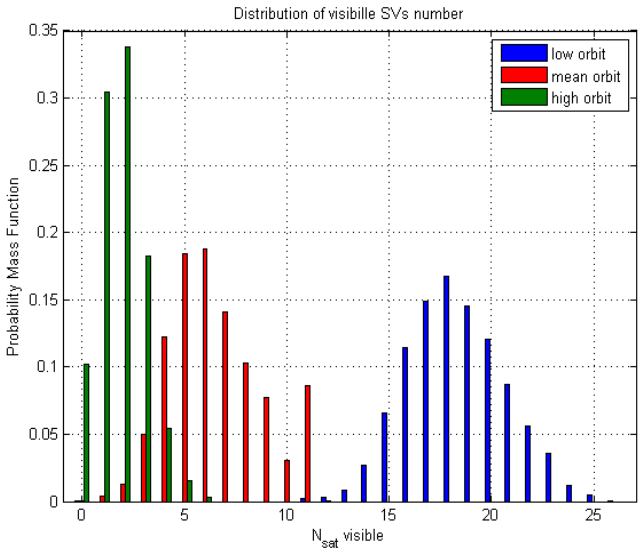

Figure V-34 Histogram of total in view satellites for the selected transfer orbit phases

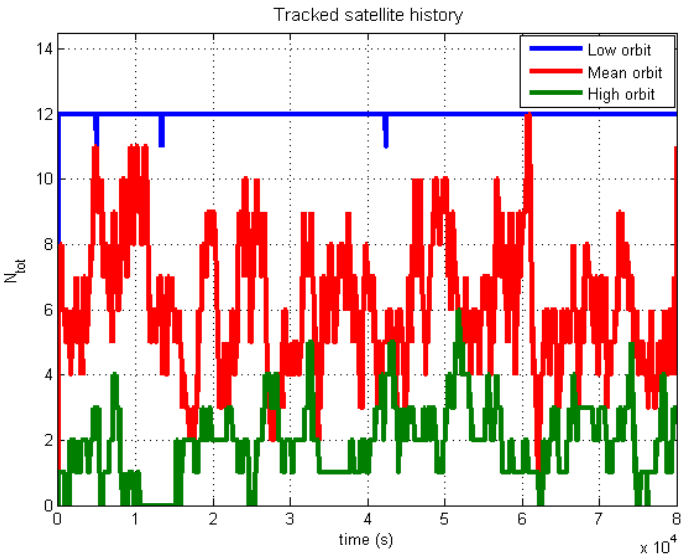

Figure V-35 Number of tracked satellite for each considered phase of the transfer orbit.

Considering kinematic solution availability (i.e. 4 satellite), Figure V-35 points out that high orbit phase results critical for almost the entire simulation. Outages are experienced for a 10% of the whole simulation time. Conversely, Low and Intermediate case are not critical confirming the readiness of SSV below the MEO strip. However, the dynamic filtering of MEONS is important also during the lower phases, since it mitigates GDOP excursion and orbit estimation continuity. In accordance to Table V-9 Spacecraft inertial and physical properties, Figure V-36 shows the simulated maximum ephemeris error experienced by tracked SVs per each considered phase. Such error envelope is used in the following section as a reference to interpret the achieved performance of CKF with respect to ranging biases.

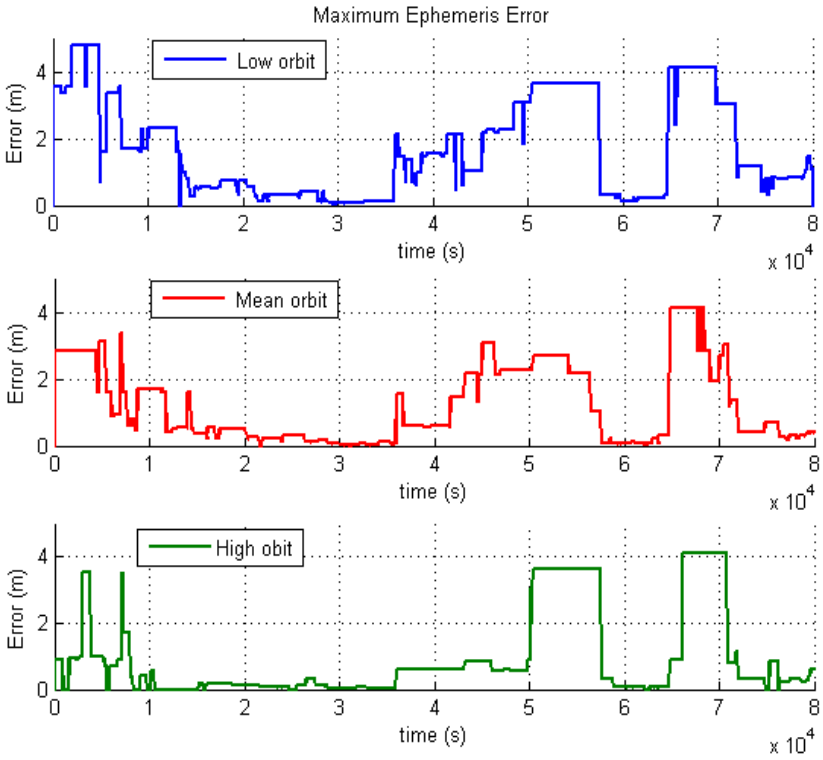

Figure V-36 Maximum experienced SVs ephemeris error for the three transfer orbit phases

C. MEONS filter configuration

MEONS filter configuration	
KF class method	Consider Extended Kalman Filter (CEKF) of [6]
Extended State Partition	The extended state $\mathbf{X}$ can be partitioned in : ➢ Reference state $\mathbf{X}^{\mathbf{x}}_{A^e} \rightarrow \mathbf{x}\ (t) = \left\{\mathbf{r}\ ,\dot{\mathbf{r}}\ ,\Delta t,\Delta\dot{t},\Delta t_{GGTO},\Delta\dot{t}_{GGTO}\right\}$ ➢ Consider parameters $\mathbf{X}^{\mathbf{p}}_{A^{cp}} \rightarrow \begin{cases}\mathbf{p}_{Pert}=\left\{\Delta C_D,\Delta C_R,a_R,a_T,a_N\right\} & \mathbf{p}_{thrust}=\left\{\Delta A,\Delta k_x,\Delta\vartheta,\Delta\phi,\Delta\eta,\Delta\zeta,\Delta m\right\}\\ \mathbf{p}_{range}=\left\{\Delta\varepsilon_1,\Delta\varepsilon_2,...,\Delta\varepsilon_n,\Delta\dot{\varepsilon}_1,\Delta\dot{\varepsilon}_2,...,\Delta\dot{\varepsilon}_n\right\}_{2n}\end{cases}$ The correspondent filter covariance $P_{\mathbf{XX}}$ is: $P_{\mathbf{XX}}=\begin{bmatrix}P_{\mathbf{X}^{\mathbf{x}}_{A^e}\mathbf{X}} & P_{\mathbf{X}^{\mathbf{x}}_{A^e}\mathbf{X}^{\mathbf{p}}_{A^{cp}}} & 0\\ P_{\mathbf{X}^{\mathbf{x}}_{A^e}\mathbf{X}^{\mathbf{p}}_{A^{cp}}} & P_{\mathbf{X}^{\mathbf{p}}_{A^{cp}}\mathbf{X}^{\mathbf{p}}_{A^{cp}}} & 0\\ 0 & 0 & P_{\mathbf{X}_B\mathbf{X}_B}\end{bmatrix}$ $P_{\mathbf{X}^{\mathbf{p}}_{A^{cp}}\mathbf{X}^{\mathbf{p}}_{A^{cp}}}=diag\left(P_{\mathbf{p}_{Pert}\mathbf{p}_{Pert}},P_{\mathbf{p}_{thrust}\mathbf{p}_{thrust}},P_{\mathbf{p}_{range}\mathbf{p}_{range}}\right)$ $P_{\mathbf{X}_B\mathbf{X}_B}=P_{\mathbf{p}_{range,n+1...N}\mathbf{p}_{range,n+1...N}}$
Stochastic model peculiarities	➢ Thrust direct feedforward, external aiding and VSD ranging errors $\mathbf{X}_B \rightarrow \begin{cases}\mathbf{X}^{\mathbf{x}_{aux}}_{B_{static}} \rightarrow \mathbf{x}_{aux}\ (t)=\left\{A,\alpha,\beta,q\ ,\omega,m_p\right\}\\ \mathbf{X}^{\mathbf{p}}_{B_{static}} \rightarrow \mathbf{p}_{range,n+1...N}=\left\{\Delta\varepsilon_{n+1},\Delta\varepsilon_{n+2},...,\Delta\varepsilon_N,\Delta\dot{\varepsilon}_{n+1},\Delta\dot{\varepsilon}_{n+2},...,\Delta\dot{\varepsilon}_N\right\}\\ \mathbf{X}^{\mathbf{p}}_{B_{prop/static}} \rightarrow \mathbf{p}_{thrust}=\left\{\Delta A,\Delta k_x,\Delta\vartheta,\Delta\phi,\Delta\eta,\Delta\zeta\right\}_{Thrust\ Off\ \ Command}\end{cases}$
Special topics and remarks	The auxiliary platform variables are included in the inactive state as the quiescent ranging and ranging rate errors of not in view SVs. If requested the filter can "switch off" also thruster consider parameters $\mathbf{p}_{thrust}$ moving them in the inactive propagated set.

Table V-11 MEONS CEKF configuration for LEO-MEO EOR

In accordance to [6], the CEKF configuration has been selected for MEONS Autonomous EOR. Information relying on firing feedforward and attitude are included as external auxiliary aiding within the estimation inactive space and, specifically, in the null partition. As described in III.3, the stochastic part of the auxiliaries is handled as dynamic parametric uncertainties by using the model consider parameters. Actually, the $x^{p}_{A^{cp}}$ partition allows desensitizing the estimation process wrt the thrust mechanization $\mathbf{p}_{thrust}$, perturbation model $\mathbf{p}_{Pert}$ and the constellation systematic biases $\mathbf{p}_{range}$. The ranging considers variables $\mathbf{p}_{Pert}$ are managed as variable state dimension block selecting active contribution in accordance to the in view SVs. During eclipses they remain active, but the sensitivity does not map their contribution in accordance with dynamic module deactivation at Generic Propagator Level. Thrust parameters can be deactivated and moved into propagated or static subspaces in order to reset the cross covariance as they lose significance after long control action switch off. All those arrangements are summarized in Table V-11.

CKF covariance configuration	
State initial covariance $\mathbf{P}_{ss}^{0}$	$\begin{cases} \sigma_{\mathbf{r}} = 10_{[m]} \quad \sigma_{\dot{\mathbf{r}}} = 0.3_{[m/s]} \\ \sigma_{\mathrm{t}}^{0} = 50_{[m]} \quad \sigma_{\dot{\mathrm{t}}}^{0} = 1_{[m/s]} \\ \sigma_{\mathrm{t}_{GGTO}} = 50_{[m]} \quad \sigma_{\dot{\mathrm{t}}_{GGTO}} = 1_{[m/s]} \end{cases}$
Parameter initial covariance $\mathbf{P}_{pp}$	$\begin{cases} \sigma_{\Delta A}^{0} = 0.009_{[N]} \quad \sigma_{\Delta m}^{0} = 2_{[Kg]} \\ \sigma_{\Delta k_{x,y,z}}^{0} = 0.001 \quad \sigma_{\Delta s_{\vartheta,\psi,\phi}}^{0} = 0.01 \\ \sigma_{\Delta C_{\xi,\eta,\zeta}}^{0} = 0.001 \quad \sigma_{\Delta C_D}^{0} = 0.15 \\ \sigma_{\Delta C_R}^{0} = 0.15 \quad \sigma_{\mathbf{a}_{R,T,N}}^{0} = 10^{-7}_{[m/s^2]} \\ \sigma_{\varepsilon_i} = 1.5_{[m]} \quad \sigma_{\dot{\varepsilon}_i} = 0.0015_{[m/s]} \end{cases}$
Process noise covariance $\mathbf{Q}_{ss}$	$\begin{cases} \sigma_{\mathbf{w_a}} = 5 \cdot 10^{-9}_{[m/s^{3/2}]} \quad \sigma_{\mathrm{w}_{\dot{\mathrm{t}}}} = 0.6_{[m/s^{1/2}]} \\ \sigma_{\mathrm{w}_{\ddot{\mathrm{t}}}} = 0.1_{[m/s^{3/2}]} \quad \sigma_{\mathrm{w}_{\dot{\mathrm{t}}_{GGTO}}} = 0.6_{[m/s^{1/2}]} \\ \sigma_{\mathrm{w}_{\ddot{\mathrm{t}}_{GGTO}}} = 0.1_{[m/s^{3/2}]} \end{cases}$
Measurement noise covariance $\mathbf{R}$	$\begin{cases} \sigma_{v_{UERE}} = \left(5.2 + \sigma_{DLL}^{2}\right)^{1/2}_{[m]} \\ \sigma_{v_{UERRE}} = 0.033_{[m/s]} \end{cases}$

Table V-12 EOR CKF setting

Aiming at pointing out relevant CEKF peculiarities, a comparison with EKF solution is hereafter performed following the approach proposed in [90] and detailed in IV.1-C for the simplified system case. Setting and tuning parameters for both filters are listed in Table V-12 and the initial state condition is affected by the same error in accordance to the initial state covariance. Specifically, a conservative degree of uncertainty has been set considering the expected specification of the actuation system and level of unknowledge on spacecraft physical properties. The measurement noise level takes into account the wider excursion of ranging noise due to C/N0 variation, so the UERE error is increased by the hardware noise σ_{DLL}^{2} modified considering eq. (3.49). Actually the information on the current C/N0 is on line provided by the equipment for each measurement channel.

D. Results

The filtering performances comparison and robustness verification against actuation errors and different orbit regimes is herein presented in term of position and velocity accuracy experienced during the three orbit phases. Figure V-37 shows the positioning 3D error, i.e. the square root of the quadratic sum of error in each component, for the low orbit phase. The maximum error is lower than 3.5m for CKF and more than 5m for EKF. Besides the reduction of the estimation error, Figure V-38 points out the capability of the consider approach to bound the error during both thruster application and eclipses. Specifically, a lower covariance is estimated, as expected, during eclipses because no thruster contribution to covariance is added. This justifies the variation of the covariance bound which shows a frequency compliant with the orbit period. The covariance bound of the EKF instead is not representative of the true error behaviour that is largely underestimated. In addition, the estimation error of the CKF shows more prominent noise-like features meaning that most of systematic error sources are correctly accounted for [93], whereas the EKF performance exhibits a higher sensitivity to the injected systematic errors.

The results confirm the bias mitigation ability of the CKF, e.g. from 40000 to 60000s where most of the ephemeris error is concentrated, the estimation is still well represented by the covariance bound.

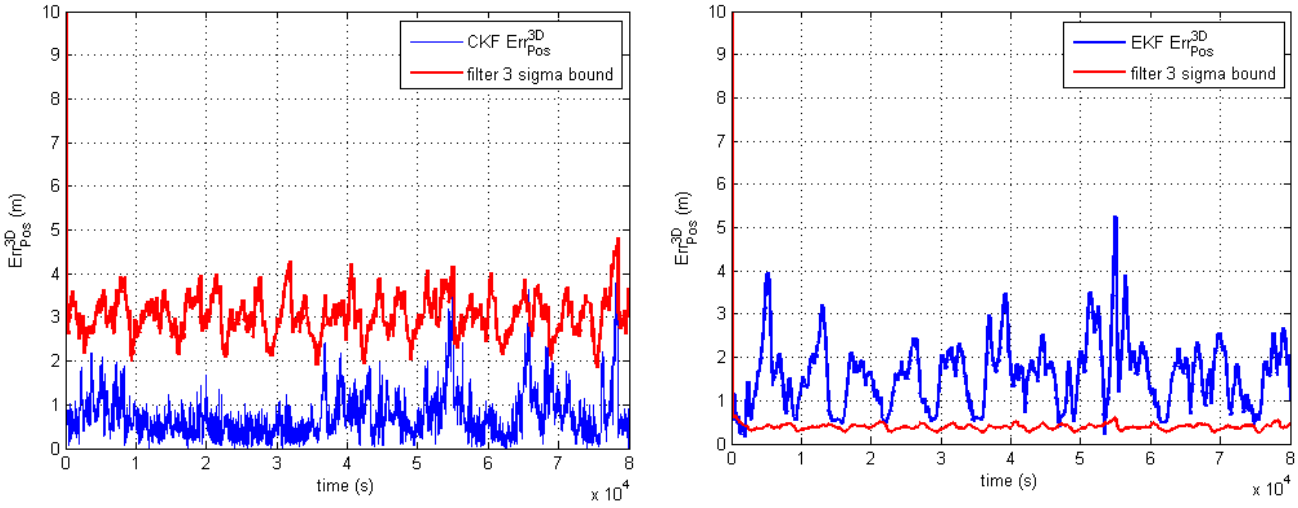

Figure V-37 EKF vs CKF 3D position error and 3σ covariance bound comparison for low orbit phase

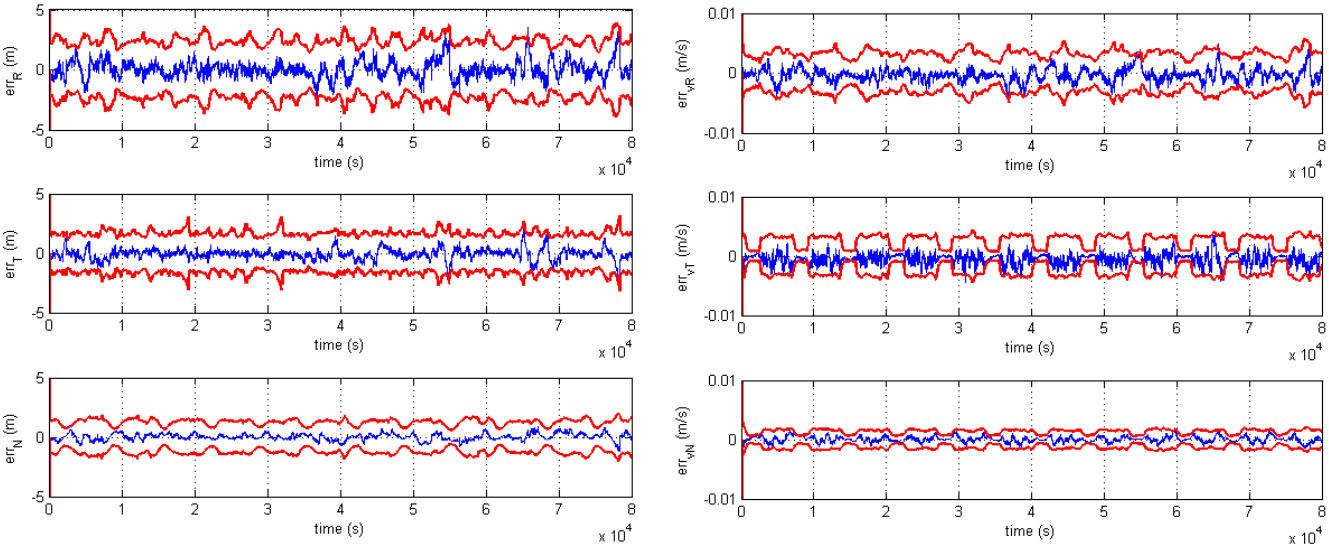

Figure V-38 CKF position, velocity error and 3σ covariance bound during low orbit phase

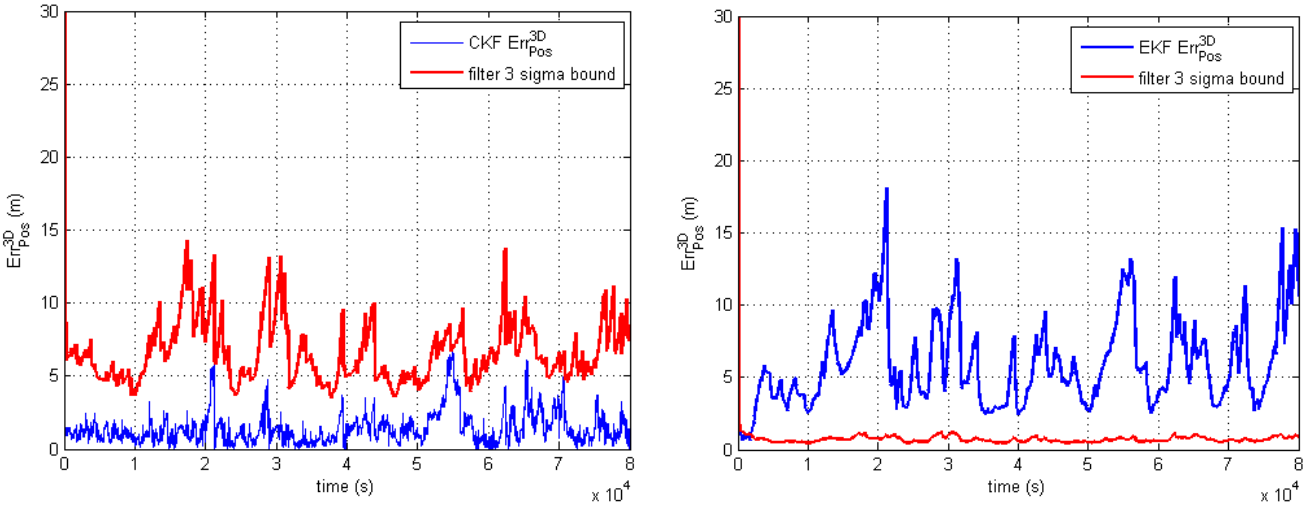

Figure V-39 EKF vs CKF 3D position error and 3σ covariance bound comparison for mean orbit phase

Figure V-39 depicts position and velocity error components together with the relevant covariance bound for the CKF during the mean orbit phase.

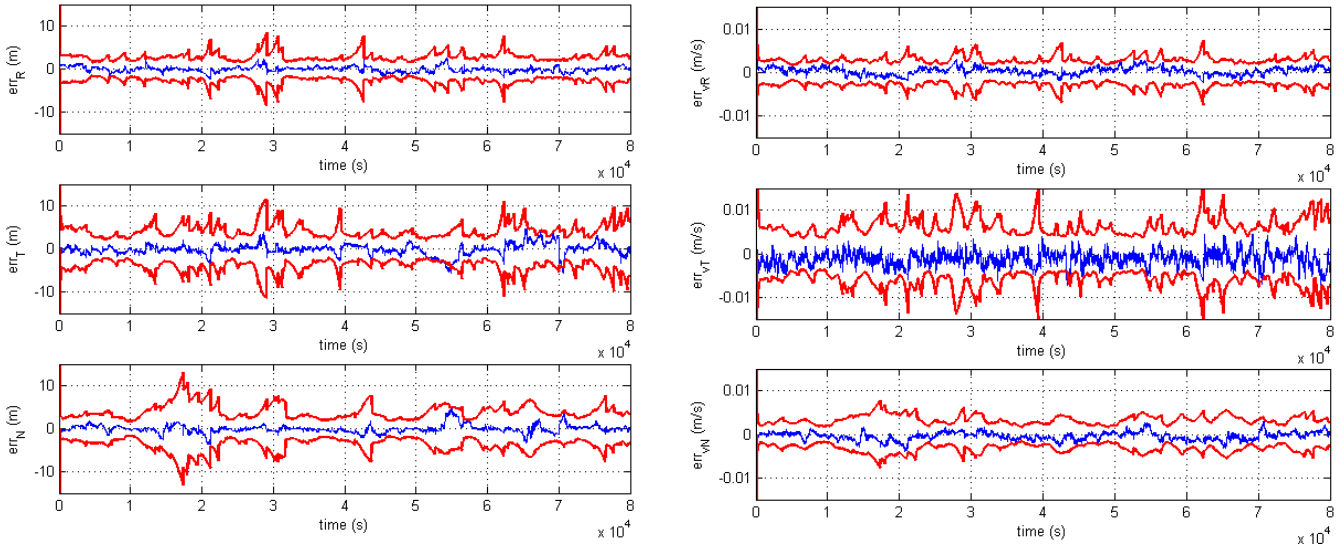

Figure V-40 CKF position, velocity error and 3σ covariance bound during mean orbit phase

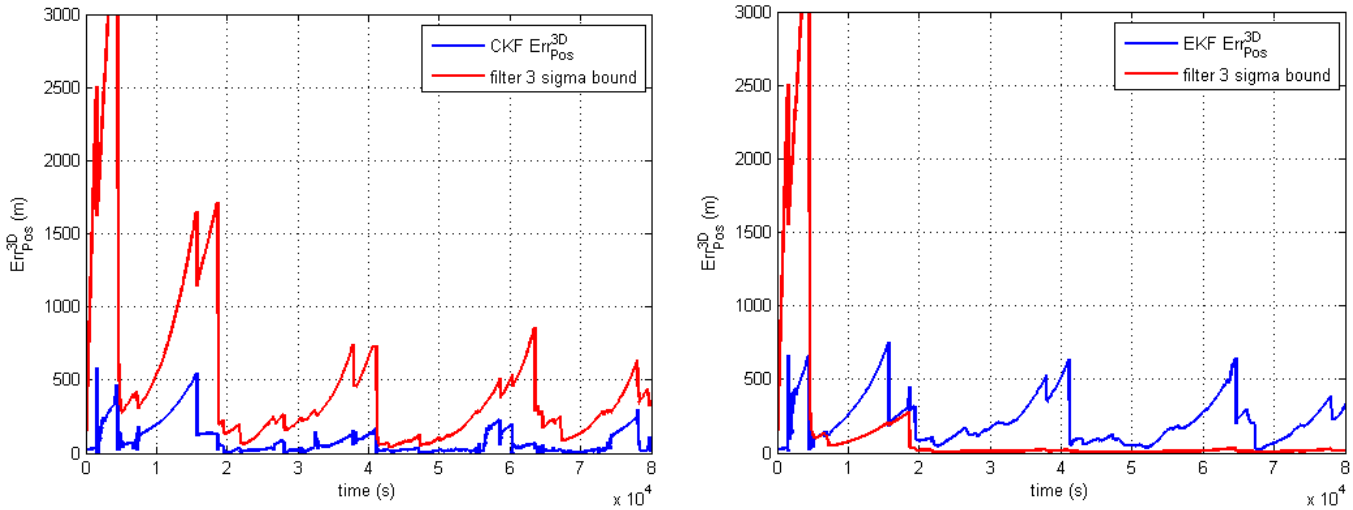

Figure V-41 EKF vs CKF 3D position error and 3σ covariance bound comparison for high orbit phase

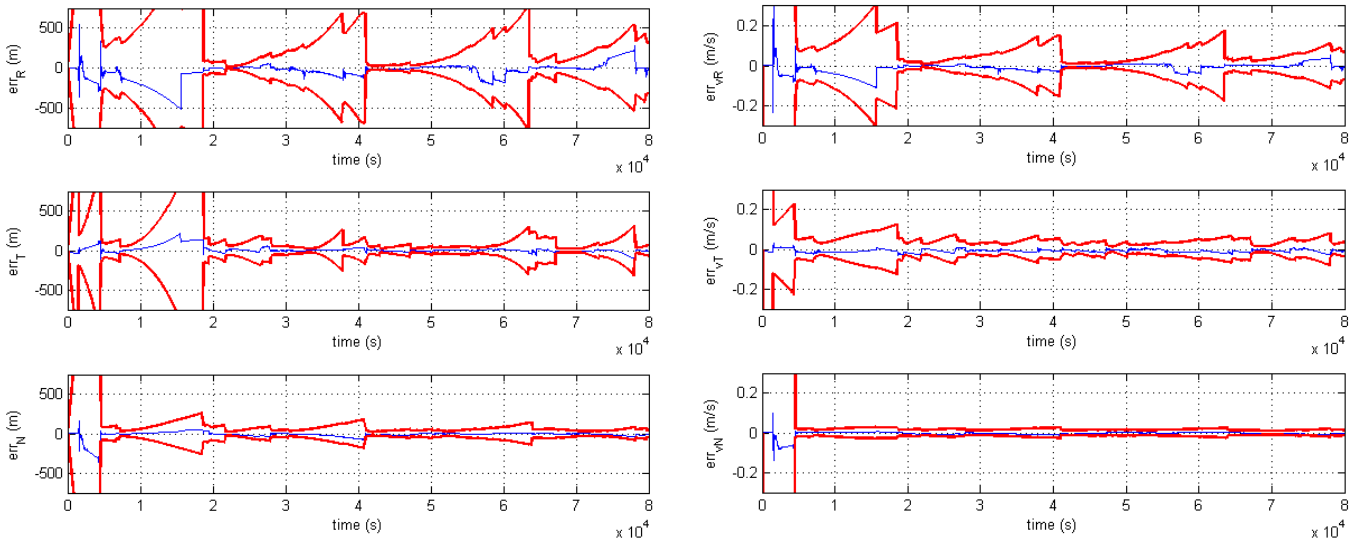

Figure V-42 CKF position, velocity error and 3σ covariance bound during mean orbit phase

The CKF positioning 3D error degrades to 4-8m (1σ) during the intermediate phase, due to the reduced number of satellites in view. Again, the EKF performance in terms of estimation error is worse than CKF, in addition it is completely inconsistent with the correspondent 3σ covariance bound.

With specific reference to Figure V-40 CKF, covariance peaks indicates phases with reduced measurement correction effect, thus the performance is more influenced by prediction. During these phases the CKF controls the error within the 3σ bound by the inclusion of thruster parameter uncertainty: it acts as an additional acceleration error contribution that increases the covariance when the measurement blending reduces. Figure V-41 shows the results for the high orbit phase. The estimation error is several tens of meters, but, after an initial transitory phase, CKF performance is stable in spite of long time spans without any GNSS satellite acquisition. The results also suggest that proper covariance evaluation via parametric uncertainty propagation in CKF is determinant also for recovering accurate positioning after long time spans of GNSS outage (see Figure 12 from 0 to 22000 s).

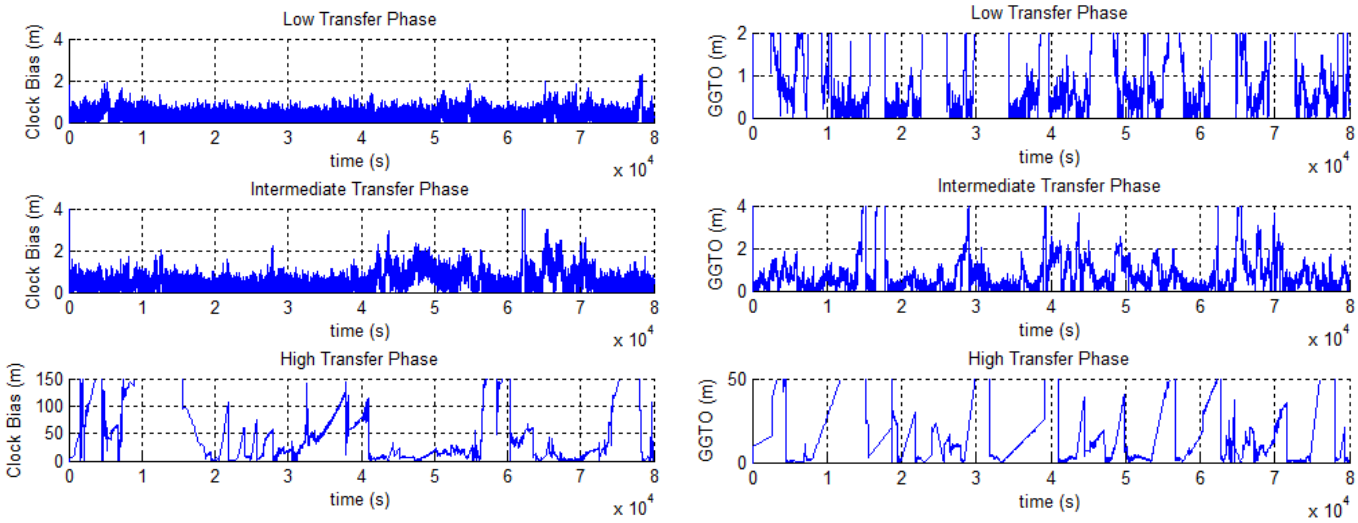

Figure V-43 Clock bias (left) and GGTO (right) estimation errors

Rising Phase			LOW ORBIT		MEAN ORBIT		HIGH ORBIT	
Filter			CKF	EKF	CKF	EKF	CKF	EKF
Mean Error	Position (m)	R	0.036	-1.024	-0.107	0.052	-42.593	-104.538
		T	-0.064	-0.291	-0.125	-4.281	15.7311	-8.971
		N	0.037	0.105	-0.022	-1.394	-9.971	-7.114
	Velocity (mm/s)	R	-0.337	-2.623	0.327	0.570	-11.413	-38.745
		T	-0.485	-1.627	-1.130	-6.135	-7.931	-18.822
		N	0.083	0.496	-0.494	-1.298	-2.991	-1.167
Std Error	Position (m)	R	0.689	1.015	0.619	1.521	88.454	156.913
		T	0.440	0.597	1.352	2.340	41.369	100.868
		N	0.274	0.537	0.987	3.473	19.925	41.596
	Velocity (mm/s)	R	1.054	1.799	0.849	1.817	22.186	33.270
		T	0.879	1.143	1.613	1.399	7.161	98.199
		N	0.468	0.772	0.934	2.113	4.318	69.315
Max Error (Module)	Position (m)	R	3.580	4.194	2.453	8.104	516.791	678.441
		T	2.581	3.643	5.760	11.220	223.001	438.969
		N	0.874	1.269	5.005	12.026	369.215	615.805
	Velocity (mm/s)	R	4.925	6.385	3.004	4.619	109.104	143.271
		T	4.343	4.159	7.674	10.404	32.627	53.340
		N	1.676	1.588	4.045	5.361	74.419	134.598

Table V-13 CKF and EKF positioning performance summary

The EKF, instead, overestimates the correction when GNSS satellites are re-tracked and so, from that moment on, it is no longer able to significantly reduce the estimation error. Figure V-42 confirms this feature for the CKF, which is able to bound the error envelope correctly also for each position and velocity component. The position performances of CKF are allowed by a proper management of the Multi-constellation estimated time delays variable $\Delta t, \Delta \dot{t}, \Delta t_{GGTO}, \Delta \dot{t}_{GGTO}$. Figure V-43 provide the CKF

clock bias and GGTO estimation errors for the tree transfer phases. The relevant effect of number of visible satellite in high scenario is outlined for both timing parameters. During lower phase, the error achieves meter accuracy and GGTO is propagated when Galileo SVs are not present in the tracking list without reacquisition issues. A summary of the achieved navigation performance statistics is provided in in terms of mean, standard deviation and maximum error in the RTN (Radial, Tangential, Normal) reference frame. CKF outperforms EKF in all the considered orbit phases.

E. Mixed Augmented-Consider filtering

As stated in IV.1-C Consider Filtering shall be intended as the minimal conservative approach (i.e. suboptimal) to be adopted in order to avoid detrimental performance degradation with respect to model errors. However, it can be also combined with direct state augmentations by promoting some consider variables in the primary state partition. A Mixed Augmented/Consider arrangement proposal is provided in Table V-14.

KF class method	Augmented/Consider Extended Kalman Filter (CEKF)
Extended State Partition	The extended state $\mathbf{X}$ can be partitioned in : ➢ Reference state $\mathbf{X}^{\mathbf{x}}_{A^e} \rightarrow \mathbf{x}\ (t) = \left\{\mathbf{r}\ ,\dot{\mathbf{r}}\ ,\Delta t,\Delta\dot{t},\Delta t_{GGTO},\Delta\dot{t}_{GGTO},\Delta A,\Delta\vartheta,\Delta\phi\right\}$ ➢ Consider parameters $\mathbf{X}^{\mathbf{p}}_{A^{cp}} \rightarrow \begin{cases}\mathbf{p}_{Pert} = \left\{\Delta C_D,\Delta C_R,a_R,a_T,a_N\right\} \quad \mathbf{p}_{thrust} = \left\{\Delta A,\Delta k_x,\Delta\eta,\Delta\zeta,\Delta m\right\} \\ \mathbf{p}_{range} = \left\{\Delta\varepsilon_1,\Delta\varepsilon_2,...,\Delta\varepsilon_n,\Delta\dot{\varepsilon}_1,\Delta\dot{\varepsilon}_2,...,\Delta\dot{\varepsilon}_n\right\}_{2n}\end{cases}$ $\mathbf{X}_{A_{ap}} \rightarrow \mathbf{p}_{thrust} = \left\{\Delta A,\Delta\vartheta,\Delta\phi\right\}$ The correspondent filter covariance $P_{\mathbf{XX}}$ is: $P_{\mathbf{XX}} = \left[\begin{array}{c\|c\|c} P_{\mathbf{X}^{\mathbf{x}}_{A^e}\mathbf{X}} & P_{\mathbf{X}^{\mathbf{x}}_{A^e}\mathbf{X}^{\mathbf{p}}_{A^{cp}}} & 0 \\ \hline P_{\mathbf{X}^{\mathbf{x}}_{A^e}\mathbf{X}^{\mathbf{p}}_{A^{cp}}} & P_{\mathbf{X}^{\mathbf{p}}_{A^{cp}}\mathbf{X}^{\mathbf{p}}_{A^{cp}}} & 0 \\ \hline 0 & 0 & P_{\mathbf{X}_B\mathbf{X}_B} \end{array}\right]$ $P_{\mathbf{X}^{\mathbf{p}}_{A^{cp}}\mathbf{X}^{\mathbf{p}}_{A^{cp}}} = diag\left(P_{\mathbf{p}_{Pert}\mathbf{p}_{Pert}},P_{\mathbf{p}_{thrust}\mathbf{p}_{thrust}},P_{\mathbf{p}_{range}\mathbf{p}_{range}}\right)$ $P_{\mathbf{X}_B\mathbf{X}_B} = P_{\mathbf{p}_{range,n+1...N}\mathbf{p}_{range,n+1...N}}$
Stochastic model peculiarities	➢ Thrust direct feedforward, external aiding and ranging errors as for Table V-12 ➢ Basically, the augmented variables $\left\{\Delta A,\Delta\vartheta,\Delta\phi\right\}$ are modelled as other thrust variables.
Special topics and remarks	The augmented variables $\left\{\Delta A,\Delta\vartheta,\Delta\phi\right\}$ are promoted at selected time/condition into the state augmentation partition in order to give evidence of the run time enabling of the calibration

Table V-14 Mixed Augmented/Consider Filtering

A rigorous approach should require the application of stochastic observability criteria [89] aiming to classify the model parameter importance. Even if some relevant tool relying on observability degree [100] are currently under investigation, these issue needs further analysis and are postponed to future works. However at design level, two fundamentals properties can be used for state variable selection:

1) strong correlation in time : assuming that a target parameter can acquire enough information along a particular trajectory (i.e. it is observable), strong correlation in time allows improving the parameter knowledge as long as the estimator continuously process measurements.

2) high level of uncertainty: considering the same weight of the variable on the stochastic system (i.e. the same observability degree) a high initial uncertainty level, represented by the parameter

covariance, will correspond in a more significant effect on the state trajectory error.

These criteria apply for thrust bias ΔA and misalignment components $\Delta\vartheta, \Delta\phi$. Actually, ranging biases $\Delta\varepsilon_1$ can be discarded as they continuously reset in accordance to visibility changes. Moreover, it is expected that the remaining perturbation parameters and other mechanization errors, still active as consider variable, can be handled as secondary order contributions. The random constant process is selected as proper auxiliary process to represent the augmented variables.

The reordering procedure allows activating, run time, the partial augmentation, so it can be configured as a MEONS Calibration Operative Submode properly defined in the MEONS EOR controller (IV.3). For the sake of brevity the test is performed on the lower and upper EOR phases. During the test, augmentation is simply activated after a certain convergence time correspondent to the acquisition of a proper positioning accuracy. Such criterion could be used as augmented model activation trigger, since parameter direct estimation generally benefit of a low error level for the other variables [100]. The start-up assumes the same covariance initialization of the IV.3-C applications, so the setting is the same of one that defined in Table V-12.

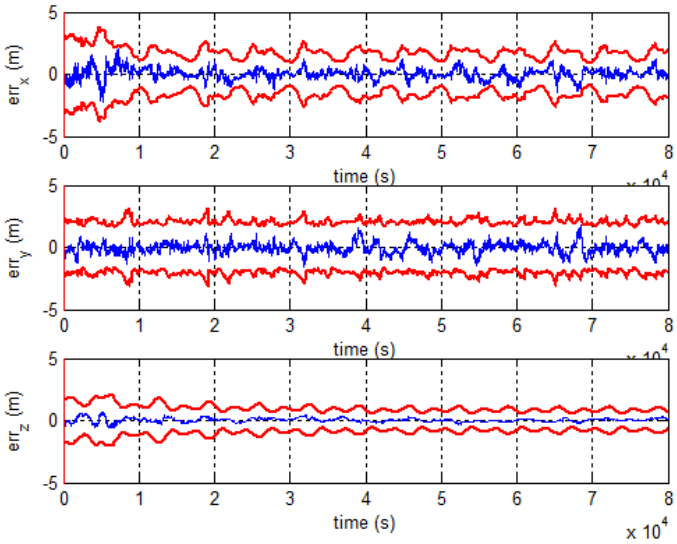

Figure V-44 AGKF Position error for the EOR LEO orbit phase

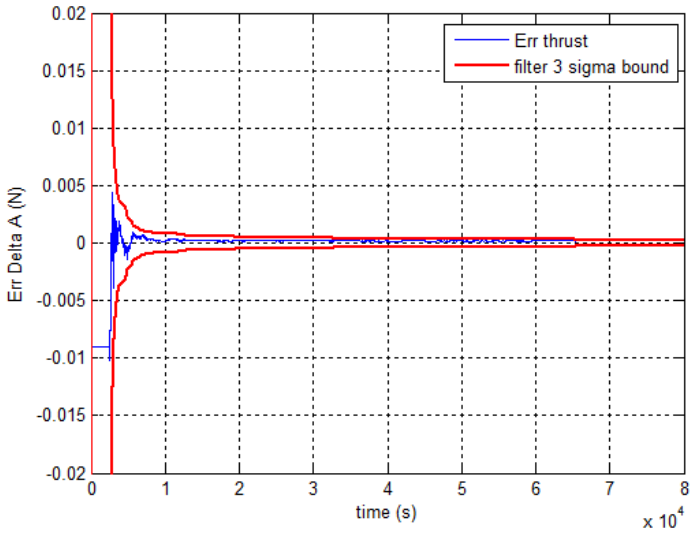

Figure V-45 Thrust bias estimation error for the EOR LEO orbit phase

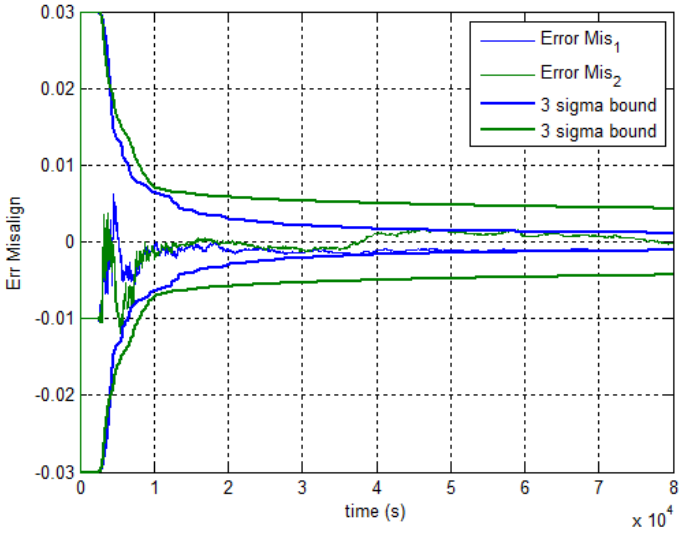

Figure V-46 Misalignment estimation for the EOR LEO orbit phase

In more details, the target state partition is activated about 2000s and 22000s respectively for the low and high orbit case. Filtering performance, relies not only to position and velocity accuracy (Figure V-44 and Figure V-47), whose statistics are synthetically provided in Table V-15, but also on thrust parameter estimation. Basically, high redundancy of information in the LEO case allows to achieve rapidly a robust parameter calibration (Figure V-45 and Figure V-46). This scenario does not consider additional possible variation during the mission, which are generally restricted to a small percentage of bias and misalignment magnitude and adsorbed by other considered parameters $\Delta k_x, \Delta\eta, \Delta\zeta$. In general, small perturbation can be conservatively dealt with by increasing uncertainty level of remaining parameters or modifying calibration thruster model. Conversely, a strong variation that could be expected after specific

operative scenarios (i.e. switch on after long transfer stop) can be handled by inactive state capability of the MEONS filter. The procedure reset the auxiliary process (i.e. the random constant), without losing position and velocity tracking in order to reinitialize the calibration and converge to another correct value.

The augmentation correctly works also during the high orbit, but a longer transient is necessary for the final performance acquisition (Figure V-48, Figure V-49). In this case position is more accurate than CEKF, due to the effect on long duration propagation phases. The calibration is basically a key element to be accounted. All the provided results are in line with the AGKF peculiarities shown in IV.1-C: the orbit estimation is improved in the Minimum Variance sense by the calibration of the parameters.

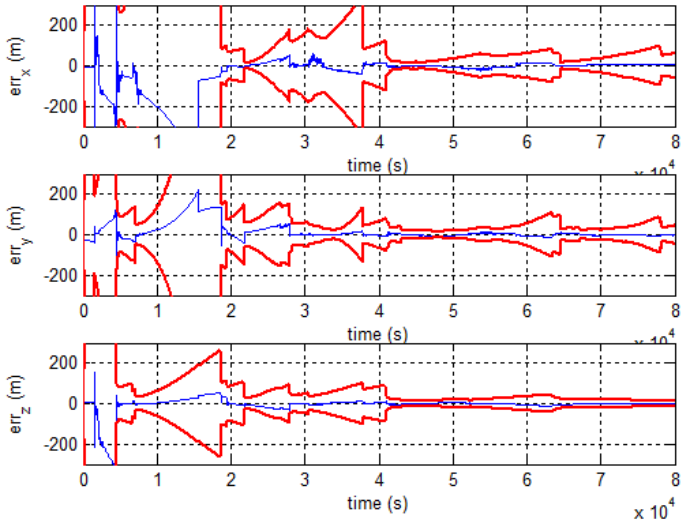

Figure V-47 CKF position, velocity error and 3σ covariance

Rising Phase			LOW ORBIT	HIGH ORBIT
Filter			AGKF	AGKF
Mean Error	Position (m)	R	0.0058	-0.8623
		T	0.0139	6.8164
		N	0.0790	-1.5525
	Velocity (mm/s)	R	0.0652	0.2076
		T	-0.0154	1.7746
		N	0.0075	-0.5073
Std Error	Position (m)	R	0.4755	17.1619
		T	0.2529	12.7959
		N	0.3737	8.7614
	Velocity (mm/s)	R	0.4431	3.6482
		T	0.1973	4.0535
		N	0.3167	2.3371
Max Error (Module)	Position (m)	R	2.3532	61.1608
		T	1.1261	53.5735
		N	1.5954	32.1399
	Velocity (mm/s)	R	3.6626	14.1756
		T	1.2996	15.6121
		N	2.4669	6.8150

Table V-15 CKF and EKF positioning performance summary

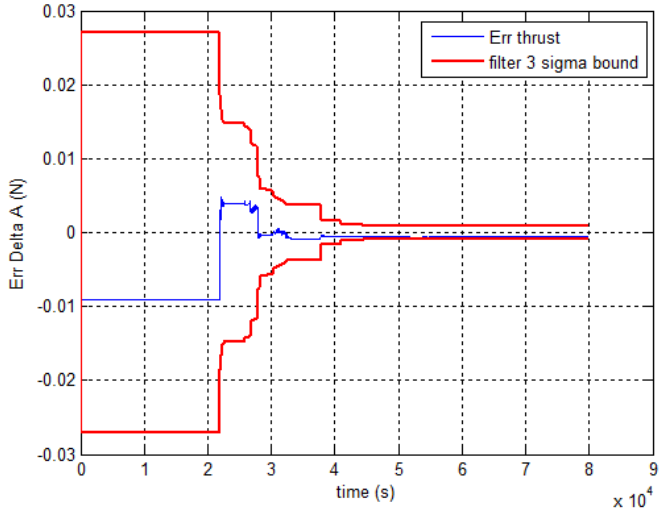

Figure V-48 Thrust bias estimation error for the EOR MEO orbit phase

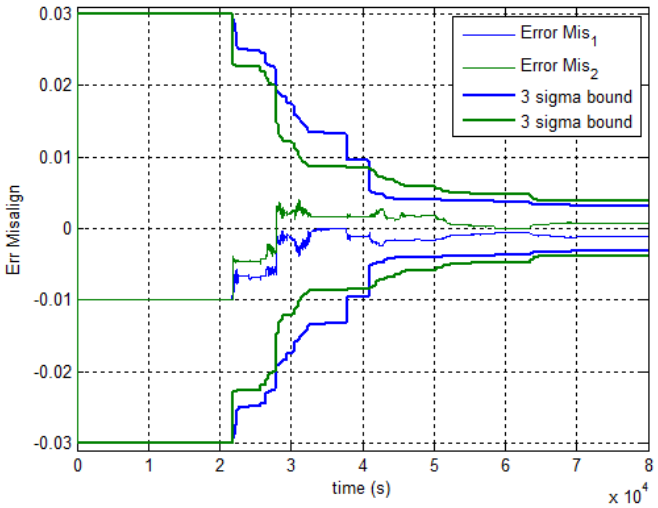

Figure V-49 Misalignment estimation error for the EOR MEO orbit phase

However it is worthy to remind here some relevant aspects. Firstly, including the other considered parameters makes reliable the calibration procedure. A test in high orbit case has been performed deactivating the other thrust consider parameter $\Delta k_x, \Delta\eta, \Delta\zeta$. The misalignment estimation does not show relevant changes, but its covariance bound becomes misleading, as shown in Figure V-50. This behaviour can be intended as a lower consistency of the parameter calibration, since the bound reduces very close to the error. The additional thruster mechanization variables can be seen as a systematic deviation on the

estimated one and the filter calibration accuracy must be limited by this contribution. Basically, other methods, as proper variable reduction and combination can be put in place in order to handle this issue. However the proposed approach results very simple from a design point of view: consider parameters works as a set of uncorrelated tuning variables that are directly mapped on the state estimate by the physical sensitivity model. The second aspect is the effect on the state augmentation of the proper choice of the auxiliary process. Only for exemplificative purposes, a process with a too low correlation time is tested, specifically a GM1 model with wrong time constant of 6000s. As shown by Figure V-52 the calibration procedure becomes quite ineffective because the estimation is not able to improve the parameter knowledge due to the sparsity of the information. The introduction of a degree of freedom is in this case useless. This condition makes the CKF competitive since it provides a design simplification, with acceptable performance, avoiding characterization of the auxiliary process.

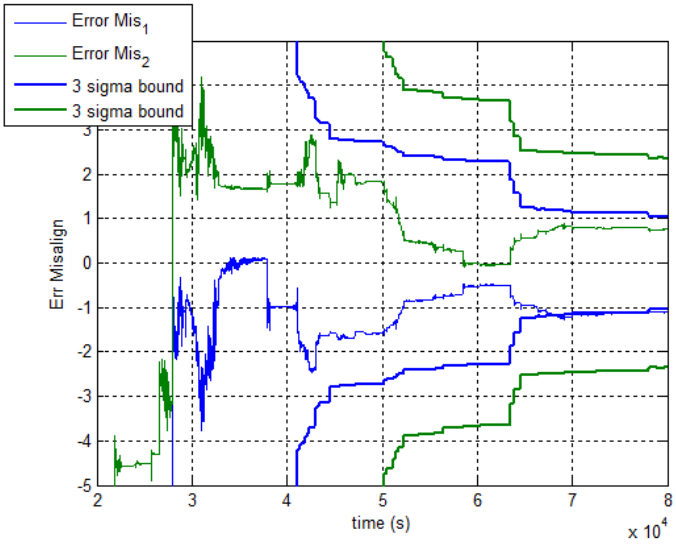

Figure V-50 Misalignment estimation without auxiliary consider parameters

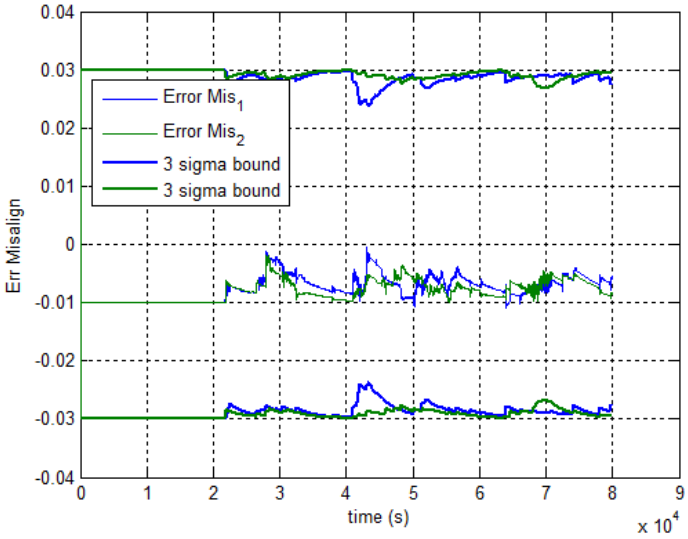

Figure V-51 Misalignment estimation with wrong selection of auxiliary process

The state augmentation hitherto proposed needs further investigation. As stated at design level the state augmentation and the consider approach represent two different philosophy that shift from accurate and sensitive solution to the suboptimal robust one. Beyond future development of criteria allowing to trade off these needs, MEONS capability with mixed augmented and considered variables has been fully verified.

V.4 MARGINALIZED CONSIDER FILTERING FOR SMALL SATELLITE AUTONOMOUS TARGET ORBIT ACQUISITION

A. Mission: Low thrust autonomous orbit acquisition for next generation small satellites.

The possibility to use MEONS during LEOP for an AAM control procedure (II.2) has been investigated in [7] for small satellite platforms. The results discussed hereafter confirm the possibility to override control navigation criticalities [118] due to manoeuvre dynamic and realize a deeper synergy between MEONS and autonomous orbit control. The specialization for AAM case of the general control architecture discussed in III.1 is reported in Figure V-52.

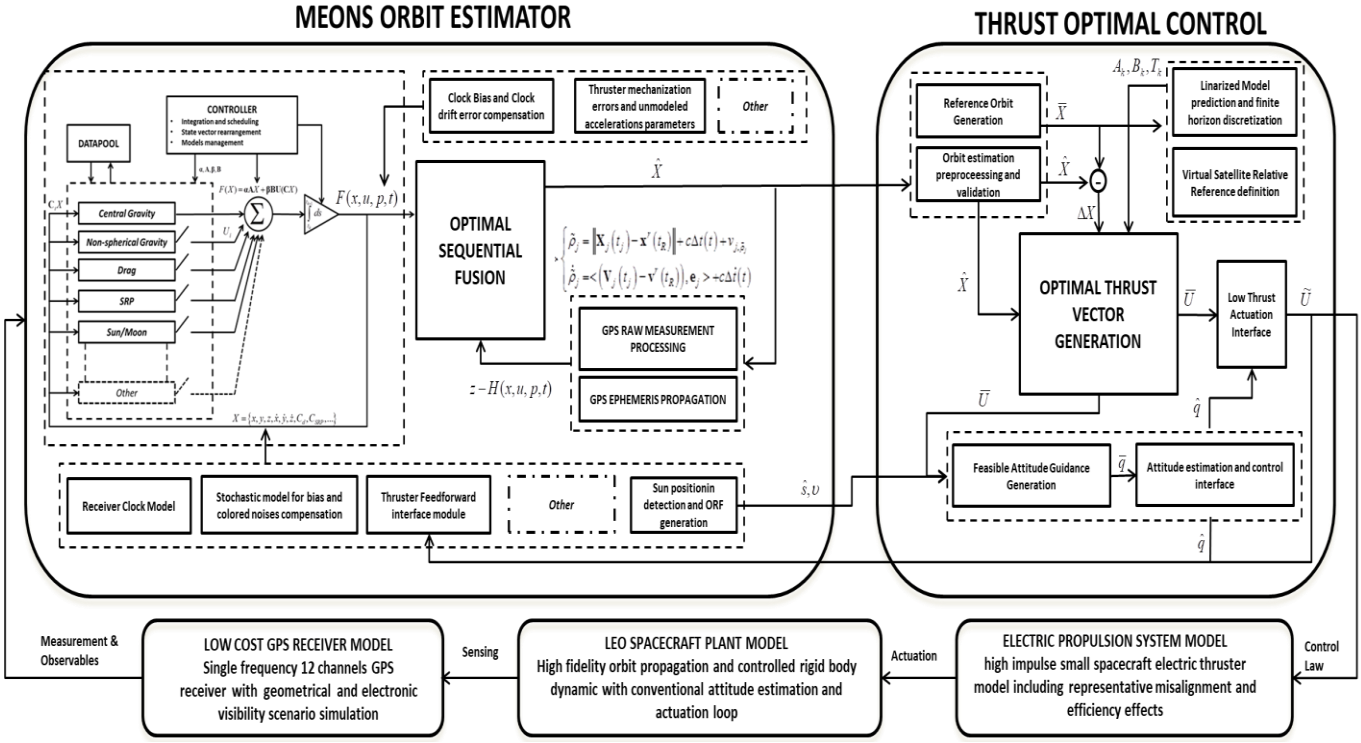

Figure V-52 Control system block diagram for Autonomous Orbit Acquisition

The target spacecraft reflects the design of a 130Kg platform embarking electrical propulsion. Common design drivers with the EOR case can be identified considering the same electrical low thrust steering framework. The propulsion system is considered mounted along the mechanical x-axis, whereas solar arrays can be reoriented around the mechanical y-axis (Figure V-53).

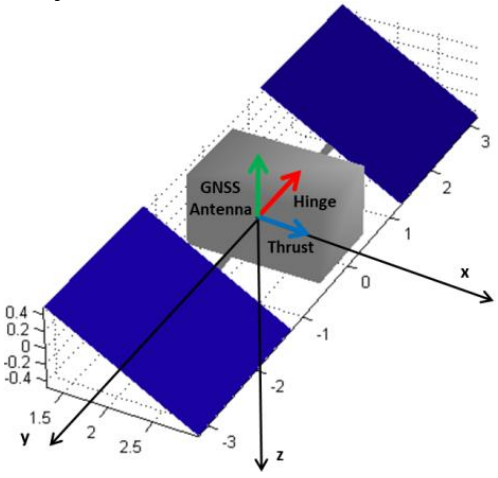

Figure V-53 Illustration of reference small spacecraft architecture

The orbit acquisition is realized through a hall thruster assembly providing a maximum actuation of 0.018N and a specific impulse (ISP) of 1300s [119] in accordance to the reduced platform resources. A scaled avionic (sensor-actuators) subsystem is considered in order to assume triaxial attitude estimation and control compatible with small satellite. The main difference with the EOR architecture relies on the navigation assembly. The satellite integrates the single board GNSS receiver within the avionic computer, allowing to track up to 12 GPS satellites. As stated in II.3 a reduced cost single chain solution shall be considered, providing single frequency/single constellation measurements. More important, differently from G2G EOR case, only one antenna is available, whose mounting direction is constrained by the mission operative attitude.

Complete DSS model		
Parameter	**Symbol**	**Value**
mass (kg)	mass (kg)	130
drag coefficient	CD	2.25
Solar Radiation Coefficient	CR	1.3
Rising starting date	y_i, m_{i-},d_i	2016, 03, 22
Reference orbit altitude	h_i	613 km
Reference orbit parameters	e_i, Ω_i, i_i	0.001, 0°, 61°
Injection error at manoeuvre start-up (ECI)	$\Delta x_{hill}, \Delta y_{hill}, \Delta z_{hill}$ $\Delta \dot{x}_{hill}, \Delta \dot{y}_{hill}, \Delta \dot{z}_{hill}$	1135.437 (m) 105.740 (m) 1879.600 (m) 3.792 (m/s) -1.489 (m/s) -3.749 (m/s)
Nominal Thrust Magnitude	A,ISP	0.03 N , 1300 m/s
Thrust Magnitude Efficiency	ε	5% of A
Thrust Magnitude Noise	ν_x, ν_y, ν_z	N(0,10-9 m/s2)
Delta Mass	Δm	1e-3Kg
Scaling errors	$\Delta k_x, \Delta k_y, \Delta k_z$	10-3
Skewing errors	$\Delta\vartheta, \Delta\psi, \Delta\varphi$	10-3
Misalignment errors	$\Delta\xi, \Delta\eta, \Delta\zeta$	10-2

GNSS Scenario Simulator			
GSS setting	**Simulation Approach**	**Parameter**	**Value**
Constellation	GPS (32 SVs)	TLE	-
Visibility analysis	Geometrical selection	FOV Rx (Half cone) FOV Tx (Half cone)	85° 85°
	Elcetronic Visibility	Acquisition Threshold	38dbHz
		λ L1/E1 , L_{SVf} , L_{IL} , L_{IMP} T_{Sys}	19 cm 1dB 2.5dB, 2.5dB,220K
Measurements	P_L1/P_E1 DL1/D_E1	Rate	1Hz

GNSS Scenario Simulator				
GNSS error source	**Simulation Approach**	**Estimation/calibration approach**	**UERE 1σ (m)**	**UERRE 1σ (m/s)**
Receiver clock bias and drift	Discrete-time model of colored noise	On line estimation	Negligible	Negligible
Satellite Ephemeris and Satellite Clock Correction	Perturbed GNSS satellite positions and velocity error per axis	Neither estimation nor calibration but modelled as considered parameters	1m-4m	0.001-0.004
Ionospheric delay	Ionospheric Error included	It is assumed a Klobukar or Nequick method for first order whereas residuals are included within ranging non-white tuning parameters	1m-4m	0.001
Multipath	Normally distributed random error	Neither estimation nor calibration, but included as equivalent ranging error non-white tuning parameters	1.0	0.010
Measurement noise	Random noise with standard deviation accounting for C/N0		σ_{DLL} (0.3-0.5)	0.010

Table V-16 AAM scenario setting

Assuming Earth pointing EO (or TLC) mission, the antenna is aligned with the negative z-axis in order to cope with Zenith pointing during payload operations. The control system attitude guidance (Figure V-52.) is one that defined in III.1-D, so the antenna boresight orientation is subordinated to thrust and Sun tracking needs. Mitigation of the expected GNSS antenna unfavourable pointing (low visibility conditions and high GDOP) is just in charge to the MEONS orbit estimation module. Spacecraft physical properties

and relevant mission data are reported in Table V-16. From an operative point of view, the steering scenario starts when safe hold conditions are achieved: after launch spacecraft initial rate has been dumped and sun pointing attitude is acquired in order to activate platform avionic and power subsystem basic functions. At this step, considering power supply and positioning as main attitude drivers, the navigation system can determine initial spacecraft position with accuracy sufficient to sense launch vehicle injection errors and start AAM. Wrong satellite displacement is evaluated comparing valid navigation solution with a reference physical trajectory that can be preliminary preloaded or computed on board [120].This study considers an initial dispersion of 2Km (3D in Hill reference frame) from a LEO circular target orbit, whose ephemeris parameters are reported in Table V-16 . As concern the OTVG the general framework and the control design drivers are ones that described in III.1-D. However, some details are provided on the developed mathematical kernel in order to address the closed loop performance analysis (a complete description is provided in[118]).

As stated in III.1-D, a general Hamiltonian for the control problem can be defined by using eq.(5.7) . It formalizes the optimization goal of bringing the S/C from an initial dispersed condition $\mathbf{X}_{in}$ to the final one $\mathbf{X}_{fin}$ in a given time window $T = t_f - t_{in}$ and minimizing consumption of fuel $\mathbf{L}$ (i.e. the square sum of thrust control variables). $\Lambda = [\lambda_1, \lambda_2, \lambda_3, \lambda_4, \lambda_5, \lambda_6]$ is the costate vector necessary to define the augmented function of the optimal control problem [61].

$$\begin{cases} H(\mathbf{X},\mathbf{U},\Lambda)=L(\mathbf{X},\mathbf{U})+\Lambda^{\mathbf{T}}\mathbf{f}(\mathbf{X},\mathbf{U}) \\ L=\int_{t_2}^{t_1}\sum_{\mathbf{i=1}}^{3}u_i^2\mathbf{d}\theta \end{cases} \wedge \begin{cases} \dfrac{d\mathbf{X}}{dt}=\mathbf{f}(\mathbf{X},\mathbf{U}) \\ \mathbf{X}(\mathbf{t}_1)=\mathbf{X}_{\mathbf{in}},\mathbf{X}(\mathbf{t}_2)=\mathbf{X}_{\mathbf{fin}} \end{cases} \tag{5.7}$$

Nevertheless, before applying Pontryagin's Minimum Principle the model shall be reviewed in order to deal with real time on board implementation.

$$\mathbf{H}(\mathbf{X},\theta,\mathbf{U})=\mathbf{L}(\mathbf{X},\theta,\mathbf{U})+\Lambda^{\mathbf{T}}[\mathbf{A}(\theta)\cdot\mathbf{X}+\mathbf{B}(\theta)\cdot\mathbf{U}]$$

$$\textbf{with} \quad \mathbf{L}=\int_{\theta_2}^{\theta_2}\sum_{\mathbf{i=1}}^{3}u_i^2\mathbf{d}\theta \quad \textit{and} \quad \begin{cases} \dfrac{d\mathbf{X}}{d\theta}=\mathbf{A}(\theta)\cdot\mathbf{X}+\mathbf{B}(\theta)\cdot\mathbf{U} \\ \mathbf{X}(\theta_1)=\mathbf{X}_{\mathbf{in}},\mathbf{X}(\theta_2)=\mathbf{X}_{\mathbf{fin}} \end{cases} \tag{5.8}$$

Specifically eq.(5.7) reduces to eq.(5.8) considering the following approximation:

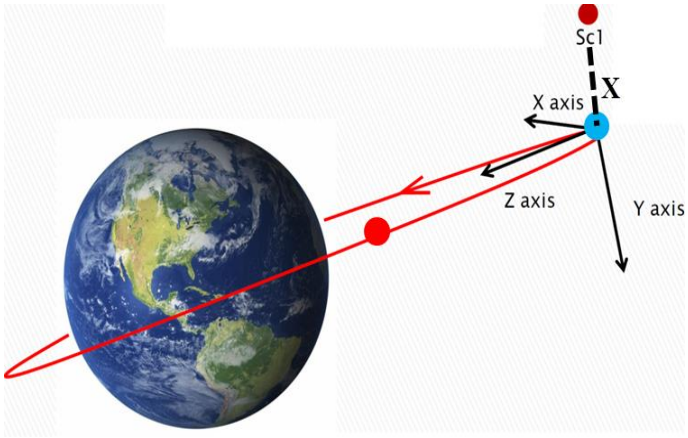

Figure V-54 Autonomous Orbit Acquisition control via Virtual Spacecraft approach

- The dynamic model is linearized along the reference target orbit $\mathbf{X}_{ref}(t)$. This trajectory is also called Virtual Spacecraft orbit (red line in Figure V-54) as it leads to the analogy with a formation flying problem.
- The dynamic model is rewritten in term of relative positioning of the S/C wrt the virtual reference (blue point in Figure V-54), thus $\mathbf{X}$ includes the relative position and velocity of the spacecraft in the Local Vertical Local Horizontal (LVLH)

- The dynamic model matrices (i.e. A and B) are obtained in term of unperturbed relative motion as

time variant function of reference orbital parameters. Details are reported in [121] and Appendix A, as they are propagation modules integrated in the Generic Propagator database.

- The final control problem solution provided in [59] expresses the optimal thrust as function of the costate vector:

$$u_j = -\frac{1}{2}\ \frac{(1-e^2)^3}{\left(1+e\cos(\theta)\right)^4 n^2}\lambda_{2j} \tag{5.9}$$

A discretization of the continuous time dependent true anomaly $\theta_k = \theta(t_k)$ allows to solve numerically the associated state and costate equations [120] providing a discrete approximation of the optimal thruster law.

This recursive implementation allows performing optimal control by simply solving a linear equation system [59] making feasible its on-board implementation. Although, the approach does not take into account nonlinear effects, perturbation effects and possible thruster errors. An open loop control could not produce satisfactory results, thus a closed loop has to be implemented in order to improve convergence properties and accuracy.

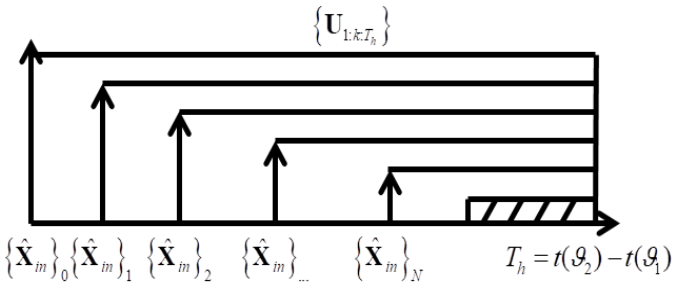

Figure V-55 Closed loop AAM control logic by using MEONS estimation for relative position reset

At each control cycle the algorithm computes a new initial relative state $\mathbf{X}_{in}$ starting from the newest estimation of MEONS orbit, and updates the optimal thruster law for the rest of the transfer time. The update rate of the loop Δt_{loop} can be selected in order to trade-off accuracy and computational effort, while the total acquisition horizon setting $T_h = t(\vartheta_2) - t(\vartheta_1)$ is the fundamental tool to make steering strategy compatible with the thrust saturation.

Δt_{loop} of 300s and T_h of 54700s are selected to cope with the assumed platform resources. The closed loop solution has been integrated in the GSS environment simulating electronic visibility selection and GNSS scenario peculiarities. Table V-16 also contain relevant setting for the GNSS equipment simulation. The ionosperic error is considered in term of systematic residuals assuming the implementation of a legacy method (i.e. Klobucar or Nequick in [122]) in order to remove the greatest first order term. The ephemeris error has been included as for V.3.

B. MEONS configuration

Similarly to the EOR case, MEONS propagation and observation equation are one that designed for low thrust control application. Eq.(3.42) and eq.(3.43) are just tailored in order to consider thrust contribution in eq.(3.29) and single constellation pseudorange and Doppler raw data processing. As for the EOR case, the Consider approach is selected as minimal conservative configuration to handle perturbation and actuation model parametric uncertainty. Actually, a robust estimation is mandatory when the orbit estimator is used in closed loop in order to ensure control stability and tracking. The uncalibrated ranging and range rate parameters are used as tuning parameters to consider the reduced performance due to single frequency application [76]. Actually, covariance consistency is fundamental as it provides the position and velocity error bound monitoring used to discard wrong correction samples or stop actuation in case of unexpected sensing failures. The final arrangement provided in Table V-17 is not very different from EOR case except for the Marginalized approach that has been used in order to handle

simultaneously numerical and linearized Taylor series methods discussed in IV.1. Actually, in the last phase of its development MEONS has been extended to this generalized nonlinear approach also in view of future extension (i.e. hybridization with attitude dynamic). The small satellite platform study has offered a test case to check this functionality.

KF class method	Consider Marginalized Unscented Kalman Filter (CMUKF) [7]
Extended State Partition	The extended state $\mathbf{X}$ can be partitioned in : ➢ Reference state: $\mathbf{X}^{\mathbf{x}}_{A^{nl}} \rightarrow \mathbf{x}\ (t) = \{\mathbf{r}\ ,\dot{\mathbf{r}}\ \}$ $\mathbf{X}^{\mathbf{x}}_{A^{l}} \rightarrow \mathbf{x}\ (t) = \{\Delta t, \Delta\dot{t}\}$ $\mathbf{X}^{\mathbf{p}}_{A^{l}} \rightarrow \{\varepsilon, \Delta\vartheta, \Delta\phi, \Delta k_x, \Delta\eta, \Delta\zeta, \Delta m, \Delta C_D, \Delta C_R, a_R, a_T, a_N\}$ ➢ Consider parameters $\mathbf{X}^{\mathbf{x}}_{A^{e}} \rightarrow \{\mathbf{r}\ ,\dot{\mathbf{r}}\ , \Delta t, \Delta\dot{t}\}$ $\mathbf{X}^{\mathbf{p}}_{A^{cp}} \rightarrow \mathbf{p}_{Pert} = \{\Delta C_D, \Delta C_R, a_R, a_T, a_N\}\ \ \mathbf{p}_{thrust} = \{\varepsilon, \Delta k_x, \Delta\eta, \Delta\zeta, \Delta m\}$ The correspondent filter covariance $P_{\mathbf{XX}}$ is: $\begin{bmatrix} \mathbf{P}_{\mathbf{x}_{A^{nl}_k}\mathbf{x}_{A^{nl}_k}} & \mathbf{P}_{\mathbf{x}_{A^{nl}_k}\mathbf{x}_{A^{l}_k}} & \mathbf{P}_{\mathbf{x}_{A^{nl}_k}\mathbf{x}_{A^{cp}_k}} & 0 \\ \mathbf{P}_{\mathbf{x}_{A^{l}_k}\mathbf{x}_{A^{nl}_k}} & \mathbf{P}_{\mathbf{x}_{A^{l}_k}\mathbf{x}_{A^{l}_k}} & \mathbf{P}_{\mathbf{x}_{A^{l}_k}\mathbf{x}_{A^{cp}_k}} & 0 \\ \mathbf{P}_{\mathbf{x}_{A^{cp}_k}\mathbf{x}_{A^{nl}_k}} & \mathbf{P}_{\mathbf{x}_{A^{cp}_k}\mathbf{x}_{A^{l}_k}} & \mathbf{P}_{\mathbf{x}_{A^{cp}_k}\mathbf{x}_{A^{cp}_k}} & 0 \\ 0 & 0 & 0 & \mathbf{P}_{\mathbf{x}_{B_k}\mathbf{x}_{B_k}} \end{bmatrix}$ $P_{\mathbf{X}^{\mathbf{p}}_{A^{cp}}\mathbf{X}^{\mathbf{p}}_{A^{cp}}} = diag\left(P_{\mathbf{p}_{Pert}\mathbf{p}_{Pert}}, P_{\mathbf{p}_{thrust}\mathbf{p}_{thrust}}, P_{\mathbf{p}_{range}\mathbf{p}_{range}}\right)$ $P_{\mathbf{X}_B\mathbf{X}_B} = P_{\mathbf{p}_{range,n+1\ldots N}\mathbf{p}_{range,n+1\ldots N}}$
Stochastic model peculiarities	➢ Thrust direct feedforward, external aiding and VSD ranging errors $\mathbf{X}_B \rightarrow \begin{cases} \mathbf{X}^{\mathbf{x}_{aux}}_{B_{static}} \rightarrow \mathbf{x}_{aux}\ (t) = \{A, \alpha, \beta, q\ , \omega, m_p\} \\ \mathbf{X}^{\mathbf{p}}_{B_{static}} \rightarrow \mathbf{p}_{range,n+1\ldots N} = \{\Delta\varepsilon_{n+1}, \Delta\varepsilon_{n+2}, \ldots, \Delta\varepsilon_N, \Delta\dot{\varepsilon}_{n+1}, \Delta\dot{\varepsilon}_{n+2}, \ldots, \Delta\dot{\varepsilon}_N\} \end{cases}$
Special topics and remarks	The reference state has been decomposed in a nonlinear and linear partition in order to verify possible extension to mixed nonlinear/linear solution

Table V-17 MEONS CMUKF configuration for LEO-MEO EOR

Unfortunately, comparison test between the MUKF arrangement and the standard equivalent EKF (both in their Consider declination) has not provided relevant improvements during nominal acquisition procedure. The AAM optimization starts when navigation has reached a minimum accuracy threshold, which is a small percentage of the expected dispersion (<30m 3D). This procedure allows making robust the first OTVG optimal control prediction. Probably, reduced dynamic range of the error, considering the nature of GNSS observable cannot trigger model nonlinearities and the solution remain in the neighbourhood of the optimal trajectory, where linearization applies.

However, as shown in the simplified example of IV.1-B, the sigma point extension can be effective in case of wrong initialization and studies as [83] confirm this peculiarity also for orbit estimation. Such condition can occur during the navigation initialization phase that precedes the AAM manoeuvre. A dedicated scenario has been generated considering the following issues:

- During receiver initialization a slow acquisition of code and carrier phase can be experienced. An exemplificative start-up phase has been generated simulating visibility escalation in Figure V-56.

MUKF covariance configuration	
State initial covariance $\mathbf{P}_{ss}^{0}$	$\sigma_{\mathbf{r}} = 10_{[m]} \quad \sigma_{\dot{\mathbf{r}}} = 0.3_{[m/s]}$ $\sigma_{t}^{0} = 50_{[m]} \quad \sigma_{\dot{t}}^{0} = 1_{[m/s]}$ $\sigma_{t_{GGTO}} = 50_{[m]} \quad \sigma_{\dot{t}_{GGTO}} = 1_{[m/s]}$
Parameter initial covariance $\mathbf{P}_{pp}$	$\sigma_{\varepsilon}^{0} = 0.05 \quad \sigma_{\Delta m}^{0} = 0.01_{[Kg]}$ $\sigma_{\Delta k_{x,y,z}}^{0} = 0.001 \quad \sigma_{\Delta s_{\vartheta,\psi,\phi}}^{0} = 0.01$ $\sigma_{\Delta c_{\xi,\eta,\zeta}}^{0} = 0.001 \quad \sigma_{\Delta C_D}^{0} = 0.15$ $\sigma_{\Delta C_R}^{0} = 0.15 \quad \sigma_{\mathbf{a}_{R,T,N}}^{0} = 10^{-7}_{[m/s^2]}$ $\sigma_{\varepsilon_i} = 2_{[m]} \quad \sigma_{\dot{\varepsilon}_i} = 0.0015_{[m/s]}$
Process noise covariance $\mathbf{Q}_{ss}$	$\sigma_{\mathbf{w_a}} = 5 \cdot 10^{-9}_{[m/s^{3/2}]} \quad \sigma_{\mathbf{w}_{\dot{t}}} = 0.6_{[m/s^{1/2}]}$ $\sigma_{\mathbf{w}_{\dot{t}}} = 0.1_{[m/s^{3/2}]} \quad \sigma_{\mathbf{w}_{\dot{t}_{GGTO}}} = 0.6_{[m/s^{1/2}]}$ $\sigma_{\mathbf{w}_{\dot{t}_{GGTO}}} = 0.1_{[m/s^{3/2}]}$
Measurement noise covariance $\mathbf{R}$	$\sigma_{v_{UERE}} = \left(5 + \sigma_{DLL}^{2}\right)^{1/2}_{[m]}$ $\sigma_{v_{UERRE}} = 0.033_{[m/s]}$

Table V-18 EOR CKF setting

- During filter initialization the estimation module can experience a high error on the initial conditions. MEONS start-up inherit the Coarse Orbit Determination module of first generation TAS-I navigation system. This module, by using the same MEONS orbit integrator propagates the orbit from a preloaded Initial State Vector (ISV), generally computed by ground flight dynamic processor, initializing the spacecraft position without using GNSS. However, taking into account injection errors, propagation from a wrong ISV and timing errors (worst case 1s correspond to 7km) can lead to more than 10 km error on the available first guess. A worst case of 10Km on each component is here considered.

Results of the performed MEONS run are shown in Figure V-57.

The simulation allows pointing out the distance between the two approaches: MUKF convergence properties are very close to UKF, outperforming the conventional EKF in critical initialization conditions. The behaviour reflects what has been shown in the two dimension example of IV.1-B.

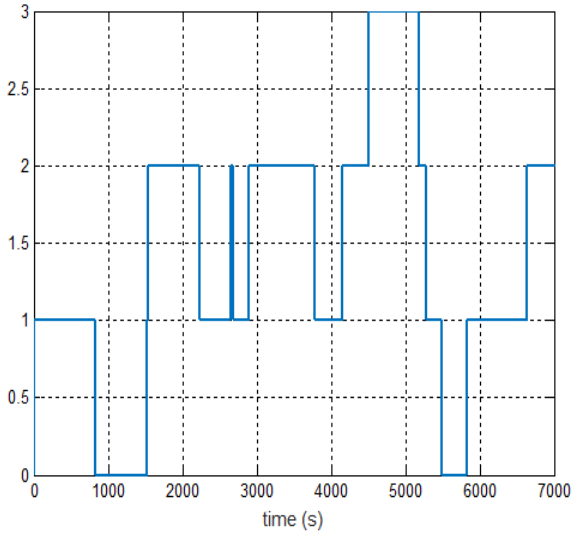

Figure V-56 : GNSS degraded signal acquisition scenario for convergence issues analysis

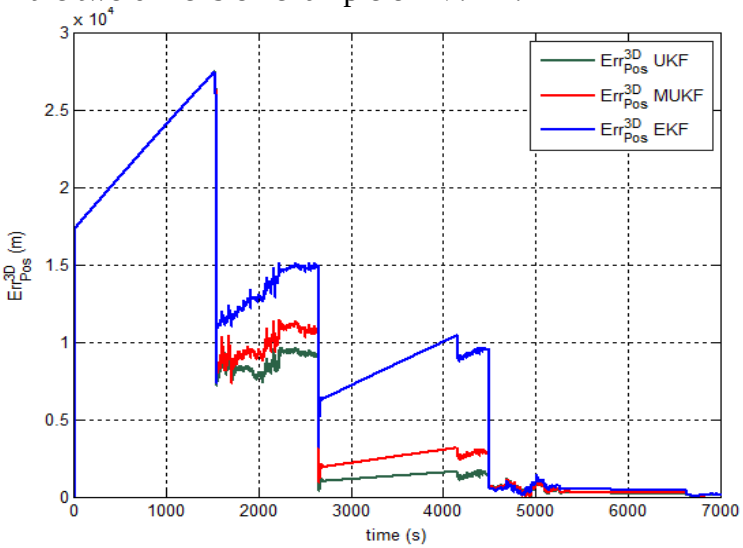

Figure V-57 : MEONS EKF, UKF and MUKF orbit estimation performance comparison

C. Results

The application of the steering law immediately points out a wide excursion of GNSS visibility conditions Figure V-58. The attitude guidance preserves desired thrust and Sunlight projections in BRF (Figure V-59) at the expense of the GNSS antenna orientation. Actually, Figure V-60 shows a periodic reduction of available GNSS measurements experienced when the antenna points far from the Zenith condition.

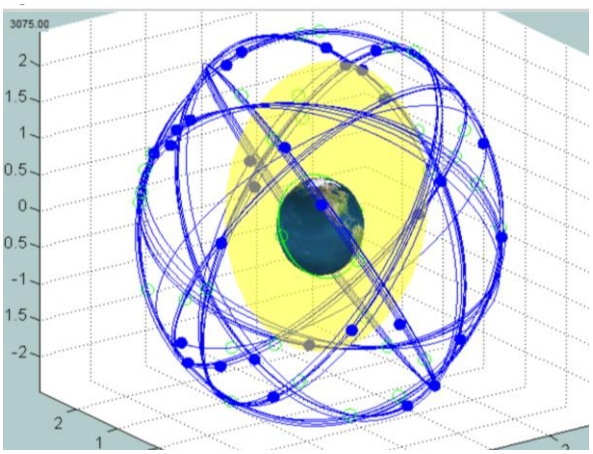

Figure V-58 : GNSS scenario simulation for Autonomous Acquisition Manoeuvre

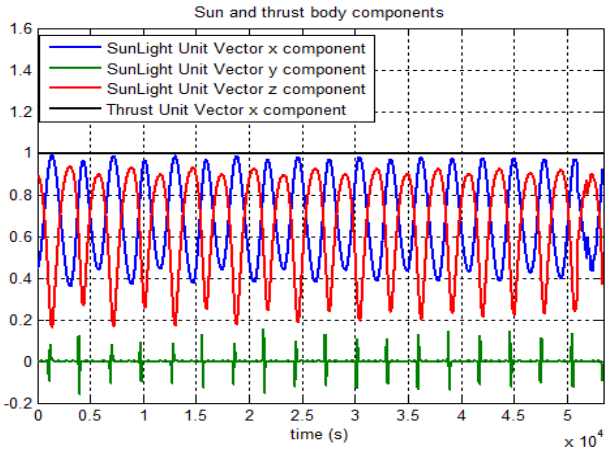

Figure V-59 : Thrust and Sunlight projection in BRF due to designed attitude guidance

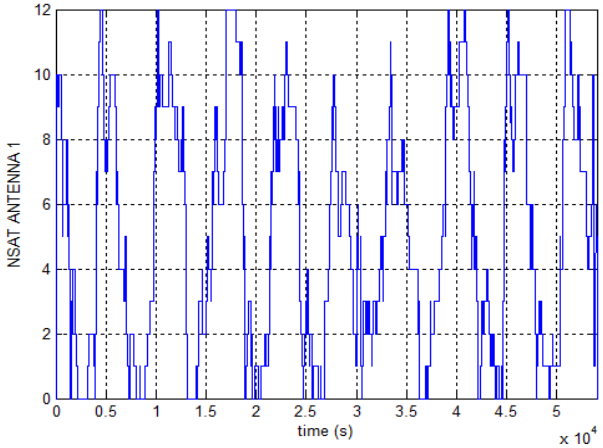

Figure V-60 : GNSS number of visible satellite during acquisition scenario

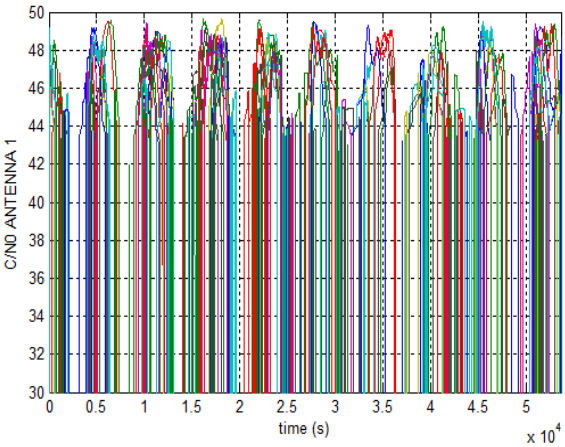

Figure V-61 : C/N0 evaluation for SVs electronic visibility selection

However, as shown in Figure V-62 and Figure V-63 MEONS estimation allows to keep navigation performance within a stable error bound achieving positioning accuracy that ranges from few meters, with more than 4 satellites, to a maximum of 20m during longer GNSS outages.

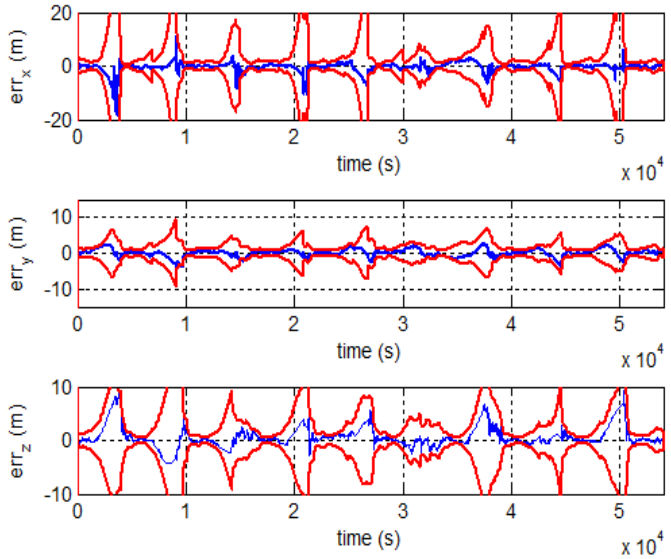

Figure V-62 CMUKF position, velocity error and 3σ covariance bound during low orbit phase

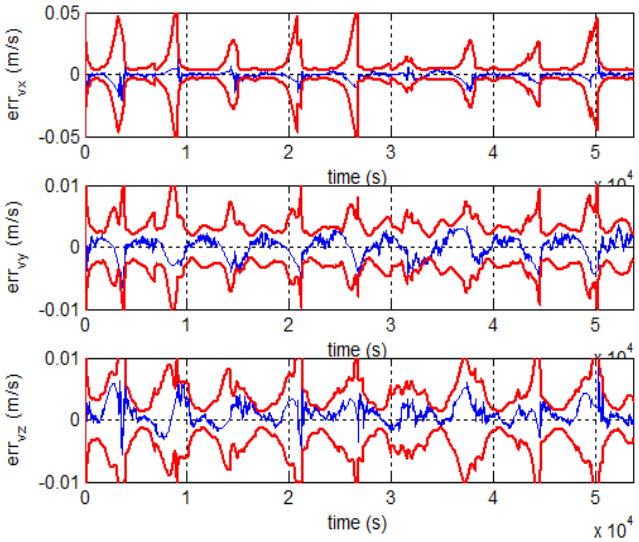

Figure V-63 CMUKF velocity error and 3σ covariance bound during low orbit phase

Actually, covariance peaks indicate phases with reduced measurement correction effect, but the filter is always able to rapidly reacquire the performance as new measurements are available.

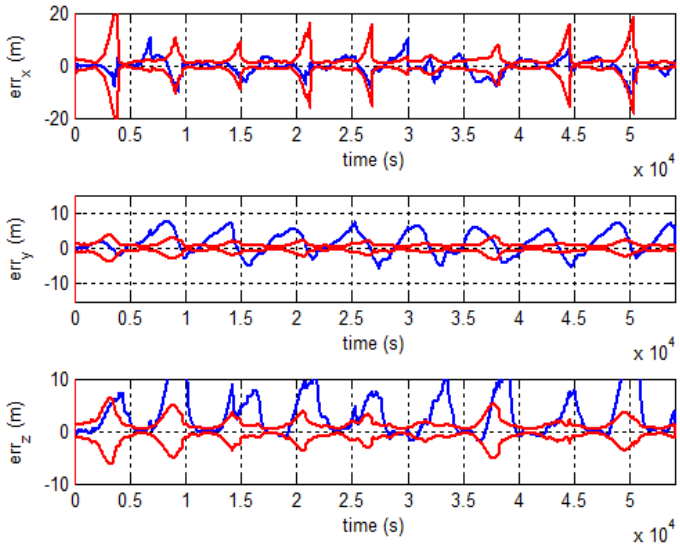

Figure V-64 Standard MUKF position, velocity error and 3σ covariance bound during low orbit phase

Similarly to the EOR case, during propagation phases the Consider solution controls the error within the 3σ bound by taking into account thruster parameter uncertainty. This feature is confirmed comparing the MEONS performance with the one obtained by a standard MUKF with increased covariance as for IV.1 C comparison example. The filter accuracy is degraded (see Figure V-64), especially on components mainly affected by the misalignment mechanization error. More important the covariance bound is not representative of the effective orbital error with clear drawbacks on the capability to monitor the effective control error. The same considerations apply for measurement systematic errors.

Not considering ranging errors determine an underestimated covariance if compared with the standard MUKF. However, Consider solution via ranging parameters can be locally too conservative as the measurement systematic error varies in accordance to the geometry and orbit arc (i.e. Ionosphere error). A proper shaping of consider covariance during the expected measurement maxima will be considered in the future to locally improve the performance.

As concern control performance, the position error (Figure V-65) and the acquisition trajectory envelope in Hill reference frame (Figure V-66) confirm the stability and robustness of the optimal control approach. The controller is able to converge to the 15m accuracy threshold (Figure V-67) within the selected acquisition window (53700s).

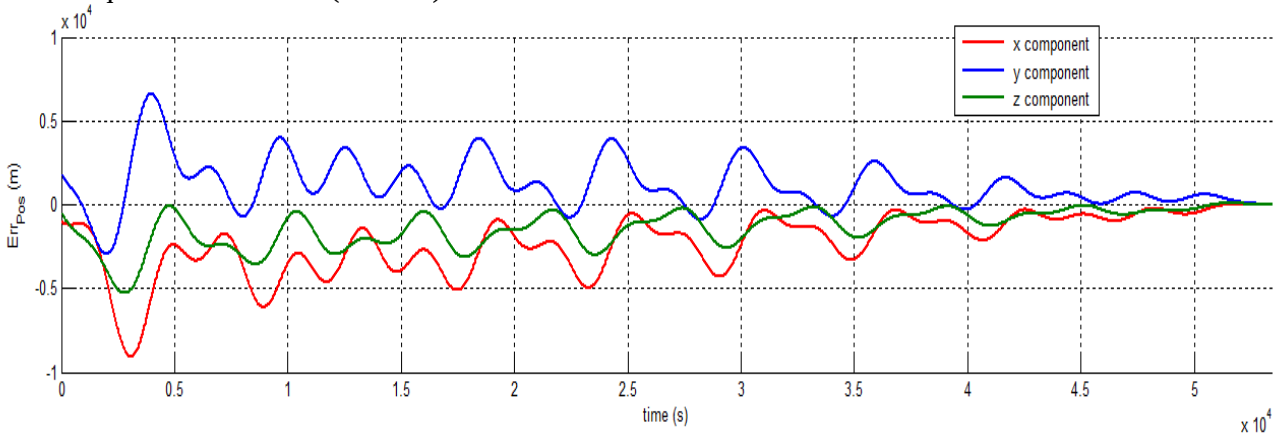

Figure V-65: Optimal Control Error in ECI reference frame.

It shall be noted that such time span allows reaching the target orbit with a maximum thrust magnitude of 0.012N compatible with actuation saturation constraints (Figure V-68). Less than 0.05Kg of propellant has been spent to perform the autonomous steering. A sensitivity analysis with respect to time horizon confirms it as the fundamental tool to control saturation.

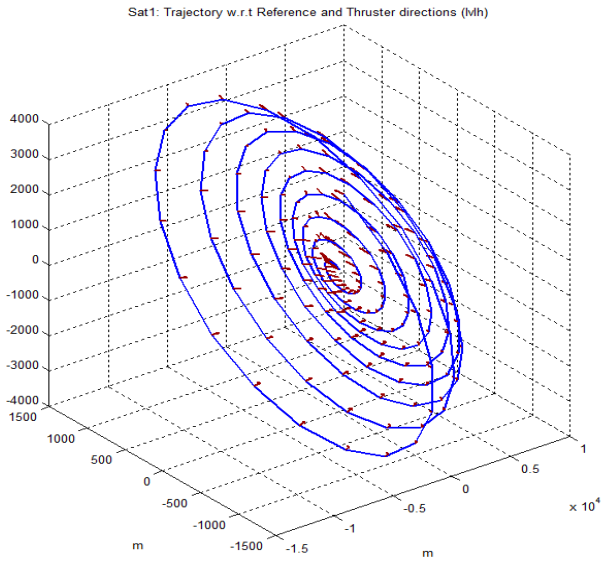

Figure V-66 : Acquisition trajectory and optimal low thrust envelope in Hill reference frame

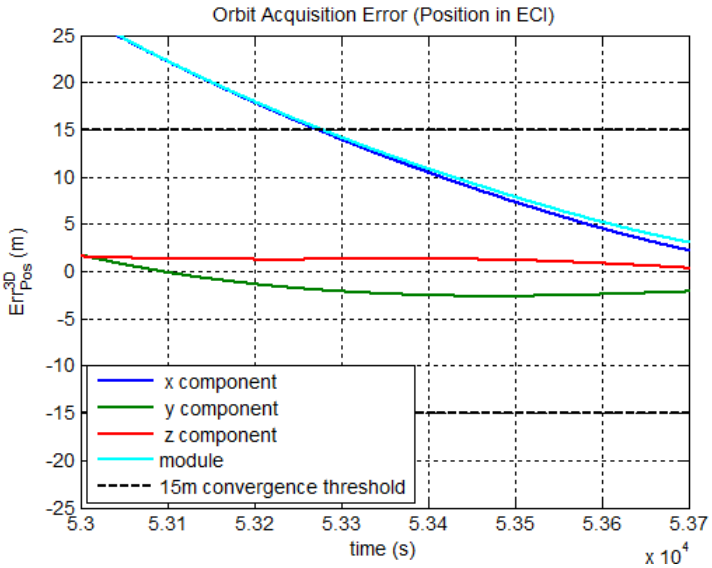

Figure V-67 : Acquisition trajectory and optimal low thrust envelope in Hill reference frame

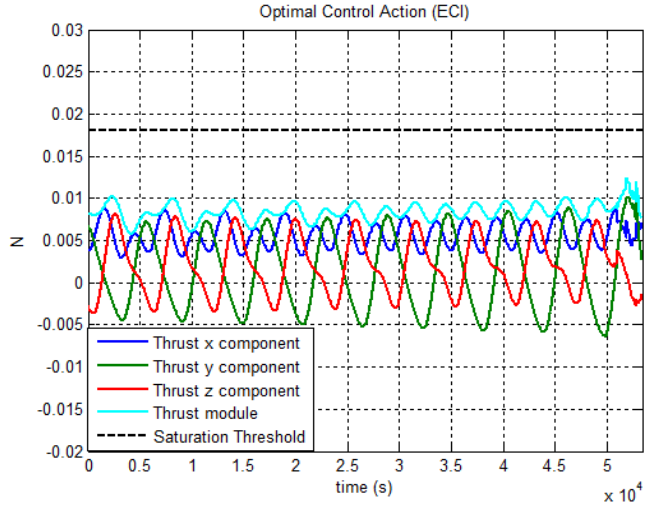

Figure V-68 Applied Low Thrust Control Action

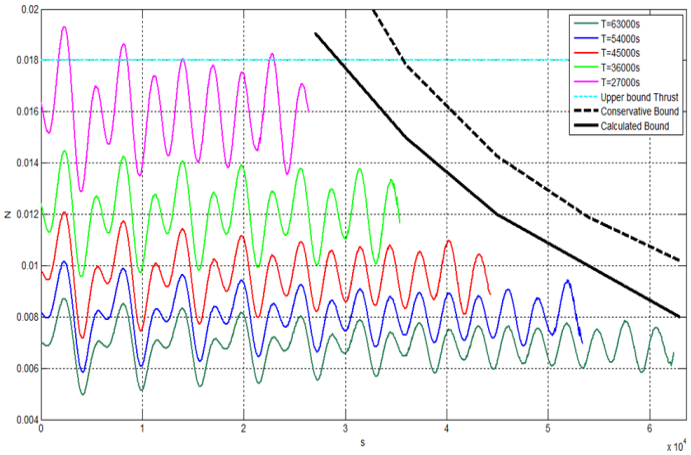

Figure V-69 Thrust magnitude variation with AAM Horizon selection

For the sake of comparison Figure V-65 shows the solution of the optimal control in case of open loop approach: without the estimation reset the controller is not able to compensate the approximation present in its internal dynamic model becoming ineffective.

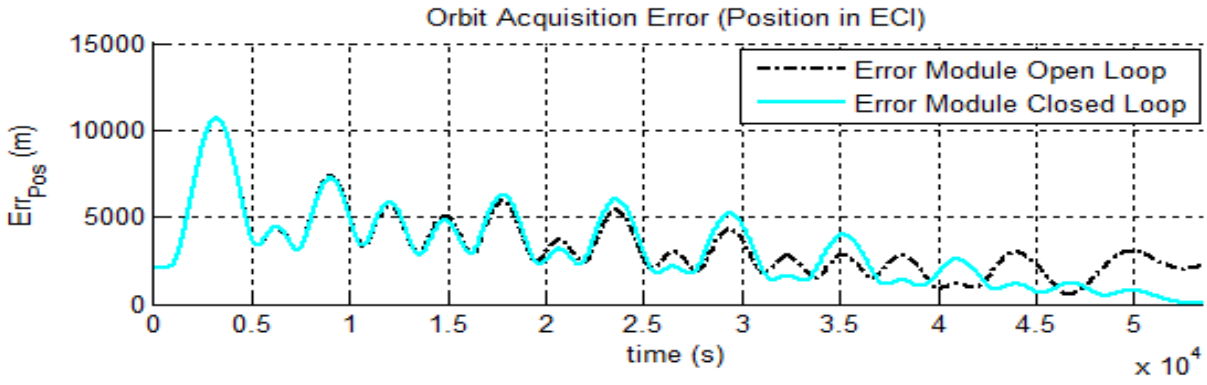

Figure V-70 Approximated optimal control performance with and without closed loop logic implementation

A conservative bound $F_{\max} \propto K(Vm/T_f), K \simeq 1.5$ has been proposed in order to improve on-board feasible optimal solution search. It is expressed as a function of the current mass m, the actuator saturation threshold, and the velocity injection error V sensed via the navigation system. Such bound provide a useful first guess reducing the number of iteration necessary to recursively exclude unfeasible control trajectories.

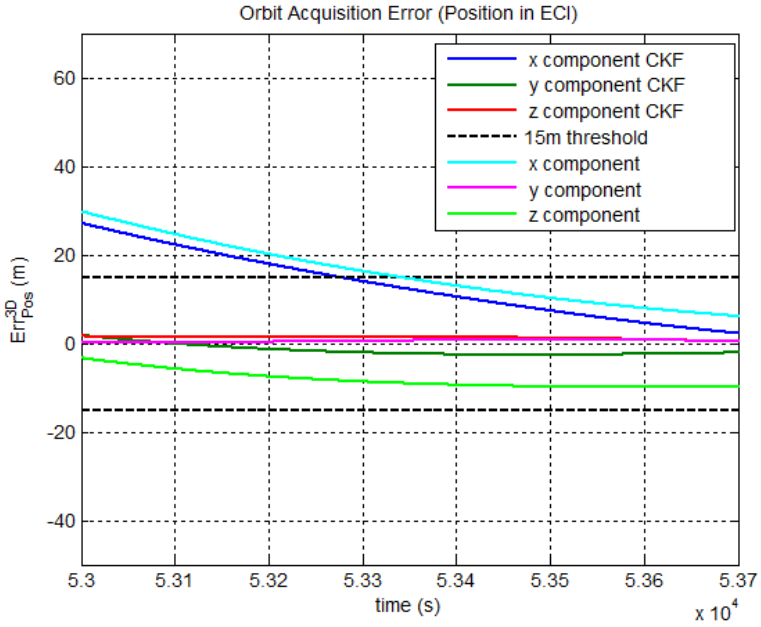

Figure V-71 AAM acquisition accuracy with and without considering effect of parametric uncertainty on the thrust actuation

The effect on control of the CKF approach is also addressed in Figure V-71. Even if the control results convergent also for the standard EKF, the final performance is basically degraded by the estimator: the error signal converges to zero, but the effective control displacement is less accurate wrt the target reference. Moreover, the propagated covariance bound is not representative of the effective orbit error tube. The analysis confirms the importance of well posed orbit estimation for closed loop low thrust control. It acts not only on the accuracy, but also on the convergence properties as well as control parameter setting.

It is worthy to remind in the end of the AAM test case that the MEONS capability to handle tracking bias will be used in the planned development in order to include the GRAPHIC approach [123] for the integrated single frequency GNSS architecture. Actually, thrusting on the reconfigurable capability of the estimator will be possible to include pseudorange-phase combination as POD submode for next generation small platform.

CHAPTER VI

CONCLUSIONS

This dissertation investigates a novel Multipurpose Earth Orbit Navigation System architecture aiming at providing a generalized GNSS based spacecraft orbit estimation kernel for next generation platforms. Specifically, the thesis aims at describing the complete system design and development activity carried out in the frame of different TAS-I programs and internal studies. Copernicus Sentinel 1, SABRINA-BISSAT formation flying mission, as well as Galileo second Generation and TAS-I next generation small platform have been the operative framework where enhancing conventional on-board solution to a multipurpose navigation paradigm. Actually, the variety of spanned navigation needs introduces two fundamental design drivers:

- the challenging navigation issue to simultaneously deal with different orbit regime and wide range of GNSS receivers configurations introduced by the novel Space Service Volume scenario

- the development of an open architecture providing a reusable and configurable AOC functionality supporting conventional (i.e. Earth Observation on board POD) and novel platform capabilities (i.e. low thrust autonomous steering).

In more details, the study contribution can be summarized as follow:

- the derivation of the complete navigation system mathematical and functional model by performing requirement flow down and high level architecture design

- a numerical testing campaign of the orbit estimation solution aiming at providing a numerical proof of concept of the achieved compatibility in different operative scenarios.

Specifically, the MEONS system is conceived as a general sequential processing module that performs the real time on-board estimation of spacecraft position, velocity and time on the basis of GNSS available measurements and all auxiliary information provided by the hosting platform. This allows focusing the investigation on the three main functionalities:

- the spacecraft orbit propagation
- the GNSS measurement processing
- the optimal sequential filtering kernel

The first block, namely referred as Generic Propagator, is mainly impacted by the compatibility with novel G2G low thrust autonomous LEO-to-MEO Orbit Rising. This work, taking advantage from former TAS-I activities, has the merit of introducing the scenario of a manoeuvring spacecraft that autonomously target itself from the low injection orbit to the higher operative one by incorporating electric propulsion. A platform that crosses a wide range of orbital regimes and operative conditions (i.e. controlled or not) poses important challenges in terms of providing a compatible performance also during long term sensor outages and GNSS critical visibility conditions. Firstly, MEONS orbit perturbation model consider all relevant gravitational and non-gravitational perturbation contribution for low to high orbit propagation. Secondly, a direct feedforward of electric thrust and attitude control action is implemented in order to reduce the effect of a continuously manoeuvring spacecraft. Specifically the actuation integration issues as well as optimal control characteristics has been analysed from a navigation point of view in order to define orbit propagation interfaces with the hosting platform. Actually, is outlined that acquiring control action and external information does not correspond to the perfect knowledge of the effective firing,

which is naturally affected by propulsion system mechanization errors. Moving the dynamic model into the stochastic state space representation, the state augmentation with uncertain parameters is identified as the proper solution for mitigating unmodelled effects.

All the introduced instances are integrated within the MEONS open state space architecture. Such solution provides an extended variational state space representation and a dynamic model decomposition allowing to operate by selecting from a wide range of state and parameter arrangements, in accordance to the extended OD paradigm. It is worthy to remind that the aim is achieving a modular solution that can be configured with respect to the target application and augmented in case of specific mission needs. The switching model capability allows selecting all dynamic contribution from a model database by activating the correspondent module also run time. Currently, the MEONS real time orbit perturbation baseline setting is in line with LEO applications demanded accuracy. Actually, the reduced dynamic approach integration aim at preserving the standard on-board POD compatibility (i.e. Earth Observation applications as S1 and SABRINA mission). Some dynamic model design criteria have been proposed in and used to confirm compatibility of real time MEONS setting with high orbit scenario. Finally, the augmentable dynamic model architecture is addressed as a powerful tool for extending the same propagation module to multiple spacecraft and multiple realizations filtering solution. The first make the design compatible with formation flying problems, the second with sigma-point based filters.

The second block, i.e. namely referred as the Generic Observer, incorporates all navigation issues derived from the analysis of different configuration of the GNSS receivers experienced within the different mission scenarios. Actually, MEONS functionality has the primary aim to interface GNSS devices by sequentially processing different kind and different combination of measurements. Properly modelling GNSS measurements reconstruction pattern has relevant impact on the orbit estimation accuracy. The G2G mission is still the scenario that introduces the relevant elements of novelties. The first is the necessity to handle GNSS geometry and visibility conditions during low to high orbit transfer (side lobe exploitation, low level of carrier to noise ratio), Actually, working within the Space Service Volume high regions does not allow overriding EOR GNSS scenario criticalities by loosely coupled approach and direct GNSS raw measurement processing must be implemented (i.e. pseudorange and Doppler observable exploitation). This allows to mitigate the reduced number of usable GNSS satellites, high GDOP (Geometric Dilution of Precision) and acquisition after significant GNSS outage periods, especially experienced during the nearly-MEO mission phase. Secondly, it is introduced the necessity to interface novel receivers architectures. The G2G mission enhances the navigation performance by using Galileo (E1)/GPS(L1) combination and Multi-antenna configuration for the hosted GNSS assembly. This correspond to properly represent at simulation level GPS and Galileo raw data and consider in the navigation task all the procedure allowing interoperability of the two constellation sources. Considering also the reference dual frequency solutions, experienced during LEO Earth Observation satellite POD application (i.e. Sentinel-1 case), this study identifies the main design driver for the MEONS measurement processing module in Multi-frequency/Multi-constellation/Multi-antenna raw measurement compatibility. It is worthy to note that not only high orbit scenario benefit of raw data processing. Critical visibility condition and sensor outages still apply for the Autonomous Acquisition Manoeuvre application aiming to enable autonomous low thrust target orbit acquisition also for next generation small LEO platform. Availability of single antenna solutions can determine unfavourable pointing of the antenna, since spacecraft attitude is primarily driven by optimal thrust direction and solar array sun exposure maximization.

Also in the case of Generic Observer, all measurement processing instances converges into the implementation of a generalized function handling pseudorange, Doppler and carrier phase measurements relative to different frequencies, different constellation and different antennas. Switching model state space representation used for propagation is considered also for the Generic Observer: measurement reconstruction patterns are stored within an observation model database and can be selected in accordance to the current GNSS receiver configuration. The state vector augmentation paradigm has been extended to

the observation processing task in order to deal with unknown calibration parameters and systematic tracking error affecting the measurements. The reconfigurable architecture allows managing intermittent measurement and channel data in accordance to the current in view satellite tracking list. The CDGPS combinations complete the MEONS measurement processing capability for formation flying missions.

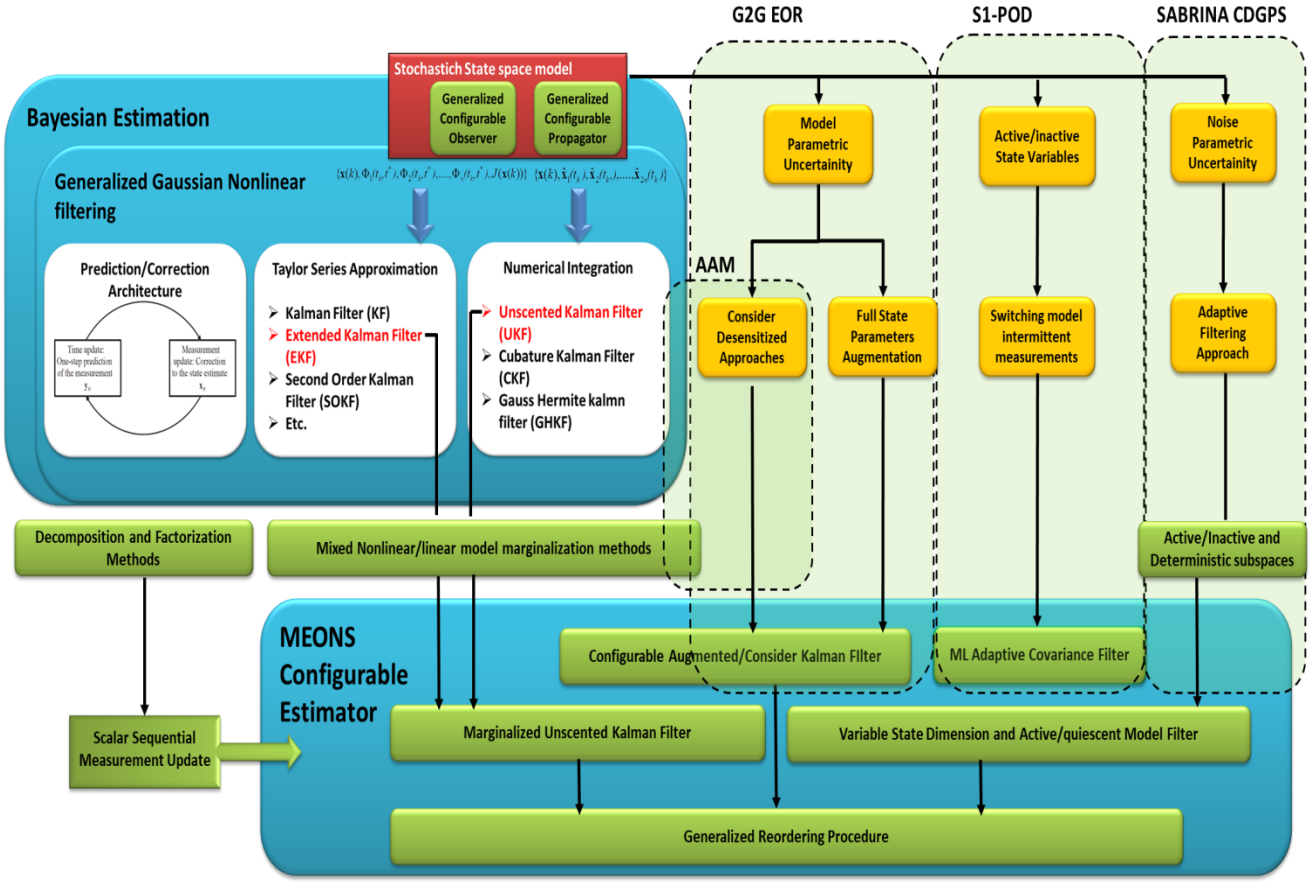

Figure VI-1 MEONS Configurable Sequential Estimation Design Process

Figure VI-1 provides a syntesis of the design process used to define the third block : the MEONS configurable estimator. The study starts from a wide spectrum overview of the state of art of advanced optimal filtering solution that can be used for navigation purposes. However, the modern estimation tecniques review is accomplished:

- with respect to the specific navigation needs of the envisaged applications
- in accordance to the idea to made available a Configurable Sequential Estimation solution that could be customized with respect to specific carachteristic of the navigation problem

Bayesian filtering has been introduced to derive the general stochastich state space framework and the prediction/correction scheme, which define the MEONS architecture and software cycle. After that, the two families of recursive General Gaussian Kalman Filtering approach i.e. the Taylor series based and the sigma-point based methods are selected in accordance to theis compatibility with the augmentable variational model available in the MEONS propagation and observation modules. Two relevant representant of the class i.e. EKF and UKF are selected, investigated and implemented within the estimation module in order to address nonlinearities issues.

The use of the proper filtering tool is integrated with the investigation at estimation level of the relevant characteristics of the encisaged physical and mathematical models.

G2G and other controlled application introduces the necessity of dealing with an optimal filtering approach in presence of several kinds of parametric uncertainty sources introduced by the control action

mechanization as well as by the GNSS measurement processing. This issue can be handled by both direct state augumentation and conservative Consider filtering apporaches. The study performs a complete analysis of peculiarities of the two approaches addressing the Consider filtering method as the minimal conservative solution. Applting it to the EOR case allows to properly control the error within a reliable covariance bound with low level of complexity. Those peculiarities are attractive also for the AAM scenario. The closed loop architectures, as one that proposed for small spacecraft optimal acquisition, has the same needs to properly weight the control feedforward with a proper level of uncertainity in order to improve stability and tracking capabilities of the filter.

The analysis of variable state dimension filtering is derived from the needs to manage intemittent carrier phase ambiguities estimation for the SABRINA CDGPS application. However, the approach is also extended to enhance GNSS raw measurement error representation. Using Consider ranging parameters is a possible method to robustify estimation with respect to unmodeled systematic contributions. The variable state dimension approach shrink the extended state in active and quiescient state vector partitions that, used in synergy with switching model peculiarity of MEONS state space model, allows run time reconfiguring estimation. The promotion or reset of a variable can be accomplished moving them within their proper active/inactive partitions and the reordering procedure can be implemented in order to rearrange the state estimation.

S1 Hardware in the loop data processing has offered the occasion to test a rapresentant belonging to the class of adaptive filtering. Actually, partial knowladge of noise covariances can jeopardize filter optimality. Several solutions are available in order to tune on-line the filtering process. Specifically, this study reports the results achieved integrating ML tecnique within the MEONS scheme. Beyond the successful tuning of the filter, the application outlines how important is the tuning in POD application in order to fullfill its stringent accuracy requirments.

The last estimation kernel design activity focuses on the possibility to optimize or merge some of the proposed methods within an integrated approach. A general framework has been found in the DMS paradigm that aim at adapting filtering to a set of sequentially more constraining state space representation. Specifically, conditionally linear/nonlinear substructure can be used to merge Taylor series and sigma point based approaches. Actually, the MUKF filtering solution, used for the AAM scenario, allows to merge UKF/EKF demonstrating an improvement in term of filtering initialization during critical statup conditions, with competive computational burden. The exploitation of active/inactive subspaces, also referred as switching model capability, coincide with the possibility to use reordering matrices for variable state dimension rearrangement. This work outline that the reordering procedure can be generalized as a powerful tool allowing to focus the Kalman Filtering method that uses model decomposition on target state partitions. Specifically, Consider and Augmented methods has been integrated within a configurable solution that uses reordering tool in order to promote consider variable in the augmented partition and process them in accordance to the new configuration. Such combination has been successfully tested on G2G scenario that verifies the possibility to run time enable thruster errors compensation as good operative condition occurs.

Numerical issues relying on the on real time has been also considered within the configurable estimation kernel developmnet. Scalar sequenial update methods and possible enhancment in term of covariance factorization methods has been considered. Those approaches allows also to extend MEONS software to multisesor applications since it can sequentially injest different observable provided by different sources. However, further activities are necessary for a full integration of the described numerical methods in view of the real time implementation.

It is worthy to note that all the selecteed methods has been tested first on simplified mathematical model and then on the target navigation scenario. The used approach allows to better understand the filtering method peculiarities and then recognize it within the final navigation results.

Navigation Scenario	Spacecraft Dynamic Model	GNSS Architecture	Filtering Tecnique	Performance	Verified capability
Sabrina Mission	Formation of two satellite in Bistatic SAR operative conditions	Carrier phase differential GNSS measurent considering dual frequency L1/L2 reciver	AGKF with state variable dimension for intermittent SD ambiguity estimation	Centimeter order accuracy of relative positioning for wide range baseline excursion	Compatibility with formation flying applications and Differential GNSS measurements
S1 HIL	Conventional platform for Earth Observation in nominal LEO operative conditions	Dual frequency L1/L2 by using improved ionofree combination	AKF for process covariance tuning	Submeter order absolute positioning in case of low level of systematic errors and optimal tuning	Compatibility with enhanced on-board POD for future fast SAR product delivery is EO SAR missions
Galileo Second Generation	Long duration optimal tranfer for low thrust LEO-to-MEO autonomous orbit risig	Multi-antenna configuration considering high sensitivity Galileo/GPS receiver	Consider Kalman Filtering for estimation in presence of parametric uncertainity	From meter order accuracy in low transfer phase to 100-150m in high orbit (improved in case of thrust calibration)	Compatibility with a low thrust autonomous orbit rising and high orbit SSV scenarios
Autonomous Orbit Acquisition	Fast manouvring LEO Spacecraft for optimal low thrust target obit acquisitionin from injection	Single antenna Single frequency reduced navigation solution and integration with AOC control task	Consider MUKF Filtering for controlled application and improved initialization	From meter order accuracy in good visibility conditions to 20m in case of unfavourable antenna pointing	Compatibility with a low thrust autonomous orbit rising and high orbit SSV scenarios

Table VI-1 Multipurpose Earth Orbit Navigation System applications summary

The four experienced scenarios provide a complete numerical test campain of the MEONS system, performed by customizing all modules on the mission carachteristics. As shown in Table VI-1, the arrangments span different combination of the obit propagation system, different GNSS receiver combinations as well as different filtering methods. The achieved level of positioning accuracy is compatible with the expected performance for the considered navigation applications.

Based on the innovative nature of the envisaged phase A/B studies, flight data are not available for almost all the investigated scenarios. As a consequence, no in-flight proof of concept of the proposed multipurpose solution has been shown in this thesis. Nonetheless, it is a fact that MEONS is a not yet available tool in the GNSS-based on board orbit estimation panorama. Indeed, MEONS covers a set of theoretical and operational solutions matching the modern navigation instance of enhanced flexibility with respect to multiple SSV applications. This thesis contributed to that topic presenting end-to-end theoretical derivation mathematical and functional model for the navigation system. Selected approaches and algorithms can be thus reasonably expected to support MEONS transitions from investigation to operation. This includes the exploitation of the proposed AOC functionality in next generation Earth orbiting platform based on a unified framework for high performance navigation capability.

REFERENCES

[1] J.R.Vetter, “Fifty Years of Orbit Determination, Development of Modern Astrodynamics Methods”, John Hopkins APL Technical Digest, Volume 27, Number 3, (2007)

[2] A. Águeda Maté, F. Martínez Fadrique, “Sequential Orbit Determination in Diverse Scenario”, 4th International Conference on Astrodynamics Tools and Techniques Madrid, Spain, April 2015

[3] Galileo 2nd Generation Satellite Study – REF: Phase A/B1 AO/2- 1607/13/NL/CVG, 2015

[4] A. Intelisano, L. Mazzini, S. Landenna, A. Zin, L. Scaciga, L. Marradi , “Recent Flight Experiences of TAS-I On-board Navigation Equipment”, 4th ESA Workshop on Satellite Navigation User Equipment Technologies, NAVITEC, 2008

[5] M. Farahman, A. Long, R. Carpenter, “Magnetospheric MultiScale Mission (MMS) Navigation Performance Using the Goddard Enhanced Onboard Navigation System”, 25th International Symposium on Space Flight Dynamics, October 2015

[6] F. Menzione, A. Renga, M. Grassi, “On-board orbit determination for low thrust LEO-MEO transfer by Consider Kalman Filtering and multi-constellation GNSS”, Acta Astronautica, Volume 138, September 2017, pp. 242-254

[7] F. Menzione, D. Sarrocco , A. Ferraro, “GNSS Based Consider Marginalized Filtering and Optimal Low Thrust Control for Small Satellite Autonomous Orbit Acquisition”, 24th Conference of the Italian Association of Aeronautics and Astronautics, October 2017

[8] M.C. Moreau, P. Axelrad, J.L. Garrison, A. Long, “GPS Receiver Architecture and Expected Performance for Autonomous Navigation in High Earth Orbits”, Navigation, Vol. 47, No. 3, 2000, pp. 191-204

[9] O. Balbach et al., “Tracking GPS Above GPS Satellite Altitude: First Results of the GPS Experiment on the HEO Mission Equator-S”, IEEE PLANS,1998, pp. 243-249

[10] J.F. Lorga and P.F. Silva, “Autonomous Orbit Determination for future GEO and HEO missions”, 5th ESA Workshop, NAVITEC, 2010

[11] B.W. Parkinson and J.J. Spilker, “Global Positioning System: Theory and Applications”, Volume I, AIAA Publications, Washington, 1997

[12] J. Roselló, P. Silvestrin, R. Weigand, G. López Risueño, G. García, “Multi-GNSS Space Receivers based on AGGA-4”, NAVITEC, 2014

[13] A. Noroozi, C.J.M. Verhoeven, G.L.E. Monna and E.K.A. Gill, “A Reconfigurable Multi-band GNSS Receiver Front-end for Space Applications: System Level Considerations”, ProRISC/ IEEE Workshop on Semiconductors, Circuits, Systems and Signal Processing, Veldhoven The Netherlands, 2008.

[14] E.D. Kaplan, C.J. Hegarty, “Understanding GPS – Principles and Applications”, 2nd Edition, Artech House, Boston/London, 2006.

[15] S. Zago, M. Visconti, A. Zin, F. Belgiovane, E. Mangolini, L. Scaciga, L. Marradi, “The LAGRANGE-2G GNSS Spaceborne Receiver Design”, NAVITEC, 2014

[16] IS-GPS-200H, GPS Interface Control Document, September 2013

[17] D. Borio, “Squaring and Cross-Correlation Codeless Tracking: Analysis and Generalisation”, IET Radar, Sonar & Navigation, Vol. 5, December 2011

[18] European GNSS (Galileo) open service signal-in-space interface control document, December 2016

[19] IS-GPS-705-D, GPS L5 Interface Control Document, September 2013

[20] A. Zin et al., “Preparing An Autonomous, Low-Cost GNSS Positioning And Timing Function On-Board A GEO Telecom Mission: a study case”, CEAS Journal, 2015

[21] J. Roselló, P. Silvestrin,G. Lopez Risueño, R. Weigand, J.V. Perelló, “AGGA-4: core device for GNSS space receivers” of this decade, NAVITEC, 2010

[22] N.Nadarajah, Peter J. G. Teunissen, G. Giorgi, “GNSS Attitude Determination for Remote Sensing: On the Bounding of the Multivariate Ambiguity Objective Function”, Earth on the Edge: Science for a Sustainable Planet, Volume 139, 2014, pp. 503-509

[23] ESA Express Procurement (EXPRO+) / Open-Competitive - Invitation to tender for Techniques for GNSS navigation at High Orbits (GEO/GTO/HEO), REF: AO/1-8349/15/NL/LF

[24] S.C. Martos et al., “Snapshot Software Receiver for GNSS in Weak Signal Environments: An Innovative Approach for Galileo E5”, Proceedings of the 23rd International Technical Meeting of the Satellite Division of the Institute of Navigation, ION GNSS 2010, Portland, Oregon, September 2010

[25] W.L. Edwards, B.J. Clark, D.M. Bevly, “Implementation Details of a Deeply Integrated GPS/INS Software Receiver”, IEEE/ION Position Location and Navigation Symposium, Indian Wells, CA, May 2010, pp. 1137-1146

[26] Report Signal Processing Techniques and Demonstrator for Indoor GNSS Positioning ESA/ESTEC Contract No. RES-PTE/GLC/ek/912.2007 DINGPOS-SRIFEN issue 1, 2010

[27] S. Fantinato , G. López-Risueño , R. De Gaudenzi , J.L. Gerner , “Turbo and LDPC Channel Coding for GNSS Data Broadcasting”, 4th. GNSS Signals Workshop, DLR, December 2009

[28] Prospect For The Small Satellite Market, http://euroconsult-ec.com/research/smallsats ,2017

[29] C. Reigber, Y. Xia,, H. Kaufmann, F. Massmann H., L.Timmen, Impact of Precise Orbits on SAR Interferometry”, ERS SAR interferometry, Proceedings of the Fringe 96 Workshop,1996

[30] M. P. Clarizia , C. S. Ruf , P. Jales , “Spaceborne GNSS-R Minimum Variance Wind Speed Estimator”, IEEE Transactions on Geoscience and Remote Sensing ,Volume: 52, Issue 11, November 2014

[31] M. Zentgraf, O. Montenbruck, C. Müller, B. Rueda, “Preparing the GPS Experiment for the Small Geo Mission”, 33rd Annual AAS Guidance and Control Conference, February 2011.

[32] V. Capuano, C. Botteron, Y. Wang, J. Tian, J. Leclère, P.A. Farine, “GNSS/INS/Star Tracker Integrated Navigation System for Earth-Moon Transfer Orbit”, Presented at ION GNSS, 2014

[33] GNSS Based Autonomous Orbit Determination in LEOP and other Non-Operative Phases, ESA REF- Invitation to Tender AO/1-7659/13/NL/EM

[34] A. Villien C. Caven J. Morand J. Borde, “Formation flying guidance navigation and control for science mission”, Proceedings of the 17th World Congress of The International Federation of Automatic Control, Seoul, Korea, July 2008

[35] S. Cesare, G. Sechi, “Satellite Formation for a next generation Gravimetry mission”, 7th Symposium on Small Satellite for Earth Observation, May 2009

[36] M. D’Errico, “Distributed Space Missions for Earth System Monitoring,” Springer Science & Business Media, 2012.

[37] F.D. Busse, “Precise Formation-State Estimation in Low Earth Orbit Using Carrier Differential GPS”, PhD-thesis, Department of aeronautics and astronautics of Stanford, University, March 2003.

[38] R. Kroes, W. Bertiger, P. Visser, “Precise GRACE baseline determination using GPS Solutions”, Volume 9, April, 2005

[39] D.B. Cox, J.D.W. Brading, “Integration of LAMBDA Ambiguity Resolution with Kalman Filter for Relative Navigation of Spacecraft”, Proceedings of The Institute of Navigation’s National Technical Meeting, August 2000

[40] U. Tancredi, A. Renga, M. Grassi, “GPS-based Relative Navigation of LEO formations with Varying Baselines”, Proceedings of the AIAA Guidance Navigation and Control Conference, 2010

[41] A. Renga, A. Moccia, M. D’Errico, S. Dellepiane, E. Angiati, G. Vernazza, P. Lombardo, F. Colone, D. Cristallini, S. Pignataro, Q. Rioli, G. Milillo, C. Bruno, F. Di Giorgio, M. Labriola, “From the expected Scientific Applications to the Functional Specifications, Products and Performance of the SABRINA missions”, Proceedings of the 2008 IEEE Radar Conference, May 2008.

[42] T. Schön, F. Gustafsson, and A. Hansson, “A Note on State Estimation as a Convex Optimization Problem”, proceedings of the IEEE International Conference on Acoustics, Speech, and Signal Processing, Volume 6, Hong Kong, 2003, pp. 61-64

[43] B. Ristic, S. Arulampalam, N. Gordon, “Beyond the Kalman Filter: Particle Filters for Tracking Applications”, Artech House, 2003

[44] S. Särkkä, “Bayesian Filtering and Smoothing”, Cambridge University Press, September 2013

[45] Z. Chen, “Bayesian Filtering: From Kalman Filters to Particle Filters, and Beyond”, Journal of Statistics, Volume 182, Issue 1, 2009, pp.1-69

[46] T.B. Schön, “Estimation of Nonlinear Dynamic Systems Theory and Applications Department”, Linköping Studies in Science and Technology Dissertations No.998, 2005

[47] P. Maybeck, “Stochastic models, estimation and control”, Vol. 1-2-3, New York Academic Press, 1982

[48] A. Gelb, J.F. Kasper, R.A. Nash, C.F. Price, A.A. Sutherland, “Applied Optimal Estimation”, The M.I.T. Press, Massachusetts Institute of Technology, 1974

[49] Y. Yanga, J. Xuc, “ GNSS receiver autonomous integrity monitoring (RAIM) algorithm based on robust estimation ”, Geodesy and Geodynamics, Volume 7, Issue 2, March 2016, pp.117-123

[50] A.C. Long, J.O. Cappellari, C.E. Velez, and A.J. Fuchs, “Goddard Trajectory Determination System (GTDS) Mathematical Theory”, National Aeronautics and Space Administration, Goddard Space Flight Center, 1989.

[51] H. Schaub, J.L. Junkins, “Analytical Mechanics of Space Systems”, Second Edition, AIAA education series, 2011

[52] B. Friedland, “Control system design: an introduction to state-space methods”, McGraw-Hill, 1986

[53] S.Wu, T.P. Yunk , C.L.Thorton , “Reduced-dynamic techniques for precise orbit determination of low earth satellites”, Journal of Guidance,Control and Dynamic, Volume 14, 1991, pp.24-30

[54] O. Montenbruck, P. Ramos-Bosch , “Precision real-time navigation of LEO satellites using global positioning system measurements”, GPS Solution, 2008

[55] D. M. Goebel, I. Katz, “Fundamentals of Electric Propulsion: Ion and Hall Thrusters”, JPL Space Science and Technology, 2012

[56] Y. E. Bar-Sever, “A new model for GPS yaw attitude”, Journal of Geodesy, Volume 70, Issue 11, November 1996, pp. 714–723

[57] B.A. Conway , “Spacecraft Trajectory Optimization”, Cambridge University Press, 2010

[58] L. Mazzini, “Finite thrust orbital transfers”, Acta Astronautica, Volume 100, 2014, pp.107-128

[59] D. Dumitriu. P. U. Lima. B. Udrea., “Optimal Trajectory Planning Of Formation Flying Spacecraft”, IFAC Proceedings Volumes, Volume 38, Issue 1, pp. 313-318, 2005

[60] L. Mazzini, F. Perrella, M. Cerreto, “Low Thrust transfers applications for Earth Orbiting Satellites and Constellations”, 6th International Conference on Astrodynamics Tools and Techniques (ICATT) 14-17 March 2016

[61] A.E. Bryson, and Y.C. Ho, “Applied optimal control”, Hemisphere Publishing Corporation, New York, 1975.

[62] F.Menzione, R.Ferraro, A.Renga, M.Grassi, “Multipurpose Earth Orbit Navigation System for autonomous orbit determination during satellite low thrust LEO-MEO transfer”, Metrology for Aerospace (MetroAeroSpace), 2016, pp. 319-324

[63] S. De Florio, S. D'Amico, “Optimal Autonomous Orbit Control of Remote Sensing Spacecraft”, 19th AAS/AIAA Space Flight Mechanics Meeting Savannah, USA, 2009.

[64] R. Ferraro , Master Degree Thesis, “Generalized GNSS Based On-Board Precise Orbit Determination for low Thrust Orbit Rising”, 2016

[65] R. Kroes ,O. Montenbruck, “Precise Relative Positioning of Formation Flying Spacecraft using GPS”, PhD-thesis, Delft, the Netherlands, March 2006

[66] O. Montenbruck. E. Gill, “Satellite Orbits Models, Methods and Applications”, 1st Edition Springer, 2000

[67] S. Casotto, M. Bardella and A. Zin, “Preliminary assessment of the orbit restitution Capability of a multiple-antenna GNSS receiver on a Highly elliptic orbit reaching above GNSS altitude”, Advances in the Astronautical Sciences, Volume 143, 2012

[68] W. Marquis, “The GPS Block IIR/IIR-M Antenna Panel Pattern rev”3, LMCO 2013, publically releasable data, September 2013,

[69] Representative Galileo EIRP patterns for space receivers – ESA Memo Ref. TEC-ETN/2012.155, v6 27/02/2013

[70] A. C. Vigneron, A.H.J. de Ruiter, B.V. Burlton, W.K.H. Soh, “Nonlinear Filtering for Autonomous Navigation of Spacecraft in Highly Elliptical Orbit”, Acta Astronautica January 2016

[71] O. Montenbruck, P. Steigenberger , A.́Hauschild, “Broadcast versus precise ephemerides: a multi-GNSS perspective”, GPS Solutions , Volume 19, Issue 2, April 2015, pp 321–333

[72] J.A. Klobuchar, “Ionosphere Effects on GPS”, Global Positioning System: Theory and Applications, Volume I, B.W. Parkinson and J. J. Spilker, AIAA Publications, Washington, 1997, pp. 485–515

[73] W.M. Lear , “GPS navigation for low-earth orbiting vehicles”, NASA 87-FM-2, JSC-32031, rev. 1, Lyndon B. Johnson Space Cent., Houston ,1987

[74] O. Julien, G. Lachapelle, M. Cannon, “Galileo L1 Civil Receiver Tracking Loops' Architecture”, IEEE International Symposium on Circuits and Systems, 2007.

[75] A. Afifi, A. El-Rabbany, “Performance Analysis of Several GPS/Galileo Precise Point Positioning Models”, Sensors, 2015

[76] J. Kong, X. Mao and S. Li, “BDS/GPS Dual Systems Positioning Based on the Modified SR-UKF Algorithm”, Sensors, 2016

[77] F. Menzione, A. Renga, M. Grassi, G. Campolo, “Dynamic Model Design For An On Board Multi-Purpose Precise Orbit Determination Scheme”, 23th Conference of the Italian Association of Aeronautics and Astronautics, Politecnico di Torino, November 2015

[78] D.A. Vallado, “An Analysis of State Vector Propagation Using Differing Flight Dynamics Programs”, AAS/AIAA Space Flight Mechanics conference at Copper Mountain, January 2005.

[79] L. Rujun, M.A. Henson, and Michael J. Kurtz, “Selection of Model Parameters for Off-Line Parameter Estimation”, IEEE Transaction On Control System Technology, Volume 12, May 2004

[80] M. Morgado, P. Oliveira, C. Silvestre, “Posterior Cram´er-Rao bounds analysis for INS/USBL navigation system”, Preprints of the 8th IFAC International Conference on Manoeuvring and Control of Marine Craft, September 2009

[81] M. Simandl, J. Krlovec, P. Tichavsk, “Filtering, predictive, and smoothing Cram´er Rao bounds for discrete-time nonlinear dynamic systems”, Automatica, Volume 37, Issue 11, November 2001, pp. 1703-1716

[82] G. Hendeby , F. Gustafsson, “Fundamental filtering limitations in linear non-Gaussian systems”, Proceedings of 16th Triennial IFAC World Congress, Prague, Czech Republic, July 2005.

[83] P.C. Pardal, H.K. Kuga, R.V. De Moraes, “Robustness Assessment Between Sigma Point and Extended Kalman Filter for Orbit Determination”, Journal of Aerospace Technology and Management, Volume5, São José dos Campos, October 2013

[84] P. Closas, C. Fernandez-Prades, “The marginalized square-root quadrature Kalman filter”, Signal Processing Advances in Wireless Communications, June 2010

[85] L. Chang, B. Hu, A. Li, F. Qin, “Strapdown inertial navigation system alignment based on Marginalised Unscented Kalman Filter”, IET Science, Measurement & Technology , Volume 7, Issue 2, March 2013

[86] Y. Bar-Shalom, X. Rong Li, T. Kirubarajan, “Estimation with Applications to Tracking and Navigation”, John Wiley & Sons, April 2004

[87] D. Simon, “Optimal State Estimation: Kalman, H Infinity, and Nonlinear Approaches”, John Wiley & Sons, 2006

[88] L.W. Nelson, E. Stear, “The simultaneous on-line estimation of parameters and states in linear systems”, IEEE Transactions on Automatic Control, Volume 12, 1967, pp. 438-442

[89] T. Lou, H. Fu, Z. Yongbo, “Consider unobservable uncertain parameters using radio beacon navigation during Mars entry”, Article in Advances in Space Research, February 2015

[90] D. P. Woodbury and J. Junkins, “On the consider Kalman filter, AIAA Guidance Navigation and Control Conference”, August 2010

[91] T. Lou, H. Fu; Z. Wang; and Y. Zhang, “Schmidt-Kalman Filter for Navigation Biases Mitigation during Mars Entry”, Journal of Aerospace Engineering, Volume 28 Issue 4, July 2015

[92] S. Schmidt, “Applications of State-space Methods to Navigation Problems”, Advances in Control Systems, Academic Press, 1966, pp. 293–340

[93] R.Y. Novoselov , S.M. Herman , S.M. Gadaleta , A.B. Poore, “Mitigating the effects of residual biases with Schmidt-Kalman filtering”, 8th International Conference on Information Fusion, July 2005

[94] G. Holt, R. Zanetti, C. D’Souza, “Tuning and Robustness Analysis for the Orion Absolute Navigation System”, Guidance, Navigation, and Control Conference, Boston, Massachusetts, August 2013

[95] Y. Yang, X. Yue, A. G. Dempster, “GPS On board real time orbit determination for LEO Satellite using Consider Kalman Filter”, IEEE Transactions on Aerospace and Electronic Systems, August 2015

[96] C. D. Karlgaard, H. J. Shen, “Desensitized Kalman filtering”, IET Radar, Sonar & Navigation, Volume 7, 2013, pp. 2-9.

[97] T. Lou, “Desensitized Kalman Filtering with Analytical Gain”, Information Theory, arXiv:1504.04916, 2015

[98] R. Zanetti, R.H. Bishop, “Kalman Filters with Uncompensated Biases”, Journal of Guidance, Control, and Dynamics, Volume 35, 2012, pp. 327-335

[99] G. J. Bierman, “Factorization Methods for Discrete Sequential Estimation”, Academic Press, New York, 1977

[100] H. Ho, H. Chun, S. Kwon, M. H. Lee, “Observability Measures and Their Application to GPS/INS”, IEEE Transaction On Vehicular Technology, Volume 57, January 2008

[101] A. H. Mohamed, K. P. Schwarz, “Adaptive Kalman filtering for INS/GPS”, Journal of Geodesy Springer-Verlag. No. 73, 1999, pp.193-203

[102] Q. M. Lam, J. L. Crassidis, “Evaluation of a multiple model adaptive estimation scheme for space vehicle’s enhanced navigation solution”, Proc. Guidance, Navigation and Control Conference, AIAA Press, August 2007

[103] D. Jwo, F. Chung, “Adaptive Kalman Filter for Navigation Sensor Fusion”, Sensor Fusion and its applications, Intech publication,2010

[104] G. Catastini. F. Menzione, “Performance Analysis of real time precise orbit determination by using adaptive Kalman filtering on HIL generated GPS receiver data”, Advances in the Astronautical Sciences Second IAA DyCoss'2014, Volume 153, 2015

[105] G. Strang, K. Borre, “Linear Algebra, Geodesy, and GPS” , SIAM, 1997

[106] T Schon, F Gustafsson, PJ Nordlund, “Marginalized particle filters for mixed linear/nonlinear state-space models”, IEEE Transactions on Signal Processing, 2005, pp. 2279-2289

[107] J. Nilsson, “Marginalized Bayesian filtering with Gaussian priors and posteriors”, Statistics Theory arXiv:1603.06462, 2016

[108] J. McCabe, K. DeMars, “Gaussian Mixture Consider Kalman Filter”, 26th AAS/AIAA Space Flight Mechanics Meeting, 2016

[109] J. Stauch, M. Jah , “Unscented Schmidt-Kalman Filter Algorithm”, Journal of Guidance Control and Dynamics, Volume 38, 2015, pp.117-123

[110] Z.Duan , X.R. Li , Chongzhao Han , Hongyan Zhu, “Sequential unscented Kalman filter for radar target tracking with range rate measurements”, 8th International Conference on Information Fusion, 2005

[111] R. Zanetti, R. H. Bishop, “Recursive Implementations of the Schmidt-Kalman Consider Filter, The Journal of the Astronautical Sciences, Volume 60, Issue 3, December 2013, pp 672–685

[112] H. Ghanbarpour, S. H. Pourtakdoust, “UD Covariance Factorization for Unscented Kalman Filter using Sequential Measurements Update”, International Journal of Mechanical, Aerospace, Industrial, Mechatronic and Manufacturing Engineering Volume1, 2007

[113] C.F. Von Loan, “Computing Integrals involving Matrix Exponential”, IEEE Transactions on Automatic Control, Volume AC-23, 1978, pp. 395-404

[114] M.Anania, D.Pascucci, “An approach for Simulation Models Standardization based on object-oriented programming: Sentinel 1 Test Environments”, The 8th International ESA Conference on GNC, 2011

[115] U. Tancredi , A. Renga , M. Grassi, “Ionospheric path delay models for spaceborne GPS receivers flying in formation with large baselines”, Advances in Space research, Volume 48, August 2011, pp. 507-520

[116] P.J.G Teunissen, “Least-squares estimation of the integer GPS ambiguities”, Section IV ,Theory and Methodology, International Association of Geodesy General Meeting, August 1993

[117] F.D. Busse, J.P. How, “Demonstration of Adaptive Extended Kalman Filter for Low Earth Orbit Formation Estimation Using CDGPS”, Navigation, Volume 50, Issue 2 Summer 2003 , Pages 79–93

[118] D. Sarrocco, Acquisition Strategies for single and multiple spacecraft, Thesis for Space Science and Technology Master, 2017

[119] The HT 100 Hall Effect Thruster, SITAEL website, http://www.sitael.com/wp-content/uploads/2015/10/HT-100.pdf

[120] A. Garulli, A. Giannitrapani, M. Leomanni, F. Scortecci, “Autonomous Low-Earth-Orbit Station-Keeping with Electric Propulsion”, Journal of Guidance, Control, and Dynamics, Volume 34, 2011, pp. 1683-1693

[121] G.Inalhan, M.J. Tillerson , J.P. How, “Relative dynamics and control of spacecraft formations in eccentric orbits”, Journal of Guidance, Control, and Dynamics, Volume 25, 2002 , pp. 48-59

[122] A. Angrisano, S. Gaglione, C. Gioia, M. Massaro, and U. Robustelli, “Assessment of NeQuick Ionospheric Model for Galileo single-frequency users”, Acta Geophysica, Volume 61, Issue 6, December 2013, pp. 1457–1476

[123] F. Wang, X. Gong, J. Sang, X. Zhang, “A Novel Method for Precise Onboard Real-Time Orbit Determination with a Standalone GPS Receiver”, Sensors, December 2015

APPENDIX A. MEONS ORBIT PERTURBATION MODULES

A. Orbit Perturbation models

Gravity

The total acceleration due to Earth's gravity is given by A.1:

$$\mathbf{A}_{grav} = \nabla\psi = \nabla\frac{\mu}{r} + \nabla\psi_p = -\frac{\mu}{r^3}\mathbf{r} + \mathbf{a}_{grav} \qquad \text{A.1.}$$

where ψ is the gravitational potential. This is simply the acceleration due to the spherically symmetric mass of the Earth plus the non-spherical perturbation $\mathbf{a}_{grav}$. The Earth's gravitational field is modeled using the standard spherical harmonic representation of the gravitational potential (which is a solution to the Laplacian $\nabla^2\psi = 0$). In this representation, the complete gravitational potential is written as the following function of the coordinates *r*, φ and λ where *r* is the distance from center of the earth and φ and λ are the geocentric latitude and longitude respectively:

$$\begin{aligned}&\psi(r,\phi,\lambda) = \\ &= \frac{\mu}{r} + \frac{\mu}{r}\sum_{n=1}^{\infty} C_n^0\left(\frac{R}{r}\right)^n P_n^0(\sin\phi) + \\ &+ \frac{\mu}{r}\sum_{n=1}^{\infty}\sum_{m=1}^{n}\left(\frac{R}{r}\right)^n P_n^m(\sin\phi)\left\{S_n^m \sin(m\lambda) + C_n^m \cos(m\lambda)\right\}\end{aligned} \qquad \text{A.2.}$$

with μ, gravitational parameter of the Earth; R, radius of the Earth; P_n^m, associated Legendre functions; S_n^m, C_n^m, harmonic coefficients: zonal harmonics (for m = 0), sectorial harmonics (for m=n), tesseral harmonics (for n > m ≠ 0). Note that $J_n = -C_n^0$. The term n = 1 is usually not present when the origin of the coordinate system is placed at the center of mass of the Earth. The total acceleration is the gradient of the gravitational potential, so making derivatives of eq.(A.2) with respect the coordinates *r*, φ and λ, we obtain the three components of the total acceleration due to Earth's gravity:

$$\begin{aligned}&\psi(r,\phi,\lambda) = \\ &= \frac{\mu}{r} + \frac{\mu}{r}\sum_{n=1}^{\infty} C_n^0\left(\frac{R}{r}\right)^n P_n^0(\sin\phi) + \\ &+ \frac{\mu}{r}\sum_{n=1}^{\infty}\sum_{m=1}^{n}\left(\frac{R}{r}\right)^n P_n^m(\sin\phi)\left\{S_n^m \sin(m\lambda) + C_n^m \cos(m\lambda)\right\}\end{aligned} \qquad \text{A.3.}$$

$$\begin{aligned}&A_{grav_r} = \frac{\partial\psi}{\partial r} = -\frac{\mu}{r^2} + \\ &-\frac{\mu}{r^2}\sum_{n=2}^{\infty}\left(\frac{R}{r}\right)^n (n+1)\sum_{m=0}^{\infty} P_n^m(\sin\phi)\left\{S_n^m \sin(m\lambda) + C_n^m \cos(m\lambda)\right\}\end{aligned} \qquad \text{A.4.}$$

$$\begin{aligned}&A_{grav_\lambda} = \frac{\partial\psi}{\partial\lambda} = 0 + \\ &\frac{\mu}{r}\sum_{n=2}^{\infty}\left(\frac{R}{r}\right)^n \sum_{m=0}^{\infty} m P_n^m(\sin\phi)\left\{S_n^m \sin(m\lambda) + C_n^m \cos(m\lambda)\right\}\end{aligned} \qquad \text{A.5.}$$

From these equations it can be seen that the total gravitational acceleration is given by the spherical symmetric acceleration term $-\mu/r^2$ (appears only in the radial component) plus the non-symmetrical terms which are given as series expansions for each of the three spherical coordinates. Note that the gravity components given above are in an Earth Centred Earth Fixed spherical coordinate system and must therefore be transformed into a Cartesian ECI coordinate system before being used within the orbit propagator. The above spherical harmonic representation of the Geopotential model can use one of several different sets of coefficients, *S* and *C*. These sets of coefficients are matched to a given value of *m* and *R*. The Geopotential model is limited to order *n=30* and degree $m \leq n$ for MEONS wide range orbit applications as discussed in III.3.

Aerodynamic drag

Rigorous treatment of the aerodynamics of free molecular flow involves the representation of the complex interaction of the atmospheric molecules with the surface molecules of the spacecraft. Differently from complete DSS model, for on-board real-time software, the following assumptions apply:

- Cannon Ball model, which means that the satellite is assumed to be a sphere;
- Only reflection is considered

The expression for the aerodynamic drag implemented is:

$$\mathbf{a}_{drag} = -\frac{1}{2} C_d \, \rho(r,\phi,t) |\mathbf{v}_r(x,y,z,t)| \mathbf{v}_r(x,y,z,t) \frac{A}{m} \qquad \text{A.6.}$$

where C_d is the drag coefficient which is expected to have a value in the range of about 2 to 3 with 2 being a typical reference value (for a spherical SC). The atmospheric density model is denoted with $\rho(r,\phi,t)$ and it is a function of ECI radius, ECI latitude and time. The satellite area and mass are represented by *A* and *m* respectively. The velocity is that of the satellite relative to the Earth's atmosphere and is calculated in the ECI frame under the assumption that the atmosphere rotates with the Earth. Thus the relative velocity $\mathbf{v}_r(x,y,z,t)$ is given by the equation:

$$\mathbf{v}_r(x,y,z,t) = \mathbf{v} - \boldsymbol{\omega} \times \mathbf{r} \qquad \text{A.7.}$$

where $\boldsymbol{\omega}$ is the angular velocity vector of the earth in the ECI reference frame. Although the exact natures of the phenomena are not well understood, there is experimental evidence that diurnal and seasonal variations, as well as effects due to changes in solar flux and geomagnetic activity, can be modeled with some degree of success. In our MEONS Generic Propagator for POD the atmospheric density, ρ, is calculated using an analytic approximation to the Harris- Priester atmospheric model. The modification attempts to account for the diurnal bulge (which is located approximately 30 degrees east of the subsolar point) and a minimum density profile at the antapex of the diurnal bulge. The density values at a fixed height *h* above the reference ellipsoid for either the minimum atmospheric density, ρ_{min},or the maximum atmospheric density, ρ_{max}, can be represented by the following analytic formula:

$$\rho_m(f,h) = A_m(f-65)^{\alpha_m} + B_m[2 - e^{-\beta_m(f-65)}] \qquad \text{A.8.}$$

where:

- ρ_m is the maximum or minimum density;
- $A_m, B_m, \alpha_m, \beta_m$ are height-dependent best-fit parameters, reported in density tables,
- f is the 10.7 cm solar flux.

The density, including the diurnal variation effect, is computed:

$$\rho = \rho_{\min}(f,h) + [\rho_{\max}(f,h) - \rho_{\min}(f,h)]\cos^n\left(\frac{\gamma}{2}\right) \quad \text{A.9.}$$

where

- γ is the angle between the satellite position vector and the apex of the diurnal bulge;
- **r,** is the satellite position vector;
- $\mathbf{U}_B$, is the unit vector directed toward the apex of the diurnal bulge.

Solar radiation pressure acceleration

Solar radiation pressure is a perturbation which becomes important at higher altitudes. Solar radiation pressure involves many problems including:

- analysis of the solar radiation to accurate model and predict the solar cycles and variations;
- evaluation of the satellite cross-sectional area;
- shadowing of the Earth and the spacecraft itself;
- studying of the specular and diffuse reflection.

Differently from DSS, MEONS baseline considers only specular reflection because diffuse reflection requires to have complex three-dimensional model of the satellite. The important aspect that we consider is the shadow of the Earth calculated taking into account the relative position between Sun, Earth and the satellite. The solar radiation pressure acceleration in MEONS Generic Propagator is the following:

$$\mathbf{a}_{SRP} = -\nu \frac{p_{SR} C_R A}{m} \frac{\mathbf{r}_{sun-sat}}{|\mathbf{r}_{sun-sat}|} \left(\frac{\mathbf{r}_{sun}^2}{|\mathbf{r}_{sun-sat}|^2} \right) \quad \text{A.10.}$$

where

- ν is the eclipse factor. It is between 0 (satellite in shadow) and 1 (satellite in sunlight);
- p_{SR} is the solar pressure, obtained dividing the solar flux [W/m^2] by the speed of light;
- C_R is the reflectivity which indicates how the satellite reflects incoming radiation. Typical values are between 0.0 and 2.0. A value of 0.0 means the object is translucent to incoming radiation and no force is transmitted. A value of 1.0 means that all radiation is absorbed and all the force is transmitted. A value of 2.0 indicates that all the radiation is reflected and twice the force is transmitted to the satellite.
- $\mathbf{r}_{sun-sat}$ is the vector from the satellite to the Sun. This means that the Solar Radiation Pressure acceleration is in the opposite direction
- $\mathbf{r}_{sun}$ is the ECI Sun position vector.

Sun-Moon third body acceleration

The gravitational attraction of Sun and Moon can be found simply applying a third body problem for both and finally summing the two contributions to obtain the total acceleration on the satellite. Let us indicate with:

- **r**, the satellite ECI position;
- $\mathbf{r}_{sat-sun}$, the vector from the satellite to the Sun;
- $\mathbf{r}_{sat-moon}$, the vector from the satellite to the Moon;
- $\mathbf{r}_{sun}$, the ECI position of the Sun;
- $\mathbf{r}_{moon}$, the ECI position of the Moon.

The satellite acceleration due to the Sun and Moon gravity are:

$$\mathbf{a}_{Sun} = -\frac{G(m_{Earth}+m_{sat})\mathbf{r}}{r^3} + Gm_{Sun}\left(\frac{\mathbf{r}_{sat-sun}}{r_{sat-sun}^3} - \frac{\mathbf{r}_{sun}}{r_{sun}^3}\right) \quad \text{A.11.}$$

$$\mathbf{a}_{Moon} = -\frac{G(m_{Earth}+m_{sat})\mathbf{r}}{r^3} + Gm_{moon}\left(\frac{\mathbf{r}_{sat-moon}}{r_{sat-moon}^3} - \frac{\mathbf{r}_{moon}}{r_{moon}^3}\right) \quad \text{A.12.}$$

Perturbation partial derivatives

A full derivation of all partial derivatives of the presented perturbation models has been developed and provided in [64]

B. Auxiliary stochastic processes

In order to account for the parametric uncertainty the following approach is considered

$$c(t) = c_{ref} + \Delta c(t) \quad \text{A.13.}$$

Indicating with *c* the generic uncertain variable , c_{ref} is a constant reference value for $c(t)$ and $\Delta c(t)$is a time varying correction factor. These correction factors can be modelled via continuous or discrete time linear stochastic process [] generally represented as :

$$\frac{d}{dt}\mathbf{\Delta c}(t) = A\mathbf{\Delta c}(t) + w_c(t) \longrightarrow \mathbf{\Delta c}_k = e^{A(t_k - t_{k-1})}\mathbf{\Delta c}(t) + \int_{t_k}^{t_{k+1}} e^{A(t_{k+1}-\lambda)}\mathbf{w}(\lambda)d\lambda \quad \text{A.14.}$$

These process can be handled via integration and discretization map developed for MEONS Generic propagator. However for the sake of completeness the well-known discrete form of the mostly used model are reported:

- Random Constant :

$$\Delta c(t_{k+1}) = \Delta c(t_k) + w_c(t_k)$$
$$Q[w_c(t_k)] = 0 \qquad Cov[w_c(t_0)] = P_0 \quad \text{A.15.}$$

- Gauss Markov (GM1), with correlation time τ_c:

$$\Delta c(t_{k+1}) = \exp[-\alpha_c(t_{k+1} - t_k)]\Delta c(t_k) + w_c(t_k)$$
$$Q[w_c(t_k)] = \sigma_{\Delta c}^2\left\{1 - \exp[-2\alpha_c(t_{k+1} - t_k)]\right\} \qquad \alpha_c = \frac{1}{\tau_c} \quad \text{A.16.}$$

Second order Gauss Markov process (GM2):, random walk (RW) and random ramp (RR are included in the A. representation and they can be referred in [105]. The empirical acceleration variable are modelled respectively as A.15 in V.3 and as A.16 in V.1 : different choice can be proposed in accordance to the dynamic scenario and filtering method used. Those accelerations are defined in the RTN reference frame, so they are properly mapped in ECI by the correspondent transformation matrix.

C. Linearized Model for optimal orbital control

The MEONS propagator has been used in V.4 also to provide to the optimal control scheme on-board integrated reference state trajectory and linearized orbit dynamic matrices. Referring to eq.(5.8) the following matrices are updated:

$$\begin{cases} \dfrac{d}{d\theta}\begin{bmatrix} x \\ \dot{x} \\ z \\ \dot{z} \end{bmatrix} = \mathbf{A}_{xz}(\theta)\begin{bmatrix} x \\ \dot{x} \\ z \\ \dot{z} \end{bmatrix} + \mathbf{B}_{xz}(\theta)\begin{bmatrix} f_x \\ f_z \end{bmatrix} \\ \dfrac{d}{d\theta}\begin{bmatrix} y \\ y \end{bmatrix} = \mathbf{A}_{xz}(\theta)\begin{bmatrix} y \\ y \end{bmatrix} + \mathbf{B}_{y}(\theta)\begin{bmatrix} f_y \end{bmatrix} \end{cases} \qquad \text{A.17.}$$

$$\mathbf{A}_{xz} = \begin{bmatrix} 0 & 1 & 0 & 0 \\ \dfrac{e\sin(\theta)}{1+e\cos(\theta)} & \dfrac{2e\sin(\theta)}{1+e\cos(\theta)} & \dfrac{-2e\sin(\theta)}{1+e\cos(\theta)} & 2 \\ 0 & 0 & 0 & 1 \\ \dfrac{2e\sin(\theta)}{1+e\cos(\theta)} & -2 & \dfrac{3+e\sin(\theta)}{1+e\cos(\theta)} & \dfrac{2e\sin(\theta)}{1+e\cos(\theta)} \end{bmatrix} \qquad \mathbf{A}_{xz} = \begin{bmatrix} 0 & 1 \\ \dfrac{-1}{1+e\cos(\theta)} & \dfrac{2e\sin(\theta)}{1+e\cos(\theta)} \end{bmatrix} \qquad \text{A.18.}$$

$$\mathbf{B}_{xz}(\theta) = \frac{\left(1-e^2\right)^3}{n^2\left(1+e\cos(\theta)\right)^4}\begin{bmatrix} 0 & 1 & 0 & 0 \\ 0 & 0 & 0 & 1 \end{bmatrix}^T \qquad \mathbf{B}_{y}(\theta) = \frac{\left(1-e^2\right)^3}{n^2\left(1+e\cos(\theta)\right)^4}\begin{bmatrix} 0 & 1 \end{bmatrix}^T \qquad \text{A.19.}$$

Where $\{\theta, e, n, \mathbf{f}\}$ are true anomaly, eccentricity, mean motion of the reference orbit [118] and $\mathbf{f}$ the a control force vector.

APPENDIX B. GNSS OBSERVATION MODULES

D. GNSS primitive measurement and error notation

Pseudorange measurement

- Pseudorange observation equation can be expressed as follow [11], [14]:

$$\tilde{\rho}_i(t) = r_i(t) + c\Delta t^r(t) - c\Delta t_i(t) + I_i(t) + E_i(t) + MP_i(t) + \nu_{\tilde{\rho}_i} \quad \text{B.1.}$$

  - $r_i = \sqrt{\left((X^{(i)} - x)^2 + (Y^{(i)} - y^r)^2 + (Z^{(i)} - z^r)^2\right)}$ is the geometrical line of sight (LOS) from the receiver $\{x, y, z\}$ to the target SVs $\{X^{(i)}\ Y^{(i)}\ Z^{(i)}\}$ at time of emission
  - Δt^r, Δt_i are respectively receiver clock bias and constellation time error
  - I_i time delay due to ionosphere;
  - η_i time delay due to receiver noise;
  - MP_i time delay due to multipath ;
  - E_i time delay due to an error in the broadcast ephemeris.

Instantaneous Doppler

- The simplified pseudorange rate model ([11], [14]) is defined as:

$$\dot{\tilde{\rho}}_i(t) = \dot{r}_i(t) + c\Delta\dot{t}^r(t) - c\Delta\dot{t}_i(t) + \dot{I}_i(t) + \dot{E}_i(t) + \dot{MP}_i(t) + \nu_{\dot{\tilde{\rho}}_i} \quad \text{B.2.}$$

  - $\dot{r}_i = \dfrac{\left[(X-x)(\dot{X}-\dot{x}) + (Y-y)(\dot{Y}-\dot{y}) + (Z-z)(\dot{Z}-\dot{z})\right]}{\sqrt{\left(X^{(i)}-x\right)^2 + \left(Y^{(i)}-y\right)^2 + \left(Z^{(i)}-z\right)^2}}$ is the geometrical range rate component projecting receiver and SVs relative velocity along the (LOS)
  - $\Delta\dot{t}_i, \dot{I}_i, \dot{E}_i, \dot{MP}$ are the propagation time delay derivatives, generally relying on high frequency residuals of the primitive source
  - η_i range rate random error due to receiver noise

Carrier Phase Measurements

- The Carrier Phase measurement observation is defined as :

$$\left(\phi_j^r(t) + A_j^r\right)\lambda = \\ = r_j^r(t) + c\Delta t^r(t) - c\Delta t_j(t) - I_j(t) + E_j(t) + mp_j(t) + \beta_j + \nu_{\phi_i} \quad \text{B.3.}$$
$$j = 1...n$$

- r_i is the geometric range as for eq. B.1
- ϕ_j^r is the phase measurement, i.e. the fractional part of carrier phase observables
- Δt^r , Δt_i Δt_i , I_i , E_i are the same time delay error of eq. B.1
- mp_j is the multipath contribution for the phase measurement
- β_j is the receiver noise figure for the phase measurement
- A_j^r is the integer ambiguity

when not modelled differently or in order to consider their stochastic residual for which apply random error assumption , the error contributions are incorporated within User Equivalent Range Error (UERE):

$$\chi^j{}_{UERE} = -c\Delta\tilde{t}_j + \tilde{I}_j^r + \tilde{E}_j + \tilde{M}P_j \qquad \text{B.4.}$$

User Equivalent Range Rate Error (UERE):

$$\dot{\chi}^j_{UERE} = -c\Delta\dot{\tilde{t}}_j + \dot{\tilde{I}}_j^r + \dot{\tilde{E}}_j + \dot{\tilde{M}}P_j \qquad \text{B.5.}$$

which are generated as uncorrelated white noises. The magnitude is computed as the Root Square Sum (RSS) of the expected error levels per each measurement typology.

GNSS observation models Partial derivatives

All the correspondent observation model as well as MEONS modules Jacobians has been fully derived in [64]

E. CDGPS SD model

Double frequency linearized observation model for CDGPS used for V.2 refer to the conventional linearization process of SD model in eq. In accordance to [65] , linearized with respect to the baseline point B, can be rewritten as follow:

$$SD_j^{AB}(t) = \left(\phi_j^A(t) - \phi_j^B\right)\lambda = -\mathbf{e}_B^j \Delta\mathbf{r}_{AB} + c\left(\Delta t^A(t) - \Delta t^B(t)\right) + I_j^{AB}(t) + mp_j^{AB}(t) + \beta_j^{AB}(t) + A_j^{AB}(t)$$

$$\mathbf{e}_B^j = \frac{(\mathbf{X}_j - \mathbf{x}_j^B)}{\left\|\mathbf{X}_j - \mathbf{x}_j^B\right\|} \qquad \mathbf{r}_{AB} = \mathbf{x}_j^B - \mathbf{x}_j^A \qquad \text{B.6.}$$

This observation model is refined for large baseline considering relative ionosperic path delay as a direct combination of the correspondent absolute contribution. This correspond to express, for estimation purposes, the SD measurements as a function of two separated VTEC :

$$(J_j^B(E_j^B)VTEC_B - J_j^A(E_j^A)VTEC_A) \qquad J_j^r(E_j^r) = \frac{82.1}{f^2(\sin(E_j^r) + \sqrt{\sin^2(E_j^r) + 0.076}} \qquad r = A, B \qquad \text{B.7.}$$

Where are the absolute mapping factor expressed as a function of the current SVs elevation.

APPENDIX C. GNSS SCENARIO SIMULATOR

G.S.S. tool has been developed for this research in the frame of MEONS project for [3] . It manages the entire simulation, providing all the necessary inputs to all the functions involved in the estimation process.

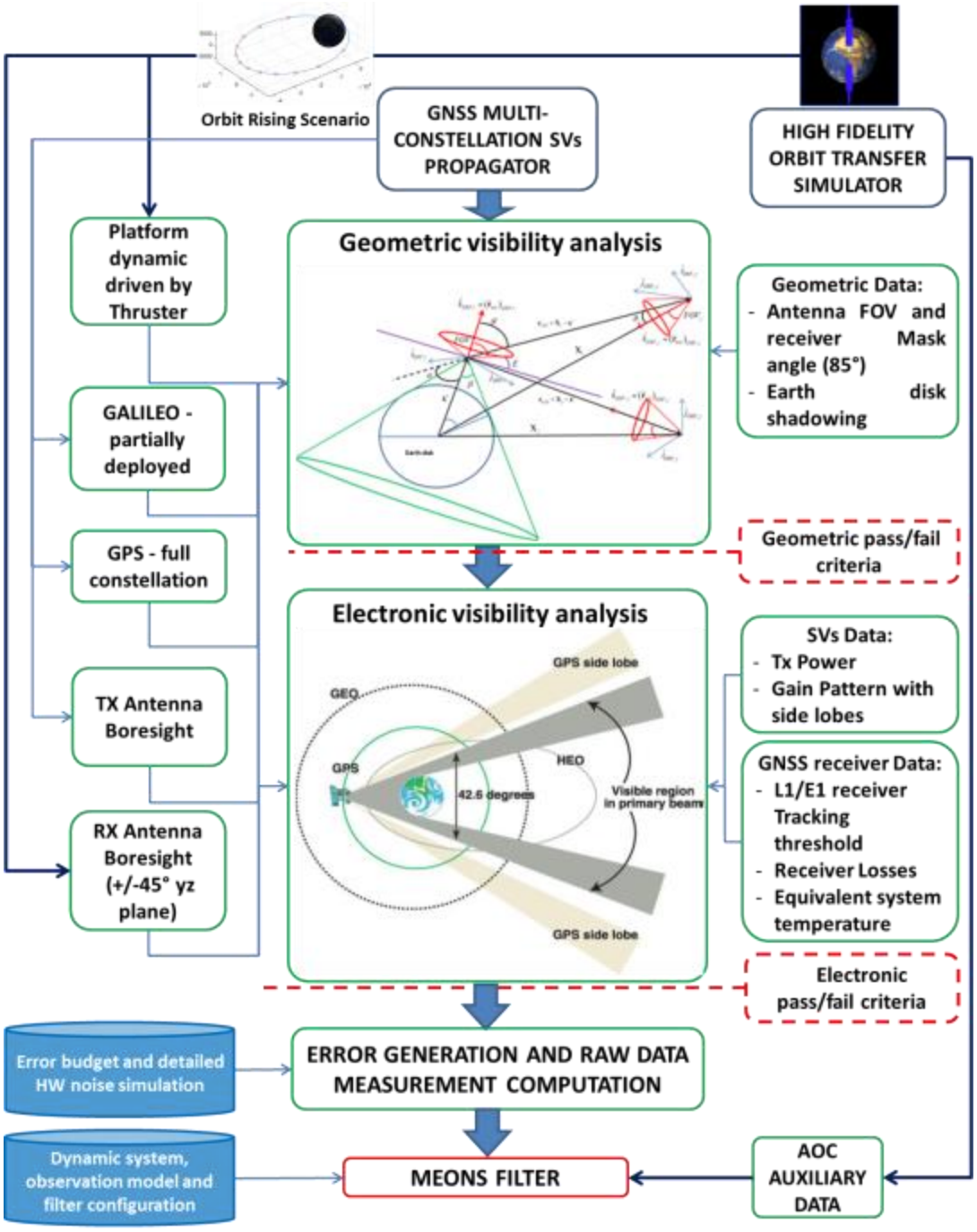

Schematic representation of the simulation process.

Observing the block diagram above the most important elements of the environment are:

- ***DSS***, High fidelity simulator

First of all, all external information are acquired. They come from a high fidelity orbit transfer simulator, which provides position and velocity of the spacecraft during orbital transfer (see III.1). These accurate position and velocity are utilized for comparison with the MEONS estimated solution. The high fidelity orbit transfer simulator provides also spacecraft attitude, which is required to obtain

receiving antenna boresight direction.

- ***SGP4/SDP4*** , Constellation Propagator

A GNSS multi-constellation propagator gives at each time instant position, velocity and transmitting antennas boresight direction of all the SVs of both Galileo and GPS constellation. The propagation starts from an input file of TLE (Two line elements) referred to the scenario simulation date: these data can be easily downloaded by the NORAD and updated in the simulated scenario periodically.

Card #	Satellite Number	Class	International Designator			Yr	Epoch Day of Year (plus fraction)	Mean motion derivative (rev/day /2)	Mean motion second derivative (rev/day2 /6)	Bstar (/ER)	Eph	Elem num	Chk Sum
			Year	Lch#	Piece			S	S .	S . S E			
1	16609	U	86017	A		93352	.53502934	.00000788	00000-0	10529-3	0	342	
2	16609		Inclination (deg)			Right Ascension of the Node (deg)		Eccentricity	Arg of Perigee (deg)	Mean Anomaly (deg)	Mean Motion (rev/day)	Epoch Rev	Chk
2	16609		51.6190			133.3400		0005770	102.5680	257.5950	15.591140704478		69

Two line elements for SVs propagation

- **GSS analysis ,** Visibility analysis

The spacecraft and constellation dynamic information integrated with receiving antenna mounting allows performing in view SVs selection considering Geometric and Electronic visibility criteria. Geometric visibility selector simply excludes the SVs which fall outside the Field of View of the receiving antenna in accordance to mask angle setting and takes into account the Earth disk, shadowing a part of the SVs of the two constellations. The electronic visibility perform link budged defined in III.2 comparing the result with the selected tracking and acquisition thresholds. The knowledge of the visible GNSS satellites makes possible to generate errors and raw data measurements within the receive module functional block.

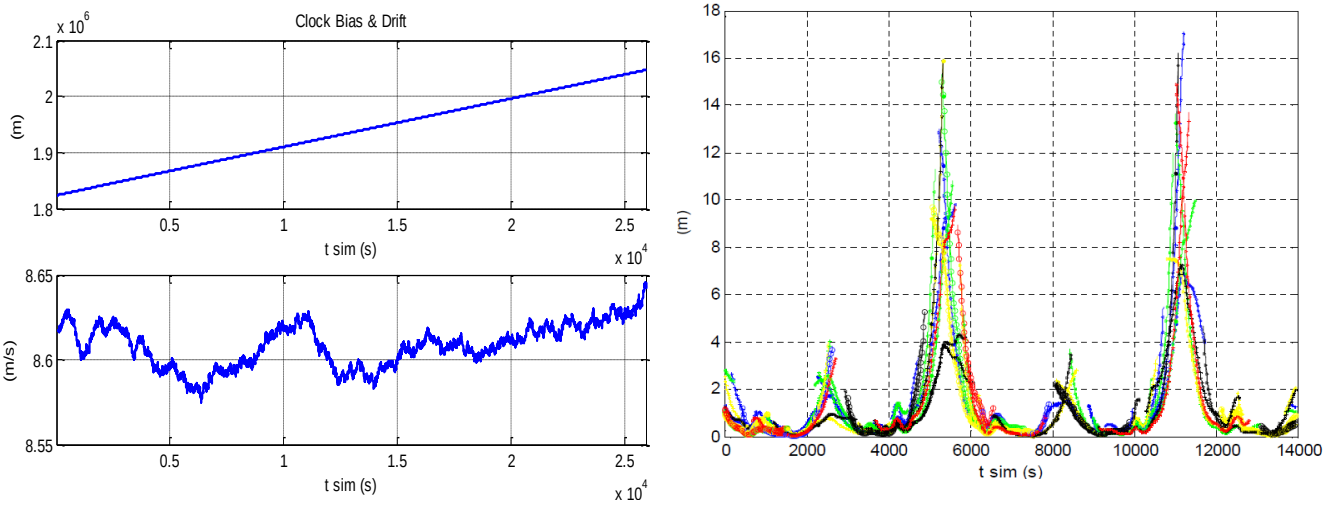

Representative example of injected error: clock bias and ionospheric path delay (high levels)

- **Receiver model,** configurable Multi-constellation,Multi-antenna,Multi-frequency equipment model

This block simulates the receiver behavior representing the correlator channels FE allocation of measurement and their kinematic navigation processing. Both pseudorange and carrier phase are provided together with the range-rate/Doppler information for each satellite in view. All the equipment functionalities have been modelled in accordance to selected target hardware [15] reproducing all relevant contribution to the navigation performance. Specifically, this block adds all error terms to the true ranging information considering hardware (i.e. clock bias and drifts, DLL and FLL noises) constellation (i.e. SVs ephemeris) and environmental (Ionosphere delay) effects. In this manner a simulated GNSS raw measurement scenario can be used to feed the several filtering algorithms.

- ***Antenna Bus/ Filter Bus***, MEONS GNSS and AOC interfaces

This antenna bus function allows to integrate several instances of the analysis in order to simulate Multi-antenna scenarios and other augmented receiver architectures described in II.1. The filter bus interface MEONS input datapool in order to acquire AOC and receiver data. This step allows to perform also closed loop for autonomous orbit acquisition test case.